THE UNIVERSITY
of EDINBURGH

The effect of insults associated with preterm birth on mouse brain development

Eamon Fitzgerald

Submitted for the degree of Doctor of Philosophy

The University of Edinburgh

2020

Declaration

I declare that the work presented in this thesis is entirely my own work, except where stated in the text. This work has not been submitted for any other degree, and to the best of my knowledge contains no material published or written by any other person, except where stated in the text.

Eamon Fitzgerald

April 2020

Acknowledgments

This PhD has only been made possible by the kindness and help of others. I'd like to start off by thanking my family, even though they have no idea what I do or have been doing, they're some of the kindest people this world has to offer and their unwavering belief in me has been central to everything I continue to do and achieve.

I am extremely grateful to the technical help of the CVS lab management team, particularly Karen French and all the technical help from the LF2 technicians, particularly Duncan and Sandra. Many people have helped me with various techniques and analysis over the years including Dr Jessy Cartier, Hannah Costello, Matthew Sinton, Dr Veronique Miron and Prof Nik Morton. I'd also like to thank Prof Megan Holmes for her advice throughout my PhD.

This PhD would not have been possible without funding from Medical Research Scotland and Aquila Biomedical and I am deeply grateful for that. I also spent 3 months with Aquila during my PhD where I was met with nothing but kindness and for this, I'd like to thank all of their staff. In particular I'd like to thank Claire Doris, Dr Hailey Gooding and Dr Jessy Cartier. Medical Research Scotland have been an amazing organisation to work with and I'd like to thank all of their board and trustees, with a particular thanks to Prof Phillip Winn and Dr Alex Graham.

I've been very lucky to have Prof James Boardman as my second supervisor throughout my PhD and I am really grateful for his input to the project throughout and his willingness to help at any given turn. I would also like to extend my thanks to the entire Boardman lab past and present and their advice on what real doctors get up to in real life.

Last but certainly not least I'd like to thank my primary supervisor Prof Mandy Drake. Throughout my PhD she has been kind, supportive and generous with her time, and for that I am forever grateful. I have also been lucky to be surrounded by a great group of people who have passed through the lab over the past few years, particularly Bonnie, Matthew and Kahyee.

Abstract

Preterm birth (PTB) is associated with an increased incidence of many neurodevelopmental disorders. The mechanisms underlying this association are unclear, but insults associated with PTB such as hypoxia, inflammation and stress can affect brain development. In this thesis I examine the effects of these insults on the mouse brain at times with neurodevelopmental relevance to PTB.

Mice when born are roughly equivalent in terms of brain development to a human at 24 weeks of gestation and mature to term equivalence by postnatal day (P) 10. As such, this course of postnatal brain development in mice provides an opportunity to study insults associated with PTB at timepoints neurodevelopmentally relevant to PTB in humans.

DNA methylation is crucial to the fine spatial and temporal control of gene expression associated with normal brain development. Altered DNA methylation (5-methylcytosine; 5mC) has been shown in the brains of individuals with autism spectrum disorders, schizophrenia and other neurodevelopmental disorders. Additionally, preterm birth is associated with altered DNA methylation at several key genes associated with neurodevelopment. However, many of these studies cannot distinguish 5mC and 5-hydroxymethylation (5hmC), which is generated from 5mC by the Ten-eleven translocation (TET) enzymes. The TET enzymes are highly susceptible to environmental perturbations and are therefore a good candidate for epigenetic dysregulation associated with PTB related insults.

I hypothesised that common PTB-related insults such as inflammation and/or hypoxia would affect the expression of the TET enzymes and this would be associated with altered DNA hydroxymethylation. To test this hypothesis, I used a forebrain slice culture model and showed that hypoxia results in increased expression of the TET enzymes. Previous studies have shown that DNA hydroxymethylation accumulates at classic hypoxic response genes following hypoxia in the cancer environment. I tested the applicability of this to brain development and found significant accumulation of 5hmC in these areas following hypoxia, demonstrating the relevance of this mechanism to neonatal hypoxia.

Early life stress is also thought to be important in PTB. To test effects of stress on brain development, I developed a novel paradigm of early life stress in mice (modified maternal separation or MMS). MMS consists of separating a pup from its mother for 1.5 hours/ day from P4-P6. During this separation period the pup is moved into a supine position, from where it will struggle to return to the prone position and the process is repeated. I hypothesised that MMS would affect the transcriptome and DNA methylome in the perinatal period and result in altered behaviour in adulthood. Using 3' mRNA sequencing and DNA methylation immunoprecipitation-sequencing I found subtle alterations in gene expression and profound alterations in DNA methylation in the hypothalamus immediately following MMS. In adulthood, I demonstrated that pups exposed to MMS have a hyperactivity phenotype in the elevated plus and open field mazes but do not display hyperactivity under habitual conditions. At 4 months of age, there were no changes in candidate gene expression in the hypothalamus, but there were changes in the expression of genes associated with stress signalling in the hippocampus following MMS. Finally, there were no persistent changes in DNA methylation in candidate regions in the hypothalamus.

I also showed an NFkB signature in the hypothalamic transcriptome following MMS. NFkB signalling is classically associated with inflammation, I therefore hypothesised that inflammation, induced by LPS, would potentiate subsequent MMS. Using immunohistochemistry, I found no difference in specific cell populations in the cortex or hippocampus. I then performed 3' mRNA sequencing to assess the transcriptome wide effect of LPS and MMS in the cortex. I showed enrichment of NFkB binding sites among differentially expressed genes in MMS but there was no additional effect of prior LPS exposure. Finally, I sought to explore whether LPS and/or MMS affected synaptic pruning in the hippocampus, however there was no evidence for altered expression of genes associated with synaptic pruning.

In summary, in this thesis I show that LPS, hypoxia and early life stress can affect mouse brain development. These results further the knowledge around how insults associated with PTB may affect brain development and neurodevelopmental outcome.

Lay Abstract

Worldwide approximately 11% of all live births occur before term. When a baby is born preterm it is at a much higher risk of atypical brain development. This can include a learning disability or a diagnosis of, among others, autism spectrum disorder and schizophrenia in later life. The reason for this is not well understood but it is thought that factors such as inflammation, hypoxia (or too little oxygen) and stress, which are all common in babies born preterm may play a role. One possibility is that these factors could affect the 'epigenome' of cells within the baby's brain and this might play a role in the increased risk of atypical brain development. The epigenome is the name for a collective of molecular signposts on DNA that are involved in deciding which proteins are made and when, in this thesis I focus on an epigenetic mark called DNA methylation. During a process as complex as brain development, the manufacturing of proteins needs to be very well controlled, and as such, things that affect DNA methylation may affect the way the brain develops. As DNA methylation is involved in the control of which bits of DNA make proteins, it is extremely diverse between tissues. This means that DNA methylation in tissues we can measure in human studies such as blood or saliva, have limited relevance to the epigenome of parts of the brain. Therefore, to better understand how factors such as inflammation, hypoxia and stress can affect DNA methylation of a preterm baby's brain we need to use models.

Mice are born with very immature brains in comparison to the human brain of a baby born at term. When they are born, mice are at a similar stage of brain development to a human at 24 weeks of pregnancy and mature to a similar stage of brain development to a full-term human baby, by their 10^{th} day of life. This means we can use new-born mice to investigate factors associated with preterm birth (PTB) during a time in which similar processes in brain development are occurring.

There are several ways to investigate brain development in mice. One way is a method called organotypic slice culture. In this method, slices of brain are cut and kept alive by giving them the nutrients they need. This method has the advantage of using fewer mice and being able to use more precise conditions, so processes can be measured without other influencing factors. I used this system to show that hypoxia results in an increased production of RNA (the precursor of protein in the cell) relating to the TET enzymes. These are a group of proteins which convert DNA methylation to another epigenetic mark, called DNA hydroxymethylation. These two marks have different properties, and this indicates these

marks may be important to the hypoxia response within the brain. I also used another model in which I isolated two types of cells called oligodendrocyte precursor cells (OPCs) and microglia. I kept these cells alive in groups without the presence of other brain cells and showed that hypoxia results in a reduced ability of OPCs to produce mature myelinating oligodendrocytes, which are important to normal brain function and often affected by PTB. I also show that LPS (lipopolysaccharide; used to mimic infection) and hypoxia can make microglia produce specific types of proteins which are involved in inflammation.

There are many mouse models to study stress in early life, but they do not always accurately replicate the stress associated with PTB. I developed a new model, which I adapted from a commonly used model called maternal separation. In my model, called modified maternal separation (MMS), mice on their 4^{th} day of life are repeatedly but gently turned on to their back for 1.5 hours on 3 consecutive days. I showed this model is not associated with changes in growth or blood glucose levels, which other models of early life stress are associated with. I also show MMS is associated with many changes in DNA methylation in the hypothalamus, a region of the brain important in the stress response. Next I demonstrated that mice exposed to MMS displayed hyperactive behaviour in a new stressful environment as adults and that this hyperactivity was not representative of normal hyperactivity during the course of a typical day.

Finally, I tested to see if MMS would be affected by prior administration of LPS. To investigate this, I used a technique called 3' mRNA sequencing, which measures what types of mRNA (the type of RNA which will form a template for a protein synthesis) are present. I did this in the cortex, a region commonly affected by PTB. However, there was little differences in which mRNA was present here when LPS preceded MMS compared to MMS alone.

In conclusion, in this thesis I present results which contribute to the wider understanding of how factors associated with PTB may affect brain development.

Abbreviations

5caC	5-carboxycytosine
5fC	5-formylcytosine
5hmC	5-hydroxymethylcytosine
5mC	5-methylcytosine
ACTH	Adrenocorticotropic Hormone
ADHD	Attention Deficit Hyperactivity Disorder
ANOVA	Analysis Of Variance
ARI	Acute Respiratory Infection
ARVCF	Armadillo Repeat gene deleted in Velo-Cardio-Facial syndrome
ASD	Autism Spectrum Disorders
AVP	Arginine Vasopressin
BAM	Binary Alignment Map
BBB	Blood Brain Barrier
BCAAs	Branched Chain Amino Acids
BDNF	Brain Derived Neurotrophic Factor
BER	Base Excision Repair
BMAL1	Brain muscle ARNT-like protein 1
BSA	Bovine Serum Albumin
CBP	CREB Binding Protein
CBR1	Cannabinoid Receptor 1
CGI	CpG Islands
CHARGE study	Childhood Autism Risks from Genetics and Environment
CHD	Congenital Heart Disease
CLOCK	Circadian Locomotor Output Cycles Kaput
CP	Cerebral Palsy
CpG	Cytosine phosphate Guanine
CREBBP	CREBP Binding Protein
CRH	Corticotrophin Releasing Hormone
CRP	C-Reactive Protein
Cry	Cryptochrome
CSMD	CUB and Sushi multiple domains

DBP	D-box binding protein
DISC	Disrupted In Schizophrenia
DIV	Days *In Vitro*
DLG4	Discs Large Homology 4
DNMT	DNA Methyltransferase
EPM	Elevated Plus Maze
FADS2	Fatty Acid Desaturase 2
FDA	Federal Drug Administration
FKBP	FK506 binding protein
FMRP	Fragile X Mental Retardation Protein
GCs	Glucocorticoids
GLAST	Glutamate Aspartate Transporter
GR	Glucocorticoid Receptor
GRE	Glucocorticoid Response Element
GWAS	Genome Wide Association Studies
HDAC	Histone deactalyse
HIF	Hypoxia Inducible Factor
hmeDIP	hydroxymethylated DNA Immunoprecipitation
HPA axis	Hypothalamus Pituitary Adrenal axis
ICF	Immunodeficiency, Centromeric region instability, Facial anomalies
IFN	Interferon
IkB	inhibitor kappa B
IKK	The IkB kinase
IP	Intraperitoneal
iPSCs	induced Pluripotent Stem Cells
LIF	Leukemia Inhibitory Factor
LPS	Lipopolysaccharide
MAPK	Mitogen-Associated Protein Kinase
MeCP2	Methyl CpG binding protein 2
meDIP	methylated DNA Immunoprecipitation
MIA	Maternal Immune Activation
MLL	Mixed Lineage Leukemia
MMS	Modified Maternal Separation

mPFC	medial Prefrontal Cortex
MR	Mineralocorticoid Receptor
MRI	Magnetic Resonance Imaging
MRS	Magnetic Resonance Spectroscopy
NFIL3	Nuclear Factor Interleukin 3 regulated
NFkB	Nuclear factor kappa B
NICU	Neonatal Intensive Care Unit
NR	Nuclear Receptor
OF	Open Field
OPCs	Oligodendrocyte Precursor Cells
P (followed by a number)	Postnatal (age in days)
PARP	Poly-ADP ribose polymerase
PBS	Phosphate Buffered Saline
PCR	Polymerase Chain Reaction
Per	Period
PET	Positron Emission Tomography
PGK1	Phosphoglycerate kinase 1
PHD	Proline Hydroxylase
PRR	Pathogen Recognition Receptor
PSD95	Post-synaptic density protein 95
PTB	Preterm birth
PVL	Periventricular Leukomalacia
PVN	Paraventricular Nucleus
RDS	Respiratory Distress Syndrome
ROR	Retinoic-acid related Orphan Receptors
RT	Reverse Transcription
SCN	Superchiasmatic Nucleus
SFR	Spontaneous Firing Rate
SHRP	Stress-hyporesponsive period
SLC	Soluble Light Chain
SNP	Single Nucleotide Polymorphism
SSRI	Selective Serotonin Reuptake Inhibitor
TBS	Tris Buffered Saline

TBST	TBS with Tween
TCA	Tricarboxylic Acid
TDG	Thymine DNA Glycosylase
TET	Ten-Eleven Translocation
TLR	Toll-like receptor
TNF	Tumor Necrosis Factor
TSC	Tuberous Sclerosis Complex
UHRF2	Ubiquitin like with PHD and ring finger domains 2
VEGFA	Vascular Endothelial Growth Factor
VIP	Vasoactive Intestinal Peptide
WGA	Whole Genome Amplification
WMI	White Matter Injury

Contents

1 Introduction

Preterm birth (PTB) is associated with various adverse neurodevelopmental outcomes, but many of the underlying mechanisms are unknown. In this thesis I explore the effect of early life insults, which are associated with PTB, on mouse brain development. I examine how perinatal hypoxia, inflammation, exogenous glucocorticoids and stress can affect the epigenome, as well as various physiological and biochemical processes integral to brain development.

1.1 Epidemiology of PTB

PTB is clinically defined as birth prior to 37 weeks of gestation [1]. In 2010, PTB accounted for 11.1% of all live births reported worldwide, with complications directly resulting from PTB accounting for approximately 1 million deaths per year [2]. Seventy five percent of all deaths in the perinatal period occur among those born preterm [3], and in 2010 the UK reported infant mortality as 1.6 and 24.3 per 1000 live births for term and preterm births respectively [4].

In recent decades, mortality associated with PTB has decreased with improved neonatal care, but with this there has been an increased diagnosis of neurodevelopmental disorders among those born preterm [5,6]. Neurodevelopmental outcome following PTB has improved since the 1990's [7], but PTB remains the single largest early life risk factor for poor long-term neurodevelopmental outcome [8–10]. PTB is associated with an increased prevalence of neurodevelopmental disorders including cerebral palsy (CP) [11], autism spectrum disorders (ASD) [12–14] and schizophrenia [15,16]. PTB is also predictive of cognitive ability at school age, with those born at earlier gestational ages typically receiving lower scores [17].

Despite the social and economic burdens associated with PTB there is still relatively little known about its aetiology. Cervical length is a major risk factor, with near universal screening now in place [18]. There may also be a genetic component, as the daughters of mothers who have given birth preterm are themselves more likely to undergo preterm labour [19]. Moreover, in a large genome wide association study (GWAS), single nucleotide polymorphisms (SNPs) in several genes (*Early B-Cell Factor 1*, *Selenocysteine-specific elongation factor*, *Type-2 angiotensin II receptor* and *WNT4*) have been associated with gestational duration [20]. Environmental factors such as socio-economic status, stress,

smoking, poor diet and drug use have also been implicated in the onset of PTB [21,22]. Infection, both maternal and intra-uterine, is also strongly associated with the onset of PTB [23,24].

1.2 PTB and neurodevelopmental disorders

Neurodevelopmental disorders are those which have origins during early brain development and, as mentioned earlier, PTB is associated with an increased risk for many neurodevelopmental disorders. In this section I will discuss this with particular attention paid to ASD and schizophrenia.

1.2.1 Autism Spectrum Disorders (ASD)

ASD diagnoses in England have increased dramatically over the last 50 years [25], likely as a consequence of broadening diagnostic criteria and increased clinical awareness. ASDs are highly heterogeneous in their aetiology, phenotype and severity. The DSM V criteria for ASD reflects this with three levels of severity, and many syndromic and non-syndromic forms have been described. ASD can be broadly defined as persistent difficulties in both verbal and non-verbal social interactions [26,27]. There is a higher prevalence of ASD in males [28], with a prevalence amongst 8-year old boys and girls in the UK of 3.8 and 0.8 per 1000 respectively [29].

Many syndromic forms of ASD are monogenic and inherited in a mendelian fashion [30,31]. *De novo* mutations in either the germline or somatic cells during early development also contribute to a small proportion of ASD cases [32]. There is also clear evidence for a large polygenic component to ASD [33,34].

Environmental factors also play a role in the aetiology of ASD. It has been shown in many studies across different populations and ethnicities that PTB is associated with an increased prevalence of ASD in offspring [12–14,35–37]. Perinatal infection has also been heavily linked to ASD [38–41] and in particular maternal influenza infection during pregnancy has been associated with an increased ASD in offspring, [42] but it should be noted this has not been replicated in other studies [43].

1.2.2 Schizophrenia

Schizophrenia is a neurodevelopmental disorder, characterized by positive (e.g. hallucinations and delusions) and negative (e.g. avolition and alogia) symptoms which typically first occur during late adolescence [44]. Schizophrenia has an incidence of 5 per 1000

in the general population [45], and there is a marked increase in prevalence amongst those born preterm [15,16,46]. Similarly to ASD, some studies have suggested a link between early life inflammation (particularly maternal influenza) and risk of schizophrenia in later life [40,41,47,48]. Increased levels of circulating maternal cytokines are also associated with an increased risk of schizophrenia in offspring [49,50]. Although the mechanisms linking maternal infection with the development of schizophrenia in offspring remain unclear, studies suggest a reallocation of resources may be involved [51–53].

Positive associations from genome wide association studies (GWAS) in individuals with schizophrenia are enriched for genes associated with astrocytes and oligodendrocytes [54]. As will be discussed later, oligodendrocytes are particularly vulnerable to PTB related brain injury, particularly hypoxia. In term born infants, perinatal hypoxia doubles the risk of psychiatric disease [55]. Schmidt-Kastner *et al* showed that 55% of genes associated with schizophrenia (through GWAS) have also been linked to hypoxia response mechanisms [56]. Therefore, neonatal hypoxia is also a plausible mechanism in the aetiology of schizophrenia.

1.2.3 Encephalopathy of prematurity

Encephalopathy of prematurity commonly results from PTB, consisting of both white matter injury (WMI) and grey matter injury [57]. WMI typically occurs in the deep white matter of the periventricular area and can result from many clinical factors such as hypoxia/ischemia, infection or nutritional deficiencies [58]. The degree of WMI is predictive of neurodevelopmental outcome [59] and a spectrum of WMI occurs following PTB. This includes three principal pathologies: diffuse non-necrotic lesions, focal macroscopic lesions and focal microscopic lesions [60]. Microscopic lesions have a similar distribution to macroscopic lesions suggesting similar underlying mechanisms [60]. However, unlike macroscopic and diffuse lesions, traditional 3T MRI techniques are unable to identify microscopic necrotic lesions, but they can be seen with higher powered 12T imaging [61]. Diffuse WMI is the most common form of WMI seen in infants born preterm and a significant contributor to this is impaired oligodendrocyte maturation [62].

CP is a neurodevelopmental disorder with characteristic motor symptoms. Periventricular leukomalacia (PVL) is a core neuropathological feature [63,64] which consists of focal necrotic lesions in the deep white matter combined with more diffuse, less severe lesions [65]. It is estimated that 2-3.5 per 1000 neonates will develop CP [66] and PTB is a major risk factor. In a

large epidemiological study from Norway, with data from almost 1.8 million births of various gestational ages over 34 years, there was an 8.5% incidence of CP in those with a gestational age at birth of 23-27 weeks, which decreased in an age dependent manner to 0.1% in those born at term [11].

Around 10% of CP cases are thought to be directly associated with fluctuating oxygenation at birth [67] and the multiple-hit hypothesis proposes that a number of distinct insults acting in synchrony may lead to the development of CP [68]. Hypomyelination as a result of oligodendrocyte cell death is a core feature of CP. Cells of the oligodendrocyte lineage are especially vulnerable to PTB related insults as their maturation coincides with the time in which PTB occurs [69] and hypomyelination is also frequently seen in PTB associated brain injury without CP [70,71].

There is extensive neurogenesis during the 3rd trimester [72] and cortical migration of GABAergic interneurons occurs until after term equivalent age [73], the routes of which may be disrupted by deep white matter injury associated with PTB.

1.2.4 Common features of neurodevelopmental disorders

The aetiology of non-syndromic neurodevelopmental disorders is often unknown and there is a large symptomatic overlap between disorders, with central diagnostic criteria such as low IQ and social difficulties listed for many disorders [74,75]. This leads to some diagnostic subjectivity and individuals therefore often have multiple diagnoses [76,77]. Many neurodevelopmental disorders are also associated with common risk factors, as discussed earlier PTB and maternal infection are associated with a marked increase of both ASD and schizophrenia. There is evidence similar mechanisms may underlie ASD and schizophrenia, with mounting evidence for synaptic involvement in both disorders. I will now discuss some common features of neurodevelopmental disorders, focusing primarily on ASD and schizophrenia.

1.2.4.1 Synaptic components of neurodevelopmental disorders

1.2.4.1.1 ASD

During the early postnatal period there is a rapid increase in the number of synapses within the brain, which peaks around 2 years of age. Henceforth, synapse number gradually decreases until mid-late adolescence, from which point synapse number remains relatively

constant [80]. The process of selective glial mediated synaptic loss is termed "synaptic pruning" and alterations in this as well as neurogenesis have long been hypothesised to be involved in the pathophysiology of many neurodevelopmental disorders [81,82].

ASD is associated with an increased synapse number in the cortex [83,84] and amygdala [85]. Cortical transcriptomes from post-mortem tissue of individuals with ASD show strong signs of synaptic and microglial alterations [33,86]. In individuals with ASD, brain size is slightly below average at birth, then significantly increased at 1 year before normalising in adulthood [87]. In post-mortem tissue from individuals with ASD there is differential DNA methylation at several loci associated with synaptic pruning (e.g. *C1q*, *CR3*, *C3* and tumour necrosis factor (*TNF)*) [88]. The Shank family of proteins interact with PSD95 (post-synaptic density protein 95) at the synapse [89]. Mutations within these proteins are associated with ASD in humans [90] and Shank3 haploinsufficiency produces an ASD like phenotype in mice which can be rescued with the HDAC (histone deacetylase) inhibitor Romidepsin [91]. The post-synaptic proteins neuroligin 3 and 4, as well as their presynaptic ligand neurexin 1 have also been linked to ASD [92].

1.2.4.1.2 Schizophrenia

Deficits in synaptic pruning have been hypothesised to underlie schizophrenia for decades [93,94]. In post-mortem tissue from individuals with schizophrenia there is a decreased synaptic density in the prefrontal cortex and hippocampus [95], as well as a decreased abundance of synaptic proteins in the hippocampus [96]. Microglia induced pluripotent stem cells (iPSCs) derived from individuals with schizophrenia also show increased levels of synaptic pruning compared to control individuals [97].

Many genes and physiological processes that are thought to play a role in schizophrenia also have roles in synaptic pruning. As mentioned previously, viral infection during pregnancy may be associated with an increased incidence of schizophrenia in offspring, and in mouse models neonatal, toll-like receptor 3 (TLR3) activation (which models viral infection) reduces spine density in a manner dependent on *DISC1* (disrupted in schizophrenia 1) [98,99]. A variant of the *C4* gene (part of the complement pathway) confers an increased risk of schizophrenia in humans. In mice, C4 is present at the synapse and has an important role in synaptic pruning [100]. *C4A* expression is increased in the cortex of individuals with schizophrenia and ASD [33]. CSMD1 (CUB and Sushi multiple domains 1) is an inhibitor of C4 and is highly expressed in

the brain [101]. A SNP within the *CSMD1A* gene is associated with schizophrenia and various cognitive attributes [102,103].

1.3 Methods and models to study human brain development following PTB

Understanding the patterns of human brain development following PTB presents a number of problems. First and foremost, the brain is a largely inaccessible organ which precludes the use of brain specific biopsies or samples taken during routine clinical practice (with the exception of CSF). I will now briefly discuss commonly used methods and models for the investigation of human brain development.

1.3.1 Humans

Brain development in humans is studied primarily using various non-invasive parameters such as epidemiology, behavioural studies and imaging modalities, such as magnetic resonance imaging (MRI), magnetic resonance spectroscopy (MRS) and ultrasound. These techniques have given crucial insights into typical brain development and how it is affected by PTB. However, they alone are unable to provide a full picture of the physiological and biochemical response to PTB. This necessitates the use of experimental models such as iPSCs, organoids and animal models.

1.3.2 Animal models

There are many animal models available to study how PTB and early life adversity affect brain development. Simple organisms such as zebrafish are useful to study fundamental, well conserved characteristics of brain development as they have short reproduction cycles (hatching occurs 3-4 days after fertilisation) and are transparent during the early stages of nervous system formation. Rodents are mammals, with short gestational cycles (birth occurs ~21 days after fertilisation) and many conserved neurodevelopmental processes making them an attractive model. Large animal models are also used as they have a higher degree of similarity to the human brain but have long gestational cycles (birth occurs ~114 days post-fertilisation in the pig for instance).

1.3.2.1 Rodents

Rodents, particularly mice and rats, are the most commonly used animal to study brain development due to genetic tractability, short gestational cycles and the presence of many well conserved processes in brain development. Compared to humans, mice are born relatively immature in terms of brain development. The bioinformatic mapping of gene

expression patterns across both human and mouse development indicates that mice when born have roughly equivalent gene expression patterns to a human at about 24 weeks of gestation and become comparable to term born humans by postnatal day (P)10 [121]. As such, insults immediately following birth occur at neurodevelopmentally comparable timepoints to preterm birth in humans.

1.3.2.2 Large animals

Large animal models such as pigs and sheep have longer periods of gestation and higher degrees of neural complexity compared to rodents. Due to this long period of gestation and the cost associated with their maintenance, large animal models are useful for evidence of efficacy before trials in non-human primates (such as a baboon model [122]) and humans. For instance, an *ex utero* incubation system has been successfully trialed in preterm sheep [123].

1.3.3 Primary culture systems

Primary culture systems are useful as the conditions in which cells grow can be accurately controlled with fewer variables than *in vivo* experimentation. They also allow experiments which would be unethical in living animals and as cells from an individual can be used in multiple treatment groups, culture systems help to reduce the number of animals used in scientific experimentation. However, they fail to account for many complexities of tissue resident cells and as such are best used in combination with *in vivo* experimentation. I will now briefly review some common culture models for the study of brain development.

1.3.3.1 Rodent primary cell culture

The heterogeneity of cell types in the brain makes it difficult to ascribe physiological function or mechanism to specific cell types. Primary cell culture is often used to look at cell type specific effects of pharmacological agents and environmental perturbations. In neonatal animals, brain tissue can be dissociated and specific cell types extracted using various techniques, before culturing.

Since the specific growth factors and nutrients needed to enable cell growth are often unknown, animal serum is commonly used in media for the culture of primary cells. As serum content is undefined and variable from batch to batch, this is a central point of variability in these systems. Further studies, such as the one by Bohlen *et al* [124], in which a protocol for the culture of murine microglia under defined conditions, are necessary to further translation in this area.

1.3.3.2 Rodent Organotypic brain slice culture

An alternative culture system which retains the complex cytoarchitecture of the brain while providing a controlled culture system is organotypic brain slice culture. In this paradigm, the brain is isolated from a neonatal animal and cut into 300µm sections, which can then be cultured for an extended period on a semi-permeable membrane at the media/air interface.

This system has been used for high throughput drug screening [125] as well as investigations of neurodegeneration [126], myelination/remyelination [127] and electrophysiological activity [128]. It is however a lower throughput approach than primary culture models (which can be scaled for use in 96 or 384 well formats). Therefore, organotypic brain slice culture systems are an intermediary between primary cell culture and *in vivo* experimentation.

1.3.3.3 Human iPSCs and organoids

The widespread use of animal models, whilst adding critical information to the field, has not resulted in a marked improvement in outcome for infants born preterm. In recent years, iPSCs and human organoid models have emerged which provide much translational promise. Human cortical organoids can produce electrical patterns similar to those seen in preterm infants [129] and work in organoids has already identified the protein unfolding response as a promising therapeutic target for neonatal hypoxia [130]. However, organoids do not recapitulate the entire cellular heterogeneity of the brain and questions remain over the reproducibility of these systems. Also, the brain does not develop in isolation and these systems cannot account for systemic influences on brain development such as sensory input.

1.4 Epigenetics

There is no consensus definition of the term “Epigenetics”, but Adrian Bird’s proposed definition of “the structural adaptation of chromosomal regions so as to register, signal or perpetuate altered activity states” [131] is a common modern definition. For the purpose of this thesis, I will focus on modifications to genomic cytosine (see Figure 1.1), which do not alter the underlying coding sequence, and refer briefly to chromosomal and RNA modifications.

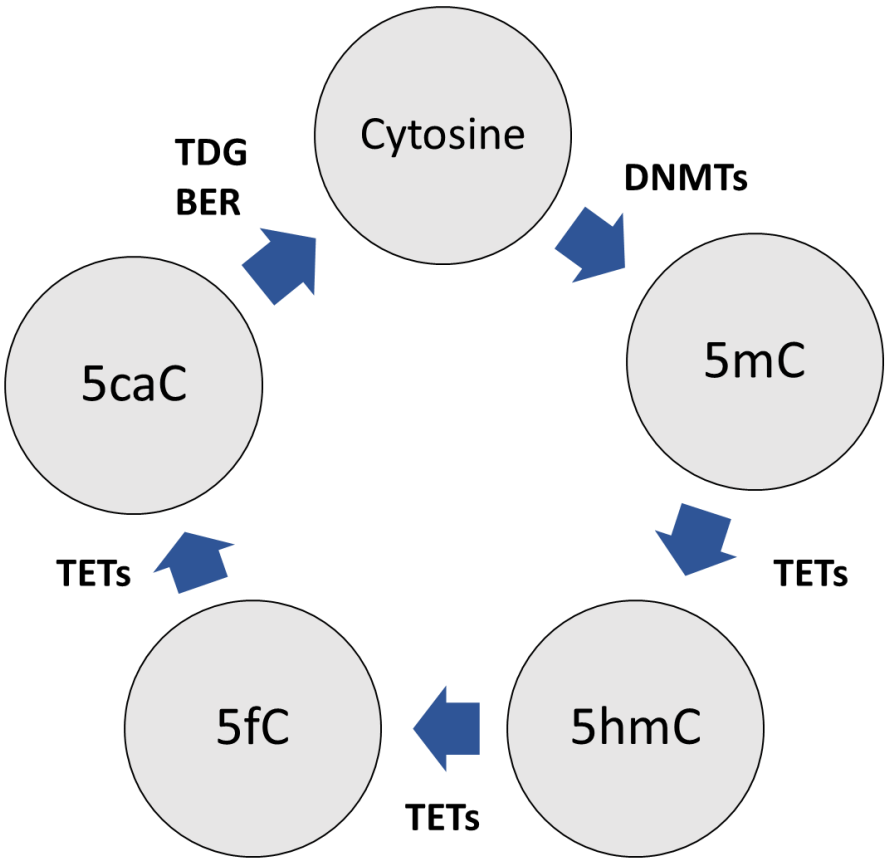

Figure 1.1 Cytosine can be converted to 5-methylcytosine (5mC) by the DNMT enzymes. This mark when present within the promoter regions of a gene is classically associated with repression of transcription. Until recently this was thought to be a permanent modification, with no known removal mechanism other than passive DNA demethylation (lack of maintenance on the de novo strand during DNA replication). However recently the TET enzymes were shown to catalyse the hydroxymethylation of 5mC to form 5-hydroxymethylcytosine (5hmC), and subsequently 5-formylcyosine (5fC) and 5-carboxylcytosine (5caC). 5fc and 5caC can then be removed and an unmodified cytosine replaced through thymine DNA glycosylase (TDG) and the base excision repair (BER) pathway.

1.4.1 DNA Methylation

DNA methylation typically occurs at the 5th carbon of cytosine residues when accompanied by a guanine residue in the sequence Cytosine phosphate Guanine (CpG) [132], to produce 5-methylcytosine (5mC). Roughly 10% of these CpG sites genome wide are present in clusters called CpG islands (CGI), which are often located in the promoter regions of key developmentally regulated genes [132–134]. Although CGIs are generally unmethylated, the

presence of 5mC in these areas is typically associated with repression of gene transcription [132]. DNA methylation is highly conserved from plants through to mammals and is widely viewed as a key mechanism in the fine spatial and temporal control of gene expression during development [132]. Low levels of 5mC are generally associated with pluripotency, where less than 30% of CpGs may be methylated as opposed to terminally differentiated cells where up to 85% of CpGs may be methylated [135–137]. The enzymes DNA methyltransferase (DNMT) 3A and 3B are responsible for *de novo* DNA methylation [138], while DNMT1 is responsible for the maintenance of 5mC on the complimentary strand during DNA replication [139].

1.4.2 DNA Hydroxymethylation and the Ten-Eleven Translocation Enzymes

The Ten-Eleven Translocation (TET) enzymes were first proposed to produce 5-hydroxymethylcytosine (5hmC) from 5mC by Tahiliani *et al* [140]. The three TET proteins (TET1-3) are part of a large group of α-ketoglutarate dependent dioxygenase enzymes which include other epigenetic modifiers such as the jumonji-containing domain histone demethylases and the proline hydroxylase (PHD) proteins (involved in the cellular response to hypoxia [141]). This group of enzymes uses the tricarboxylic acid (TCA) cycle metabolite α-ketoglutarate and oxygen as essential substrates and Fe_{2+} as an essential co-factor [22,142].

TET1 and TET2 have overlapping functions [143], whilst TET3 is important during reprogramming within the oocyte [144,145] but is also important at later developmental stages within the retina [146]. These are the only enzymes which are known to produce 5hmC and its subsequent metabolized forms of 5-formylcytosine (5fC) and 5-carboxylocytosine (5caC) [147,148]. 5hmC, 5fC and 5caC are present in the genome at decreasing quantities (with 5hmC being the most prevalent). This is due to a conformational change which occurs during the act of 5hmC production, resulting in reduced TET affinity for the subsequent derivatives [149].

1.4.3 Dynamics of DNA Methylation and Hydroxymethylation

Both 5mC and 5hmC are dynamically present in the brain throughout development in rodents and humans [110,163,164] and, as will be discussed later, are altered in many neurodevelopmental disorders. A gradual increase in 5hmC is seen at developmentally primed genes through brain development, with particular enrichment at Fragile X Mental Retardation Protein (FMRP) binding sites [163,165]. In mouse embryonic stem cells 5hmC is found both intragenically at sites of active transcription genes and at extended promoters of polycomb repressed genes [166]. In the adult brain 5hmC is present throughout gene bodies at much higher levels than in ESCs

and for the most part absent at transcription start sites, where 5hmC is typically enriched in ESCs [163]. 5mC and 5hmC are present in cell type specific patterns and can be used to predict neuronal subtype [167]. There is also minimal 5hmC on the X chromosome in both male and female rodents and humans [163].

5mC is a stable modification, meaning it is covalently bound to cytosine and produces distinct effects on chromatin architecture and transcription. 5hmC is also associated with distinct effects on the genome. However only a few 5hmC binding partners have been characterized to date. Spruijt *et al* [168] demonstrated the ubiquitin like with PHD and ring finger domains 2 (UHRF2) protein binds and recruits other complexes to 5hmC. Mellen *et al* showed that methyl CpG binding protein 2 (MeCP2) can also bind to 5hmC with high affinity [169].

1.5 Epigenetics and neurodevelopmental disorders

Several neurodevelopmental disorders are associated with genetic alterations in epigenetic proteins. Rett syndrome is caused by mutations of the DNA methylation reader *MeCP2* [176]; ICF (Immunodeficiency, Centromeric region instability, Facial anomalies) syndrome is associated with a mutation in the *de novo* DNA methyltransferase *DNMT3b* [177] and fragile X syndrome is associated with an expanded CGG repeat in the promoter of the *FMR1* gene, which results in its hypermethylation and subsequent silencing [178]. Also, the imprinting disorders Angelman syndrome and Prader-Willi syndrome are caused in most cases by mutations or deletions within imprinted genes (reviewed by Rangasamy *et al.* 2013 [179]). These are examples of syndromic neurodevelopmental disorders and, as discussed previously with respect to ASD, can be classified by their known aetiology and characteristic symptoms.

Much of the research on epigenetic alterations in neurodevelopmental disorders focuses on these syndromic forms, but as mentioned previously these account for a small percentage of overall individuals with a diagnosed neurodevelopmental disorder. In the next section, I will discuss the evidence for epigenetic alterations in both in cases of non-syndromic neurodevelopmental disorders and following PTB.

1.5.1 Epigenetic alterations following PTB

Cruickshank *et al* examined blood at birth and at 18 years of age, from infants born extremely preterm (less than 31 weeks of gestation) and compared DNA methylation profiles to term born infants. Differences were found at birth but not at 18 years of age [180]. Similar results

have been shown in other studies, comparing infants born preterm and at term [181–183]. However, as discussed earlier, DNA methylation is highly dynamic throughout development. As these studies are comparing DNA from infants born at different ages, it is therefore not necessarily surprising to see differences.

To address this, Sparrow *et al* analyzed DNA taken from buccal cells of infants born preterm at term equivalent age (i.e. 40 weeks from conception) and term born controls. Here, altered DNA methylation was seen at several genes with important functions in neural development [184]. However, this differential methylation is not present at largely 1 year of age [185]. One of the differentially methylated proteins in the Sparrow *et al* study was soluble light chain 7a5 (*SLC7A5*), an amino acid transporter present, among other areas, in endothelial cells and therefore at the blood brain barrier (BBB) [184]. Tărlungeanu *et al* demonstrated that *SLC7A5* deletion from endothelial cells results in abnormal behaviours in mice, which were improved with intraventricular administration of BCAAs (branched chain amino acids). In this study they also identified individuals with ASD who had mutations within the *SLC7A5* gene [186]. Therefore, considering SLC7A5 has been shown to be differentially methylated in infants born preterm and to have a role in neurodevelopmental disorders, it is an intriguing candidate for the investigation of PTB related brain injury.

1.5.2 Epigenetic alterations in ASD

Differential DNA methylation has been identified at many loci in post-mortem tissue of individuals with ASD, including in the prefrontal cortex, temporal cortex and cingulate gyrus [88,187]. Key inflammatory mediators, such as TNF have been shown to be both differentially methylated and expressed in post-mortem prefrontal cortices of individuals with ASD [88,188]. Differential DNA methylation in blood [189] and buccal cell [190] derived DNA from monozygotic twins discordant for ASD has also been described.

Differential acetylation genome wide of the H3K27ac histone modification is seen in individuals with ASD (when compared to age matched typical developing controls) in the prefrontal cortex, temporal cortex and cerebellum of individuals with ASD compared to typically developing controls [191]. Genes related to synapses and ion channels [188] are particularly enriched among those showing differential histone acetylation [188,191,192]. In a large cohort of Danish children, prenatal exposure to the HDAC inhibitor, Valproate, was shown to lead to an increased incidence of ASD in offspring [193]. Moreover, mutations in the histone

acetyltransferase *CREBBP* (CREBP binding protein) are associated with altered neurodevelopmentally regulated behaviours [194].

1.5.3 Epigenetic alterations in schizophrenia

In post-mortem frontal cortical tissue from individuals with schizophrenia, there are widespread changes in DNA methylation, including in the promoter of *DNMT1* [195]. Using an unbiased clustering algorithm to analyse the DNA methylome of these individuals, there was strong clustering within the schizophrenia and control groups, indicating a specific DNA methylation landscape in the brain of individuals with schizophrenia [195]. Another study found *DNMT1* to be overexpressed in layer I GABAergic interneurons of the prefrontal cortex in individuals with schizophrenia or bi-polar disorder, which was also associated with alterations in DNA methylation at some candidate genes [196]. Another study of DNA methylation in post-mortem frontal cortical tissue in individuals with schizophrenia and age matched controls, showed differential methylation in genes associated with glutamatergic and GABAergic signaling [197]. Using DNA isolated from blood in 689 individuals with schizophrenia, differential methylation has been reported at several genes central to neural development [198]. Therefore, there is good evidence for deregulation of DNA methylation in frontal brain regions and in whole blood of individuals with schizophrenia.

There is also mounting evidence also for alterations in histone modifications among individuals with schizophrenia and I will now briefly summarize some of these findings. In a GWAS of individuals with/without schizophrenia Shi *et al* identified a key chromosomal area, in which many histone modifiers and immune regulators are present, which confers an increased risk of schizophrenia [199]. Histone deacetylase 1 (HDAC1) and HDAC2, which remove acetyl marks from histones, have both been implicated in schizophrenia [200,201]. Tang *et al* showed alterations in the lifetime trajectory of the histone mark H3K14ac in the prefrontal cortex of individuals with schizophrenia [202]. There is also evidence for altered histone methylation in the frontal cortex of individuals with schizophrenia [203].

Therefore, there is evidence for epigenetic alterations in individuals born preterm and those with diagnosed neurodevelopmental disorders when compared to term born or typically developing individuals respectively. It is however unclear whether the changes in these marks occurs as a result of pathogenic processes and are therefore not the primary drivers of

atypical brain development or whether early life events cause fundamentally altered epigenetic trajectories which are causative of atypical neurodevelopment.

This is further confused by the techniques used in these studies. As outlined previously, 5hmC and its subsequent derivatives have only recently been described and traditional bisulphite based techniques cannot discriminate between 5mC and its subsequent derivatives. In theory, a reduction in 5mC could be accompanied by a concomitant increase in 5hmC resulting in no net change when analysed using bisulphite sequencing. More in depth evaluation of 5mC/5hmC through the genome is needed in these studies, as has been done by Spiers *et al* 2017 [204].

As discussed previously there is a clear genetic component to neurodevelopmental disorders but even the most recent polygenic associations [34] cannot explain all cases, implying a clear role for environmental factors such as PTB. Therefore, a major outstanding question is how PTB related brain insults (i.e. hypoxia, inflammation, glucocorticoids and early life stress) can affect brain development and interact with the genetic component of neurodevelopmental disorders to modulate risk increased risk. I will now discuss the insights animal models have given into these insults, with reference to human literature.

1.6 Insults associated with preterm birth

1.6.1 Hypoxia

Respiratory distress syndrome (RDS) is a condition associated with very preterm birth in which underdeveloped lungs are unable to produce surfactant, so that systemic hypoxia may occur with associated brain injury [205–208]. There is no consensus as to the appropriate level of oxygen to administer infants born preterm and this can lead to fluctuations between hypoxia and hyperoxic states [209]. In term born neonates, congenital heart disease (CHD) is the most common major complication following birth, and is associated with an increased incidence of neurodevelopmental disorders [210–212]. CHD is also associated with decreased cerebral oxygenation [213,214] and impaired cortical development in fetuses [215,216]. This implies that perinatal hypoxia exposure regardless of gestational age at birth can be a significant contributor to atypical neurodevelopment.

In mice, prolonging *in utero* like oxygenation is associated with decreased levels of short and long term oxidative stress [217]. Hyperoxia in neonatal mice is associated with a decreased breathing rate post-hyperoxia [218] and with hypomyelination of the white matter [219].

1.6.1.1 Hypoxia and the epigenome

Hypoxia can affect the α-ketoglutarate dependent dioxygenase family of epigenetic modifiers in several ways. It can directly alter TET enzyme activity through reduced oxygen availability, which as discussed earlier is an essential substrate for their activity . Hypoxia can indirectly affect their function through disruption of the TCA cycle and resulting reduced α-ketoglutarate (which is also an essential substrate for the α-ketoglutarate dependent dioxygenases) availability and increased succinate and fumarate levels (which are inhibitors of the α-ketoglutarate dependent dioxygenases) [220]. Moreover, during hypoxia, α-ketoglutarate can be metabolized by malate dehydrogenase and lactate dehydrogenase to L-hydroxyglutarate or D-hydroxyglutarate both of which are also potent inhibitors of the α-ketoglutarate dependent dioxygenases [221] (see Figure 1.2).

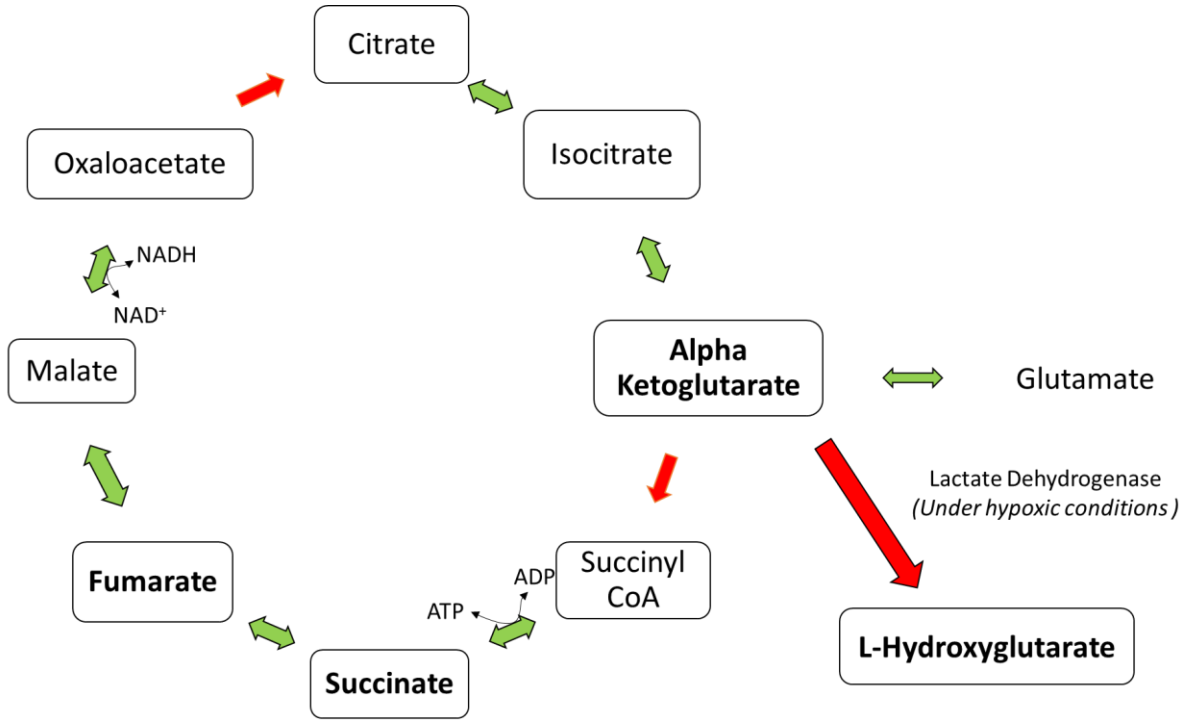

Figure 1.2 Schematic of the TCA cycle outlining irreversible conversions in red and reversible conversions in green. During hypoxia the cell quickly enters NAD⁺ and ATP debt resulting in a flux towards succinate production, which can inhibit the α-ketoglutarate dependent dioxygenase enzyme activity. Also, during hypoxia α-ketoglutarate can be converted to L-hydroxyglutarate which is a potent inhibitor of the α-ketoglutarate dependent dioxygenases.

HIF-1α and HIF-2α are the core hypoxia response unit in the cell [231]. The PHD proteins are part of the α-ketoglutarate dependent dioxygenase family and as such are sensitive to oxygen levels. During normoxia, there is sufficient oxygen present in the cell to catalyze the PHD mediated hydroxylation of HIF-1α and HIF-2α, which signals for their ubiquitylation and subsequent destruction. During hypoxia there is insufficient oxygen for this to occur and HIF-1α and HIF-2α accumulate and can dimerize with HIF-1β before nuclear translocation and induction of expression of target genes [231–233].

The TET enzymes are increased in expression following hypoxia across a range of cell types and following hypoxia there is an accumulation of 5hmC at classic hypoxia response genes [153,234]. It is, however, unknown whether neonatal hypoxia disrupts 5hmC dynamics in the brain during development.

1.6.2 Inflammation

Early life inflammation can be primary or secondary and acute or chronic in nature [235] as well as of maternal or neonatal origins [236]. Chorioamnionitis is a, typically bacterial, infection of the chorion, amnion and placenta [237,238] and can occur following premature rupture of membranes or systemic maternal infection [238,239]. It is a common cause of PTB but even in individuals born at term there is a 4-fold increase in risk of CP following chorioamnionitis [240]. Sepsis is also more common in preterm infants and is associated with adverse outcome, which will be discussed next.

1.6.2.1 Sepsis

Sepsis is an infection within the sterile structures of the body. Early onset sepsis is that which occurs before the third postnatal day and the infection is typically of maternal origin. Late onset sepsis occurs after 3 days and typically comes from the environment [241,242]. Over 20% of very low birth weight (>1500g) infants will develop late onset sepsis, which is associated with increased mortality and prolonged hospital stays and there is an inverse correlation with gestational age and incidence of late onset sepsis [243].

The EPIPAGE study of births in France up to 32 weeks of gestation, found no effect of early or late onset sepsis on cognitive performance at 5 years of age, but did see an association of early life sepsis with a diagnosis of cerebral palsy at 5 years of age [244]. An earlier study found an association between late onset sepsis and cognitive impairment in babies born before 32 weeks of gestation, when followed up at 6-9 years old [245]. A study examining brain

morphology in infants born preterm (median age of 26 weeks gestation) saw increased diffusivity in the left frontal lobe and right cingulum bundle at term equivalent age in babies with sepsis compared to those without, but no effect was seen with sepsis alone on behaviour at 2 years of age [246]. Conversely, in a cohort of very preterm infants, culture confirmed infection was correlated with neurodevelopmental outcome at 9 years of age, whereas in a subset of infants in which sepsis was suspected but not confirmed by culture, there was no such correlation [247].

1.6.2.2 Models of inflammation

Inflammation induced by infection can be modelled in a number of ways, most of which consist of agonists of one or more members of the TLR family. TLR3 and TLR4 are the most commonly studied receptors with respect to neonatal infection induced inflammation and are stimulated by the agonists lipopolysaccharide (LPS) and Poly I:C respectively. TLR4 is localized to the cell membrane, while TLR3 is located in endosomes within the cytoplasm [248]. LPS is a component of the bacterial cell wall and is commonly used to model bacterial infections. Poly I:C is a mimic of double stranded RNA and is commonly used to model viral infection. It should be noted that while LPS and poly I:C are used to model bacterial and viral infections through TLR4 and TLR3 agonism respectively, other members of the TLR family are associated with the inflammatory response to pathogens which are not modelled with LPS or poly I:C use alone (see Kawai and Akira, 2010 for a full review [249]).

Neonatal inflammation can also be modelled with the administration of individual cytokines. For instance, repeated systemic neonatal administration of IL1β replicates many key features of PTB related brain injury including hypomyelination and oligodendrocyte death [250]. Using this model it has been shown that PSD95 [251] and Wnt/β-catenin signaling [252] play a crucial role in the microglial response to neonatal inflammation, that neonatal inflammation disrupts interneuron development [253] and histamine receptor 3 antagonism may abrogate myelination deficits associated with neonatal inflammation [254].

1.6.2.3 Microglia, inflammation and synaptic pruning

Under quiescent states, microglia are the predominant immune cell within the brain. Following neonatal brain injury systemic immune cells can be recruited into the brain and contribute to inflammation [267]. *In vivo* single cell imaging has shown that in mice microglia are very long lived cells, with a median life of over 15 months [268]. Microglia are present mostly

in white matter during early postnatal development before migrating to grey matter regions and assuming a more diffuse presence by P14. They also have an ameboid phenotype in the early postnatal period compared to the ramified phenotype seen in quiescent adult states [269]. The microglial transcriptome in mice is most comparable to that of humans during early life and diverges rapidly with aging, perhaps implying divergent methods of maturation in humans and mice [270].

In 3 month old mice, LPS challenge can alter the long term histone acetylation profile of microglia and alter the response to subsequent insults [271]. Maternal immune activation (MIA) using poly I:C, is associated with a microglial transcriptomic signature which is enriched for genes associated with mature microglia [272]. This assumption of a more mature phenotype associated with early life immune challenge may affect microglial mediated synaptic pruning during early development. This has not yet been investigated in a neonatal setting.

1.7 Early life stress

A variety of early life stresses, including abuse, neglect or parental mental illness are strongly associated with an increased prevalence of a wide range of psychiatric disorders throughout life in a variety of ethnicities [280]. Exposure to prenatal stress such as maternal depression or anxiety is associated with an increased risk of preterm birth [281,282].

Hyperactivity of the hypothalamic-pituitary-adrenal (HPA) axis is common in depression [283] and early life stress is a major predictor of later life depression [284]. Early life stress produces a range of HPA related dysfunctions in later life [285]. These effects seem to be primarily predicted by early life stress and not the sequence of adverse life events which early life stress may cause [286].

1.7.1 The role of the Hypothalamic-Pituitary-Adrenal (HPA) axis and hippocampus in stress

The HPA axis is an integrated system which responds to environmental stress (illustrated in Figure 1.3). The HPA axis has various outputs and many functions but the circadian secretion of glucocorticoids under basal and stress conditions is one of the most important. Glucocorticoids are secreted from the zona fasciculata of the adrenal gland, which is stimulated by ACTH. ACTH is formed from its precursor, pro-opiomelanocortin, the production of which is stimulated in the anterior pituitary by corticotrophin releasing

hormone (CRH) which is released from the paraventricular nucleus of the hypothalamus. The ventral hippocampus through hypothalamic input can mediate this CRH release [287].

The hippocampus is classically associated with inhibition of the HPA axis, as hippocampal stimulation results in decreased glucocorticoid release in adult rats [288,289]. Corticosterone has a dose-dependent effect on hippocampal plasticity [290] and the licking and grooming behaviour of a mother to a pup is associated with the complexity of dendritic branching in the CA1 region of the hippocampus in adulthood [291].

In the hippocampus there is a distinct transcriptional profile associated with different forms of stress in adult mice i.e. acute, chronic and recovery [292]. Adult mice allowed to recover from chronic stress have a distinct transcriptome when compared to stress naïve mice and have differential responses to subsequent stress [292]. The HPA axis is therefore shaped by previous experiences and each individual stressful experience is associated with a distinct response and a subsequently distinct baseline.

1.7.2 Stress associated with PTB

Very preterm birth often necessitates long stays in the neonatal intensive care unit (NICU), which is associated with stressful events such as invasive procedures, excessive lighting, noise and sleep disturbances. The circadian secretion of glucocorticoids does not occur until approximately 2 months after birth [293] and the nature of the stress response in preterm infants in early postnatal life is not fully understood.

In human studies neonatal stress is difficult to study as traditional biomarkers such as cortisol are not yet rhythmic and are highly variable [293] and objective parameters such as the number of invasive or painful procedures or time spent in the NICU are invariably confounded by the severity of a baby's clinical condition. Nevertheless, many studies have attempted to control for these factors and interpret the effect of postnatal stress on outcome. The Neonatal Infant Stressor Scale evaluates exposure to a number of NICU associated stressors [294] and using this scale infants with a higher score (indicating a higher level of stress exposure) have anatomical differences and altered diffusion parameters on MRI at term equivalent age when compared to age matched controls [295]. Other studies have shown that stress related to pain in very preterm infants was predictive of cortical thickness [296] and cortisol levels [297] at 7 years of age.

Surgery in children with CHD is a form of severe early life stress. Morning cortisol levels in children (measured at 3-5years) are significantly lower in those who have undergone surgery than those with the condition but did not undergo surgery in early life [298].

1.7.3 Neonatal models of stress

Due to the difficulty in assessing stress in preterm infants and the lack of mechanistic insight available, rodent models are often used. I will now briefly discuss common models of early life stress but first I will outline some points of note.

There are strain specific responses to stress in mice: adult BALB/c mice show a greater HPA axis response to stress than C57BL/6J mice [299] but it is unclear if this pertains to the neonatal period. There is also moderate evidence to suggest differential behavioural and epigenetic responses to maternal separation in C57BL/6J and DBA2J mouse strains [300]. Additionally, P1 to P12 in rodents is associated with a stress-hyporesponsive period (SHRP), as defined by reduced glucocorticoid response to several stressors, including maternal separation [301] . This is primarily due to decreased adrenal activity in response to ACTH, but the hypothalamus and pituitary gland are responsive to stress during this period [302]. This may be a mechanism to protect the developing brain from high levels of circulating glucocorticoids or to facilitate maternal association and bonding before fear learning.

1.7.3.1 Maternal separation

Interaction between the mother and infant immediately following birth is very important. During this time the neonate is dependent on the mother for food, water, warmth and protection but this time is also important in building a maternal-infant bond and preventing this interaction is a strong stressor. Therefore, the most used animal model of early life stress is maternal separation.

1.7.3.1.1 Rodents

In rodents, maternal separation consists of removing the pup from the home cage for between 3-8 hours per day from 1-14 days. Maternal separation (3 hours/day from P1-P10 in mice) is associated with altered corticosterone levels as well as transcriptomic and DNA methylation changes in the hypothalamus in adulthood [303]. Rat pups subjected to this model have shown decreased weight gain and circadian rhythm alterations in adulthood [304]. Rat pups separated from their mother for 24 hours at P3 show a hyper-responsive HPA axis in

adulthood, whereas 24 hours of maternal separation on P7 results in a hypo-responsive HPA axis in adult animals [305].

There are however conflicting results using rodent maternal separation models with respect to key adult behavioural phenotypes[306,307]. Whilst genetic differences between inbred colonies and strains as well as inter-unit differences may offer an explanation for this, there is also evidence that in repeated daily maternal separation models, an increase in maternal care upon returning pups to the dam may offset some effects of the paradigm [308]. Additionally, pups at this age are dependent on their mother for food and water and therefore in cases of prolonged maternal separation, findings may be due to nutritional deficiencies, most importantly glucose. Indeed, blood glucose is significantly lower in pups following maternal separation than in control animals [309] and neonatal hypoglycaemia is independently associated with adverse neurodevelopmental outcome [310]. It has also been suggested that maternal separation paradigm more accurately models maternal neglect, rather than stress caused by preterm birth and a NICU setting [307].

1.7.3.1.2 Non-human primates

In non-human primates, infants may be removed from their mothers if they show behaviour which will harm the infant. This may result in human hand rearing or peer-rearing in which the infant is fostered onto a proven mother. In Rhesus monkeys, maternal separation for the first month of life and peer raising for the rest of childhood results in abnormal social behaviours throughout life, lower basal cortisol and a delayed response to acute stressors [311]. Rhesus monkeys have also shown alterations in circadian locomotor behaviours, which can be modulated with melatonin administration (via drinking water) following peer-rearing [312]. In pigtailed monkeys, 10 days of maternal separation is associated with changes in the circadian alteration of heart rate and body temperature [313].

1.7.3.2 Limited bedding and nesting material model

Another model of early life stress is the limited bedding and nesting model, which as the name suggests comprises of greatly reducing the amount of bedding and nesting material in the home cage. This induces maternal stress and results in fragmented maternal care, as such this most accurately models maternal neglect. A variation of this is introducing a wire mesh to the floor of the cage which works in a similar manner. This is typically carried out from P2-P9, and is a chronic, unrelenting form of stress (as opposed to the intermittent stress

associated with repeated maternal separation). Unlike maternal separation models, under this model neonatal animals are exposed to sensory stimuli such as ultrasonic vocalisations, social interaction with peers and thermal regulation, which are important in early life [314,315]. In rats [316,317] and mice [318,319] this model is associated with elevated basal corticosterone levels in pups, altered social and depressive like behaviours and enhanced amygdala activity. Similar to maternal separation studies, this model has produced conflicting results with some studies suggesting offspring exposed to this model have depressive like symptoms in adulthood, while other studies do not see this effect [307,320].

1.7.3.3 Other models

One of the earliest paradigms used to induce neonatal stress was daily handling of pups for 15 minutes [321] which produces acute HPA axis responses in the neonatal period [322] and in adult animals [323]. Chronic unpredictable stress exposure to a mother is also used. This consists of combinations of stressors which may include intruder mice, introduction of scents, decreased bedding or nesting material or restraint stress administered at unpredictable intervals. The offspring of dams subjected to chronic unpredictable stress display altered wheel running activity as adults [324]. In rats, neonatal exposure to a stressed dam for 30 minutes/day for the first 7 days of life results in alterations in DNA methylation at both neonatal and adult stages [325–327]. A similar model has also shown impairments in adult hippocampal neurogenesis as well as various behavioural alterations [328]. Corticosterone administered maternally via drinking water has been used to look at the effects of elevated maternal corticosterone on murine pups. This results in alterations in the immune response in the neonatal period [329]. Other models include combinations of maternal separation, hypoxia/hyperoxia and cold exposure [330] and maternal deprivation, in which animals are removed from their mother's care for 24 hours [331].

Overall these models have produced compelling evidence to suggest that early life stress is associated with alterations in brain development and alterations in adult behaviours. The variable results reported between studies and the relevance to human early life stress, particularly stress associated with the NICU, remains a concern. As noted earlier, the variable results may be due many reasons. There is significant variation with respect to the length of exposure and protocols used in maternal separation paradigms. The models outlined here also lack an active component, i.e. the animals are placed in a novel stressful environment, but they are not forced to engage with this environment. For instance, during maternal

separation paradigms this could manifest as higher levels of sleep in some pups compared to others which could result in a variable level of stress exposure. These models also do not accurately recapitulate stress associated with the NICU, which is associated with sleep deprivation, excessive lighting and so on.

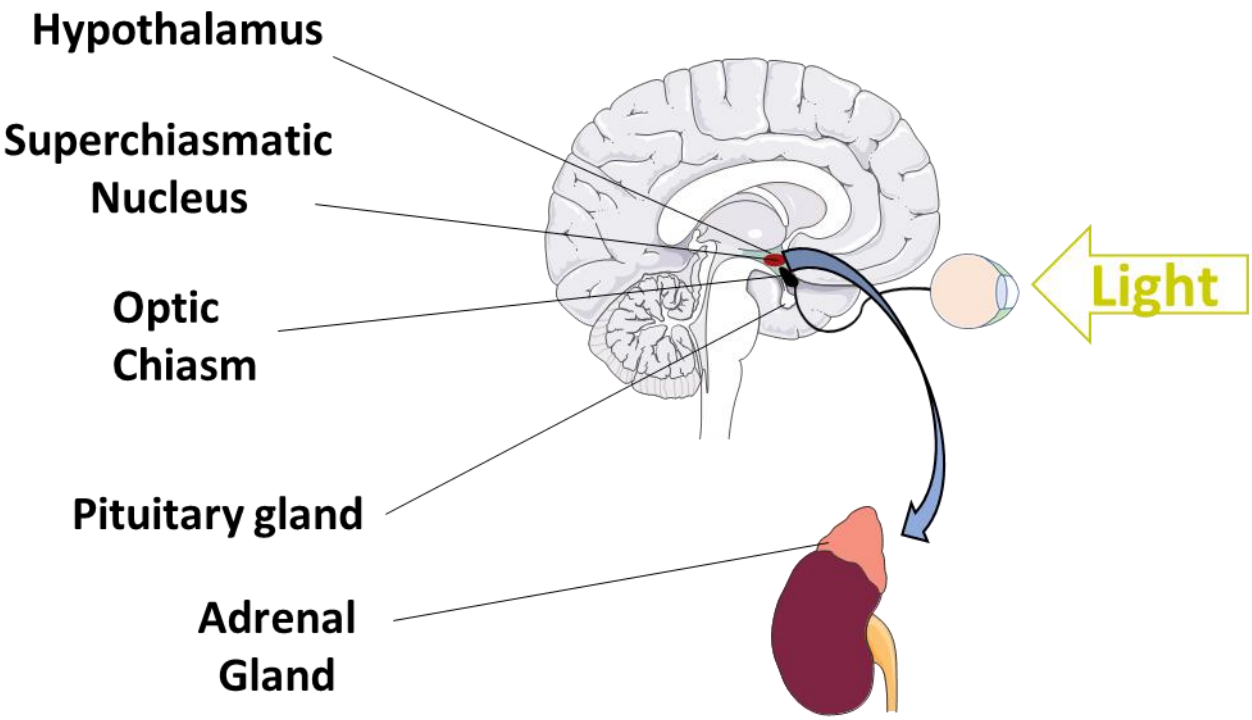

Figure 1.3 The HPA axis is shown, along with the machinery for the regulation of circadian rhythms. The superchiasmatic nucleus (SCN) of the hypothalamus receives input from light stimuli via the retino-hypothalamic tract. This acts via a hierarchy of clocks to synchronize clocks through the body to the natural day/night cycle. The SCN is at the top of this hierarchy, and through paracrine and neuronal signaling, synchronizes circadian oscillation of central and peripheral clocks including that of the adrenal gland, which secretes glucocorticoids in circadian fashion. Glucocorticoids act to synchronize clocks throughout the periphery through a glucocorticoid receptor mediated mechanism.

1.7.3.4 Stress and epigenetic alterations

A lot of work in this area has focused on DNA methylation at the GR (encoded by the gene *NR3C1*), which was stimulated by the controversial findings of differential methylation in the promoter region resulting from different levels of maternal lick/grooming behaviour in rats [332]. In humans, maternal separation has been associated with increased methylation in the 1-F promoter region of *NR3C1* in preterm infants with at least 4 days' maternal separation [333]. Maternal stress can also increase methylation of the *NR3C1* gene in the offspring [334], with

the level of methylation correlated to the subjective level of stress. A neuronal specific promoter of the *NR3C1* gene has previously been shown to be differentially methylated in post-mortem hippocampal tissue from suicide victims with a history of child abuse when compared to suicide victims without a history of child abuse [335]. However, these results remain controversial, The GR is universally expressed and as such the promoter region is typically completely unmethylated. The changes described at the *NR3C1* promoter are typically very small and perhaps not physiologically relevant.

However, stress has been convincingly shown to affect DNA methylation at several other loci following early life stress. For instance, maternal anxiety levels have also been correlated with DNA methylation alterations at various sites throughout the genome in cord blood of the new born infant [336]. In prepubertal girls, early life stress is associated with differential methylation at many loci in saliva derived DNA [337]. Early life stress has also been associated with alterations in DNA methylation in adulthood at the *FKBP5* (*FK506 binding protein*) locus [338,339], which is important in glucocorticoid signaling as I will discuss later.

Maternal separation in neonatal mice has been shown to alter DNA methylation within the hypothalamic paraventricular nucleus at the *arginine vasopressin* (*AVP)* [303] and *NR3C1* [340] loci. There is evidence this could be caused by neuronal activity through upregulation of calmodulin-dependent protein kinase II and MeCP2 [303]. The polycomb repressor complex and the TET proteins also interact with the *AVP* locus prior to changes in DNA methylation associated with maternal separation [341]. However, the exact mechanism behind stress mediated alterations in DNA methylation remain unknown.

1.7.4 Glucocorticoid signaling

1.7.4.1 Glucocorticoid receptor (GR)

The GR is a member of the nuclear receptor family of transcription factors and is near ubiquitously expressed in the brain. The GR is present in the cytoplasm but upon ligand binding it homodimerizes (heterodimerisation is also possible and will be discussed later) and translocates to the nucleus to induce cell and context specific transcriptional alterations through binding to glucocorticoid response elements (GREs) [344] (illustrated in Figure 1.4). The primary endogenous ligand for the GR is cortisol in humans and corticosterone in rodents. The GR also has high affinity for synthetic glucocorticoids such as Betamethasone and Dexamethasone, to which preterm infants are commonly exposed.

In ligand free conditions, the GR is bound to several chaperone proteins in the cytoplasm including HSP70 and HSP90 [345]. The sensitivity of the GR to ligands is dependent on many co-chaperone molecules, including FKBP51 and FKBP52 (encoded by the genes *FKBP5* and *FKBP4* respectively) [346]. FKBP51 inhibits and FKBP52 promotes nuclear translocation of the GR through interaction with dynein [347]. The GR is also controlled through phosphorylation at various residues [348].

1.7.4.2 Mineralocorticoid receptor (MR)

Aldosterone is the primary physiological ligand for the MR and has crucial roles in the kidney and Renin-Angiotensin system. However, aldosterone does not cross the BBB in large amounts and is present only at low quantities in some parts of the brain [349]. Therefore, cortisol or corticosterone in humans or rodents respectively, are the primary occupants of the MR in the brain.

The MR has a high affinity for glucocorticoids and as such, the receptor remains fully bound even during the nadir in glucocorticoid diurnal expression. In comparison, during this same period only about 10% of the GR remains bound to corticosterone [350]. The MR and GR share a large amount of homology in their DNA binding domains, however the *MR* is only expressed in subsets of neurons in the brain, such as the hippocampus and amygdala [351].

There is high *MR* expression in the hippocampus and as the *MR* is constitutively occupied by GC under non-stress conditions its expression governs the baseline stress response in the hippocampus [352,353]. During ligand free conditions the MR is predominantly located in the cytoplasm but maintains some nuclear localisation [354]. In the cytoplasm it is bound to similar chaperone proteins as the GR, which aid in its nuclear translocation upon ligand binding [355]. The MR binds DNA either as a homodimer or a heterodimer with the GR [356] and GR/MR heterodimers have an important role in stress mediated GR regulation of gene expression in the hippocampus following stress in adult rodents [357]. Several SNPs within the *MR* locus are associated with an increased or decreased HPA axis activity depending on genotype [358,359].

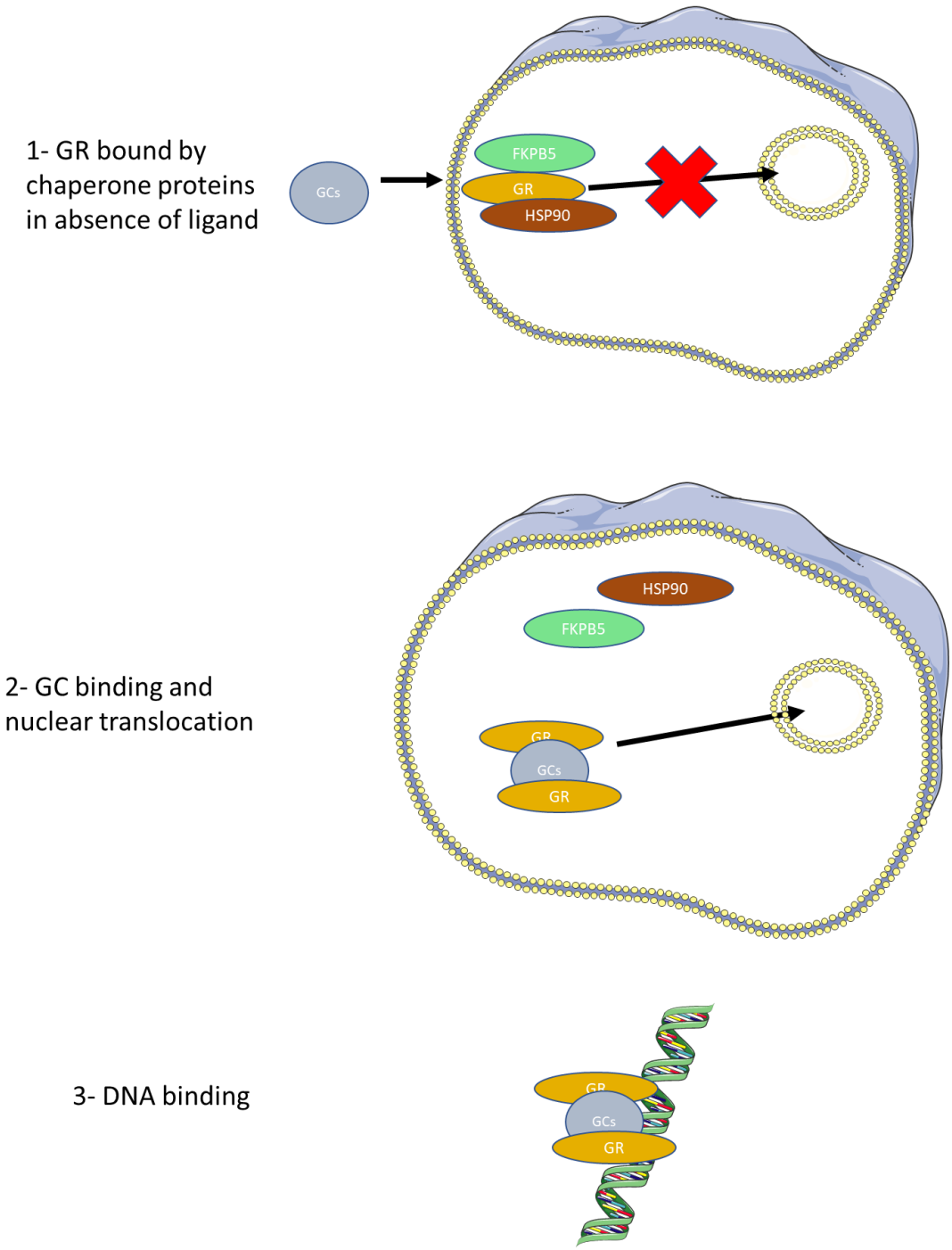

Figure 1.4 Outline of classic glucocorticoid (GC) signalling through GR. Under ligand free conditions, as seen in 1) the GR is bound by chaperone proteins such as FKBP5 and HSP90 (among others) which prevent its nuclear localisation. In 2) glucocorticoids enter the cell and displace the chaperone proteins and result in receptor dimerization (homodimerization is shown here but as mentioned heterodimerisation with the MR is also possible) which enables nuclear translocation. In 3) the induction of target gene expression is shown by the GR in response to ligand binding.

1.7.4.3 FKBP51 and FKBP52

FKBP51 is a cytosolic protein which acts as chaperone molecule and scaffolding protein[360]. It acts to oppose the function of FKBP52, its most closely related relative, with respect to nuclear translocation of the GR via interactions with dynein [361]. Both FKBP51 and FKBP52 have enzymatic subunits but little is known about the function of these domains [346] and it is their scaffolding function which has garnered most research interest.

Polymorphisms associated with the *FKBP5* gene are associated with an increased recurrence of depressive episodes in depressed individuals suggesting an important role in neuropsychiatric disorders [367]. Early life stress in humans is associated with differential DNA methylation at glucocorticoid response elements at the *FKBP5* locus [368]. Alterations in *FKBP5* expression have also been reported in individuals with ASD [369], schizophrenia [370], ADHD [371] and anxiety disorders [372]. In mice, chronic exposure to corticosterone reduces DNA methylation at the *FKBP5* locus which correlates with increased expression [373].

1.7.4.4 Synthetic glucocorticoid exposure

Synthetic glucocorticoids have been routinely administered to pregnant females at risk of delivering prematurely for decades [377–379], as they readily diffuse across the placenta [380] and act to accelerate fetal organ maturation and improve outcome without adverse maternal side-effects [381]. However, in cases of extreme preterm birth and severe bronchopulmonary dysplasia, glucocorticoids may be administered postnatally, which has been associated with improved neonatal outcome [382] but also an increased risk of cerebral palsy in some instances [383].

1.7.4.5 Glucocorticoid signaling through membrane receptors

Studies in amphibians were the first to demonstrate that glucocorticoids could bind to membrane receptors [384]. Corticosterone can, within seconds of administration, inhibit ATP mediated currents in cultured rat neurons. This is maintained when corticosterone is conjugated to bovine serum albumin, which cannot cross the cell membrane [385]. These effects may be mediated by membrane bound GR or MR, but *MR* knockout mice do not show increased glutamate release in response to corticosterone in the hippocampus [386] and a similar effect has been described for GR in the amygdala [387]. However, both the GR and MR lack transmembrane domains and it is unclear how they associate with the membrane.

Membrane mediated glucocorticoid signalling has also been described in the rat hypothalamus, which is not affected by GR or MR inhibition. In hypothalamic slices, both Dexamethasone and corticosterone produce a rapid inhibition of glutamatergic signalling, an effect which is blocked with CBR1 (cannabinoid receptor 1) inhibition. This implies the immediate effects of glucocorticoids on excitatory signalling is mediated by retrograde endocannabinoid release in the paraventricular nucleus (PVN) of the hypothalamus [388]. Endocannabinoids are also released in response to electrical activity in the rat hypothalamus [389] which may indicate CBR1 activation functions as an endogenous brake for neuronal activity in the hypothalamus. However, further research is needed to fully clarify these interactions.

Glucocorticoids have also been shown to interact with various protein kinases to mediate rapid non-transcriptional effects [390,391]. However, the primary mechanism of these effects is still unknown.

1.7.4.6 Interaction between stress and inflammation

As discussed previously, early life stress has been widely implicated in anxiety related outcomes later in life, but it is also closely associated with inflammation throughout the life course. In the Dunedin Multidisciplinary Health and Development Study, early life stress predicted plasma C-reactive protein (CRP; general inflammation marker) and fibrinogen level as well as white blood cell count at 32 years of age [392]. Similar results were found in a British study which showed that being bullied between the ages of 7 and 11 was correlated with an increased CRP at 45 years of age [393]. Moreover, the inflammatory mediator IFNγ (interferon) partially mediates the effects of early life stress on emotional processing in humans [394]. In humans, older individuals show a lower NFkB response to stress then younger counterparts and the high NFkB response was associated with lower cortisol levels after stress in peripheral blood mononuclear cells [395]. Stress during pregnancy but not before conception is also associated with increased maternal expression of classic pro-inflammatory genes in the third trimester, an effect which is driven by NFκB and AP1 (activator protein 1) [396]. These studies show early life stress can independently predispose to an altered inflammatory profile in later life, however, to investigate the mechanisms which account for these correlations animal models are needed.

There is also an interaction between stress and inflammation at the molecular level, as indicated in animal models. For instance, LPS given to rats at P14 results in altered fear

extinction behaviours in adulthood [397]. IFNβ administration during pregnancy potentiates the effects of subsequent maternal separation (3 hours/day for 2 weeks from P1) [398]. LPS induced NFκB mediated gene transcription in the hippocampus is also potentiated by stress in rodent models of chronic adolescent stress [399]. GR and NFκB signalling can regulate each other through PKA mediated phosphorylation *in vitro* and *in vivo* [400]. Therefore, it is clear that there is substantial interaction between stress and inflammation, but relatively little is known about this with respect to PTB.

1.8 Circadian rhythms

Circadian rhythms are signals which repeat over a 24 hour cycle. They are a highly evolutionarily conserved concept of timekeeping; even bacteria show evidence of circadian rhythms [401]. In mammals, circadian rhythms pervade every aspect of biology as they exist on genetic (transcription-translation feedback loops) through to a behavioural levels (sleep-wake cycles).

Every cell in the body has its own transcriptional clock, and these clocks are arranged in a hierarchal structure where the clock within the superchiasmatic nucleus (SCN) of the hypothalamus synchronizes clocks throughout the body in response to light [402]. Peripheral clocks are maintained in the absence of a functional SCN, but become dyssynchronous over time [403]. Estimates suggest that up 42% of genes are subject to circadian oscillation in at least one tissue, with the same study suggesting over 50% of FDA (federal drug administration) approved drugs target these genes [404]. As such understanding the mechanisms of circadian physiology is crucial to effectively understand and treat many common disorders.

Many hormones, such as glucocorticoids are secreted in a circadian fashion. Glucocorticoid concentrations are characteristically high in the morning and low in the evening in humans. These rhythms are commonly disrupted in many neurodevelopmental disorders which will be discussed later, first I will introduce the mechanisms of circadian regulation of gene expression.

1.8.1.1 Signaling in the SCN

The SCN contains pacemaker neurons which set circuit level properties of the system and these are necessary for the circadian oscillation of gene expression. The spontaneous firing rate (SFR) is the main output of the SCN [405]. There is typically little electrical activity in the

SCN during the night with steady pace action potentials starting near dawn and persisting through the day [406]. This is the same in both nocturnal (e.g. rodents) and diurnal (e.g. humans) species as it encodes solar time rather than behaviour [405]. The SCN has direct projections to other areas of the hypothalamus, the brain stem and subcortical areas [407]. Alterations in the SFR of the SCN can affect core circadian transcription-translation feedback loops [408] and many genes involved in electrical activity and membrane potential are under the control of these loops, illustrating electrical-transcriptional bidirectional coupling [405].

1.8.1.2 Circadian Rhythm Regulation

The SCN synchronizes cellular clocks in response to light stimuli (as shown in Figure 1.3). Melanopsin expressing cells in the retina receive light stimuli and pass this information to the SCN via the retino-hypothalamic tract [416]. In animal models SCN ablation causes systemic disruption of metabolism [417], immune responses [418] and altered sleep dynamics [419]. There are sex differences in circadian rhythmicity: men and women display functional circadian differences following a forced desynchrony program, with women subject to greater levels of circadian modulation and decreased cognitive performance in the morning [420].

1.8.2 Core transcription-translation feedback loops

Transcription-translation feedback loops are the fundamental unit of circadian rhythms (illustrated in Table 1.1). They consist of several interacting transcriptional loops, with members of each loop acting to increase transcription of another member which represses the initial activating member. Alterations in the transcription dynamics of the members of these loops may alter cell and tissue wide circadian rhythms.

In humans, brain muscle ARNT-like protein 1 (*BMAL1*) transcription increases in the morning, BMAL1 then heterodimerizes with the circadian locomotor output cycles kaput (CLOCK) protein, whose expression remains relatively constant through the day [421]. This heterodimer acts as transcription factor and binds to E-box motifs throughout the genome, driving transcription [422]. The period (Per1-3) and cryptochrome (Cry 1-2) genes are upregulated in this fashion [423]. Per and Cry proteins accumulate gradually through the day and become phosphorylated by the serine/threonine kinases casein kinase 1δ and 1ε (CK1δ and CK1ε), then Per/Cry heterodimerize before nuclear translocation. The Per/Cry heterodimer inhibits *BMAL1* transcription, thereby decreasing their own transcription. Per and Cry are degraded

via ubiquitylation and subsequent proteasomal degradation at which point *BMAL1* expression increases and the transcriptional cycle restarts [423].

A second transcription loop occurs as the CLOCK-BMAL1 heterodimer also interacts with the promoter region of *NR1D1* (nuclear receptor 1D1) and *NR1D2* (nuclear receptor 1D2) (REV-ERBα and REV-ERBβ respective proteins) to promote their transcription. REV-ERBα and REV-ERBβ compete with RAR-related orphan receptor α, β and γ (RORα, RORβ and RORγ) for binding sites at retinoic acid-related orphan receptor binding elements [424,425]. REV-ERBα acts to repress BMAL1 out of phase with Per expression patterns and while not essential for circadian rhythms, is central to length of oscillation [425].

A third transcriptional loop occurs as CLOCK-BMAL1 bind to and promote transcription of *DBP* (D-box binding protein), thyrotroph embryonic factor and hepatic leukaemia factor. These 3 proteins compete with the repressor NFIL3 (nuclear factor, interleukin 3 regulated) for binding at D-box motifs [402]. The interaction between CLOCK -BMAL1 and the E-box motif at *DBP* is unstable and stochastic with evidence suggesting CLOCK-BMAL1 may be immediately degraded by the proteasome after binding to *DBP* [426].

These three loops generate rhythms with different oscillation patterns with affinity for different binding motifs and can therefore induce diverse gene expression patterns.

Table 1.1 Central circadian regulators along with their mechanism of circadian regulation and the phenotype of animals in which the respective genes are deleted.

Protein	Mechanism	Phenotype of knockout mice	Ref
BMAL1	E-box motif binding	Severe disruption in all aspects of circadian rhythms	[427]
CLOCK	E-box motif binding	Rhythms maintained but altered behavioural response to light	[428]
PER1/2/3	Disruption of BMAL1/CLOCK	Rhythms maintained with any deleted. Severe alterations in circadian rhythms with the deletion of multiple.	[429,430]
CRY1/2	Disruption of BMAL1/CLOCK	Rhythms maintained with either deleted. Severe disruption in circadian rhythms with the deletion of both.	[431]
REV-ERB α/β	RORE motif binding	Rhythms maintained with either deleted. Severe disruption of circadian rhythms with the deletion of both	[432]
RORα/β/γ	RORE motif binding	Cerebellar defects, ataxia and metabolic defects with deletion of both. Limited disruption with either deleted alone.	[433,434]
DBP	D-box motif binding	Mice maintain rhythms but altered circadian behaviour in a free running state	[435]

1.8.3 Circadian secretion of glucocorticoids

ACTH and CRH are secreted in a diurnal pattern [439] and glucocorticoids are secreted in an ultradian pulsatile fashion with overlying circadian rhythmicity [440]. Classic studies in rats have shown that the SCN is necessary for corticosterone rhythms [441] but the peripheral adrenal clock is also necessary for glucocorticoid rhythms [442]. The synthetic glucocorticoid, Dexamethasone, is able to reset peripheral clocks but not in the SCN, as the GR is not expressed here [443].

The magnitude of the HPA axis response to a stressor is dependent on time of day as well as the type of stressor [444] and the circadian rhythmicity of glucocorticoid secretion is important for maintaining normal behaviour patterns. For instance an increased amplitude of glucocorticoid secretion without a difference in total secretion results in anxiety like behaviour in mice [445]. Chronic restraint stress in adult mice causes phase shifts in circadian gene expression in peripheral organs as well as the cortex and hippocampus but not in the SCN [446].

In terms of mechanisms, CRY1 and CRY2 interact with the GR when it is occupied, and act to reduce expression of glucocorticoid target genes. *CRY1* or *CRY2* null mice show higher circulating levels of corticosterone, and Dexamethasone exposure in these mice produces increased expression in twice as many genes than in wild type mice exposed to the same concentration [447]. *Per1* expression is altered following stress in adult mice with glucocorticoids having a spatial and stress specific effect [448]. Increased *Per1* expression is also seen in the paraventricular nucleus of the hypothalamus following inflammation and physical stressors (forced swim and immobilisation) [449]. As such, stress and circadian rhythms are thoroughly interlinked.

1.8.4 Circadian rhythms in neurodevelopmental disorders

Disruption of circadian rhythms including sleeping pattern is common in many neurodevelopmental disorders and *t*he presence of a typical sleep pattern at the age of 2 in babies who were born preterm is associated with a higher IQ at 3 years [450]. Moreover, in term infants the quality and duration of sleep is associated with more mature facial processing as measured by eye tracking at 12 months [451]. However, despite the high burden associated

with sleep disorders, relatively little is known about their mechanistic underpinnings in neurodevelopmental disorders.

1.8.4.1 ASD

Children with ASD show an elevated cortisol response to expected stressors but an unchanged baseline cortisol level [452], suggesting fundamental alterations in HPA axis functionality. Sleep disorders are very common in children with ASD [453], but even in those without diagnosed sleeping disorders there is evidence for altered sleeping patterns [454]. Adults with ASD and a diagnosed sleep disorder have higher rates of unemployment than those without a diagnosed sleep disorder [455]. This may be mediated in part by melatonin secretion: individuals with ASD have less melatonin than typically developing individuals at both diurnal and nocturnal stages of melatonin release [456,457].

Many animal models of ASD show circadian rhythm disturbances. The valproic acid rat model of ASD produces abnormal expression of genes involved in circadian rhythm regulation [458] and altered sleep dynamics [459]. Animal models of Prader-Willi syndrome [460], 16p11.2 deletion syndrome [461], fragile X syndrome [462] and Rett syndrome [463] (all syndromic forms of ASD) also show evidence for circadian rhythm abnormalities.

1.8.4.2 Other Neurodevelopmental Disorders

Actigraphy measurements taken as part of UK Biobank indicate that altered circadian activity is predictive of many mood related disorders and various mental health outcomes [464]. Individuals with schizophrenia show high levels of circadian disruption which is independent of medication and other factors [465] and commonly used mouse models of schizophrenia also exhibit circadian abnormalities [466]. Bipolar disorder is also associated with an abnormal circadian signature [467] and individuals who respond well to treatment with lithium have normalised circadian activity in fibroblast cells compared to those who do not respond well [468]. Finally, altered expression of oscillating genes in various brain regions has been identified in post mortem brain tissue from individuals with major depressive disorder [469].

1.8.5 The developing HPA axis and circadian rhythms

The HPA axis is functional in humans by the second trimester [470] and the SCN appears as a visible structure at 27 weeks of gestation [471]. Development of the adrenal cortex is dependent on age from point of conception rather than postnatal age [472]. In contrast, cortisol rhythmicity

is associated with postnatal age, with term infants showing cortisol rhythms by 1 month of age [473] and preterm infants showing cortisol rhythms at one month of term corrected age [293]. It should however be noted, there is large variation in perinatal rhythmicity, particularly in preterm infants, which makes firm conclusions difficult. Also, very preterm infants show circadian rhythms in oxygen consumption and temperature shortly after birth [474,475], variables which are under the control of the SCN. Infants born very preterm (less than 32 weeks of gestation) show improved weight gain, shorter NICU stay and increased daytime activity after exposure to an alternating light/dark cycle in the NICU, when compared to continuous light exposure [476,477]. Other studies however have seen no effect of NICU lighting regime on circadian rhythm or sleep development [478].

Animal models allow for the measurement of circadian gene expression in tissue and rats carrying the *Per1*: *luc* transgene allow for *in vivo*, real-time measurement of *Per1* expression. In these rats, Per1 expression is seen in the uterus of pregnant dams by E10, with expression exponentially increasing until birth, diurnal rhythms in *Per1* expression begin at E12 [479]. However the rat SCN does not form until E17 [480], as such these are weak, peripherally mediated oscillations. Synchronised rhythmic expression within the rat SCN isn't seen until birth [481]. This indicates peripheral clocks in rodents may operate with autonomy until birth, when the SCN initiates rhythmic expression and the synchronisation of peripheral clocks.

1.9 Conclusions

As I have outlined here, PTB is associated with adverse neurodevelopmental outcome but the mechanistic underpinnings are largely unknown. PTB is also associated with many factors such as hypoxia, inflammation and stress which can affect brain development and epigenetic modifications in the brain. In this thesis, I will explore the effect of these factors and how they affect brain development with specific emphasis on cytosine modifications.

1.10 Aims and hypotheses

Chapter 3

In this chapter I hypothesized that:

- Dexamethasone, LPS and/or hypoxia induce transcriptomic differences in a forebrain slice culture model
- These changes in transcription will associate with changes in genomic 5hmC in a forebrain slice culture model
- Dexamethasone, LPS and or/hypoxia will produce functional alterations in primary glial cultures

I aimed to test these hypotheses in the following ways:

- To compare *ex vivo* cultured forebrain slices to littermate *in vivo* tissue at similar ages and identify optimum culture length
- To investigate the dose at which Dexamethasone, LPS and hypoxia produce a physiological response under *ex vivo* culture conditions
- To evaluate the effect of these factors independently and in combination on candidate gene expression
- To evaluate 5hmC at candidate loci using DNA hydroxymethylation immunoprecipitation following Dexamethasone, LPS and/or hypoxia
- To investigate the effect of these factors on the differentiation and cytokine secretion of primary cultured mouse OPCs and microglial respectively

Chapter 4

In this chapter I hypothesized that:

- MMS will induce changes in the transcriptome and DNA methylome of the hypothalamus
- MMS will result in altered behaviour in the adult period

I aimed to test these hypotheses in the following ways:

- To assess growth and blood glucose dynamics associated with MMS
- To use immunohistochemistry to evaluate glial proportions in the hypothalamus following MMS

- To investigate the effects of MMS on the hypothalamic transcriptome in the neonatal period
- To investigate the effects of MMS on the hypothalamic DNA methylome in the neonatal period
- To examine the effect of MMS on behaviours during adulthood
- To assess the effect of MMS on candidate gene expression in the HPA axis in adulthood
- To assess the effect of MMS on DNA methylation at candidate loci in the hypothalamus in adulthood

Chapter 5

In this chapter I hypothesized that:

- Administration of LPS potentiates the effects of subsequent MMS in the hippocampus and cortex

I aimed to test these hypotheses in the following ways:

- To assess the effect of LPS and/or MMS on weight gain
- To investigate the expression of inflammation related genes in the brain 24 hours after LPS (which would be the onset of the MMS paradigm)
- To examine aspects of synaptic pruning in the hippocampus following LPS and/or MMS
- To investigate glial cell populations in the cortex following LPS and/or MMS
- To examine the cortical transcriptome following LPS and/or MMS
- To compare the cortical and hypothalamic transcriptomes after MMS to identify common regulators

2 Materials and methods

2.1 *In vivo* procedures

2.1.1 Mice

All mice were kept and procedures carried out in accordance with the University of Edinburgh's Policy on the Use of Animals in Research and with Home Office regulations. Mice were kept in controlled temperature (22˚C) conditions with a 12-hour light/dark cycle (7.00-19.00), and *ad libitum* access to food and water. Sexually mature C57BL/6JOlaHsd wild-type mice were obtained from Harlan (Harlan, UK), one male and two females were housed per cage and allowed to mate. Females were replaced after 6 litters and males replaced after 10 months of age. Both male and female mouse pups were used for slice culture experiments, while only males were used for MMS experiments. Male pups were identified using anogenital distance [495].

2.1.2 Randomisation

Throughout this thesis, randomisation was done where appropriate. To do this, a random number list was generated in Microsoft Excel and a number assigned to each mouse. The random number list was then sorted using the "sort" function in Excel, from smallest to largest. The mice were then assigned to a pre-determined group based on experimental design. For instance, the first half of the mice (i.e. those with the smallest numbers) were assigned to the control group, while the second half of the mice (i.e. those with the larger numbers) were assigned to the MMS group.

2.1.3 Subcutaneous and intraperitoneal (IP) injections

Mice were taken at postnatal day (P)3 and injected subcutaneously on the footpad of the hindlimb with ink for identification purposes. This pattern was visible until P14 at which time the mouse's ears were an appropriate size to be clipped for future identification.

For *in vivo* LPS experiments, on P3 at 1pm pups were administered a single dose of 1µg/kg LPS or the same volume of vehicle (PBS; phosphate buffered saline) via IP injection into the lower left abdominal quadrant. The maximum volume injected was 100 µl/10 g.

2.1.4 Modified maternal separation (MMS) paradigm

MMS was carried out from P4 for 1.5 hours at 1pm for 3 consecutive days. The MMS paradigm consisted of removing designated pups from the home cage and placing them on

a heated pad covered with a paper towel. A cotton bud was then used to gently move each pup into a supine position whenever they settled into a prone position. After 1.5 hours, the pups were returned to the home cage. MMS was carried out adjacent to the home cage to allow for ultrasonic communication between pups and dam.

Control pups were left in the home cage throughout whilst MMS was carried out on their littermates. All pups were handled at the start of the experiment for identification purposes.

2.1.5 Physiological Measurements and Dissections

The weight of all mice was taken prior to injection and prior to MMS each day. At the end of the experiments, mice were killed by decapitation. Using EDTA coated tubes, trunk blood was collected immediately following decapitation. Blood was kept on ice until centrifugation at 12000 RPM for 10 minutes at 4˚ C. Plasma was then isolated before storage at -80˚ C.

To remove the brain, the skin at the rear of the head was cut and the skull exposed, an incision was made at the base of the skull and a line cut from the base of the skull to the snout and the brain then fully exposed with forceps. The brain was then extracted after severing of the cranial nerves. Dissection was then immediately carried out on a glass platform covered with filter paper and surrounded by ice. Tissue was dissected before storage at -80˚ C.

2.1.6 Tail venesection

Adult mice at 3 months of age were restrained in a tube and their tail isolated. Using a scalpel, a small incision was made along the tail and blood was encouraged to exit the wound through palpation of the tail. Blood was collected using capillary action with EDTA coated tubes. Once sufficient blood was obtained, pressure was applied until blood stopped flowing and the mouse was then returned to its home cage. This was done at 7am and 7pm on the same day for each mouse for the evaluation of corticosterone.

2.1.7 Glucose measurement

Glucose was measured in the neonatal period immediately following decapitation using the Accu-Chek Performa glucometer. A glucose measuring strip was inserted into the machine and upon the prompt blood was applied to the strip. A reading of glucose concentration was then given and noted for each mouse.

2.1.8 Behaviour

For the elevated plus maze, open field and tail suspension tests, mice were brought to the behavioural testing area at least 1 hour before testing to acclimatise to the novel surroundings. Mice were then brought into the testing room one at a time for testing and then returned to their home cage afterwards. Mice which had been tested and those that were still to be tested were kept separate to avoid unnecessary agitation. Testing was done at the same time of day for all mice in a given behavioural task. Behavioural testing was done in a noise free environment and I was out of sight during the testing period. The elevated plus maze, open field and tail suspension tests were evaluated at 3 months of age and behaviour analysed with the PhenoMaster at 4 months of age.

2.1.8.1 Elevated plus maze

The apparatus was of the classic plus sign shape (width 5 cm and arm length 25 cm), with 2 opposing closed arms (15 cm in height and 2.5 lux) and 2 opposing open arms (45 lux). The arms intersected at an open centre area. Mice were placed in the centre of the apparatus facing a closed arm and allowed to explore the maze for 5 minutes. The test was automatically started by the AnyMaze software (ANY-maze, Stoelting Co.,Wood Dale, IL, USA), when I left the video frame. AnyMaze recorded all activity during the testing period and analysed the movement of all mice accordingly. The maze was cleaned thoroughly with 70% ethanol between mice.

2.1.8.2 Open field

Behaviour in the open field task was evaluated 24 hours after the elevated plus maze. The open field consisted of the classic square structure (50 cm x 50 cm, with 30 cm walls). The mice were placed in the centre of the maze and again the test was automatically started by the AnyMaze software once I left the frame and the mouse's movement was subsequently tracked and analysed. The mouse was allowed to explore the maze for 5 minutes before it was returned to its cage and the apparatus cleaned with 70% ethanol before testing the next mouse.

2.1.8.3 Tail suspension

The tail suspension test was carried out on the same day as the open field test. The mouse was suspended by the tail with a 17 cm piece of tape attached to an elevated area 50 cm from the ground. A cone was place around the mouse's tail to prevent climbing. The mouse was suspended for 6 minutes and recorded with a Canon IXUS 185 digital camera. The test

was then evaluated for mobility time, which was defined as active torso movement (i.e. not passive swinging from a previous movement), combined movement of front and rear legs or intense movement of a single set of limbs. Outside of these criteria the mouse was said to be immobile. For analysis the videos were duplicated and anonymized, through random number generation in Excel by an independent person. I was blind to the groups during analysis. After analysis duplicate values were averaged to obtain a score for a single mouse which was then used for subsequent statistical analysis.

2.1.8.4 PhenoMaster

To analyse indirect calorimetry, movement and food intake over the course of a 24-hour period, I used the TSE PhenoMaster system (TSE systems, Germany). Mice were single housed for 4 days before evaluation using the PhenoMaster system to allow acclimatisation to the novel water bottle used in the PhenoMaster system.

The mice were then transferred to the PhenoMaster, which is a closed system allowing for the quantification of O_2 intake and CO_2 output, and the calculation of the respiratory exchange ratio. The system was also fitted with food and drink sensors to monitor food and water intake, infrared laser beams also enabled the quantification of movement. The mice were allowed to acclimatise to the system for 24 hours and measurements were then taken every 15 minutes for a further 3 days. Food and water intake were monitored closely and any mouse not drinking was given water in their cage using an upturned bijous cap. Data were exported to Excel where subsequent sorting and analysis was done before statistical analysis.

2.2 *In vitro* procedures

2.2.1 Organotypic forebrain slice culture

C57BL/6JOlaHsd pups were taken at P1 and killed with an overdose of Pentobarbitone administered via intraperitoneal injection at 150mg/kg. Whole brains were dissected into ice-cold L15 media. Next, 300µm coronal sections were cut using a McaIlwain Tissue Chopper (Campden Instruments LTD). Brains were then transferred to a petri-dish containing ice cold slice culture media (see Table 2.1 for details), where brain slices were separated using a Wild Heerbrugg 1x objective for the Wild M8 Stereo Zoom Microscope and 24G needles. After separation, slices were transferred using a spatula onto Millicell culture inserts in a 6-well plate with 1 ml/well of slice culture media. Forebrain slices were kept in an incubator at 37˚ C with 5 % CO_2 unless otherwise stated.

Table 2.1 Recipe for slice culture media

Reagent (Manufacturer)	**Catalogue number**	**Volume to use (mls)**
EBSS (Thermo fisher Scientific)	24010043	62.8
BME media (Thermo fisher Scientific)	21010046	167
D-(+) Glucose solution (Sigma)	G8769	2.7
Heat inactivated horse serum (Thermo fisher Scientific)	26050088	12.5
Pen/ strep (Sigma)	P4333	2.5
GlutaMAX-I Supplement(Thermo fisher Scientific)	35100000	2.5

2.2.2 Dexamethasone, LPS and reconstitution

Dexamethasone was reconstituted in 100% ethanol and LPS was dissolved in slice culture media to the concentrations indicated with each experiment. These vehicles were co-administered to the control group during administration.

2.2.3 Primary culture of mouse microglia and oligodendrocyte precursor cells

2.2.3.1 Neural Tissue Dissociation

Whole brain tissue was extracted from C57BL/6JOlaHsd mouse pups between P0-P2 and dissociated using the neural tissue dissociation kit from Miltenyi as per kit instructions. Whole brain tissue was weighed in 1 ml HBSS (without Ca^{2+} and Mg^{2+}), an appropriate amount of enzyme P and buffer X (50 µl and 1900 µl respectively per 400 mg of tissue) was warmed to 37˚ C in a Miltenyi C-tube. The enzyme/buffer mix was then added to the tissue and attached to a gentleMACS dissociator and program m_brain_01 was initiated. The mixture was then incubated under slow rotation at 37˚ C for 15 minutes. Next the C-tube was attached to the gentleMACS dissociator and program m_brain_02 was initiated. Then an appropriate amount of enzyme A and buffer Y (10 µl and 20 µl per 400 mg tissue respectively) was added to the C-tube followed by a further 10 minutes of slow continuous rotation at 37˚C. The C-tube was then attached to the gentleMACS dissociator and program m_brain_03 was ran before a final 10-minute incubation at 37˚ C under slow continuous rotation. The cell dissociation was then passed through a 70 µm cell strainer and washed with 10 mls of HBSS (with Ca_{2+} and Mg_{2+}) per 400 mg of tissue. The mixture was centrifuged at room temperature for 10 minutes at

2000 RPM. Supernatant was discarded, and the pellet was resuspended in 1 ml of 0.5 % filtered bovine serum albumin (BSA) in PBS. Cells were then counted in a 1:1 dilution of Tryphan Blue using the Countess II FL Automated Cell Counter and Countess cell counting chamber slides.

2.2.3.2 PDGFRα isolation and culture conditions

Once dissociated cell number was assessed, PDGFRα positive cells were isolated using PDGFRα (CD140α) Miltenyi microbeads as per manufacturer's instructions. Briefly, dissociated cells were centrifuged at room temperature for 10 minutes at 2000 RPM. Supernatant was discarded, and pellet resuspended in 90 µl 0.5 % BSA in PBS per 10^7 live cells. The dissociated tissue was next incubated with 10 µl FcR blocking reagent per 10^7 live cells (included with PDGFRα cell isolation kit) for 15 minutes at 4˚ C. Then, 10 µl of PDGFRα microbeads per 10^7 live cells was added and the mixture was incubated for 15 minutes at 4˚ C. Cells were then washed in 2 mls of 0.5 % BSA in PBS per 10^7 cells and centrifuged for 10 minutes at room temperature at 2000 RPM. Supernatant was discarded, and cells resuspended in 90 µl of 0.5 % BSA in PBS per 10^7 cells. The autoMACS Pro Separator was then primed for use with a wash program. Columns were changed every 2 weeks or every 10^8 cells. A positive selection programme was then run, with the positive fraction collected in position C and the negative fraction collected in position B of a rack pre-chilled to 4 ˚C. Cells were then counted as outlined previously using the Countess automated cell counter. A 96 well flat-bottomed plate was coated the previous day with 5µg/ml Poly D-Lysine and left overnight at 37 ˚C. Before seeding the plate was washed three times with sterile PBS and allowed to air dry under sterile conditions. Cells were then seeded at a density of 10,000 cells per well in media (for recipe see Table 2.2) supplemented with PDGF-AA and NT-3 (see Table 2.4) and maintained at 37 ˚C with 5 % CO_2 unless otherwise stated.

2.2.3.3 CD11b isolation and culture conditions

Dissociated cell number was determined and CD11b positive cells were isolated with the CD11b Miltenyi microbead kit. The isolation method was identical to the PDGFRα isolation protocol outlined previously with the following exceptions. As per manufacturer's instructions the cells were not incubated with FcR blocking reagent and cells were resuspended in 90 µl of 0.5 % BSA in PBS per 10^8 cells following incubation with microbeads and subsequent centrifugation.

Once isolated CD11b+ cells were counted as previously outlined and seeded at a density of 25,000 cells/well in media of a 96 well plate (see Table 2.2) supplemented with TGF-β2, ovine cholesterol and IL34 (see Table 2.4). The plates were not coated prior to use.

Table 2.2 Formula for media in which isolated glial cells were cultured. Recipe for SATO media and details of glial specific additives are found in the following tables. Media was stored at 4 ˚C and used within 1 month.

Reagent	Amount/Volume	Catalogue Number
Neurobasal medium (without glutamine)	240 mls	21103049
DMEM-high glucose	240 mls	10566016
Glutamax	2.5 mls	35050061
ITS-G (100X)	5 mls	I3146-5ml
B27 Supplement (50X)	10 mls	17504044
Biotin (10µg/mL stock)	500 µl	B4639-100MG
NAC (50 mg/mL stock)	500 µl	A9165-5g
100 X SATO	5 mls	
Penicillin/ Streptomycin	5 mls	15140122

Table 2.3 Recipe for 100x SATO which was added to the base media for glial culture, outlined in the previous table. Aliquots of 5mls were made and stored at -20 degrees until use.

Reagent	Amount/Volume	Catalogue Number
DMEM-high glucose	50 mls	10566016
Apo-transferrin	500 mg	T1147-100mg
BSA	500 mg	A7638
Progesterone solution:	12.5 µL	

Progesterone	2.5 mg	FP8783-1G
Ethanol 100%	100 µl	
Putrescine (80mg/ml)	1000 ul	P5780-5G
Sodium selenite solution:	500 µl	
Sodium selenite	4 mg	S5261-10G
0.1N NaOH	100 µl	
DMEM-high glucose	10 mls	10566016

Table 2.4 Growth factors and cytokines added to base media previously outlined. PDGF-AA and NT-3 were added to PDGFRα positive cells and TGF-β 2, ovine cholesterol and IL-34 were added to cultures containing CD11b positive cells.

Reagent	**Concentration in Media**	**Catalogue Number**
PDGF-AA	10 ng/ml	100-13A-10ug
NT-3	5 ng/ml	450-03-10ug
TGF-β 2	2 ng/ml	100-35B-2UG
Ovine Cholesterol	1.5 µg/ml	7000000P-100mg
IL-34 CF	100 ng/ml	5195-ML-010/CF

2.3 Extractions

2.3.1 RNA Extraction

RNA was extracted using Qiazol, a tissue homogenizer and the RNeasy mini kit. First 1 ml of Qiazol was added to 25 mg of tissue. Tissue was then disrupted using a Qiagen TissueLyser II at 2000 RPM for 2 minutes. Next 200 µl of chloroform was added and the tube briefly inverted and left for 5 minutes at room temperature. Samples were then centrifuged at 10,000 RPM for 10 minutes at 4 ˚C. The upper aqueous was removed and an equal volume of 70 % ethanol added before mixing by inversion. The sample was transferred to a RNeasy mini spin column and centrifuged for 30 seconds at 10,000 RPM and flow through discarded.

Next 700 µl of RW1 buffer was added to the column before centrifugation for 30 seconds at 10,000 RPM. In a similar fashion 2x500 µl of RPE buffer was added before centrifugation. RNA was then eluted with 40 µl of RNAse free water and centrifugation at 10,000 RPM for 1 minute. RNA yield was then quantified, and integrity assessed via gel electrophoresis before storage at -80 ˚C.

2.3.2 Quantification of RNA yield and assessment of integrity

RNA yield was quantified using the Qubit RNA broad range assay. In Qubit tubes, 1 µl of sample RNA was added to 199 µl of a 1:200 dilution of Broad Range assay reagent in Broad Range buffer and RNA concentration assessed using the Qubit Fluorometer 2.0.

Next 6x loading dye was appropriately diluted in 250 ng of RNA before gel electrophoresis at 120 V for 45 minutes on a 1 % agarose gel containing gel red (final concentration of gel red 0.005%) for nucleic acid visualisation. Appropriate RNA integrity was characterised as 2 distinct bands indicating the 28s and 18s subunits of ribosomal RNA, with the 28s subunit appearing with approximately twice the intensity of the 18s subunit.

2.3.3 DNA Extraction

DNA was extracted using the Qiagen DNeasy Blood and Tissue kit. First, 50 mg of tissue was cut into small pieces before addition of 120 µl of buffer ATL and 20 µl Proteinase K solution, sample was incubated at 56 ˚C overnight in a Thermomixer at 1000 RPM. Sample was vortexed for 15 seconds before addition of 20 µl of RNase and incubated at room temperature for 2 minutes following mixing by inversion. Next, 200 µl of Buffer AL was added before further vortexing. Then, 200 µl of 100 % ethanol was added before vortexing. Sample was then added to a DNeasy spin column. The column was centrifuged at 8,000 RPM for 1 minute and flow through discarded. Next, 500 µl of Buffer AW1 was added to the column before centrifugation at 14,000 RPM for 1 minute, again flow through was discarded. Similarly, 500 µl of Buffer AW2 was added to the column before centrifugation. DNA was then eluted using 100 µl of Buffer AE and centrifugation for 1 minute at 14,000 RPM. Once eluted, DNA was kept on ice before quantification of concentration and ultimate storage at -4 ˚C.

2.3.4 Quantification of DNA concentration

DNA yield was quantified using the Qubit DNA broad range assay. In Qubit tubes, 1 µl of sample DNA was added to 199 µl of a 1:200 dilution of Broad Range assay reagent in Broad Range buffer and DNA concentration read using the Qubit fluorometer 2.0.

2.3.5 Protein extraction from cultured brain slices

Protein was extracted from either fresh or frozen cultured slices stored at -80 ˚C. Slices were incubated with 100 µl of RIPA buffer and 1 µl of cOmplete protease inhibitor under rotation at 4 ˚C for 1 hour with vortexing before and after. Sample was then centrifuged at 12000 RPM for 15 minutes at 4 ˚C. Supernatant was removed and protein concentration assayed before storage at -20 ˚C.

2.3.6 Quantification of protein concentration

Protein was quantified using the Biorad DC protein assay as per manufacturer's instructions. In summary, a 1.5 mg/ml concentration of BSA in RIPA buffer was serially diluted to create a standard curve. Next 5 µl of each standard and sample was added in duplicate to a 96-well microplate, a blank well was included to account for background. 20 µl of reagent S was added to 1 ml of reagent A to create working reagent A, 25 µl of working reagent A was added to each well. Next 200 µl of reagent B was added to each well and the 96 well plate was gently agitated for 15 minutes. Absorbance at 750 nm was then read, the blank was subtracted, and concentrations of samples extrapolated from a standard curve generated using standard functions in Microsoft Excel.

2.3.7 Western blotting

Western blotting was carried out using the Invitrogen XCell II apparatus for mini gels. 40 µg of protein was diluted in 1x loading dye, made to 30 µl with water and heated for 5 minutes at 95 ˚C, followed by cooling for 5 minutes on ice. The apparatus was appropriately assembled as indicated by the manufacturer, using a ThemoScientific 4-20% gel. The inner chamber was filled, and the outer chamber half filled with freshly made running buffer (see Table 2.5 for all buffers or solutions used in western blotting). 30 µl of sample was added per well, 4 µl of Chameleon pre-stained protein ladder was also used. Electrophoresis was then carried out at 120 V for 2 hours. After electrophoresis, the gel casing was opened, the cassette was discarded and the gel sandwich was appropriately assembled, as per manufacturer instructions, with filter paper and PVDF membrane in preparation for blotting.

The blotting apparatus was then assembled, and blotting carried out at 200 mA or 400 mA (for 1 or 2 gels respectively) for 2 hours at 4 ˚C.

Following blotting, the membrane was removed and washed in distilled water. The membrane was incubated under rotation with Ponceau red stain for 5 minutes, followed by 3 brief washes with distilled water, to assure successful transfer of protein.

The membrane was stained for total protein using the Licor Revert Total Protein Stain as indicated by the manufacturer. In summary, the membrane was incubated with 5 mls of Total Protein stain for 5 minutes at room temperature under gentle agitation. The membrane was next washed twice with 5 mls of Wash Solution under gentle agitation, followed by imaging using the Licor Odyssey CLx system.

The membrane was then blocked using 5 % non-fat milk powder in TBS-T (Tris buffered saline with 0.01% Triton) for 1 hour at room temperature. Washing was then carried out 3 times with TBS-T before incubation with an appropriate concentration of primary antibody (diluted in TBS-T) overnight under gentle agitation at 4 ˚C. Washing was then carried out 3 times with TBS-T before incubation with secondary antibody diluted at an appropriate concentration in TBS-T for 1.5 hours under gentle agitation at 4 ˚C. Before imaging the membrane was once more washed 3 times with TBS-T.

The stained membrane was imaged using the Odyssey CLx system, and quantified relative to total protein using the lmageStudio lite software.

Table 2.5 Table of solutions used for western blotting

Solution	Recipe
PAGE Running Buffer (10x)	1.9M Glycine
	250mM Tris
	pH to 8.3 (before SDS)
	1% Sodium Dodecyl Sulphate (SDS)
	1x made on day of use (1:10 dilution)
Transfer Buffer (10x)	1.9M Glycine
	250mM Tris
	pH to 8.3

	1x made on day of use with 20% Methanol
Tris-buffered Saline (TBS, 10x)	500mM Tris
	1.5M NaCl
	pH to 7.6
TBS with Tween (TBST, 1x)	1:10 dilution of TBS 10x
	0.1% Tween

2.4 ELISAs

2.4.1 Cytokine ELISAs

All ELISA's were performed in 96 well plates and in triplicate. The capture antibody was diluted as indicated by the manufacturer in 1x coating buffer and 100 µl/ well was incubated overnight at 4 ˚C to coat the plate. Next the capture antibody was aspirated (for list of ELISAs used to evaluate cytokine levels in culture media see Table 2.6), and wells were washed 3 times with 250 µl/ well of washing buffer, with 1-minute incubation time between each wash. The plate was then blotted on a paper towel to remove excess washing buffer and blocked for 1 hour with 100 µl per well of 1x ELIASPOT diluent (made from a 5x stock with deionized water). During this time the provided standards were appropriately reconstituted as indicated by the manufacturer and an 8 point standard curve made with 1x ELIASPOT diluent. After blocking, 100 µl of standards and samples were added to wells and incubated overnight at 4 ˚C for maximum sensitivity. Next the plate was washed 5 times with wash buffer, with 1-minute incubation times between each wash. The detection antibody was then prepared according to manufacturer's instructions and 100 µl was added per well. This was left to incubate for 1 hour at room temperature before 5 washes with washing buffer and 1-minute incubations between washes. The Avidin-HRP was then prepared in line with the manufacturer's instructions and 100 µl/ well added to the plate for a total of 30 minutes. Next, in line with the previously outlined washes, 7 washes were carried out followed by the addition of 100 µl/ well of TMB solution for 15 minutes. Finally, 50 µl/ well of stop solution was added and the plate was read at 450 nm. A standard curve was generated, and data analysed using Microsoft Excel.

Table 2.6 List of ELISA's used and source

Target Protein	Catalogue Number
TNFα	88-7324-88
IL1β	88-7064-88
IL6	88-7013-88

2.4.2 Plasma corticosterone ELISA

Plasma corticosterone was measured by ELISA using the Enzo kit following the manufacturer's instructions. Briefly, 10 µl of sample was added to 10µl of appropriately diluted steroid displacement reagent and left at room temperature for 5 minutes. Next, samples were diluted with 480 µl of assay buffer in a glass tube. 1 ml of ethyl acetate was added, samples were inverted, and the aqueous phase was transferred to a fresh tube. This was repeated a further 2 times with 1 ml of ethyl acetate and the aqueous phase of the samples were dried under nitrogen until a powder formed. The powder was then dissolved in 750 µl of assay buffer.

The ELISA was conducted as follows, 100 µl of samples and standards were added to wells with 50 µl of assay buffer, 50 µl of yellow antibody and 50 µl of blue conjugate. Appropriate controls were included as indicated by the manufacturer. The plate was incubated under gentle agitation at room temperature for 2 hours. The plate was then washed 3 times with 300 µl of wash solution per well. 200 µl of pNpp substrate was added to each well and incubated for 1 hour under gentle agitation at room temperature. After, 50 µl of stop solution was added and the absorbance was read immediately at 405 nm. Subsequent analysis was done in Microsoft Excel.

2.5 Microtome Sectioning

Brain tissue was fixed overnight in 4 % paraformaldehyde, then transferred to 70 % ethanol for temporary storage before embedding in paraffin wax.

Before sectioning, paraffin blocks were placed on ice to cool for at least 1 hour. Coronal sections were cut to 5 µm using a Leica 2M2125 RTS microtome, with ultrahard blades. Sections were then transferred to a water bath (Thermo Fisher Scientific, digital selection

flotation bath), set at 42 ˚C until flattened, after which they were transferred to a Superfrost slide. Three consecutive sections from a single sample were placed on each slide. Slides were then dried overnight at 37 ˚C and stored at room temperature until staining.

2.6 Immunohistochemistry

2.6.1 Immunohistochemistry on paraffin embedded sections

Before staining, paraffin wax was removed from slides through a series of washes: 100 % xylene (5 minutes), 100 % xylene (5 minutes), 100 % ethanol (3 minutes), 100 % ethanol (3 minutes), 90 % ethanol (3 minutes), 80 % ethanol (3 minutes), 70 % ethanol (3 minutes), water.

Slides were immersed in sodium citrate buffer (pH adjusted to 6) and boiled for 20 minutes, and then left to cool for a further 20 minutes. Slides were then washed twice in PBS for 5 minutes. Sections were encircled with a lipid pen and incubated with 200 µl of PBS with 10 % horse serum in a humid chamber for 1 hour and 30 minutes at room temperature to block against non-specific binding. Meanwhile, the primary antibody (see Table 2.7) was diluted in PBS with 10 % horse serum at the desired concentration. Blocking solution was then removed and 200 µl of primary antibody mixture applied. Slides were kept in a humid chamber overnight. Next the slides were washed 3x 10 minutes with PBS. The secondary antibody was diluted in PBS with 10 % horse serum and then applied to sections for 1 hour and 30 minutes. Slides were then washed 3x 10 minutes in PBS. Mounting media and coverslips were then applied to slides, which were then left to dry overnight in the dark at room temperature.

Slides were imaged using the Zeiss AxioScan Z1 system using a 10x objective. Files were then exported with original metadata to a Tiff format before downstream analysis.

Table 2.7 Antibodies used for immunohistochemistry

Antibody	Catalogue number	Dilution
IBA1	13481357	1 in 750
GFAP	ab7260	1 in 2000
Olig2	NBP1-28667	1 in 1000
MBP	ab40390	1 in 1000
DAPI	D9542	1 in 1000
Anti-rabbit Alexa 488	A-11034	1 in 750

2.6.2 Image analysis

Cell counts were carried out on IBA1 and Olig2 stained sections. Fluorescent images were exported with automatic exposure chosen in the Zen2 lite software. Cells were counted manually using the Cell Counter tool within the ImageJ software. Three consecutive sections per mouse were quantified and results averaged to produce a single biological replicate.

GFAP staining was analysed with respect to percent area. Fluorescent images were exported to a Tiff file with a universally applied brightness setting. Regions of interested were drawn in Image J and the Yen threshold was applied [496]. The image was then made binary and percent area quantified using the area function in ImageJ. Three consecutive sections per mouse were quantified and results averaged to produce a single biological replicate.

2.7 Golgi-Cox staining

Golgi staining was performed on cultured slices using the sliceGolgi kit from Bioenno. Staining was performed as detailed in the manufacturer's protocol. Briefly, fresh slices were fixed using fixative solution, after 30 minutes the solution was refreshed and left for a further 3 hours. Fixed slices were then washed 3 times with PBS-T for 15 minutes. Next the slices were covered with impregnation solution and left in a humid chamber for 6 days. Sections were then washed 3 times in PBS for 5 minutes/wash. Slices were then incubated with Solution C for 5 minutes followed by a 1 wash in PBS-T. Sections were then immersed in Solution D and finally washed 3x 5 minutes in PBS-T. Sections were then transferred to slides and mounted as previously outlined in the previous section and visualized under brightfield using a Zeiss Z1 Imager microscope.

2.8 Immunocytochemistry of OPC cultures

Media was removed from the 96 well plate and cells were washed twice with 100 µl of PBS and then fixed in 50 µl of 4 % PFA for 25 minutes. PFA was then removed and cells were washed three times for 5 minutes with 100 µl PBS. 100 µl of 10 % horse serum in PBS was then applied for 1 hour at room temperature. The primary antibody was diluted in 10 % horse serum in PBS and applied overnight at 4 ˚C. Primary antibody solution was then removed and cells were washed 3 times for 5 minutes in PBS. Secondary antibody was diluted in blocking buffer a volume of 50 µl was applied per well and left for 2 hours at room temperature. Secondary antibody was removed and cells washed 3 times for 5 minutes with PBS. The cells were left in PBS at 4 ˚C to avoid dehydration.

Fluorescently labelled cells were imaged using the Incucyte S3 system. Quantification of percent area was done using the Incucyte S3 software.

2.9 Confocal microscopy of cultured brain slices

To asses cell death in cultured brain slices, propidium iodide was diluted in culture media for 1 hour. Slices were then washed 4 times for 5 minutes in 1xPBS before fixation with 4% paraformaldehyde for 15 minutes. Slices were then washed 3x 5 minutes with 1x PBS and stained with DAPI for 15 minutes. Slices were again washed 3x 5minutes with 1x PBS and mounted and coversliped in line with method used for microtome cut sections.

Slides were imaged using the Leica TCS SP5 confocal microscope, using the 20x objective.

2.10 Reverse transcription (RT) and qPCR

RNA (1 µg) was DNAse treated as per manufacturer's instructions. Briefly, 1 µl DNAse, 1 µl RNAse inhibitor and 1 µl DNAse buffer were added to RNA and made to 10 µl with nuclease free water in PCR tubes. Samples were incubated at 37˚ C for 30 minutes, stop solution (1 µl) was then added and incubated at 6 5˚C for 10 minutes.

Reverse transcription was performed using the Applied Biosystems RT kit as per manufacturer's instructions. To DNAse treated RNA 2 µl of 10x random primers, 2 µl of 10x RT buffer, 0.8 µl of dNTPs, 1 µl of RT enzyme and nuclease free water to a final volume of 20 µl (no RT enzyme was added to the no RT control). Reverse transcription was then carried out using a G-storm thermocycler using the conditions outlined below in Table 2.8.

Table 2.8 Conditions used for reverse transcription of RNA to cDNA using a G-storm thermocycler

Temperature (˚C)	**Duration (minutes)**
25	10
37	120
85	5
4	Infinite

The cDNA was then diluted 1:15 with nuclease free water and 2.4 µl added to 1 well of a 384 well plate, with 5µ l of Qanta fastmix II, 0.2 µl of 100 µm forward primer, 0.2 µl of 100 µm

reverse primer (primers were designed using the UPL assay design software), 0.1 µl of designated UPL probe and 2.6µl of nuclease free water. All samples were assessed in triplicate. No RT and water controls were included for each assay. The plate was then sealed, and qPCR carried out using the Roche Lightcycler 480 using the cycling conditions outlined in Table 2.9, which were optimised for 6-Carboxyfluorescein (FAM) hydrolysis.

Table 2.9 Cycling conditions used for FAM hydrolysis probe-based analysis of reverse transcribed RNA using the Roche 480 LightCycler

Stage	Temperature (˚C)	Duration (mm:ss)	Ramp	Number of Cycles
Preincubation	95	5:00	4.8	1
Program	95	0:10	4.8	50
	60	0:30	2.5	
Cool	40	0:30	2	1

Samples of cDNA were pooled from all experimental groups and a serial dilution carried out to create a standard curve with concentrations 1:2, 1:4, 1:8, 1:16, 1:32, 1:64, 1:128. A set of arbitrary concentrations correlating to their dilution was attached to the standard curve points. The concentration of each of the samples was then extrapolated from the standard curve and normalised to the extrapolated concentration of the house keeping gene, *TBP* (see Table 2.10 for a full list of primers used in qPCR).

Table 2.10 List of primers and associated UPL probe used in this thesis for the assessment of gene expression

Gene	Forward primer sequence (5'→3')	Reverse primer sequence (5'→3')	Probe
TBP	gggagaatcatggaccagaa	gatgggaattccaggagtca	97
TNF alpha	ctgtagcccacgtcgtagc	ttgagatccatgccgttg	25
IL-6	gctaccaaactggatataatcagga	ccaggtagctatggtactccagaa	6
IL-1 alpha	tccataacccatgatctggaa	ttggttgagggaatcattcat	29
MBP	cctcagaggacagtgatgtgttt	agccgaggtcccattgtt	16
PGK1 L	ccaaggctttggagagtcc	gatcagctggatcttgtctgc	72

VEGFA L	gtacctccaccatgccaagt	tcatgggacttctgctctcc	64
SLC1A2	atactggctgcaccaatgc	cccaaatgaatggggtcat	58
SLC7A5	cctttacgctgtagcagttcac	gaagctgccaagctcgtg	34
TREM2	gtggtgttgagggcttgg	gctgctggcaaaggaaag	2
FKBP5	tctgacaggccgtattccat	tcgtgaaagagaagggaactg	20
DNMT1	gctaccagtgcacctttggt	atgatggccctccttcgt	1
DNMT3a	ggtgcactgaaatggaaagg	gaagaggtggcggatgac	13
ARCVF	atggcctggaggatgataca	tcatctgctgtgtcttcaaagg	1
DLG4	cgctaccaagatgaagacacg	caatcacaggggagaattg	10
Aif1 (iba1)	tgggatcatcgaggaattg	ggatttgcagggaggaaaa	3
Car9	attcctgcttcactgctggt	ctttggtcccacttctgtgc	16
C4b	tctcacaaacccctcgacat	agcatcctggaacacctgaa	10
C1q	gaagatgtctgccgagcac	tcctttaaaacctcggatacca	1
Cx3cr1	ggcctagagctcaaagaaatcc	cacagaccttcgatcccagt	16
Cx3cL1	cgcgttcttccatttgtgt	cacatgatttcgcatttcgt	74
HLA-A2	accagaaaatgacaaaagacttca	caggaggacaggaacgtcat	41
MEGF10	caccccactacaggccatt	tcagcgcacacactgtcac	16
Mertk	ctgaggactgcttggatgaac	cacagagaaggtgggtcgat	67
Lgals3 (Galectin 3)	gtgaaacccaacgcaaaca	ctcattgaagcgggggtta	97
TGF beta 1	ctgggcaccatccatgac	cagttcttctctgtggagctga	15
vGLUT1 (slc17a7)	gcaggaggagtttcggaag	agtgtgcgtggtcactgg	47
Synapsin	ggacggaagggatcacatta	tgagctgcttgtcttcatcc	25
Per1	accactgagagcagcaagagt	ctcaggaggctgtaggcaat	3
Nr3c1	cagtgttttctaatggatattcaagc	ggagcacaccaggcagag	10
NR3C2	gccggcatgaacttagga	ccctcttctgggctctgg	5
Fos	gggacagcctttcctactacc	agatctgcgcaaaagtcctg	67
CRH	gaggcatcctgagagaagtcc	tgttaggggcgctctcttc	34
POMC	gcttgcaaactcgacctctc	ttttcagtcaggggctgttc	72
CRHR1	cttctccttctggggctga	aggtgccaatgaggtccac	10
HSD11b1	tctacaaatgaagagttcagaccag	gccccagtgacaatcacttt	1
Cyp11b1	agctcagacttggtgcttcag	gcccatggaatacagattcac	3
stAr	aaggctggaagaaggaaagc	ccacatctggcaccatctta	2
MC2R	caccacaatcctctaccctca	ggtgctgagaacttttccaataa	55

2.11 3’ mRNA Sequencing

Sequencing was done on 12 samples per chip for both the hypothalamus (6 control and 6 stress) and cortical (3 control, 3 LPS, 3 stress and 3 LPS+stress) sequencing datasets.

Sequencing was carried out by staff at the Wellcome Trust Clinical Research Facility at the Western General hospital, University of Edinburgh. RNA quality was assessed using the Agilent Bioanalyser, with an average RNA integrity number of 9.3 across all sequenced mRNA samples, with all samples above 9.0. Library preparation was done using the QuantSeq 3’ mRNA-Seq Library Prep Kit following manufacturer’s instructions. Briefly, oligodT priming was initiated and reverse transcription of the first strand done before RNA was removed and second strand synthesized using random priming to create a double stranded cDNA library, followed by magnetic bead-based purification. The cDNA library was then amplified for 11 cycles before another magnetic bead-based purification step.

Template was prepared using the Ion PI Hi-Q OT2 200 kit as indicated by the manufacturer. Sequencing was done using the Ion PI Chip Kit v3, and the Ion Hi-Q Sequencing 200 Kit and the Ion Proton platform was used.

2.11.1 3’ mRNA sequencing analysis

Raw pH DAT files were produced directly from the Ion Proton platform, which were then converted to flow signals. In total an average of 7.7 million reads and 8.4 million reads per sample were achieved for the hypothalamic and cortical dataset, respectively. Polyclonal (21.8% for the hypothalamic dataset, 21.9% for the cortical dataset) and low quality reads (6.9% for the hypothalamic dataset, 5.4% for the cortical dataset) were filtered out before data alignment to the mm10 reference genome using STAR 2.5.3a in an automated workflow. Of the filtered reads 99.3% were successfully aligned to the genome in both datasets. Further downstream analysis was done using Degust and differential gene expression done using the Voom/limma and the Voom with sample weights methods for the hypothalamic and cortical datasets, respectively. Voom with sample weights was used to correct for within group variation in the smaller cortical dataset.

2.12 Hydroxymethylated and methylated DNA immunoprecipitations

DNA was extracted as previously described using the Qiagen Blood and Tissue kit, and subsequently measured using the Qubit broad range double strand DNA assay.

2.12.1 DNA sonication

DNA was sonicated using the Covaris E220 Focused Ultrasonicator. 5 µg of DNA was diluted in 130 µl of TE in a Covaris crimp cap microTUBE. Sonication was for 18 cycles of 30 seconds on/ 30 seconds off at the conditions specified in Table 2.11. Sonication quality was assessed by gel electrophoresis using a 1% agarose gel at 90 v for 90 minutes. A 100 BP DNA ladder was used to check size of sonicated DNA. A range of lengths between 100 and 600 base pairs with a mean of 200-300 base-pairs was deemed adequate (see Figure 2.1 for an example). DNA concentration was measured once more by the Qubit high sensitivity assay after sonication.

Table 2.11 Conditions for DNA sonication using 130 µl Covaris microtubes with the Covaris E220 Focused Ultrasonicator

Peak Incident Power (W)	175
Duty Factor	10%
Cycles per Burst	200
Treatment time (s)	305
Temperature (^{o}C)	7

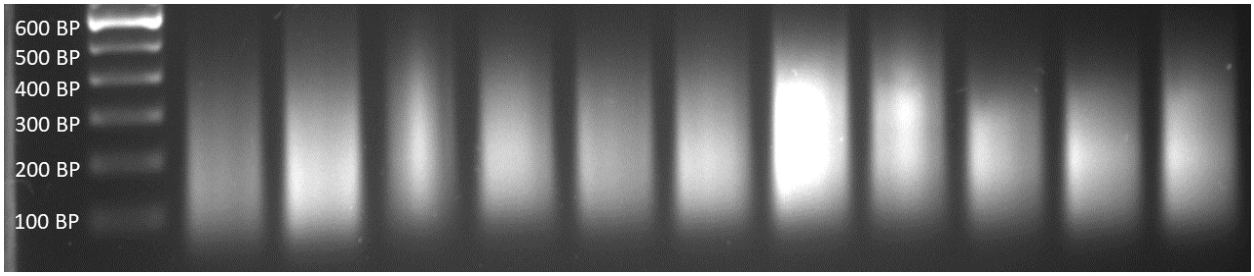

Figure 2.1 UV picture of DNA sonicated as outlined using the Covaris E220 Focused Ultrasonicator for DNA immunoprecipitations. DNA is fragmented to a 100-600BP range with a peak around 200BPs

2.12.2 Immunoprecipitation

2.5 µg of sonicated DNA was diluted in 450 µl of TE and heated for 10 minutes at 95 ˚C. 50 µl of 10x IP buffer was added per sample (see Table 2.12 for a list of solutions used in DNA immunoprecipitations). From each sample, 10 % input was taken and stored at 4 ˚C. 1 µl of anti-5hmC antibody was added to each sample followed by incubation under rotation at 4 ˚C for 3 hours.

40 µl of magnetic protein G Dynabeads were washed with 800 µl of PBS-BSA 0.1 % for 5 minutes at room temperature. The beads were then collected with a magnetic rack and supernatant aspirated. This was repeated a total of 3 times, after the final wash the beads were resuspended in their original volume with 1x IP buffer. Washed beads were then added to the DNA-antibody mix and incubated under rotation for 1 hour at 4 ˚C.

Magnetic beads were then collected and supernatant aspirated. Beads were washed 3x with 1 ml of 1x IP buffer. Beads were then incubated with 250 µl of digestion buffer and 20 µl of 20m g/ml proteinase K and incubated overnight on a Thermoshaker at 1000 RPM and 55 ˚C.

The beads were removed with a magnetic rack and supernatant containing DNA immunoprecipitated fragments used for the following steps.

Table 2.12 Solutions used for DNA immunoprecipitations

Solution	Reagent	Quantity
IP buffer (10x)	100 mM Na-Phosphate pH 7.0 (mono and dibasic)	1 mls
	1.4 M NaCl	2.8 mls
	0.5 % Triton X-100	0.5 mls
	H2O	5.7 mls
	0.22uM sterile filter	
Proteinase K digestion buffer	50 mM Tris pH 8.0	500 ul
	10 mM EDTA	200 ul
	0.5 % SDS	250 ul
	H2O	9.05 mls
	0.22uM sterile filter	
PBS-BSA 0.1%	PBS	9 mls
	BSA 10 mg/ml stock	1 ml

2.12.3 DNA Clean up

Immunoprecipitated DNA and input DNA were then processed with the Qiagen PCR purification kit, used as per manufacturer's protocol. Briefly, 20 µl of 3 M sodium acetate, pH 5, was added to each sample. 1 ml of buffer PB was then added and samples were applied to a column before centrifugation at 12000 RPM for 1 minute. Flow through was discarded and 750 µl of Buffer PE added to the column before further centrifugation at 12000 RPM for 1 minute. Flow through was discarded and column was dried via centrifugation at 12000 RPM for 30 seconds. DNA was eluted with 20 µl of nuclease free water. DNA was stored at -20 ˚C for future use.

2.12.4 qPCR of immunoprecipitated DNA

Sonicated DNA from samples was pooled and a standard curve made with a serial dilution (1:2, 1:4, 1:8, 1:16, 1:32, 1:64). To assess non-specific antibody binding an IgG control was included during immunoprecipitation and a water control included during PCR amplification.

Samples, inputs and controls were diluted with 100 µl of nuclease free water. 3 µl of sample was loaded per well with 5 µl of qPCR master mix with SYBR green ,0.02 µl of both forward and reverse primer (100 µM), and 1.96 µl of nuclease free water. Plates were centrifuged at 2000 RPM for 2 minutes prior to thermal cycling with the LightCycler 480 Instrument (cycling conditions outlined in Table 2.13).

Positive and negative control candidate regions taken from Thomson *et al*, 2015[497] to ensure efficient immunoprecipitation and that minimal bias was introduced from whole genome amplification. See Table 2.14 for a list of primers used.

Similar to the analysis of cDNA qPCR data, sample values were extrapolated using a standard curve but normalised to input rather than a house keeping gene. If evaluating PCR bias from whole genome amplification, raw Ct values of the samples were compared, as normalisation would hide bias.

Table 2.13 Cycling conditions for qPCR analysis of DNA products using SYBR green fluorescence based LightCycler

Stage	Temperature (˚C)	Duration (mm:ss)	Ramp	Number of Cycles
Activation	95	10:00	4.8	1
Denaturation	95	0:15	4.8	70
	60	1:00	2.5	
Melting Curve	95	0:05	4.8	1
	65	1:00	2.5	
	75		0.11	
Cooling	40	0:10	2.5	1

Table 2.14 List of primers used for candidate assessment of immunoprecipitated DNA throughout this thesis

Gene	Forward primer (5'→3')	Reverse primer (5'→3')
Car9	AAGCTGAGCTGGTGATCCTGA	GGTTCTGTCTGGCCCTATGC
VEGFA	AGAGTTCCCAAAGGTGCGGG	TCTCACCCTGTCACCCACG
PGK1	TGGTGGGAAGAGGAAAACGG	TGCCTTGTGGACTGATTGCT

BNIP3	CCTAAACAGCCCCTTGGGTT	CCAGCCTGCATGAGACACTT
GR	CACACTGCTGGGGCTTGATA	CAGGGGTGCAAAGCTCAATG
AVP	TTTAACCGTGTGGGGCAAGA	GCCCAGGACTTTAACCGTGT
Auts2	TGTATCTGGCCCACCACAAC	TGGCTTGAGTTGAGTGCTGT
Astn2	GCAAGGCTTAACGGCATCAC	CAGTGGTCAGAGTCAGAGAGAC
Tex19.2 (Positive control)	GGGAGATATGTAAATGAGCTGG	CATCCTTACCTCCCTGACTGAG
GAPDH (Negative control)	CCACTCCCCTTCCCAGTTTC	CCTATAAATACGGACTGCAGC

2.12.5 Whole genome amplification (WGA)

The SeqPlex Enhanced DNA Amplification Kit was used for WGA as per manufacturer's instructions. 10 µl of immunoprecipitated DNA was used, with 15 PCR cycles used in the amplification step. Prior to adapter removal, concentration was assessed using the Nanodrop. For the sample with the lowest concentration the volume containing 2.1 µg of DNA was calculated and this volume was used for adapter removal in all samples. Final elution was done in 30 µl of nuclease free water for sequencing.

2.12.6 Ion torrent proton sequencing

Three samples were sequenced per chip, with a total of 9 samples sequenced. Three samples from both the control and stress group were included, along with a single pooled input from each group and an IgG control sample to account for non-specific binding.

Sequencing was carried out by the staff at the Wellcome Trust Clinical Research Facility at the Western General Hospital in Edinburgh. Sample concentration was determined using the Qubit DNA high sensitivity assay and 100 ng of DNA was used for library preparation using the Ion Xpress Plus Fragment Library Kit. Amplification was carried out for 8 cycles and purified using the Agnecourt AMPure XP PCR clean up kit. Libraries were then checked for quality and concentration using the Agilent Bioanalyser DNA high sensitivity kit before pooling in equal concentration and templates prepared using the Ion PI Hi-Q OT2 200 kit and sequencing carried out using an Ion PI Chip kit.

2.12.7 meDIP sequencing analysis

Before sequencing sample quality was assessed using the Agilent Bioanalyser DNA High sensitivity kit to ensure appropriate sample quality. As part of an initial, onboard quality control step reads below 50bps were excluded, as sequencing accuracy dramatically decreases below this threshold [497]. This and conversion to binary alignment map (BAM) files were done using the Ion Torrent Suite software version 4.0.2.

Further analysis was done using Galaxy. Using the "bamCompare" tool BAM files were divided into 150BPs and normalisation of data to the input and IgG controls was done. The resulting output of this analyses were BIGWIG files which were converted to WIG files using the in-built "bigwigtowig" tool. WIG files were then aligned to the mm10 reference genome using the "convert genome coordinates" tool, which were then sorted by genome locus and sliding window analysis carried out using the "sliding window over length normalised regions of interest" tool, with the length of each gene normalised to 100%. Analysis of differentially methylated regions was done using DeSeq2 (version 1.12.3). Matthew Sinton helped with meDIP sequencing analysis.

2.13 Statistical analysis

Further statistical analysis was carried out for all comparisons (excluding sequencing datasets, which were analysed as described above) using the SPSS v24 software (IBM). Tests for homogeneity of variance and normality were done for each analysed variable, with no non-normal distributions identifeid. An independent t-test was used to analyse 2 independent groups. A one-way ANOVA was used to assess differences between 3 independent groups. A two-way ANOVA was used to evaluate differences between 2 independent variables across multiple groups.

Data collation and organisation was done in Microsoft Excel and GraphPad Prism v5 was used to make graphs. A p value of less than 0.05 was taken to be statistically significant.

Table 2.15 List of products used, manufacturer and catalogue number

Product	Manufacturer	Catalogue number
LPS	Sigma-Aldrich	L4391
EDTA coated tubes	Sarstedt	16.444

L15 media	Thermo Fisher Scientific	31415086
Millicell culture inserts	Millipore	PICM0RG50
Dexamethasone	Sigma-Aldrich	D4902
Neural tissue dissociation kit	Miltenyi	130-092-628
Miltenyi C-tube	Miltenyi	130-093-237
GentleMACS dissociator	Miltenyi	130-093-235
70µm cell strainer	Millipore	10788201
Tryphan Blue	Thermo Fisher Scientific	15250061
Countess II FL Automated Cell Counter	Thermo Fisher Scientific	AMQAF1000
Countess cell counting chamber slides	Thermo Fisher Scientific	C10228
PDGFRα (CD140α) Miltenyi microbeads	Miltenyi	130-01-502
AutoMACS Pro Separator	Miltenyi	130-092-545
Poly D-Lysine	Sigma-Aldrich	P6407
CD11b Miltenyi microbead kit	Miltenyi	130-049-601
Qiazol	Qiagen	79306
RNeasy mini kit	Qiagen	74106
Qubit RNA broad range assay	Thermo Fisher Scientific	Q10211
Qubit tubes	Thermo Fisher Scientific	Q32856
6x loading dye	Thermo Fisher Scientific	Q32856
Gel red nucleic acid stain	Biotium	41003
DNeasy Blood and Tissue kit	Qiagen	69506
Qubit DNA broad range assay	Thermo Fisher Scientific	Q32853
RIPA buffer	Thermo Fisher Scientific	89900
Complete protease inhibitor	Roche	4693116001
Biorad DC protein assay	Biorad	5000111
Bovine serum albumin	Sigma-Aldrich	A9418
Western blot loading dye	Licor	928-40004
4-12% gels for western blotting	Thermo Fisher Scientific	XP04205

Chameleon pre-stained protein ladder	Licor	928-60000
Filter paper and PVDF membrane	Bio-rad	162-0260
Ponceau red stain	Sigma-Aldrich	P7170
Licor Revert Total Protein Stain	Licor	926-11010
Corticosterone ELISA	Enzo Life Sciences	AD1-900-097
Ultrahard blades	Thermo Fisher Scientific	3053835
Superfrost slide	Thermo Fisher Scientific	J1800AMNZ
Lipid pen	Vectorlabs	H-4000
Mounting media	Sigma-Aldrich	F4680
Coverslips	VWR	631-0137
SliceGolgi kit	BioEnno	0.00376
Paraformaldehyde	Sigma	252549
DNAse	Promega	M6101
PCR tubes	Starlab Group	I1402-3700
Applied Biosystems RT kit	Applied Biosystems	4374996
Nuclease free water	Qiagen	129114
384 well plate	Sarstedt	72.1985.202
Qanta fastmix II	Quantabio	95118-012
UPL probe library	Roche	4683633001
Plate seals	VWR	391-1295
QuantSeq 3’ RNA-Seq Library Prep Kit	Lexogen	012.24A
Ion PI Hi-Q OT2 200 kit	Thermo Fisher Scientific	A26434
Ion PI Chip Kit v3	Thermo Fisher Scientific	A26433
Ion Hi-Q Sequencing 200 Kit	Thermo Fisher Scientific	A26433
Ion Proton Platform	Thermo Fisher Scientific	2456290-0449
100BP DNA ladder	Thermo Fisher Scientific	15628019
Magnetic rack	Thermo Fisher Scientific	CS15000
Proteinase K	Roche	115879001
PCR purification kit	Qiagen	28104

SYBR green qPCR master mix	New England Biolabs	M30004E
SeqPlex Enhanced DNA Amplification Kit	Sigma-Aldrich	SEQXE

3 The effects of LPS, hypoxia and Dexamethasone in Organotypic forebrain slice culture and primary OPC and microglia cultures

3.1 Introduction

PTB is often associated with antenatal exposure to synthetic glucocorticoids, hypoxia and inflammation. In preterm neonates these factors are rarely present in isolation and the nature of their interaction, and the physiological consequences of this for brain development are largely unknown.

The difficulty in assessing cellular and biochemical parameters of the brain in neonatal infants necessitates the use of animal models. Most studies investigating the effect of early life insults on brain development use mice due to genetic tractability, quick reproduction and the presence of many conserved mechanisms and processes. I took advantage of the trajectory of postnatal brain development in mice to model factors associated with PTB, at times with neurodevelopmental relevance to PTB in humans. I used an *ex vivo* mouse forebrain slice culture model as well as primary cultures of mouse microglia and oligodendrocyte precursor cells (OPCs) to model the effects of Dexamethasone, LPS and/or hypoxia on various physiological and biochemical parameters.

Epigenetic marks such as DNA methylation and hydroxymethylation are potential mechanisms through which PTB associated factors may mediate an effect. They are dynamically present in the brain during development [110,204] and are altered in neurodevelopmental disorders [187] and following preterm birth [184]. I therefore used this forebrain slice culture model to assess the effect of Dexamethasone, hypoxia and/or LPS on the expression of candidate modifiers of DNA methylation state.

Human studies have identified genetic variants associated with the genes *FADS2* (Fatty acid desaturase 2), *ARVCF* (Armadillo repeat gene deleted in Velo-Cardio-Facial syndrome) and *DLG4* (Discs Large Homology 4) as conferring susceptibility to WMI in preterm infants [251,498].

I therefore also investigated the effect of Dexamethasone, hypoxia and/or LPS on expression of these candidate genes to understand the mechanisms and interactions involved in their relationship with PTB and WMI.

Sparrow *et al* [184], identified differential methylation associated with several genes involved in neurodevelopment (e.g. *SLC7A5*, *SLC1A2* and *TREM2*) in buccal cells of preterm infants at term equivalent age. However, the relevance of this to the brain and the underlying causative mechanisms are unclear. Therefore, I investigated the expression of these candidate genes in the forebrain slice culture model outlined above during Dexamethasone, LPS and/or hypoxia exposure.

As discussed previously understanding the neonatal response to hypoxia and how this contributes to atypical neurodevelopment is crucial for the development of novel therapeutics. 5hmC is dynamically present through neurodevelopment [204], enriched in neurons [147] as well as genes associated with neurodevelopment and ASD [499]. Previous studies have demonstrated 5hmC is enriched at hypoxia response genes following hypoxia in cancer cells [234]. I tested the relevance of this to early brain development in the organotypic forebrain culture model using a candidate approach. As discussed previously, 5hmC at certain genomic elements is associated with active transcription, so understanding its involvement in the hypoxia response would provide valuable mechanistic insight.

WMI is a common result of preterm birth and may be caused by several factors. WMI is of particular importance as it is an indicator of future neurodevelopmental outcome [59]. OPCs are neural stem cells committed to the oligodendrocyte lineage and, as discussed earlier, they are particularly susceptible to PTB related factors. OPC proliferation and differentiation dynamics are crucial to correct myelination, therefore I investigated the effect of Dexamethasone, LPS and/or hypoxia on the ability of primary cultured mouse OPCs to produce mature myelinating oligodendrocytes.

A high incidence of inflammation is associated with PTB and microglia are one of the primary cellular mediators of inflammation within the brain. As such understanding the microglial response to PTB related factors is important. Microglia are also crucial to several homeostatic developmental processes such as myelination and synaptic pruning [500,501]. Microglia are also important in the pathogenesis of neurodevelopmental disorders with the cortical transcriptome of individuals with ASD showing a specific signature indicating microglial

dysfunction [33]. Therefore, I also investigated the effect of Dexamethasone, hypoxia and/or LPS on the secretion of cytokines from primary microglia isolated from neonatal mice.

3.2 Aims and hypotheses

3.2.1 Hypotheses

1. Dexamethasone, LPS and/or hypoxia induce transcriptomic differences in a forebrain slice culture model
2. Changes in transcription will associate with changes in genomic 5hmC in a forebrain slice culture model
3. Dexamethasone, LPS and or/hypoxia will produce functional alterations in primary glial cultures

3.2.2 Aims

1. To compare *ex vivo* cultured forebrain slices to littermate *in vivo* tissue at similar ages
2. To investigate the dose at which Dexamethasone, LPS and hypoxia produce a physiological response under *ex vivo* culture conditions
3. To evaluate the effect of these factors independently and in combination on candidate gene expression
4. To evaluate 5hmC at candidate loci using DNA hydroxymethylation immunoprecipitations following Dexamethasone, LPS and/or hypoxia
5. To investigate the effect of these factors on the differentiation and cytokine secretion of primary cultured mouse OPCs and microglial respectively

3.3 Methods

3.3.1 Animals

Adult mice were housed 3 per cage (2 females and 1 male) for breeding, and offspring were killed on P0/P1 or P8 as indicated below with an overdose of anaesthetic. Brains were extracted from both sexes for all experiments.

3.3.2 Forebrain slice cultures

In order to identify the optimal forebrain slice culture period, I undertook initial characterisation experiments in which 300µm forebrain sections were cultured for 7 or 10 days. At the end of the culture period slices were exposed to propidium iodide for 1 hour to label dead cells, then slices were washed 3 times in PBS and fixed in 4% PFA before washing and staining with DAPI to label all cells. Slices were then visualised using confocal microscopy.

For all forebrain slice culture experiments, an n of 1 was defined as a single forebrain slice from a single animal. Forebrain slices were maintained at 37˚C and 5% CO_2 unless otherwise stated.

To compare the *ex vivo* slice culture period to *in vivo* development, after birth half of the litter was randomly assigned to either a culture or non-culture group. The culture group were killed, and forebrain slices cultured as per the protocol described previously. The non-culture group remained with their mother until the end of the culture period (P8) after which they were killed before their brains removed and forebrain isolated. Tissue was either fixed for immunohistochemistry and Golgi-cox staining or snap frozen on dry ice for subsequent RNA extraction.

To evaluate optimum doses of Dexamethasone and LPS and which concentration of oxygen to use, dose-response curves were generated with increasing concentrations of each condition. RNA was extracted and cDNA generated before qPCR analysis of a well characterised response gene for each condition.

For gene expression profiling, slices were cultured for 7 days before incubation with 100nM Dexamethasone for 5 hours, before media removal and washing with PBS. On the subsequent day, slices were exposed to 100ng/ml of LPS for 5 hours before washing with PBS and fresh media replacement, followed by immediate incubation under 1% oxygen for 24 hours. Slices were then snap frozen on dry ice for subsequent RNA extraction and gene expression profiling via qPCR.

3.3.3 DNA hydroxymethylation immunoprecipitation (hmeDIP)

To assess 5hmC at candidate regions, I used hmeDIP. DNA was extracted from cultured forebrain slices using the Qiagen blood and tissue DNA extraction kit as per manufacturer's instructions. Next, 2.5 µg of DNA was sonicated to a mean length of 250 base pairs using a Covaris Ultrasonicator. Sonicated DNA was incubated with anti-5hmC antibody, which was then pulled down using magnetic protein A coated beads. The beads were washed thoroughly in buffer as described previously and enriched 5hmC released by an overnight digestion with proteinase K at 55 ˚C. DNA enriched for 5hmC was then purified using the Qiagen PCR purification kit. Candidate regions were interrogated using qPCR, with primers designed using the UCSC genome browser and primer BLAST. Regions were normalised to 10% input. An IgG and a water control were included with each experiment.

OPC cell differentiation and microglial cytokine production

The effect of Dexamethasone, LPS and/or hypoxia on OPC cell differentiation and microglial cytokine production was examined using primary mouse cell cultures. Mice at P0-P1 were killed by overdose of anaesthetic and brains extracted. Whole brain tissue from 4 pups was dissociated using the Miltenyi Neural Dissociation kit (for an n of 1). PDGF-Rα or CD11b coated beads were used for MACS isolation of OPCs or microglia respectively. Cells were seeded into 96 well plates at 12,500 or 25,000 cells per well for OPC and microglia culture respectively and maintained at 37˚C and 5% CO_2 unless otherwise stated. Experiments were done in triplicate and averaged to produce an n of 1.

Cells were cultured for 24 hours before exposure to Dexamethasone, LPS and/or hypoxia. Similar to the forebrain slice culture paradigm, primary cells were exposed to 100nM Dexamethasone for 5 hours and subsequent washing with PBS, followed by exposure to 100ng/ml LPS for 5 hours and subsequent incubation under 1% oxygen for 24 hours. Media from cultured microglia was collected at the end of the culture period for cytokine ELISAs, while OPC cultures were differentiated for 3 days in the presence of LIF before fixation and MBP staining.

3.4 Results

3.4.1 Comparison of candidate gene expression in cultured slices and non-cultured littermate tissue

In Figure 3.1, candidate gene expression was measured in cultured slices and non-cultured tissue. As seen in Figure 3.1A, a range of candidate genes showed no difference in expression following the culture period when compared to non-culture littermates. However, a difference was seen in the expression of *DNMT1* and a trend was seen for *HIF1α*, as seen in Figure 3.1B and C respectively.

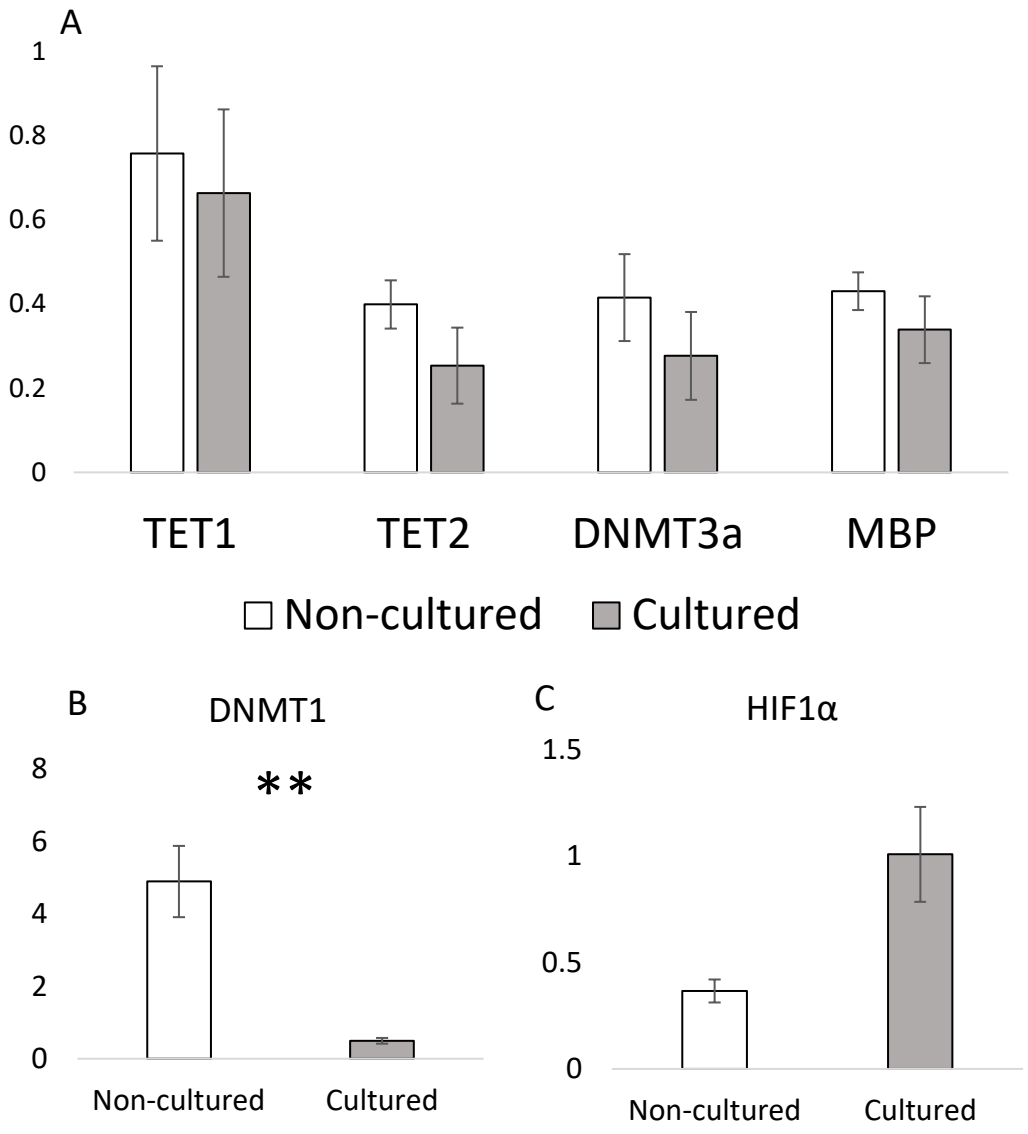

*Figure 3.1 Relative expression of candidate genes in forebrain slices cultured for 7 days and forebrain tissue from P8 littermates. (A) no significant difference in expression of TET1, TET2, DNMT3a or MBP (degrees of freedom (df)=6 for all 4, p=0.665, 0.196, 0.362 and 0.332 respectively) between non-cultured tissue (white columns) and cultured (grey columns) slices was seen. In (B) downregulation of DNMT1 expression during the culture period (df=5, p=0.001) was identified. In (C) a trend towards an upregulation of HIF1α in cultured slices compared to non-cultured tissue (df=6, p=0.015) was seen. N=6 and 7 for cultured and non-cultured groups respectively. Data were analysed using an independent t-test, error bars indicate standard error of the mean. A p-value<0.008 was statistically significant after Bonferroni correction for multiple comparisons. ** indicates p<0.01. Expression was normalised to TFRC and TBP.*

3.4.2 Dexamethasone, LPS and hypoxia induce physiological responses in an ex vivo forebrain slice culture model

I tested the ability of Dexamethasone, LPS and hypoxia to produce physiological responses in the forebrain slice culture model. Slices were incubated with varying concentrations of Dexamethasone, LPS or Oxygen. RNA was then extracted, and expression of well characterised response genes was measured. As seen in Figure 3.2A, the expression of *FKBP5* increased following all doses of Dexamethasone. In Figure 3.2B, the expression of *IL-1α*, *IL-6* and *TNF-α* increased in a dose-dependent fashion with LPS. Similarly, in Figure 3.2C, the expression of *PGK1* (phosphoglycerate kinase 1) and *VEGFA* (vascular endothelial growth factor A) increased in a dose-dependent fashion in response to decreasing oxygen concentrations. Also, in 1% oxygen there was an accumulation of the HIF1α protein (Figure 3.2D). Subsequent experiments were carried out using 100nM Dexamethasone, 100ng/ml LPS and 1% Oxygen.

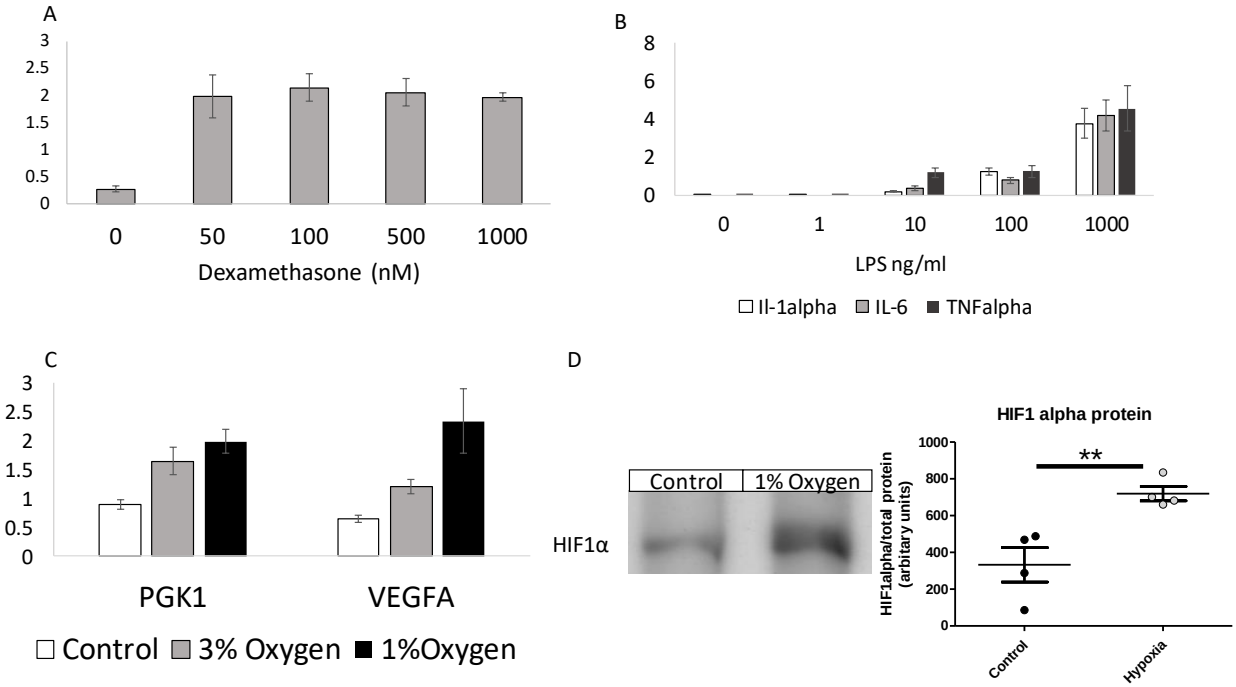

Figure 3.2 Dexamethasone, LPS and hypoxia produce physiological effects in the forebrain slice culture paradigm. (A) relative expression of FKBP5 increases with exposure to 5 hours of Dexamethasone. (B) following 5 hours of LPS exposure the expression of IL1α, IL6 and TNFα (represented in open, grey and black bars respectively) increased in a dose-dependent fashion with LPS concentration. (C) there was a dose-dependent increase in the relative expression of PGK1 and VEGFA in response to decreasing oxygen concentrations. The control condition (21%

*oxygen) is represented by the open bars and hypoxic conditions of 3% and 1% groups are represented by grey and black bars respectively. (D) HIF1α protein was assessed by western blot, with representative bands shown, and normalised to total protein showing an increase in presence at 1% oxygen (df=3, p=0.009) as indicated by an independent t-test. ** indicates p<0.01. For all experiments shown n=4-8 and error bars indicate standard error of the mean. Gene expression was normalised to TFRC and TBP.*

3.4.3 PTB related factors alter the expression candidate genes following combinations of Dexamethasone, LPS and hypoxia

I tested the immediate transcriptional response of candidate genes to all combinations of Dexamethasone, LPS and hypoxia. These candidate genes were taken from a number of sources, including previously described modifiers of DNA methylation (*TET1*, *TET2* and *DNMT3a*), candidates identified by Sparrow et al (*TREM2*, *SLC7A5* and *SLC1A2*) and candidates are involved in perinatal WMI (*FADS2*, *DLG4* and *ARVCF*). In FIGURES I show the genes which show consistent trends or which achieve statistical significance, but all statistical comparisons are shown in Table 3.1.

As seen in FIGURE, I investigated the independent effect of Dexamethasone, LPS or hypoxia on candidate gene expression using qPCR. As can be seen in FIGURE A, there were no significant effects of Dexamethasone on expression of these genes. As can be seen in FIGURE B, there were also no significant effects of hypoxia on candidate gene expression but there was a non-significant trend towards an increase in *TET1*, *TET2* and *SLC7A5* expression. Similarly, as seen in FIGURE C, there were also no significant effects of LPS alone on the expression of candidate genes.

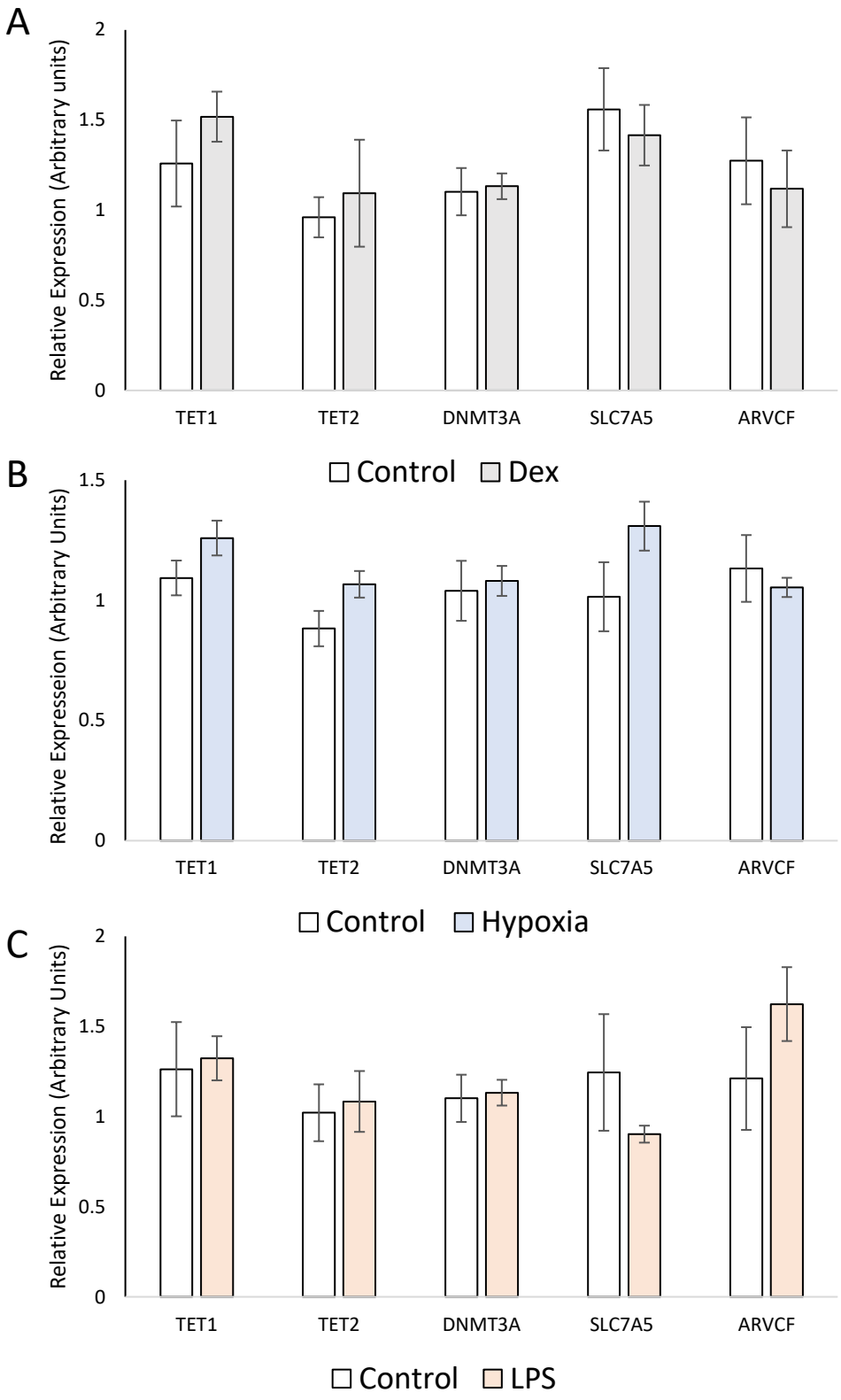

Figure 3.3 Relative expression, normalised to TBP of Dexamethasone (A), hypoxia (B) and LPS (C) in the forebrain slice culture model, of candidate genes. In A, there was no difference in expression of TET1 (p=0.841, df=9), TET2 (p=0.963, df=9), DNMT3A (p=0.485, df=9), SLC7A5 (p=0.108, df=9) or ARVCF (p=0.68, df=12) following Dexamethasone. In B, following correction for multiple comparisons there was no difference in expression of TET1

(p=0.013, df=12), TET2 (p=0.013, df=21), DNMT3A (p=0.835, df=11), SLC7A5 (p=0.007, df=21) or ARVCF (p=0.283, df=9) following hypoxia. In C, there was no difference in expression of TET1 (p=0.07, df=15), TET2 (p=0.894, df=15), DNMT3A (p=0.835, df=11), SLC7A5 (p=0.117, df=15) or ARVCF (p=0.326, df=5) following LPS. All comparisons were made using an independent t-test following Bonferroni correction for multiple comparisons. Data are expressed as mean and standard error bars.

Next, I investigated the effect of combinations of these insults on the expression of the same genes by qPCR. As seen in FIGURES A and B there were no significant effects on gene expression for the "Dexamethasone and hypoxia" or "Dexamethasone and LPS". However, there was a non-significant trend towards an increase in expression of *TET1* and *TET2* following Dexamethasone and hypoxia, as seen in FIGURE A. I next looked at the effects of "LPS and hypoxia" and "Dexamethasone, LPS and hypoxia" in FIGURE C and D, respectively. In FIGURE C, *ARVCF* was significantly increased in both groups. As seen in FIGURE D, *TET2* was significantly increased with "Dexamethasone, LPS and hypoxia", but a similar trend was observed for "LPS and hypoxia" as seen in FIGURE C. Trends towards an increase in expression were also seen for *TET1* and *SLC7A5* in both groups.

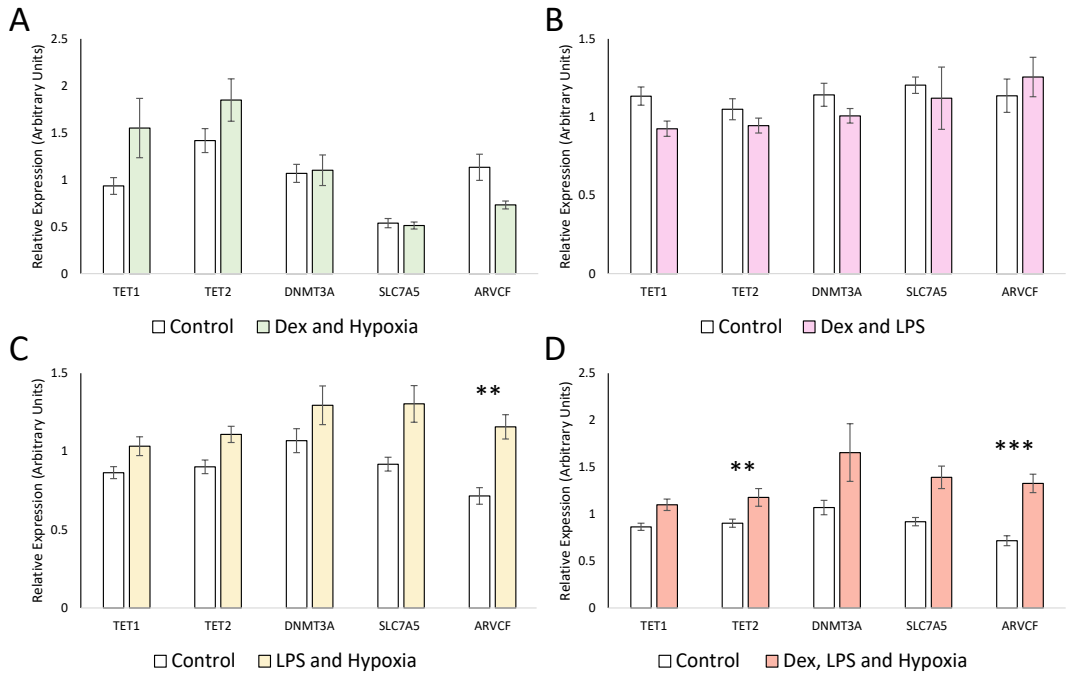

Figure 3.4 Outline of candidate gene expression following Dexamethasone (Dex) and hypoxia (A), Dex and LPS (B), LPS and hypoxia (C) and Dex, LPS and hypoxia (D). In A there were no differences in candidate gene expression following Dexamethasone and hypoxia of TET1 (p=0.014, df=22), TET2 (p=0.102, df= 22), DNMT3a (p=0.861, df=28), SLC7A5 (p=0.704, df=14) or ARVCF (p=0.012, df=17) after correction for multiple comparisons. In B, there were no differences in expression of TET1 (p=0.029, df=13), TET2 (p=0.572, df=11), DNMT3A (p=0.258, df=15), SLC7A5(p=0.207, df=21) or ARVCF (p=0.391, df=10) following Dexamethasone and LPS, after correction for multiple comparisons. In C, ARVCF (p=0.001, df=19) was significantly increased but no difference was seen in expression of TET1 (p=0.018, df=16), TET2 (p=0.007, df=20), DNMT3A (p=0.11, df=21) or SLC7A5 (p=0.018, df=21) following LPS and hypoxia. In D, TET2 (p=0.001, df=21) and ARVCF (p=0.0003, df=19) were significantly increased in expression, but there were no differences in TET1 (p=0.028, df=16), DNMT3A (p=0.441, df=18) or SLC7A5

*(p=0.01, df=19) after Dexamethasone, LPS and hypoxia. ** indicates p<0.006 (adjusted threshold for statistical significance, *** indicates p<0.001. All comparisons were made using an independent t-test and followed by a Bonferroni correction for multiple comparisons. Data are expressed as mean and standard error bars.*

Table 3.1 Table showing the p-value (with degrees of freedom) in all candidate genes and conditions analysed. Each condition was compared with their own control group using an independent t-test with a Bonferroni correction post-hoc. The adjusted p-value threshold for statistical significance was p<0.006. All comparisons which met this criteria are highlighted in bold.

	Unadjusted p-value (degrees of freedom)						
Gene	Dex	LPS	Hypoxia	Dex and LPS	Dex and Hypoxia	LPS and Hypoxia	Dex, LPS and Hypoxia
TET1	0.841 (9)	0.07 (15)	0.013 (12)	0.029 (13)	0.014 (22)	0.018 (16)	0.028 (16)
TET2	0.963 (9)	0.894 (15)	0.013 (21)	0.572 (11)	0.102 (22)	0.007 (20)	**0.001 (21)**
DNMT3A	0.485 (9)	0.835 (11)	0.368 (14)	0.258 (15)	0.861 (28)	0.11 (21)	0.441 (18)
ARVCF	0.638 (12)	0.326 (5)	0.283 (9)	0.391 (10)	0.012 (17)	**0.001 (19)**	**0.0003 (19)**
DLG4	0.84 (12)	0.068 (6)	0.173 (13)	0.248 (12)	0.173 (14)	0.071 (20)	0.101 (20)
FADS2	0.325 (12)	0.366 (5)	0.894 (15)	**0.004 (15)**	**0.004 (21)**	0.286 (20)	0.309 (19)
SLC7A5	0.108 (9)	0.117 (15)	0.007 (21)	0.207 (15)	0.704 (14)	0.018 (21)	0.01 (19)
SLC1A2	0.108 (13)	0.929 (12)	0.341 (12)	0.057 (15)	0.486 (13)	0.046 (24)	0.971 (24)
TREM2	0.045 (14)	0.503 (4)	0.798 (12)	0.373 (15)	0.248 (14)	0.809 (14)	0.1 (12)

3.4.4 There is no change in 5hmC at the SLC7A5 locus following LPS and/or hypoxia

SLC7A5 was subject to the highest level of differential methylation in Sparrow *et al* and I found it to be increased in expression following various combinations of hypoxia. I also saw a similar pattern with the TET enzymes (see **Error! Reference source not found.**), and as discussed in the introduction, 5hmC is thought to mark sites of active transcription when located within the gene body. Therefore, I next assessed 5hmC levels within well conserved regions of the *SLC7A5* gene body following LPS and/or hypoxia. I used hmeDIP and assessed enrichment through qPCR at candidate regions. The regions assessed within the *SLC7A5* mouse gene can be seen in Figure 3.3A, alongside an indication of human conservation. There were no differences in 5hmC following LPS and/or hypoxia at any of the regions assessed, see Figure 3.3B. Fitting with the previous literature, 5hmC levels across these 3 loci were correlated with each other, see Figure 3.3C.

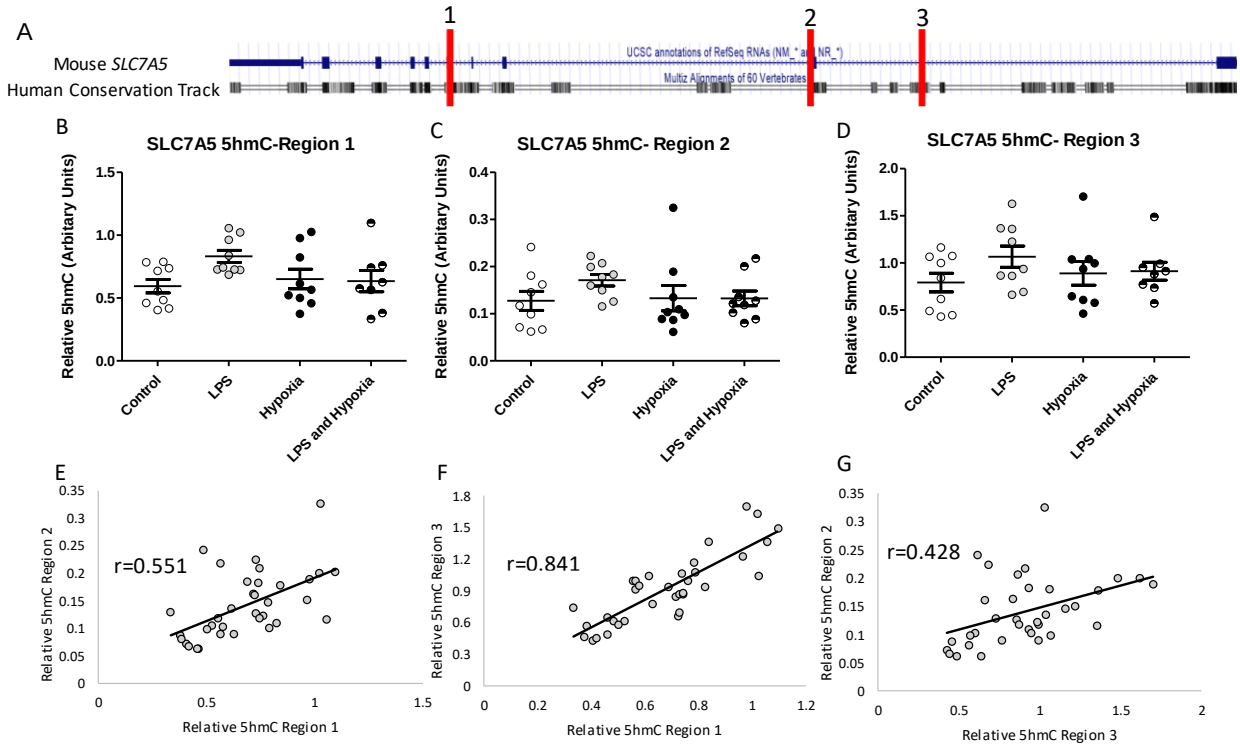

Figure 3.3 5hmC was assessed at the SLC7A5 locus following LPS and/or hypoxia. In A) the mouse SLC7A5 gene as seen through the UCSC genome browser is seen in the top blue track, with exons represented as thicker segments. Underneath, the black track represents the degree of conservation with the human SLC7A5 locus, thick segments represent regions of high conservation. The red vertical lines indicate the regions assessed for 5hmC and are numbered as they are referenced in the subsequent graphs (B-G). In B-D, the level of 5hmC (normalised to 10% input) at different intragenic regions of the 5hmC locus is shown (B- p=0.085 LPS, 0.907 hypoxia and 0.068 interaction; f-statistic= 3.298, 0.014 and 4.695 respectively; df=32) (C- p=0.258, 0.679 and 0.538; f-statistic=1.357, 0.177 and 0.393, respectively; df=32) (D- p=0.098, 0.531, 0.83; f-statistic=4.01, 4.07 and 0.47, respectively; df=32), no differences were found across any of the regions and conditions assessed but there was a trend towards an interaction between LPS and hypoxia in region 1 (B, p=0.068). In E-F the correlation between 5hmC at the 3 different regions was examined with Region 1 showing a positive correlation with Region 2 (panel E; p=0.001 and r=0.551) and Region 3 (panel F; p<0.001 and r=0.841), and also 5hmC in Region 2 was positively correlated with 5hmC in Region 3 (panel G, p=0.01 and r=0.428). A two-way ANOVA was used to analyse data represented in B-D, with error bars representing standard error of the mean. A Pearson's correlation was carried out in E-G.

3.4.5 Accumulation of 5hmC at hypoxia response genes following LPS and/or hypoxia

I saw an increase in expression of the *TET* enzymes following hypoxia, and 5hmC has been implicated in the hypoxia response in cancer [234]. Therefore, I looked at the presence of 5hmC at these loci following LPS and/or hypoxia. As seen in Figure 3.4A there was an interaction

between LPS and hypoxia at the *Car9* locus. There were no effects of LPS and/or hypoxia at the *PGK1*, *VEGFA* or *BNIP3* loci, as seen in Figure 3.4 B-D.

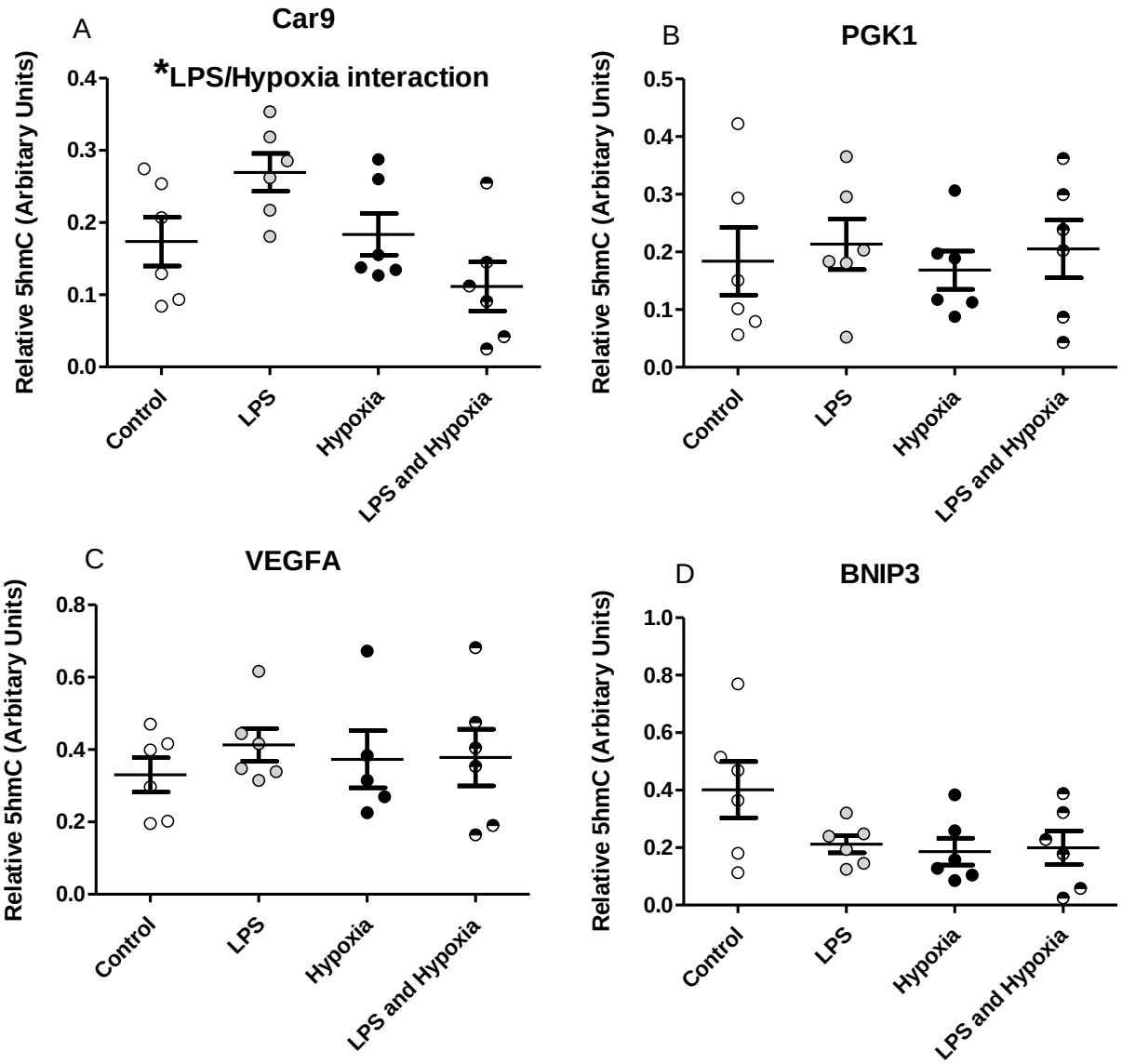

*Figure 3.4 5hmC at candidate regions associated with classic hypoxia response genes following LPS and/or hypoxia. In A) 5hmC associated with the Car9 locus was affected by hypoxia (p=0.026, f-statistic=5.768, df=20) and an interaction between LPS and hypoxia (p=0.013, f-statistic=7.423, df=20) was seen with no effect of LPS (p=0.704, f-statistic=0.149, df=20). Similar graphs are shown in B, C and D for the PGK1 (p=0.805, 0.491 and 0.937; f-statistic=0.062, 0.491 and 0.006 for hypoxia, LPS and an interaction, respectively, df=20), VEGFA (p=0.948, 0.498 and 0.547; f-statistic=0.004, 0.478 and 0.376 for hypoxia, LPS and an interaction respectively) and BNIP3 (p=0.419, 0.542 and 0.478; f-statistic=0.666, 0.377 and 0.511 for hypoxia, LPS and an interaction, respectively, df=20) loci respectively, none of which showed alterations in 5hmC at the candidate regions tested. A two-way ANOVA was used to analyse all data. Error bars are indicative of standard error of the mean. * indicates p<0.05.*

3.4.6 Morphological assessment of primary mouse OPCs and microglia after LPS

In Figure 3.5, primary mouse OPCs and microglia isolated from the neonatal mouse forebrain were imaged using brightfield before and after LPS administration. Under normal conditions (Figure 3.5A) OPCs display a typical bipolar morphology. Following exposure to LPS (Figure 3.5C), some cells retain this morphology, but some cells appear with a more rounded cell body, indicative of a mature oligodendrocyte. Under normal LPS-free conditions (Figure 3.5B) microglia have a characteristic elongated morphology. Following exposure to LPS (Figure 3.5D), they assume a more ramified morphology with a rounder cell body which is typical of a transition to an inflammatory phenotype.

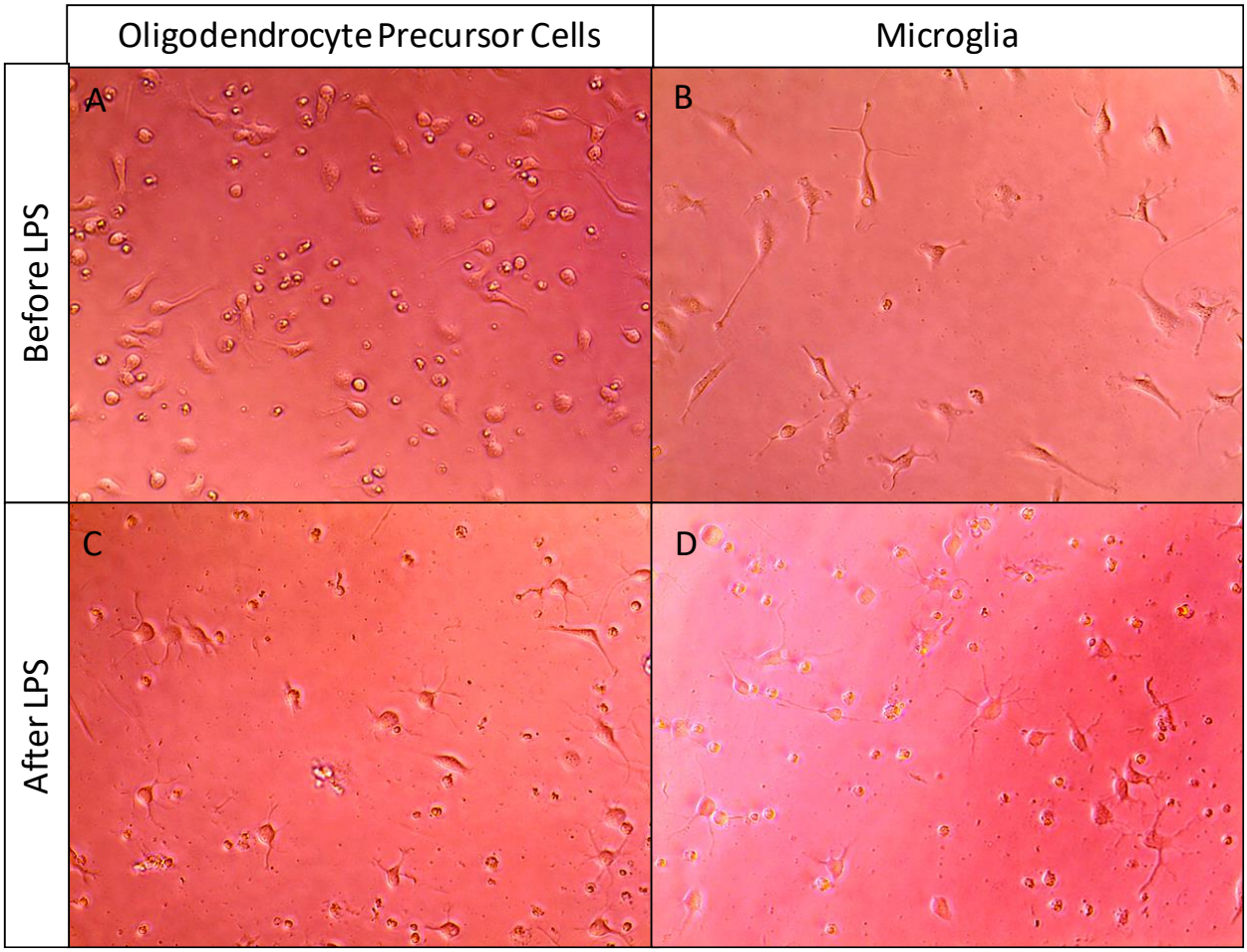

Figure 3.5 Assessment of primary mouse OPC and microglia cultures before (A and B) and after (C and D) LPS. In A) a bipolar morphology can be seen, which is characteristic of OPCs, after LPS treatment (C) these cells display a more ramified morphology which is consistent with a mature oligodendrocyte. In B) under homeostatic conditions, microglia have an elongated cell body and long processes which is typical of quiescent state microglia. In D) after

exposure to LPS microglial cell bodies become rounded and have a more ramified structure, a phenotype typically associated with inflammatory conditions.

3.4.7 LPS and hypoxia increase microglial cytokine release

Microglia are one of the primary mediators of neuroinflammation, and the elevated presence of cytokines in the blood is associated with adverse neurodevelopmental outcomes [502]. As such, the local microglial production of cytokines in response to PTB related factors may also have and important role. To overcome the problem of cellular heterogeneity, I isolated and cultured microglia from the forebrain of neonatal mice and exposed them to Dexamethasone, LPS and/or hypoxia and measured cytokine secretion into the media, a schematic of the paradigm is shown in Figure 3.6A. In Figure 3.6B, TNFα was increased following LPS with undetectable levels in control conditions. There was no independent or interaction effect associated with Dexamethasone or hypoxia. In Figure 3.6C, IL1β was increased following hypoxia. There was no independent or interaction effect associated with Dexamethasone or LPS. In Figure 3.6D, IL6 was increased following LPS. There was no independent or interaction effect associated with Dexamethasone or hypoxia.

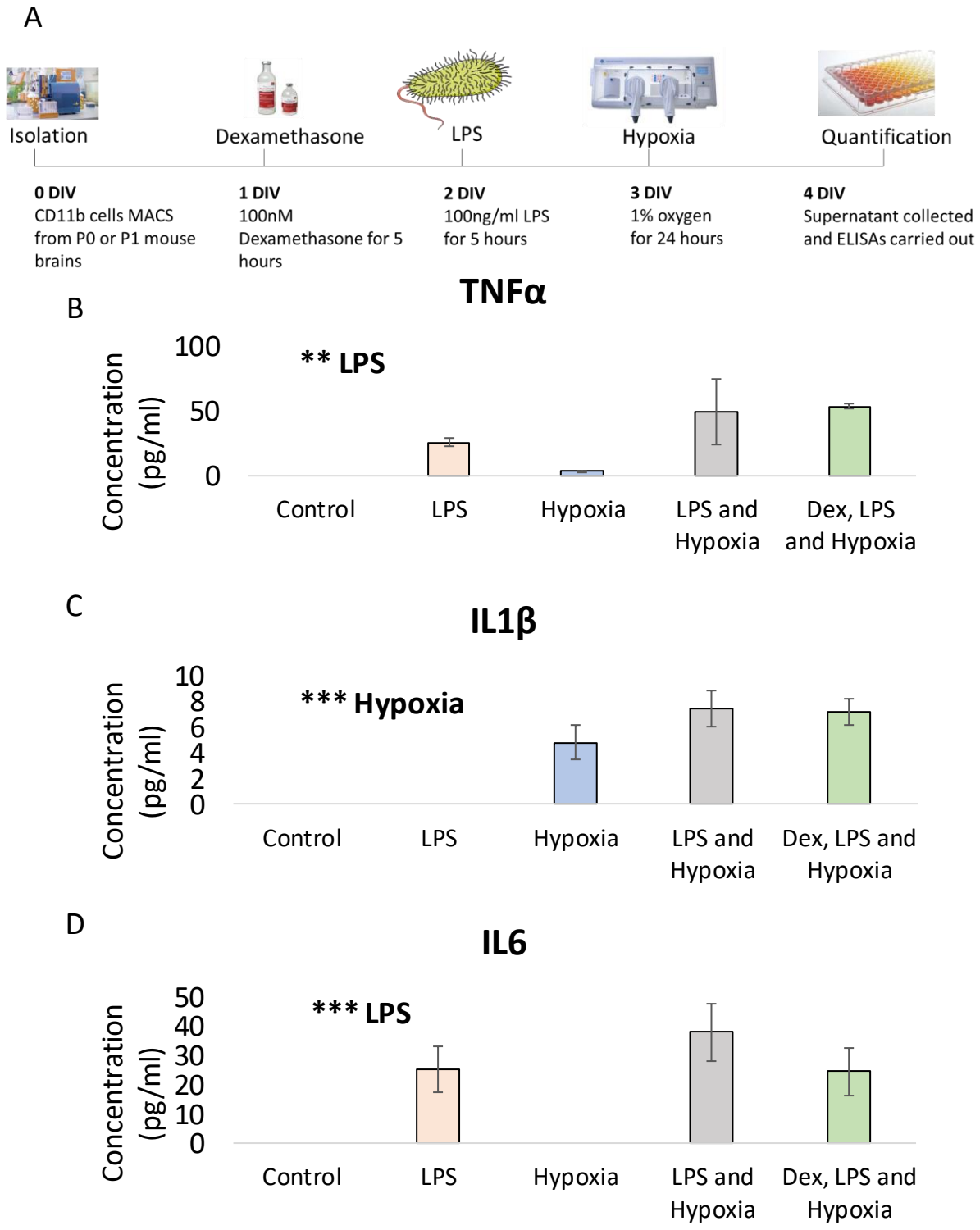

Figure 3.6 The effect of LPS, hypoxia and Dexamethasone on TNFα (B), IL1β (C) and IL6 (D) production in primary cultured microglia. In A) a schematic of the experimental design shows CD11b cells were isolated from neonatal mouse forebrains and cultured in the presence of Dexamethasone, LPS and/or hypoxia before quantification of cytokines from the supernatant using an ELISA. In B) TNFα was increased in the media following LPS (p=0.003, f-statistic=14.385, df=15) with no effect of hypoxia (p=0.177, f-statistic=2.054, df=51), Dexamethasone (p=0.809, f-

*statistic=0.061, df=15) or interaction (p=0.291, f-statistic=1.22, df=15) between the factors. In C) IL1β was increased following hypoxia (p<0.001, f-statistic=27.084, df=15) with no effect of LPS (p=0.279, f-statistic=1.25, df=15), Dexamethasone (p=0.88, f-statistic=0.024, df=15) or interaction (p=0.279, f-statistic=1.25, df=15) between the factors. In D), IL6 was increased following LPS exposure (p<0.001, f-statistic=29.981, df=15) with no effect of hypoxia (p=0.294, f-statistic=1.203, df=15), Dexamethasone (p=0.145, f-statistic=2.425, df=15) or interaction (p=0.294, f-statistic=1.203, df=15) between the factors. ** indicates p<0.01 and *** indicates p<0.001. Data were analysed using a three-way analysis of variance (ANOVA). A p-value<0.016 was said to be statistically significant following Bonferroni correction for multiple comparisons. Error bars show standard error of the mean. N= 4-6 for all groups.*

3.4.8 Hypoxia is associated with a decreased production of mature myelinating oligodendrocytes in primary cultured mouse OPCs

Reduced numbers of mature myelinating oligodendrocytes may cause hypomyelination and facilitate WMI. As such, it is important to understand the factors associated with PTB which may affect the production of mature oligodendrocytes from OPCs. To examine this, PDGF-Rα+ cells were isolated from neonatal mouse forebrain tissue and exposed to Dexamethasone, LPS and/or hypoxia. The ability of these cells to produce mature myelinating oligodendrocytes was then measured (described in Figure 3.7A).

In Figure 3.7B, hypoxia decreased the percentage of MBP positive oligodendrocytes at the end of the differentiation period. There was a trend towards the same effect for LPS and there was no interaction between the factors.

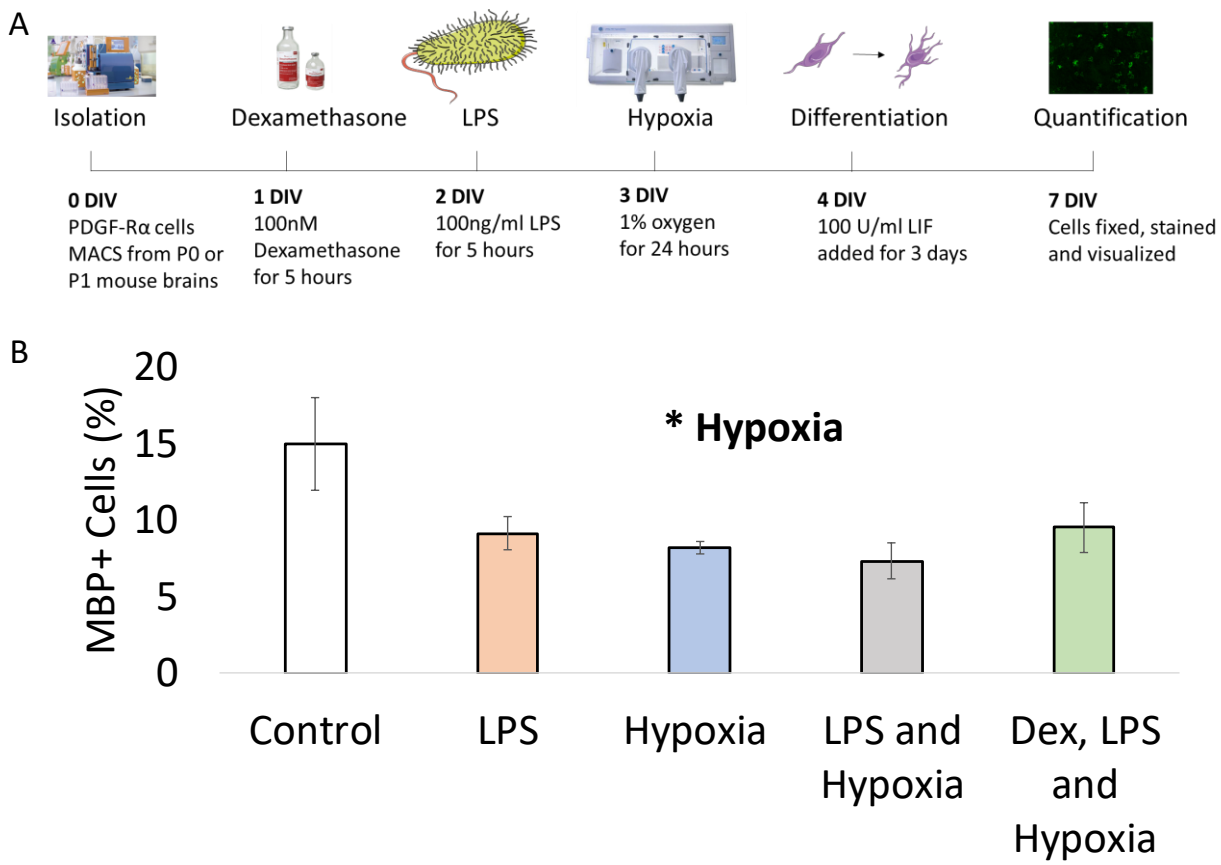

*Figure 3.7 The effect of LPS, hypoxia and Dexamethasone on OPC differentiation. In A) a schematic of the experimental design shows PDGF-Rα cells were isolated from neonatal mouse forebrains and cultured in the presence of Dexamethasone, LPS and/or hypoxia before addition of 100units/ml of Leukemia inhibitory factor (LIF), to stimulate differentiation, for 3 days. Cells were then fixed, stained and imaged. In B) there was a decrease in the proportion of MBP positive cells following hypoxia ($p=0.016$, $f\text{-statistic}=7.067$, $df=15$) and a trend towards a decrease associated with LPS ($p=0.051$, $f\text{-statistic}=4.365$, $df=15$), with no effect of Dexamethasone ($p=0.319$, $f\text{-statistic}=1.052$, $df=15$) or an interaction between the factors ($p=0.141$, $f\text{-statistic}=2.371$, $df=15$). * indicates $p<0.05$. Data were analysed using a three-way ANOVA. Error bars show standard error of the mean. N= 4-6 for all groups.*

3.5 Discussion

In this chapter I show that:

1. There is comparable candidate gene expression between cultured slices and non-cultured littermates but there were significant differences in *DNMT1* and *HIF1α* expression
2. Dexamethasone, LPS and hypoxia produce physiological responses under *ex vivo* culture conditions
3. There was limited interactions between Dexamethasone, LPS and hypoxia in terms of candidate gene expression
4. When assessing 5hmC, there was a significant interaction between LPS and hypoxia at Car9, a classic hypoxia response gene
5. There were no significant interactions found between LPS and hypoxia in terms of microglial cytokine secretion and OPC differentiation in primary glial culture systems

3.5.1 Forebrain slice culture model

Multiple forebrain slices can be obtained from a single animal and a single animal can therefore be represented in multiple groups of the *ex vivo* forebrain slice culture model. As such each group is composed of very similar tissue composition, thereby reducing variation between groups and reducing the number of animals used. It also provides more defined conditions than an *in vivo* environment, facilitating the analysis of specific pathways and mechanisms.

The experimental design for the initial experiments (Figure 3.1-3.5) described in this chapter were suboptimal. A separate control group was used for the comparison with each individual group which hinders comparisons across groups. Future studies should design experiments so that an individual control group is compared across all experimental conditions. This would facilitate statistical analysis with an ANOVA and accordingly increase statistical power.

3.5.2 Dexamethasone

I used 100nM of Dexamethasone in these experiments. This is a relatively low dose and was used to model the *in utero* exposure to Dexamethasone many preterm infants receive. This concentration has been used previously in various brain culture paradigms [503,504] but to my knowledge, this is the first instance of this concentration being used to examine factors associated with early life brain development.

I used expression of *FKBP5* as a marker of Dexamethasone exposure. Transcription of *FKBP5*, as discussed in the introduction, is directly induced by the GR when a ligand is bound and FKBP51 (protein of the *FKBP5* gene) acts to negatively regulate GR mediated effects. In Figure 3.2, the expression of FKBP5 saturates at the very low dose of 50nM of Dexamethasone. This implies a low threshold at which transcription of FKBP5 is maximally induced by Dexamethasone. A previous study saw a similar result using cortisol exposure in cultured human adipose tissue [505]. Considering there is not a consensus Dexamethasone concentration to use in culture which models prenatal Dexamethasone exposure, I proceeded with 100nM as it has previously been used in the literature and my dose-response experiment demonstrated a clear induction of *FKBP5* expression at that concentration implying a physiological response.

As outlined previously, *ex vivo* slices, or primary cultured cells were exposed to Dexamethasone for 5 hours on the day prior to LPS exposure. The *in vivo* half-life of Dexamethasone is 36-72 hours [506], as such the 5 hour exposure used here was low. LPS exposure was not initiated until 19 hours after Dexamethasone was removed from the slices, and from this timepoint it was a further 29 hours before the slices were processed and analysed (5 hours of LPS and 24 hours of hypoxia). It is therefore likely that any effects of Dexamethasone administration had subsided by the time of analysis. However, my primary interest in this study was to investigate the relationship between LPS and hypoxia in the context of prior Dexamethasone exposure and to investigate whether this had any 'programming' effect on this interaction.

3.5.3 Relevance of hypoxia

The forebrain slice culture paradigm is done using a semi-permeable membrane with the slices maintained at the liquid-air interface. The slices were maintained under control conditions at room oxygen levels of 21% (a partial pressure of 160mmHg). Research in the awake adult mouse brain shows that physiological oxygen concentrations in the forebrain vary between 80mmHg in larger arterioles and 20mmHg or below in the capillary bed [507]. These values are likely to be similar, if not lower, in the neonatal brain where hypoxia is a critical mediator of normal brain development [508]. Therefore, one major limitation of this study is the supraphysiological oxygen concentrations used for the control group.

As seen in Figure 3.1, *HIF1α* gene expression was increased in cultured forebrain tissue in comparison to *in vivo* conditions. Upregulation of *HIF1α* expression has previously been seen

in response to hyperoxia in tumours [509]. Therefore, the exposure to supraphysiological oxygen concentrations is a possible cause of the increased *HIF1α* expression seen in the forebrain slice culture. Despite this, a dose-dependent increase in the expression of classic HIF1α response genes (*PGK1* and *VEGFA*) was seen following hypoxia. There was also an increase in HIF1α protein (Figure 3.2) after 1% oxygen exposure which indicates a physiologically relevant response to hypoxia in this model.

3.5.4 Effects on candidate gene expression

As seen in **Error! Reference source not found.**, both *TET1* and *TET2* were increased in expression following hypoxia both independently and with various combinations of Dexamethasone and LPS. Previous studies have shown increased expression of the *TET* enzymes following hypoxia occurs in some, but not all, cell lines [153]. To my knowledge, upregulation of *TET1* and *TET2* during hypoxia has not previously been reported during early postnatal brain development. As discussed in the introduction, the TET enzymes are members of the α-ketoglutarate dependent dioxygenase family and are therefore dependent on oxygen as an essential substrate. Therefore, it is somewhat paradoxical that a lack of oxygen should upregulate the expression of these enzymes. However, Laukka *et al* demonstrated that the K_m of TET1 and TET2 for oxygen is 30μM and therefore, they can maintain normal activity even under hypoxic conditions [510].

HIF1α has been shown to recruit TET1 to HIF1α target sites across the genome to mediate 5mC conversion to 5hmC and facilitate subsequent hypoxia induced gene expression changes in cancer cell lines [234]. TET1 has also been reported to interact with HIF1α and HIF2α in a fashion independent of its catalytic subunit. Wang *et al* show TET1 binds to HIF1α and acts to stabilise its C-terminus, while TET1 competes with PHD2 for hydroxylation sites on the HIF2α protein, and in doing this reduces HIF2α hydroxylation and therefore its degradation [511]. However, this work was carried out in cancer cell lines and its relevance to other, non-cancerous cells and *in vivo* conditions is unclear.

Future work in this area should consider whether TET mediated hydroxymethylation is integral to the hypoxia response *in vivo* and if this involvement is a transient mechanism to facilitate hypoxic gene expression or part of a pathogenic series of events which themselves can alter brain development and neurodevelopmental outcome. The manipulation of 5hmC

is a key tool for understanding its importance in these processes. Typically, cytosine analogues such as 5-azacytidine are used to cause experimental non-specific DNA demethylation through their integration during DNA repair or replication instead of resident cytosine nucleotides. However, to understand the accumulation of 5hmC during hypoxia at hypoxia response genes, site specific manipulation of 5hmC is needed. A recent tool described by Xu *et al*, uses the fusion of a Cas9 (with disabled endonuclease activity) to the TET3 catalytic domain, which can be recruited in a site-specific manner to DNA by guide RNAs to facilitate 5hmC induction [512]. This technology may prove to be a useful tool in the elucidation of 5hmC importance during hypoxia and normal development.

As seen in **Error! Reference source not found.**, in my *ex vivo* forebrain slice culture paradigm, *SLC7A5* expression is specifically increased in all instances of hypoxia (except for Dexamethasone + hypoxia). *SLC7A5* expression has previously been shown to be upregulated during hypoxia in various cancer cell lines [513–516] but to my knowledge this has not been shown in non-cancerous brain tissue or indeed using an *ex vivo* mouse forebrain culture system. Tarlungeanu *et al* showed that deletion of *SLC7A5* from endothelial cells produces abnormal neurodevelopmentally-regulated behaviours in mice and these are rescued with leucine and isoleucine intra cerebroventricular administration. They also demonstrated that mutations within *SLC7A5* are associated with ASD in humans [186]. Previously, Sparrow *et al* showed that *SLC7A5* is differentially methylated in buccal swabs taken at term equivalent age from infants born preterm, when compared to term born controls [184]. Dysregulation in SLC7A5 (whether this be upregulation or downregulation) may therefore play a role in adverse perinatal events and affect neurodevelopmental outcome.

LPS has been shown to sensitise to subsequent hypoxia exposure in previous studies [517]. Here I provide limited support for this hypothesis. The expression of *ARVCF* (**Error! Reference source not found.**) was not changed by LPS or hypoxia independently but was increased when LPS preceded hypoxia and this was not affected by Dexamethasone. The inability of Dexamethasone to ameliorate this alteration in expression may be because it was transiently present in the media and the anti-inflammatory effects of Dexamethasone (which as discussed previously are primarily mediated through increased *NFKBIA* transcription) have subsided by the time of LPS exposure. Another possibility is that, as NFKBIA acts to limit the activation of the NFkB pathway, the interaction between LPS and hypoxia occurs independently of NFkB. For example a signal could be propagated through IRF5 or MAPK/AP-

1, which can mediate a response to LPS independently of NFkB signalling [518] and which are also involved in hypoxia signalling [519].

3.5.4.1 5hmC at hypoxia response loci

I found an interaction between hypoxia and LPS at an analogous region of the *Car9* gene which was enriched in Mariani *et al* [234]. I also found an effect of hypoxia alone but the presence of a interaction with LPS makes inferring biological significance from this difficult, as can be seen with a visual inspection of the data (Figure 3.4). There were no changes in 5hmC among other hypoxia response genes and this may be for a number of reasons. Firstly, the previous study looked primarily in human immortalised cancer cell lines which typically have dramatically reduced 5hmC levels [520]. If this was true for the cell lines used in the Mariani *et al* study, then small effect sizes would result in significant enrichment, but the physiological relevance of the changes may be questionable. Secondly, I used mouse cultured tissue, whereas Mariani *et al* used human cells. There may be species specific differences in the mechanistic response to hypoxia. Finally, Mariani *et al* used a genome wide approach to assess 5hmC whereas here I used a candidate approach. As such, I may have missed regions of 5hmC enrichment through the candidate nature of my approach.

The interaction between LPS and hypoxia with respect to 5hmC at the *Car9* locus is interesting. As previously discussed, there is evidence that LPS can potentiate a subsequent hypoxia exposure. A potential mechanism for this may be epigenetic remodelling of DNA and/or chromatin by LPS, which may affect the ability of transcription factors and DNA binding proteins, associated with hypoxia, to bind DNA [521]. However, this needs a more comprehensive study using *in vivo* models of hypoxia and inflammation with sequencing-based approaches to fully understand.

A more comprehensive study using *in vivo* hypoxia exposure to pups should be done using sequencing methods to assess the effect of hypoxia on 5hmC. This could also be validated in infarct regions of human neonatal brain tissue, using the contralateral uninjured hemisphere as a control. A candidate ChIP for TET1-3 at hypoxia response genes could also be done to identify specific mediators of these effects. Finally, the effect of hyperoxia and its interaction with hypoxia should be assessed. As discussed previously, preterm infants are often exposed to intermittent episodes of hypoxia and hyperoxia. As such, the evaluation of this more clinically relevant combination should be assessed. For instance, an experiment could include

4 groups: control, hypoxia, hyperoxia and intermittent hypoxia/hyperoxia. Dissection of various brain regions could be done and genome wide hydroxymethylation assessed.

Effect of PTB associated factors on primary cultured mouse glial cells

My finding that there is a reduction in myelin producing mature oligodendrocytes following hypoxia (see Figure 3.7) is one that has been previously reported in the literature [522,523]. I also saw a trend toward a decrease in the number of myelin producing mature oligodendrocytes following LPS exposure. However, this trend falls just outside statistical significance. Inflammation induced hypomyelination is a common feature in perinatal brain injury models [251]. This experiment was underpowered to detect a difference in mature myelinating oligodendrocytes at the effect size seen here. For future studies, to achieve a power of 0.8 the sample size of each group would need an additional 5 samples.

I showed that hypoxia upregulated IL1β secretion from primary cultured microglia, but no effect or interaction was seen with LPS. Considering IL1β is implicated in classic LPS signalling, this was somewhat surprising. Studies have shown that IL1β is involved in the immediate response to LPS but is also maintained with LPS exposure in peripheral macrophages [524,525]. However, the dose of LPS used in my study was relatively low and microglia have distinct characteristics to other macrophage populations. It is possible that IL1β is transiently produced by primary cultured mouse microglia in response to low dose LPS but to my knowledge, this has not previously been reported. IL1β has previously been identified as a HIF1α target [526,527], but to my knowledge this is the first description of such an effect in cultured primary murine microglia.

I show that OPC exposure to hypoxia results in a reduction in MBP positive cells after the induction of differentiation, and I show a similar but not significant trend for LPS (Figure 3.7B). I was therefore surprised that the effect size was not larger in the LPS + hypoxia group compared to either factor independently, this may be due to several reasons. Firstly, an effect for LPS fell just outside the threshold for statistical significance of $p<0.05$. However as described previously, this study was underpowered to detect a change at the effect size observed and a reduction in myelinating oligodendrocytes following inflammation has previously been reported in the literature [250]. Therefore, a larger sample size is required to test this hypothesis. Secondly, impaired OPC differentiation, increased OPC cell death, increased mature oligodendrocyte cell death or decreased OPC proliferation are examples of

mechanisms which may result in a decreased percentage of MBP positive cells in this assay. It is therefore possible LPS and hypoxia act either through a similar mechanism which saturates, or through different mechanisms which interact in an unknown fashion to limit adverse outcome.

In conclusion, in this chapter I have characterised a forebrain slice culture paradigm and have shown it is comparable, in terms of glial populations, neuronal morphology and candidate gene expression patterns, to littermates which are left with their mother through the culture period. I established factors associated with PTB, such as Dexamethasone, the inflammatory mimic LPS and hypoxia produce physiological responses in this forebrain slice culture paradigm. I have also shown these factors produce differential expression of several candidate genes associated with cytosine modifications and WMI in PTB. I demonstrated using primary mouse OPC cultures that hypoxia results in a decreased production of mature myelinating oligodendrocytes. Finally, I also show in primary mouse microglia cultures a differential cytokine response to LPS and hypoxia.

4 Characterisation of MMS in the neonatal and adult periods

4.1 Introduction

As discussed in the introduction, PTB is associated with an increased risk of lower IQ [528] and with various neurodevelopmental disorders [529], but the mechanisms behind these associations are largely unknown. Early life stress interacts with, and regulates gene networks which are enriched for variants associated with schizophrenia and major depressive disorder [530]. Moreover, early life stress in the form of temporary childhood neglect is associated with an increased incidence of ADHD and a lower IQ in later life [531]. However, the relevance of this to stress associated with PTB is unknown. Therefore, understanding the mechanisms of stress PTB may give important insight into the atypical neurodevelopment associated with PTB.

PTB is often accompanied by extended stays in the NICU, which is associated with stressors such as invasive procedures, sleep deprivation, excessive light and noise. However, the investigation of stress associated with PTB in humans is difficult, as stressful experiences such as painful procedures are invariably confounded by the severity of any associated pathology. This means independently assigning effects to stress is challenging in the preterm environment. Despite these difficulties, exposure to painful procedures has been independently associated with reduced MRI metrics in grey and white matter at term equivalent age, when various confounders are corrected for [532].

Canonical glucocorticoid signalling occurs through the binding of glucocorticoids to cytosolic GR and MR which then heterodimerise and elicit gene expression changes through direct DNA binding. Therefore, understanding transcriptomic changes following stress may provide insights into mechanisms and processes affected. This can be done by exploring the expression of candidate genes with qPCR, e.g. genes with well characterised responsiveness to GR signalling, such as *Per1* [533]. Alternatively, unbiased transcriptome-wide approaches (e.g. 3' mRNA sequencing) can be used to investigate the differential expression of mRNA [534]. Previous studies using a combination of maternal separation and limited nesting models have used RNA sequencing to profile gene expression in regions of the brain associated with reward, and have demonstrated that transcription factors may play a key role in the consequences of early life stress [535,536]. Therefore, investigating the enrichment of transcription factor binding sites in sequencing datasets may indicate transcription factors which drive any transcriptome alterations seen.

PTB and neurodevelopmental disorders are associated with alterations in various epigenetic marks, including DNA methylation; for example early life stress has also been associated with altered DNA methylation in humans [537] and animal models (maternal separation) [303]. It has been proposed that stress may alter DNA methylation through glucocorticoid and FKBP51 (encoded by *FKBP5*) signalling [366]. This may play an important role in stress associated learning, as exposure to early life stress can modify the subsequent response to stress [538]. As such, understanding the effect of early life stress on DNA methylation may provide insights into processes and mechanisms involved. A commonly used technique to assess both genome wide (with sequencing) or candidate (with qPCR) alterations in DNA methylation is DNA methylation immunoprecipitation (meDIP) [497]. This is similar to the technique used in the previous chapter to assess the presence of DNA hydroxymethylation.

To understand the effects of early life stress on adult outcome in animal models, behavioural tests are commonly employed. As early life stress in humans is associated with an increased risk of anxiety and depression in adulthood, tests of anxiety and depression are commonly used in models of early life stress. The elevated plus maze (EPM) and open field (OF) are used as tests of anxiety in rodents [539], where increased activity in exposed areas (i.e. the open arms in the EPM and the centre zone in the OF) is proposed to associate with reduced anxiety. The tail suspension test is a commonly used measure of depression like behaviour in mice [540], and has previously been used in the analysis of behaviour following early life stress [541].

As discussed in the introduction many neurodevelopmental disorders are associated with circadian rhythm abnormalities [542]. Some of these have been replicated in animal models, for example classic studies in non-human primates have shown circadian rhythm alterations in temperature regulation follow maternal separation [543]. The limited nesting material model in rodents also disrupts patterns of activity and sleep [544]. The monitoring of in cage habitual behaviour over the course of a normal day following early life stress would therefore provide valuable insights into the consequences of early life stress.

The most commonly used model of early life stress is maternal separation, in this model pups are removed from the home cage for 3+ hours per day for 10+ consecutive days. However, the mother is the sole source of nutrition during this developmental period and extended periods of maternal separation can produce hypoglycaemia in pups [309]. The neonatal brain is particular susceptible to fluctuations in glucose concentrations [545] and therefore distinguishing between the effects of nutrition and stress is difficult in this model. Maternal

separation may also be associated with variable stress exposure, as during the paradigm some pups may fall asleep while others may engage more with the stress, possibly leading to the conflicting results seen in this model. Moreover, traditional maternal separation models do not accurately recapitulate stress associated with the NICU, where frequent manual manipulations and sleep deprivation are common. Other models of early life stress such as the limited nesting model are models of fragmented maternal care and may be less relevant to stress associated with PTB. To better understand the consequences of stress associated with the preterm environment on brain development, better animal models are needed.

Therefore, in this chapter I developed a novel model of early life stress, modified maternal separation (MMS), which is relevant to PTB. I characterise the effect of MMS in both the neonatal and adult periods.

4.2 Hypotheses

1. MMS will induce changes in the transcriptome and DNA methylome of the hypothalamus
2. MMS will result in altered behaviour in the adult period

4.3 Aims

1. To assess growth and blood glucose dynamics associated with MMS
2. To use immunohistochemistry to evaluate glial proportions in the hypothalamus following MMS
3. To investigate the effects of MMS on the hypothalamic transcriptome in the neonatal period
4. To investigate the effects of MMS on the hypothalamic DNA methylome in the neonatal period
5. To examine the effect of MMS on behaviours during adulthood
6. To assess the effect of MMS on candidate gene expression in the HPA axis in adulthood
7. To assess the effect of MMS on DNA methylation at candidate loci in the hypothalamus in adulthood

4.4 Methods

4.4.1 Animals and MMS

Only C57BL/6JOlaHsd male animals were used in the following experiments. For breeding, 2 females and 1 male were kept in a single cage. On P3, male pups were randomised to control or MMS groups and received a subcutaneous ink injection to the footpad for identification purposes. On P4, pups assigned to the MMS group were removed from their home cage and placed on a heating pad. They were repeatedly inverted to the supine position for 1.5 hours/day for 3 consecutive days (P4-P6). MMS was carried out adjacent to the home cage to allow for communication through ultrasonic vocalisation. Control pups were left in the home cage whilst MMS was carried out. Both groups were handled at the start of the paradigm in a similar manner.

Following MMS, one cohort of animals was killed, and brains extracted. The brain was divided in half along the midline, with one half snap-frozen on dry ice for subsequent RNA/DNA extraction and the other half fixed overnight in 4% paraformaldehyde for paraffin embedding, sectioning and immunohistochemistry. An n of 10/group was used for this set of experiments, with the specific n for each experiment identified in their associated figure legends in the results section.

Following MMS, a second cohort were returned to the home cage and allowed to mature without further intervention. They were weaned at P21, with control and MMS littermates housed together. At P90-P130 behavioural testing was carried out. Animals were then killed by cervical dislocation, tissue extracted and snap frozen for subsequent analysis. An n of 11/group was used for these experiments, with the specific n for each experiment mentioned in the associated figure legend in the results section.

4.4.2 Immunohistochemistry

Following embedding in paraffin, 5µm coronal forebrain sections were cut using a microtome. Sections were arranged, 3/slide and deparaffinisation and immunohistochemistry was carried out as previously described. Images were taken using an AxioScan slidescanner and quantification was done using image J. 3 consecutive sections per animal were quantified and averaged to obtain an n of 1. Iba1+ and Olig2+ cells were normalised to area, while GFAP+ cells were quantified as percent coverage.

4.4.3 RNA profiling (qPCR and 3' mRNA sequencing)

RNA was isolated from frozen tissue as previously described. For candidate gene analysis with qPCR, 1 µg of RNA was reverse transcribed into cDNA following DNAse treatment. Expression of candidate genes was measured using FAM hydrolysis on a Roche 480 LightCycler and normalised to expression of *TBP*.

3' mRNA sequencing was carried out by staff at the Wellcome Trust Clinical Research Facility, at the Western General Hospital, Edinburgh. Library preparation was done with 500ng of RNA, and sequencing carried out with 12 samples per chip. Data were mapped to the mm10 genome and differential gene expression analysis done using Degust with the Voom/limma method.

4.4.4 meDIP sequencing

DNA was isolated from the hypothalamus as previous described. Immunoprecipitation was carried out on 2.5µg of sonicated DNA after aliquoting 10% input for normalisation. An IgG control was included with each immunoprecipitation. Whole genome amplification was done before sequencing and efficiency of immunoprecipitation and homogeneity of whole genome amplification were assessed using qPCR for previously identified positive and negative regions [497].

Ion torrent sequencing was done by the staff at the Wellcome Trust Clinical Research Facility, at the Western General Hospital, Edinburgh. 3 samples were sequenced per chip and data mapped to the mm10 genome annotation. Downstream analysis was done using Galaxy.

4.4.5 Elevated plus maze (EPM)

Animals were tested with the EPM at P90-P100. Animals were habituated to the novel holding area outside the testing room for at least 1 hour prior to testing. Then animals were taken in one at a time for testing. They were placed in the centre of the maze facing the closed arm and allowed to explore the maze for 5 minutes. Their movement was tracked and quantified by the AnyMaze software. The maze was cleaned with 70% ethanol and residual ethanol allowed to evaporate for 5 minutes prior to testing the next animal.

4.4.6 Open field (OF) maze

Animals were tested in the OF 24 hours after the EPM. The animals were also habituated to the holding area for 1 hour prior to testing and animals tested one at a time. For testing, animals were taken into the testing room and placed in the centre of the OF and allowed to

explore the maze for 5 minutes. Similar to the EPM the animal's movement was tracked and quantified with the AnyMaze software and the apparatus was cleaned with 70% ethanol between tests with 5 minutes evaporation time allowed for residual ethanol.

4.4.7 Tail suspension test

The tail suspension test was carried out 1 hour after the OF. An 18 cm piece of tape was attached to the mouse's tail, which was then attached to an edge 50 cm above the floor. The mouse was left for 6 minutes and its activity recorded. The total time immobile for each animal was quantified blindly.

4.4.8 In cage monitoring

Circadian metabolic and activity parameters were measured use the TSE-Systems PhenoMaster. Animals were single housed for habituation to the novel spout of the water bottle used with the system for 4 days prior to measurement. Animals were introduced to the system and left for 4 days; data from the first 24 hours were discarded as mice acclimatised to the novel environment. During this time mice had *ad libitum* access to food and water as usual. For normalisation of calorie expenditure data, TD-NMR was performed before and after the PhenoMaster, with the averaged lean mass of the 2 measurements used for normalisation.

4.5 Results

4.5.1 Assessment of growth, blood glucose dynamics, corticosterone and candidate gene expression following MMS

Considering the potential nutritional deficiencies associated with other models of early life stress, I first assessed growth dynamics during MMS and blood glucose levels immediately following MMS. As seen in Figure 4.1A, there were no differences in weight gain between the control and MMS groups. There was no difference in weight at the start of the paradigm on P4 (see Figure 4.1B), the brain/body weight ratio on P6 (see Figure 4.1C) or blood glucose levels at P6 (see Figure 4.1D). I next tested plasma corticosterone levels on P6 in both control and MMS groups, as it is the principal hormonal stress mediator in rodents. As seen in Figure 4.2, there were no differences between groups in plasma corticosterone as measured by ELISA.

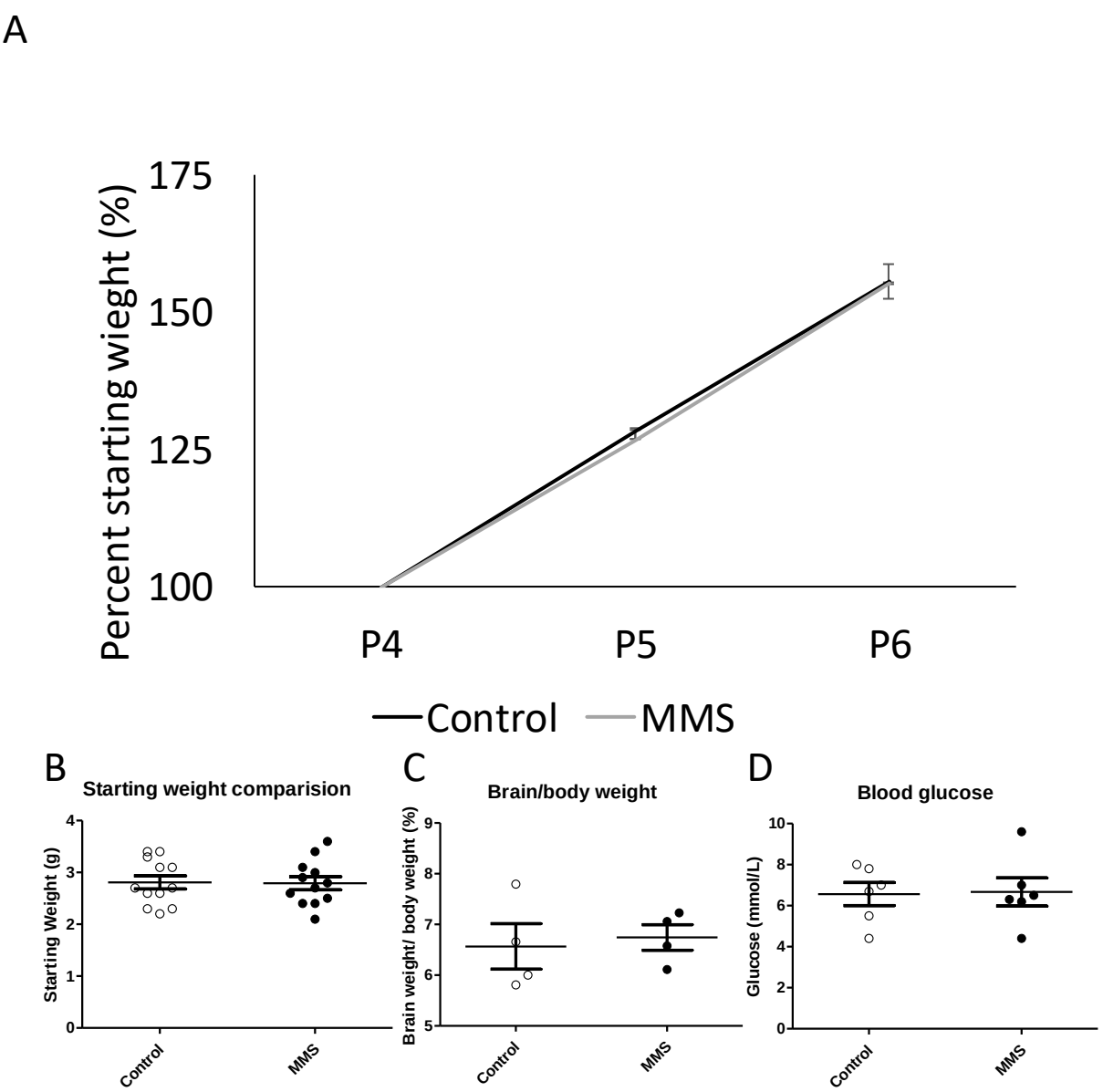

Figure 4.1 Weight was measured immediately before MMS in both control and MMS groups from P4-P6. In A, weight was normalised to the starting weight at P4, with no effect of MMS on weight gain (control-black line, MMS-grey line)(p=0.94, f-statistic=0.015, df=60), n=11/group. B shows there was no difference between control and MMS groups in starting weight (p=0.95, df=18), n-=11/group. C demonstrates MMS was not associated with an altered brain/body weight ratio at P6 (p=0.45, df=3), n=4/group. In D, blood glucose measured immediately following the paradigm on P6 shows no difference between groups (p=0.91, df=5), n=6/group. In B-D, the control group are represented by the clear circles with the MMS group represented by the black filled circles. A was compared using a repeated measures ANOVA and B-D were compared using an independent t-test. Error bars indicate standard error of the mean.

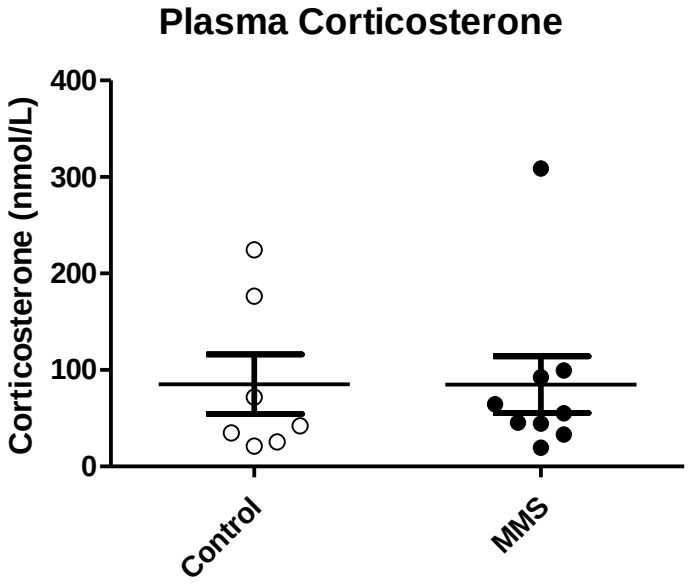

Figure 4.2 Corticosterone was measured by ELISA in plasma isolated immediately following MMS on P6. There was no difference between the control group (clear circles) and the MMS group (black filled circles) (p=0.29, df=6) as indicated by an independent t-test, n=7-9. Error bars indicate standard error of the mean.

I next investigated candidate gene expression in the hypothalamus of control and MMS groups using qPCR. As seen in Figure 4.3, *Per1* and *DNMT1* were increased in expression following MMS, but there were no differences in the expression of the *GR*, *MR* or *DNMT3a*.

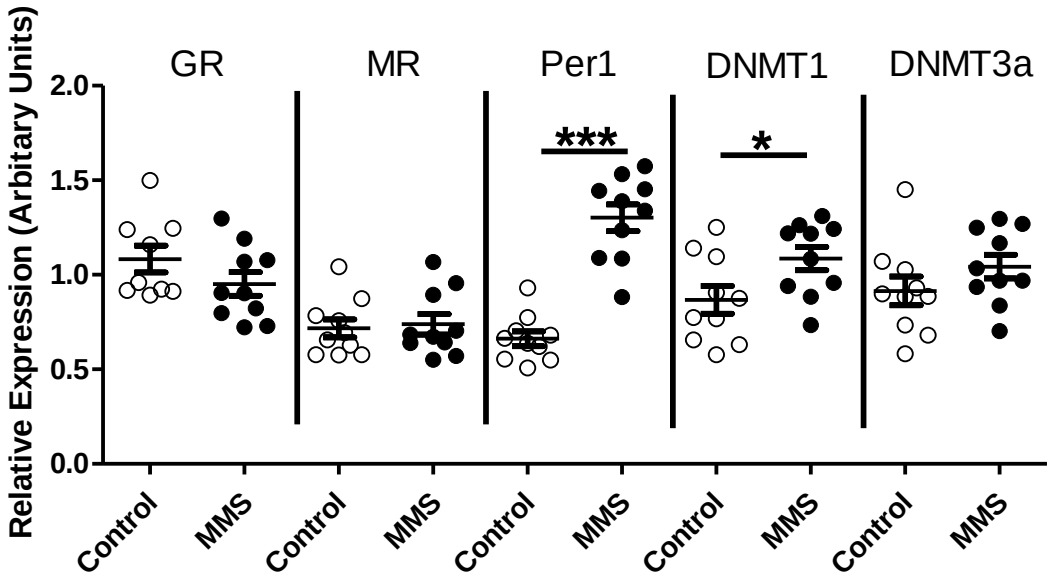

Figure 4.3 Candidate gene expression in hypothalamic tissue immediately following the paradigm on P6 was measured by qPCR and normalised to the expression of TBP. There were no differences in the expression of the GR (p=0.053, df=9), MR (p=0.49, df=10) or DNMT3a (p=0.09, df=9) but Per1 (p=0.009, df=9) and DNMT1 (p=0.03, df=9)

*were increased in expression as indicated by independent t-tests, n=9-11. The control group are represented by clear circles and the MMS group by black filled circles. * indicates p<0.05, *** indicates p<0.001. Error bars indicate standard error of the mean.*

4.5.2 Iba1+, Olig2+ and GFAP+ cell proportions in the hypothalamus following MMS

Glial cells are crucial to typical brain development and are very plastic to insults. The *GR* is ubiquitously expressed in the brain and therefore glucocorticoid signaling may affect these cells. Therefore, I investigated the proportion of GFAP+ astrocytes, Iba1+ myeloid cells and Olig2+ cells of the oligodendrocyte lineage using immunohistochemistry. As seen in Figure 4.4, there were no differences in the proportion of GFAP, Iba1 or Olig2 labelled cells in the hypothalamus immediately following the paradigm at P6.

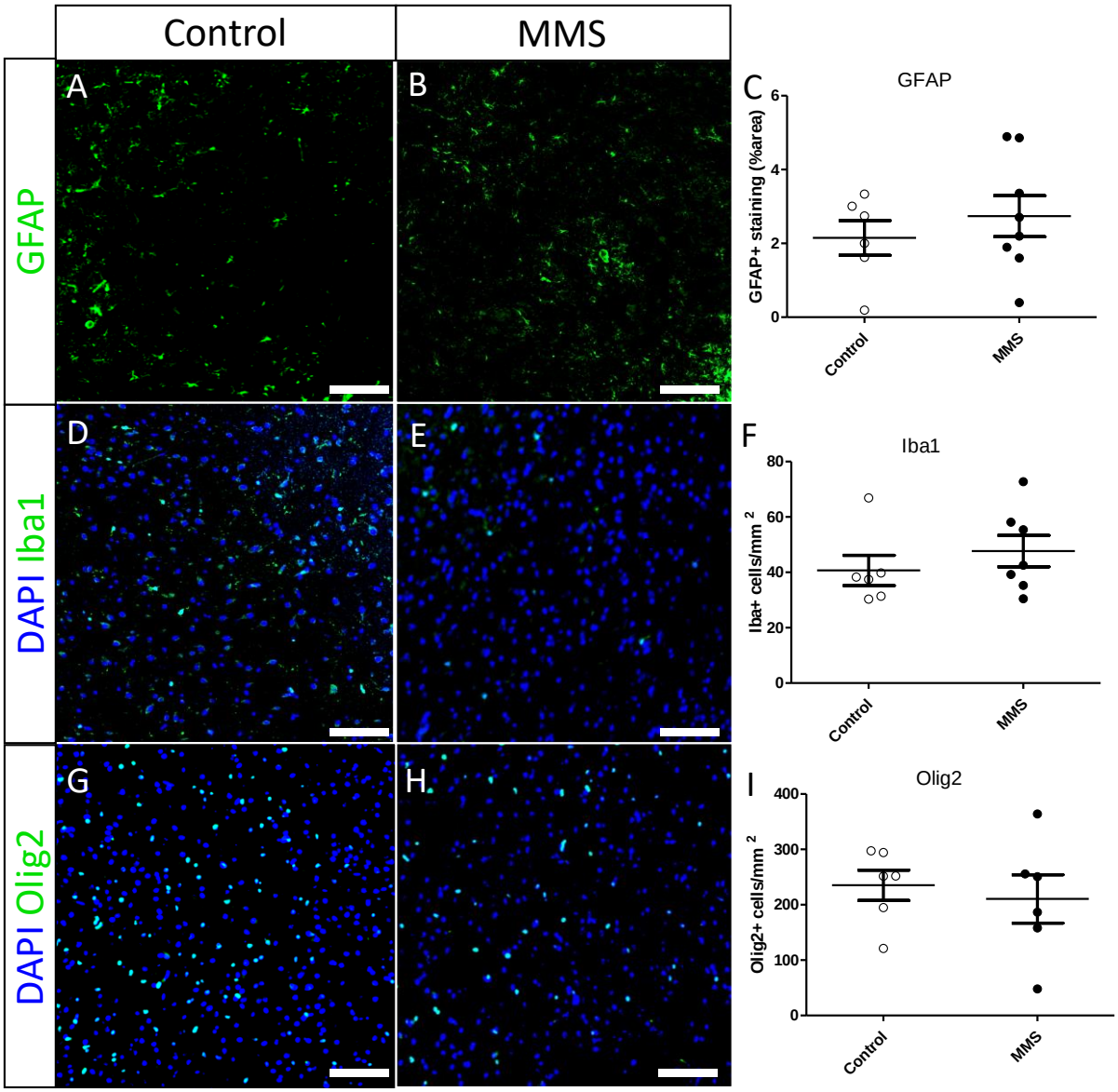

Figure 4.4 Paraffin sections were stained for GFAP, Iba1 and Olig2. In A and B, representative images of GFAP+ staining from the hypothalamus are shown. In C, GFAP+ cells are quantified as percent coverage in control (clear circles) and MMS (black filled circles) pups with no differences found (p=0.867, df=5). In D and E, representative images from Iba1 (green) and DAPI (blue) stained hypothalamic sections are shown, which are quantified in F as cells/mm^2 for control (clear circles) and MMS (black filled circles) pups, no differences were found (p=0.311, df=4). In G and H, representative images of Olig2 (green) and DAPI (blue) stained hypothalamic sections are shown, which are quantified in I as Olig2+ cells/mm^2 for control (clear circles) and MMS (black filled circles) pups (p=0.791, df=5). Scale bar indicates 100µm. All statistical comparisons were made using independent t-tests, n=6-9. Error bars indicate standard error of the mean.

4.5.3 Assessment of the hypothalamic transcriptome using 3' mRNA sequencing

As there were changes in candidate gene expression (see Figure 4.3) following MMS in the hypothalamus, I next evaluated transcriptome wide disruptions in the hypothalamic mRNA using 3' mRNA sequencing. As seen in Figure 4.5A, there was only a single gene with an FDR corrected <0.05 (*D630033O11Rik;* FDR of 0.002131, unadjusted p-value of 4.92E-08, logFC of 2.662301), and using an MDS plot to cluster the samples in an unbiased fashion there was no discernable pattern (see Figure 4.5B). This indicates that MMS resulted in minimal and only subtle transcriptional changes in the hypothalamus at P6.

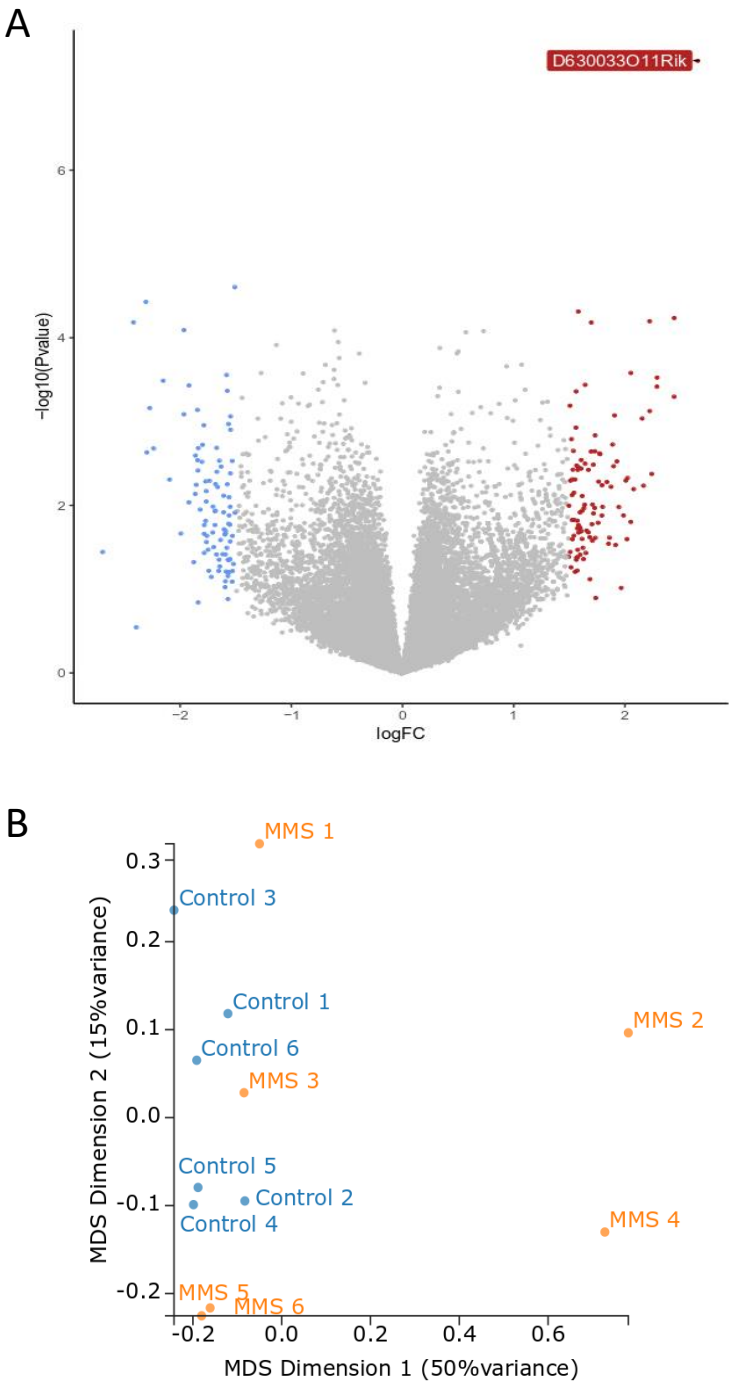

Figure 4.5 3' mRNA sequencing was done on RNA extracted from the hypothalamus of control and MMS groups (n=6/group). In A, a volcano plot shows all genes which were analysed for differential expression using the Voom/limma method. Blue and red dots indicate genes which had a logFC less or more than 1.5, respectively. Only 1 gene had an FDR corrected of<0.05, D630033O11Rik, which is indicated with its name. In B an MDS plot is used to cluster all samples in an unbiased fashion. The x-axis represents Dimension 1, which accounted for 50% of the variation in the data. The y-axis represents Dimension 2, which accounted for 15% of the variation in the dataset. There were no distinct clustering patterns between control (blue dots) and MMS (orange dots) samples.

I then used the genes with a logFC greater than 1.5 (as indicated by the blue and red dots in Figure 4.5A) for gene ontology analysis to indicate broad processes which are involved in subtle transcriptional changes. As seen in Figure 4.6A, there was enrichment in the cellular component and biological process categories for terms related to motile cilia. Also, under molecular function, terms enriched included “DNA-binding RNA pol specific” and “ligand-gated cation channel activity”. Two genes which were included under these terms were *NR4A3* and *FOS* respectively. These genes were validated by qPCR and showed significant upregulation, confirming the validity of this method (see Figure 4.6B).

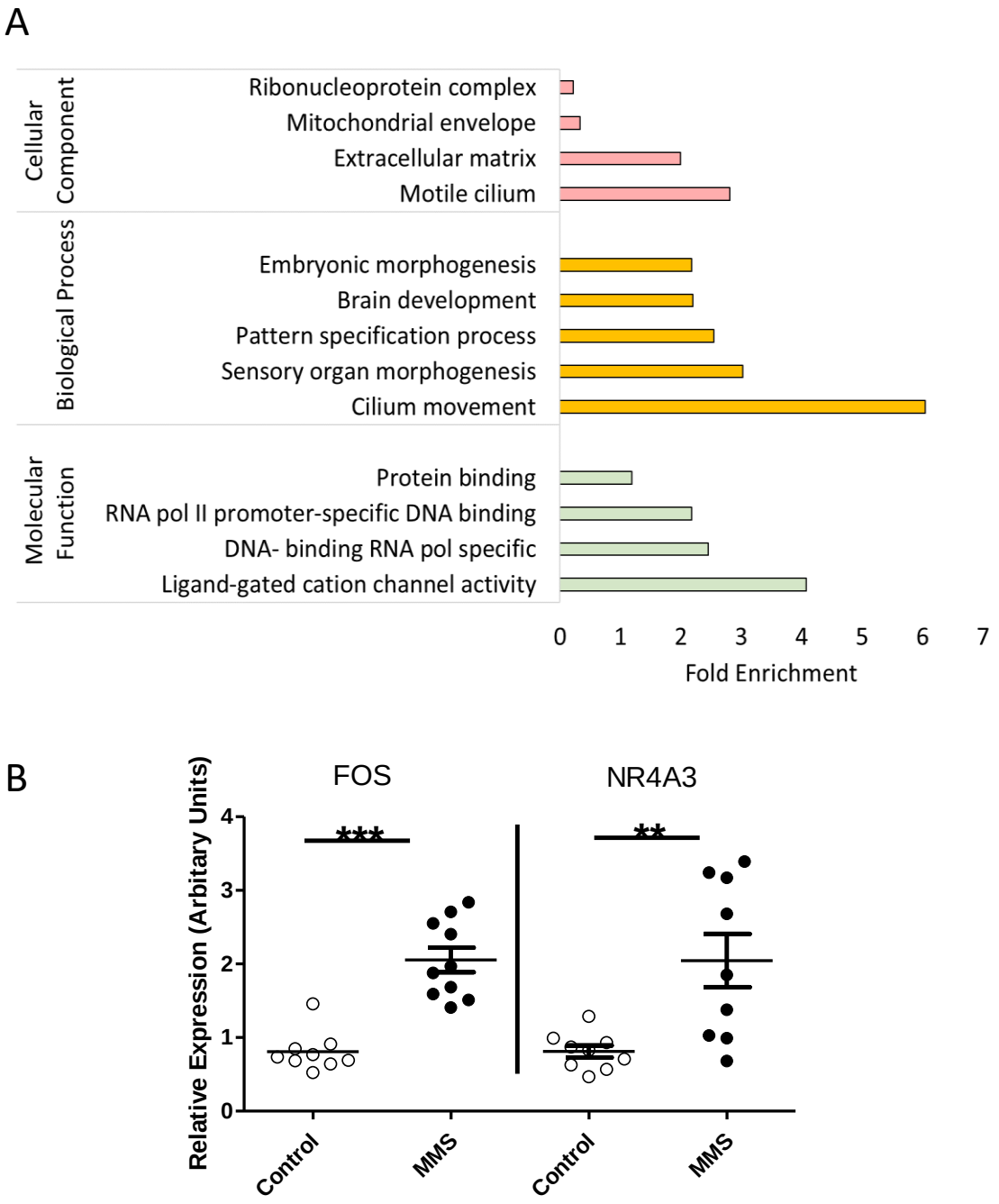

*Figure 4.6 In A, the results of a gene ontology analysis are shown. Analysis was done for genes with a logFC change of greater than 1.5. Enriched terms were classified under cellular component (pink), biological process (yellow) and molecular function (green). Examples of enriched terms are those relating to the cilium and neuronal activity. Genes identified in the "DNA-binding RNA pol specific" and "Ligand-gated cation channel activity" included NR4A3 and Fos, respectively. In B, they were validated by qPCR and were significantly increased (p=<0.001 and 0.002 for FOS and NR4A3, respectively, df=16) in their expression as indicated by an independent t-test, n=9-10. ** indicates p<0.01, *** indicates p<0.001. Error bars indicate standard error of the mean.*

Using the same threshold of a logFC greater than 1.5, I carried out a transcription factor enrichment analysis with the Opossum software, to identify motifs associated with the binding of particular transcription factors which were enriched among the genes. The results, which are presented in Figure 4.7, show enrichment for transcription factors of the NFkB family and other transcription factors such as Klf4 and SP1, which are important in a variety of pathways including neuronal differentiation and activation.

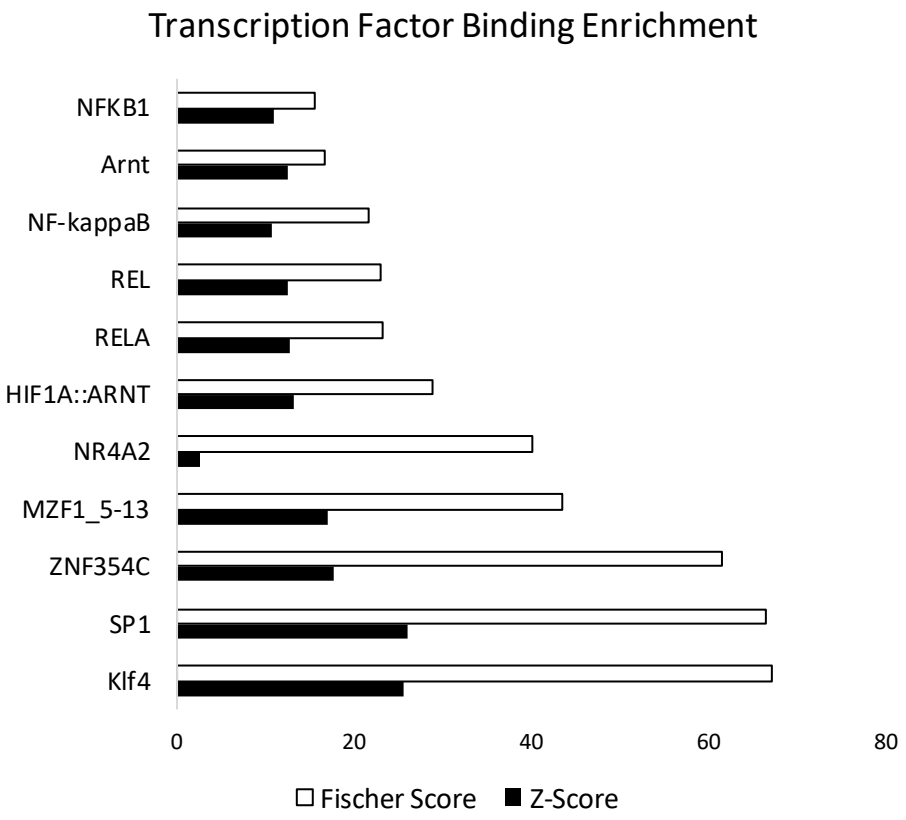

Figure 4.7 Transcription factor binding enrichment analysis of genes with a logFC of greater than 1.5 indicates enrichment for motifs associated with the NFkB pathway and pathways involved in differentiation and neuronal activity (i.e. KLF4 and SP1). For each transcription factor 2 metrics of enrichment, Fischer score (clear bars) and z-score (black bars) are included. Analysis was done using the Opossum software.

4.5.4 Investigation of DNA methylation in the hypothalamus following MMS

As I saw increased expression of the DNA methylase, *DNMT1*, in the hypothalamus following MMS (see Figure 4.3), I chose to investigate broad patterns of DNA methylation in the hypothalamus using meDIP (see Figure 4.8A for a schematic describing this approach). Differentially methylated regions were identified using the DESeq2 method, which showed substantial overlap with an alternative method, edgeR (see Figure 4.8B). Differentially methylated regions were annotated and catalogued as to their genomic association (as seen in Figure 4.8C). Regions which could not be annotated such as long repetitive regions were omitted at this stage. Of these regions, those annotated to protein coding regions were further subdivided into their respective genomic locations (see Figure 4.8D). The 4501 (see Figure 4.8C "protein") identified differentially methylated regions associated with protein coding regions, were associated with 2594 unique genes, which were then analysed used gene ontology.

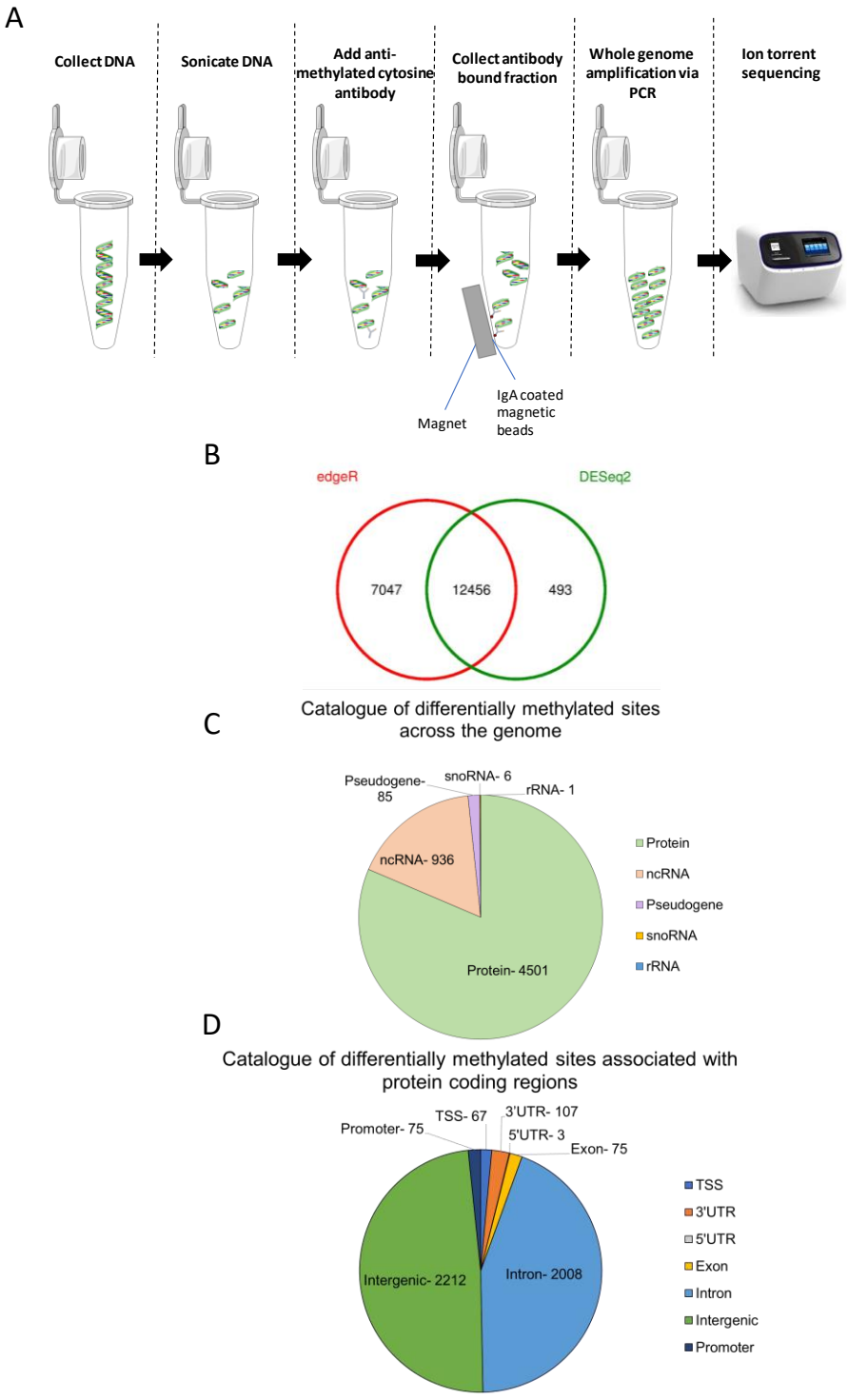

Figure 4.8 A) shows a schematic of the meDIP protocol. DESeq2 was used to assess differential methylation. B) shows there was substantial overlap between DESeq2 (green circle) and edgeR (red circle) methods (numbers indicate quantity of differentially methylated regions found using each method). In C, annotated regions which were differentially methylated between control and MMS groups are catalogued by their associated genomic elements. In D, the differentially methylated regions from the "protein" category in C are further subdivided into their genomic locations.

Unbiased clustering of all differentially methylated regions, using a principal component analysis (see Figure 4.9A), demonstrated MMS had a specific and distinct effect on DNA methylation within the hypothalamus. In Figure 4.9B, a volcano plot of all regions assessed for differential methylation is shown, with significantly differentially methylated regions shown in pink. All significantly differentially methylated regions were then grouped into a heat map and clustered by Euclidean distance (see Figure 4.9C). Samples were then correlated using a correlation heatmap, as seen in Figure 4.9D.

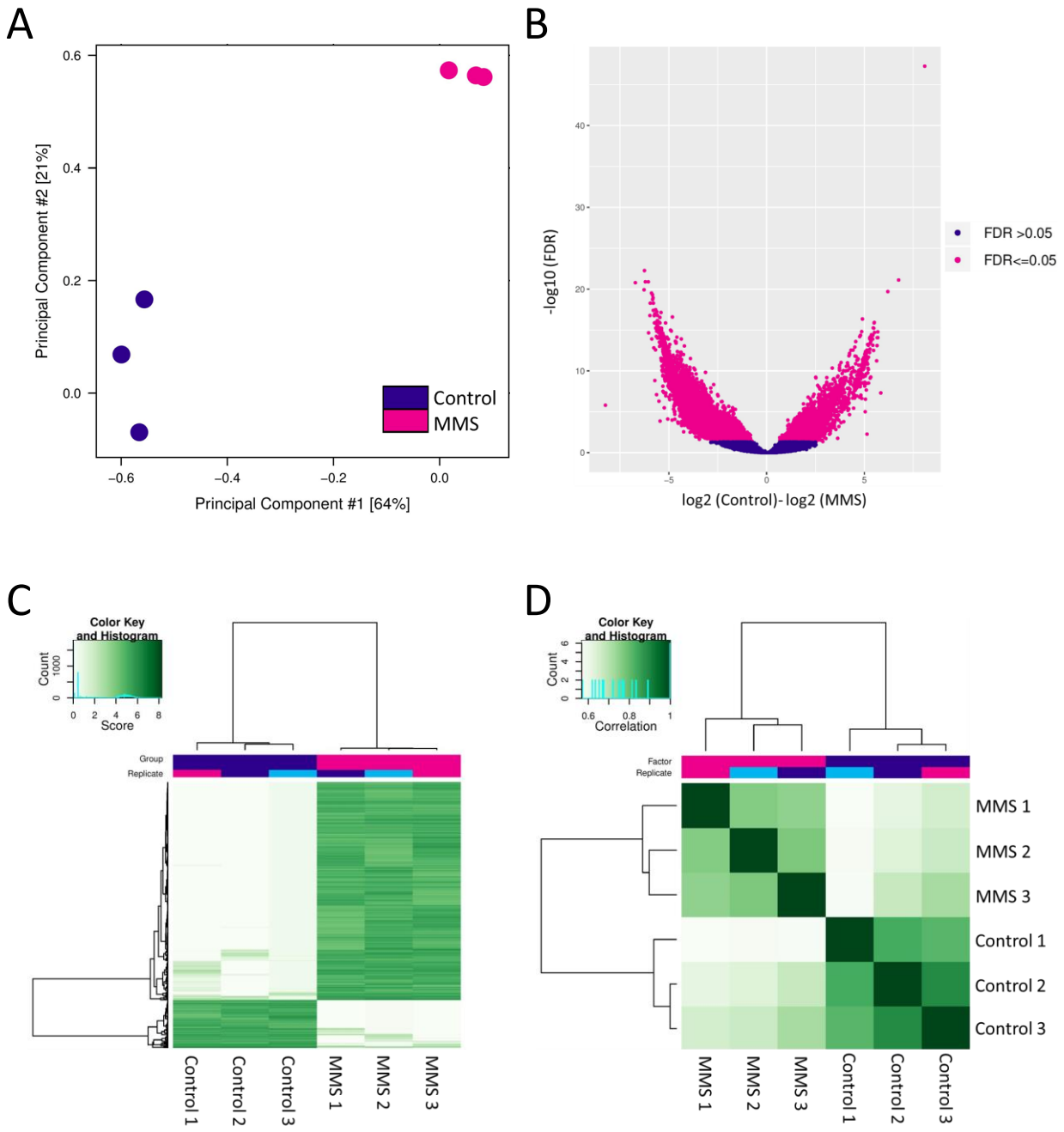

Figure 4.9 In A, a principal component analysis of samples from control (dark blue) and MMS (pink) groups shows a distinct and specific effect of MMS on DNA methylation. In B, a volcano plot of all regions assessed for differential methylation is shown. Samples with an FDR corrected <0.05 are indicated in pink, while those with an FDR corrected >0.05 are shown in dark blue. In C, a heatmap shows all differentially methylated regions clustered by Euclidian distance, with dark green indicating an increase in methylation with white indicating a decrease in methylation. A correlation heatmap is shown in D, with dark green indicating a higher degree of correlation and white indicating a lesser degree of correlation.

Gene name	Neurodevelopmental relevance	Reference
Cdon	Involved in neuronal migration	Powell, 2015 [546]
Gprin1	SNPs implicated in schizophrenia	Qin, 2005 [547]
Dnajc14	Decreased expression in the PFC of individuals with Schizophrenia	Arion, 2007 [548]
Fzd1	Involved in differentiation and presynaptic function	Varela-Nallar, 2009 [549]
Mast1	Mutations associated with cerebellar hypoplasia, corpus callosum and cortical abnormalities	Tripathy, 2018 [550]
Zbtb16	Corticosteroid responsive transcription factor	Fahnenstich ,2003 [551]
Adarb1	Decreased expression in postmortem tissue of individuals with schizophrenia and bipolar disorder	Kubota-Sakashita, 2014 [552]
Uhrf2	Reader of 5mC and 5hmC, shown to interact with DNMT1	Zhang,2011 [553] and Zhou, 2014 [554]
Cdh10	SNPs implicated in ASD and associated with excitatory/inhibitory balance	Wang, 2009 [555] and Smith,2017 [556]
Atf7	Involved in NFkB signaling and subsequent telomere shortening in neonatal infants	Lazarides, 2019 [557]
Wbscr17	Deleted (1 of 26 genes) in Williams-Beuren syndrome and SNPs in mothers increase risk of ASD in offspring	Connolly, 2017 [558]
Robo3	Mutations cause horizontal gaze palsy and progressive scoliosis due to abnormal axon guidance	Fricke, 2001 [559]
Usp44	Loss of function mutation associated with intellectual disability	Harripaul, 2018 [560]
Mlxipl	Involved in Williams-Beuren syndrome	Cairo, 2001 [561]
Diaph3	Involved in cell migration and guidance, may function down stream of SHANK3. Implicated in ASD	Vorstman, 2011 [562]
Kiz	Implicated in ASD	Alonso-Gonzalez, 2019 [563]
Trim32	Implicated in neurodevelopmental disorders including ASD and ADHD	Lionel, 2014 [564]

Snrpn	Methylation level at this locus, in blood, is associated with adult and childhood cognitive abilities	Lorgen-Ritchie, 2019 [565]
Lypd1	Plays a role in anxiety related behaviour	Tekinay, 2009 [566]
Pla2g4a	SNPs implicated in Schizophrenia	Peet, 1998 [567]
Bmp3	SNPs near locus associated with cognitive decline in patients with schizophrenia	Hashimoto, 2013 [568]

Figure 4.10 Genes with a previously identified role in neurodevelopment or neurodevelopmental disorders which were found among the top 100 differentially methylated regions identified by meDIP sequencing, along with their relationship with neurodevelopment.

Many of the genes found to be differentially methylated have also been associated with neurodevelopmental disorders, see

Figure 4.10 for more information. Therefore, I performed a gene ontology analysis of all significantly differentially methylated regions which were annotated to protein coding genes (see Figure 4.11). Under the category of cellular component, all enriched terms were associated with the synapse. Under molecular function, enriched terms were associated with cell adhesion and transcription factor binding. Under the category of biological processes, synaptic and cell adhesion terms once more appeared.

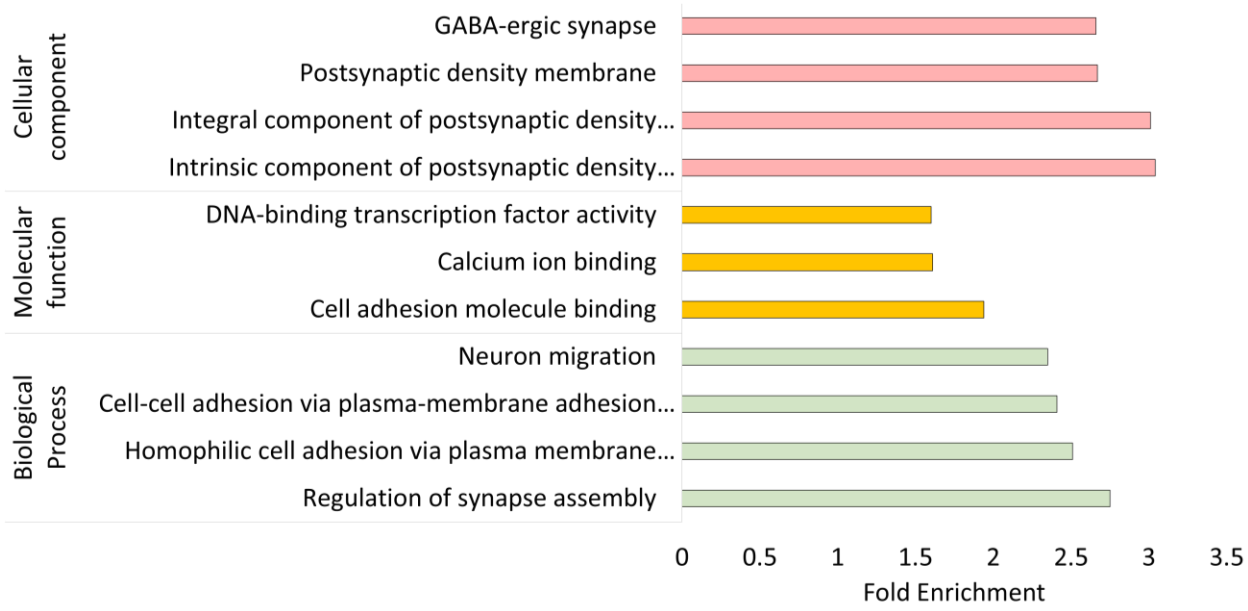

Figure 4.11 Gene ontology analysis of differentially methylated regions associated with protein coding regions was done for terms associated with cellular component (pink), molecular function (yellow) and biological processes

(green). Enriched terms included terms related to synaptic elements in the cellular component and biological processes categories

As the term "DNA-binding transcription factor activity" was enriched, I decided to look for enrichment of transcription factor binding motifs around differentially methylated genes. As seen in Figure 4.12 this was done for all synapse associated genes as indicated by the Gene Ontology analysis. All transcription factors with a Fisher score higher than 7 are shown in Figure 4.12A, with a subset listed underneath in Figure 4.12B with their function indicated. In Figure 4.12C, the same analysis is done but for genes with differential methylation in the promoter region. Only two transcription factors had a Fisher score of higher than 7, both of which have important roles in cell proliferation.

A

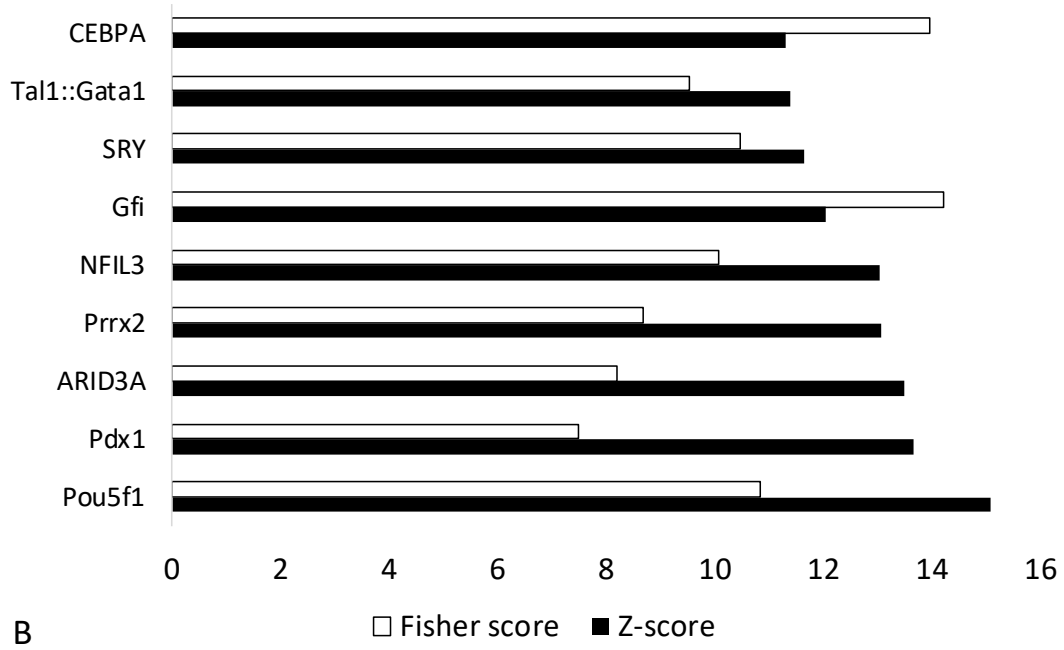

B

Synapse related genes			
Transciption Factor	**Information**	**Z-score**	**Fisher score**
Pou5f1	Master regulator of stem cell self renewal (Oct4 is coding protein)	15.098	10.84
NFIL3	Key regulator of circadian rhythms	13.047	10.078
SRY	Master regulator of male sexual development	11.654	10.492

C

Differentially methylated promoter regions			
Transcription factor	**Information**	**Z-score**	**Fisher score**
Klf4	Stem cell self renewal, dysregulation in mice leads to hydrocephalus	11.921	10.61
Zfx	Overexpressed in gliomas	10.615	7.842

Figure 4.12 Transcription factor binding enrichment analysis was done for differentially methylated regions associated with synaptic genes (A and B) and genes which had differential methylation in their promoter regions

(C). In A, transcription factors with a Fischer score of higher than 7 are shown, with Fischer score (clear bars) and z-score (black bars) indicated. In B, candidate transcription factors from A are listed. In C, all transcription factors with a Fischer score of greater than 7 for differentially methylated regions in characterized promoters are listed.

Next I evaluated the relationship between DNA methylation and expression. I identified all common genes with a logFC change in expression greater than 0.5 and those which were also differentially methylated. The expression of these genes was not correlated with their methylation, see Figure 4.13.

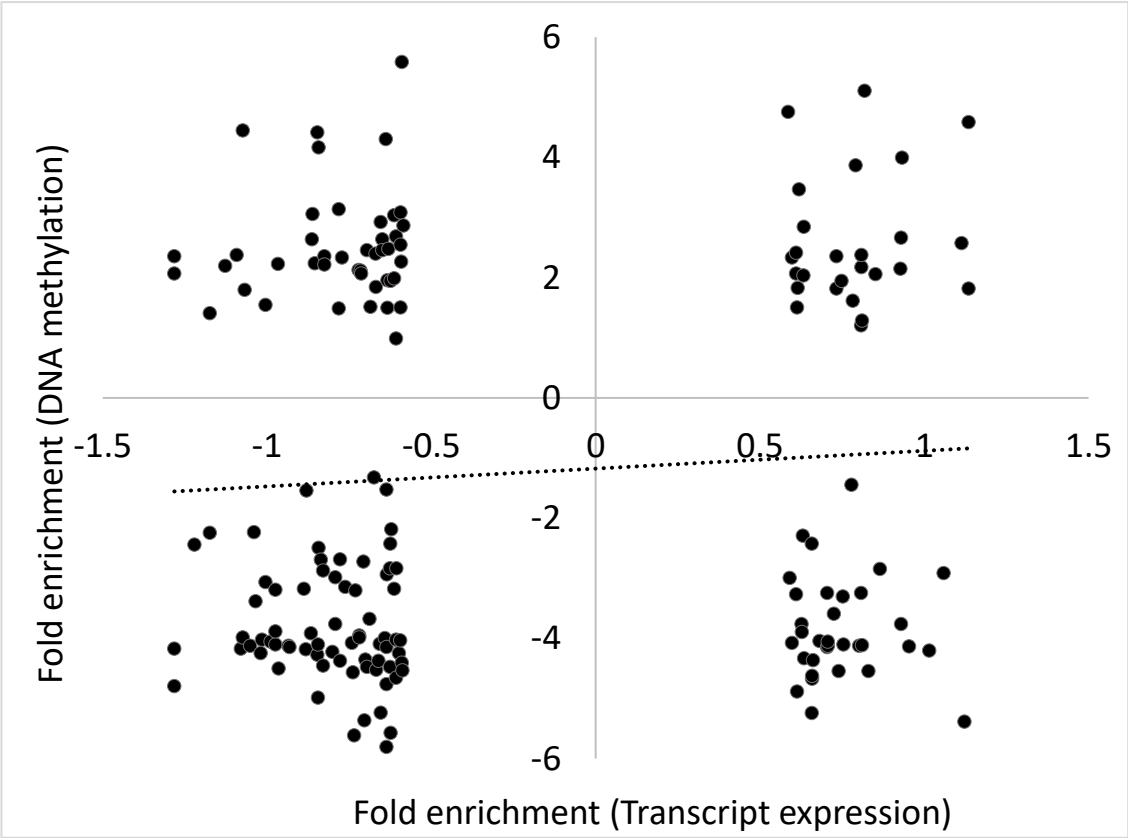

Figure 4.13 Genes with a change in expression of logFC of 0.5 or more as indicated by 3' mRNA sequencing and which were associated with a differentially methylated region (greater than or equal to 2-fold change) were correlated using a Pearson correlation. There was found to be no correlation with transcript expression and differential methylation (correlation coefficient=0.07 and p=0.36).

4.5.5 The effect of MMS on behaviours during adulthood

Next, I investigated the effect of MMS on behaviour during the adult period using the EPM at 3 months of age. Representative track plots from control and MMS groups can be seen in Figure 4.14A and B respectively, with the location of the open and closed arms indicated in

A. Animals from the MMS group travelled further during the testing period but did not have an altered preference for the open arms, closed arms or centre zone, as seen in Figure 4.14C and D respectively. The MMS group also had a higher average speed and a higher mobile time, as seen in Figure 4.15A and B. The MMS group travelled further in the closed arm but had the same average duration of visit, as seen in Figure 4.15C and D. However, there were no differences between the control and MMS group in distance travelled in the open arm or the average duration of visit to the open arm, as seen in Figure 4.15E and F.

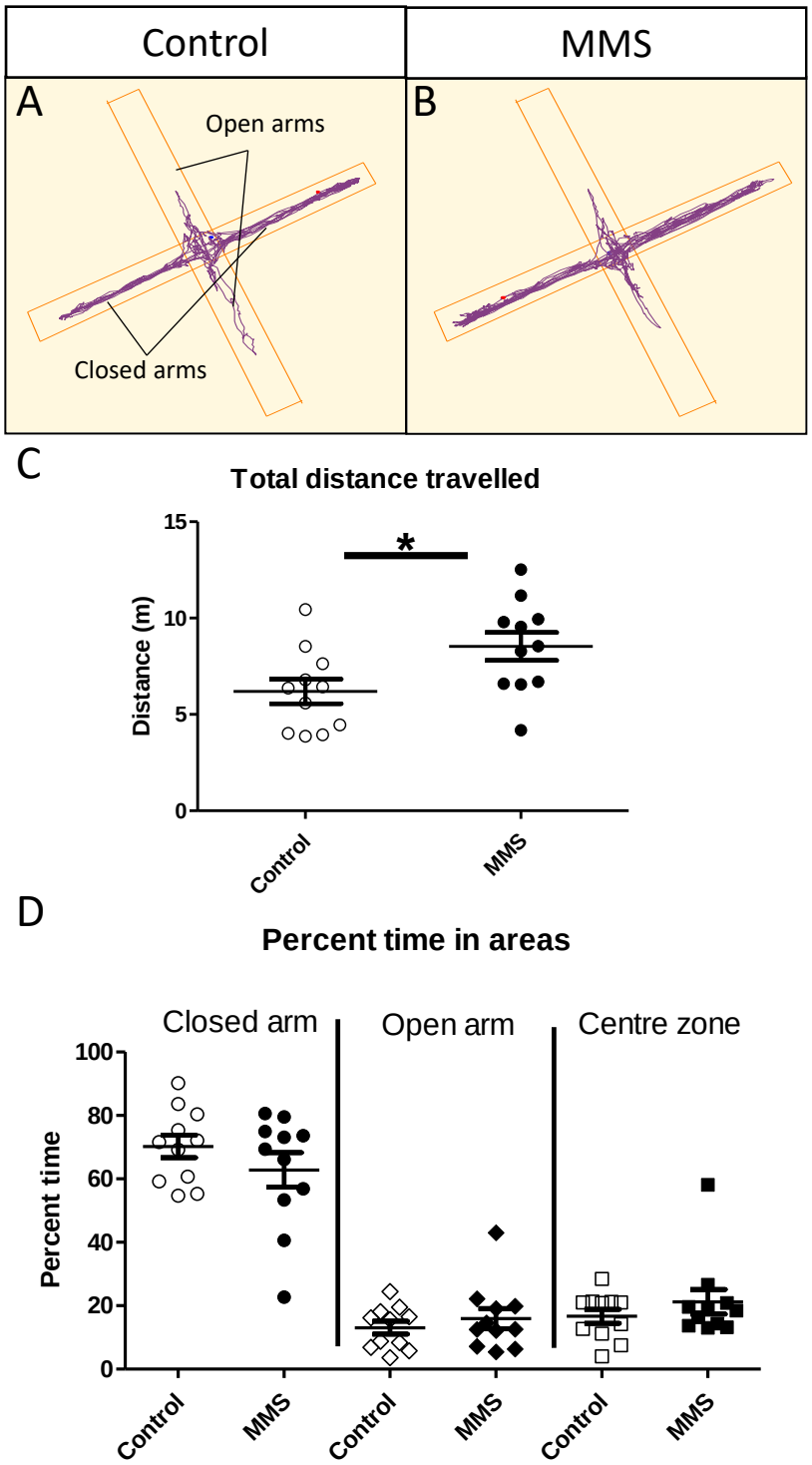

*Figure 4.14 At 3 months of age mice were tested with the EPM. In A and B representative track plots can be seen, with the open and closed arms indicated in A. The MMS group travelled further during the testing period (p=0.02, df=20) with no difference in time spent in the open arms, closed arms or centre zone (p=0.46, 0.27 and 0.32 respectively, df=20 for all zones). All statistical comparisons were made using independent t-tests, n=11 for all groups in all graphs. * indicates p<0.05. Error bars indicate standard error of the mean.*

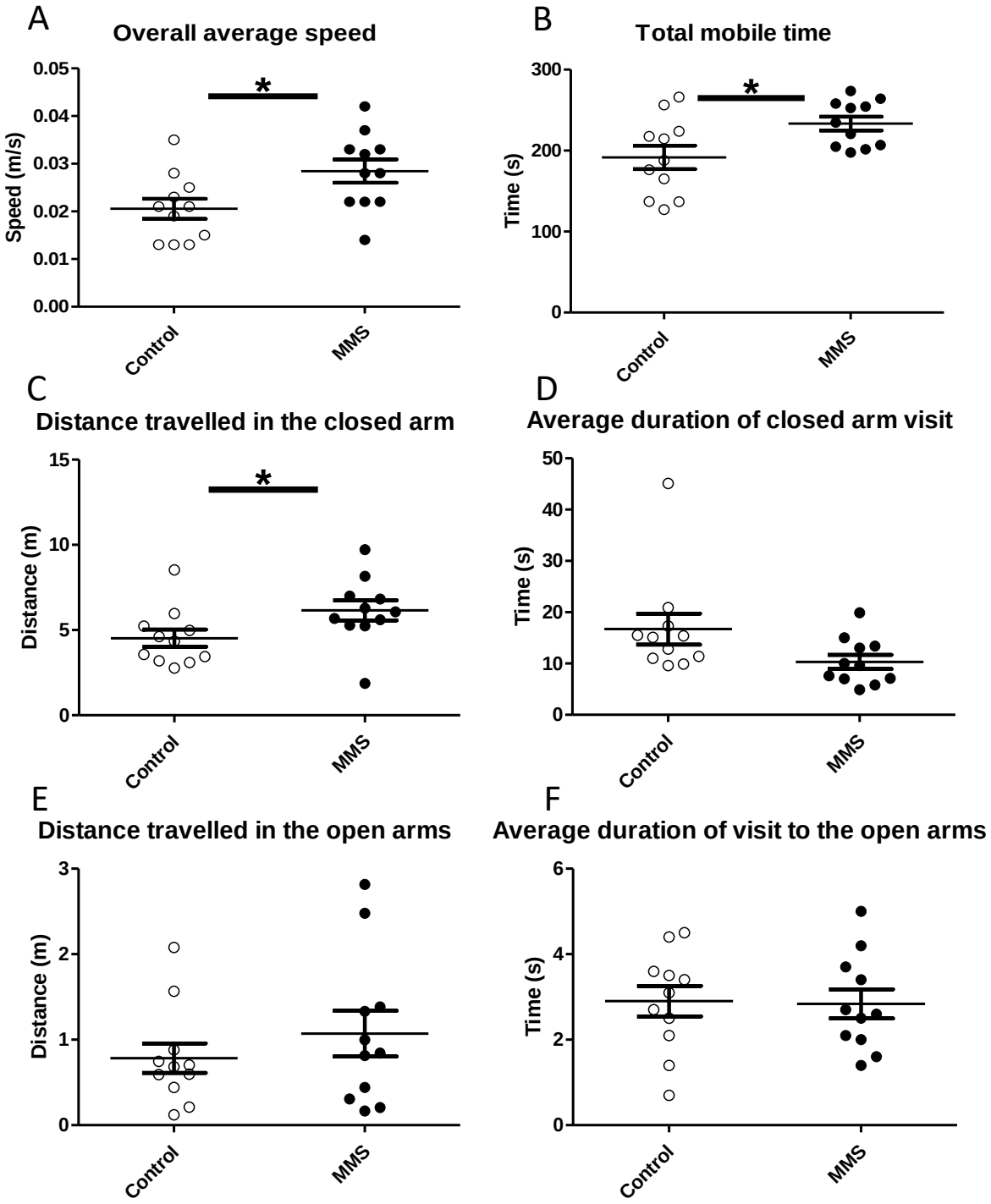

Figure 4.15 Further results from the EPM. The MMS group travelled at a faster overall speed (p=0.02, df=20) and spent a greater amount of time mobile (p=0.02, df=20), as seen in A and B respectively. In the closed arm only, the MMS group travelled further (p=0.048, df=20) but spent the same amount of time there during each visit (p=0.27, df=20), as seen in C and D respectively. In the open arms only, there were no differences between control and MMS groups in distance travelled (p=0.38, df=20) or duration of visit (p=0.90, df=20), as seen in E and F respectively. All

*statistical comparisons were made using independent t-tests, n=11 for both groups in all graphs. * indicates p<0.05. Error bars indicate standard error of the mean.*

Mice were then tested in the OF, representative track plots for control and MMS groups can be seen in Figure 4.16A and B with the inner and outer zones of the OF indicated in A. Similar to the EPM, the MMS group travelled further with no altered preference for time spent in the inner or outer zones during the course of the test, as can be seen in Figure 4.16C and D. The MMS group also moved faster with a higher total mobile time, see Figure 4.16and F. The MMS group travelled further in the outer zone, but had a shorter average length of visit, as seen in Figure 4.16G and H. Mice from the MMS group also travelled further within only the inner zone, with no difference in the average length of their visit to this zone, as seen in Figure 4.16I and J.

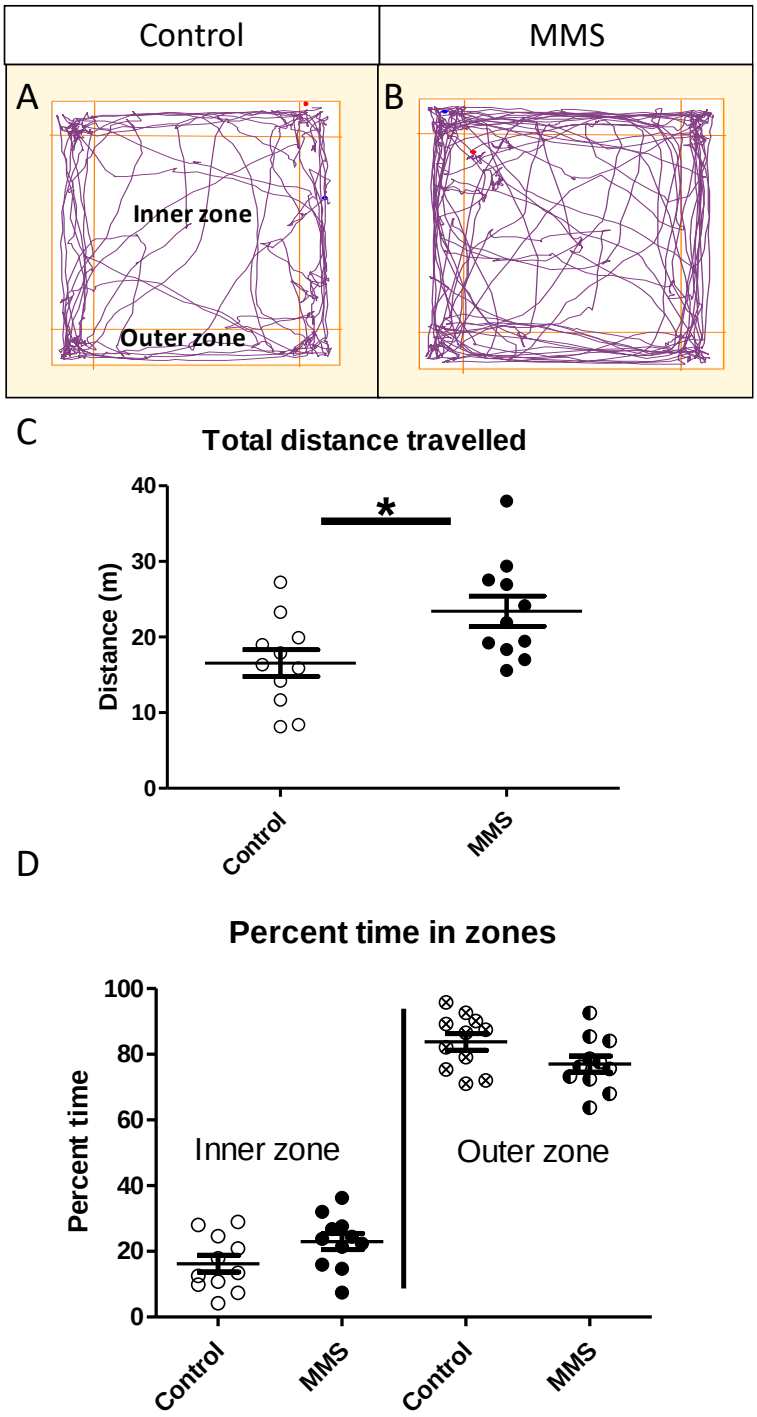

*Figure 4.16 Mice were tested in the OF 24 hours after the EPM. Representative track plots of control and MMS animals can be seen in A and B respectively, with the inner and outer zone indicated in A. Mice from the MMS group travelled further than the control group (p=0.02, df=20), without an altered proportion of time spent in the inner or outer zones (p=0.07 and 0.07 respectively, df=20 for both), as seen in C and D. All statistical comparisons were made using independent t-tests, n=11 for both groups in all graphs. * indicates p<0.05. Error bars indicate standard error of the mean.*

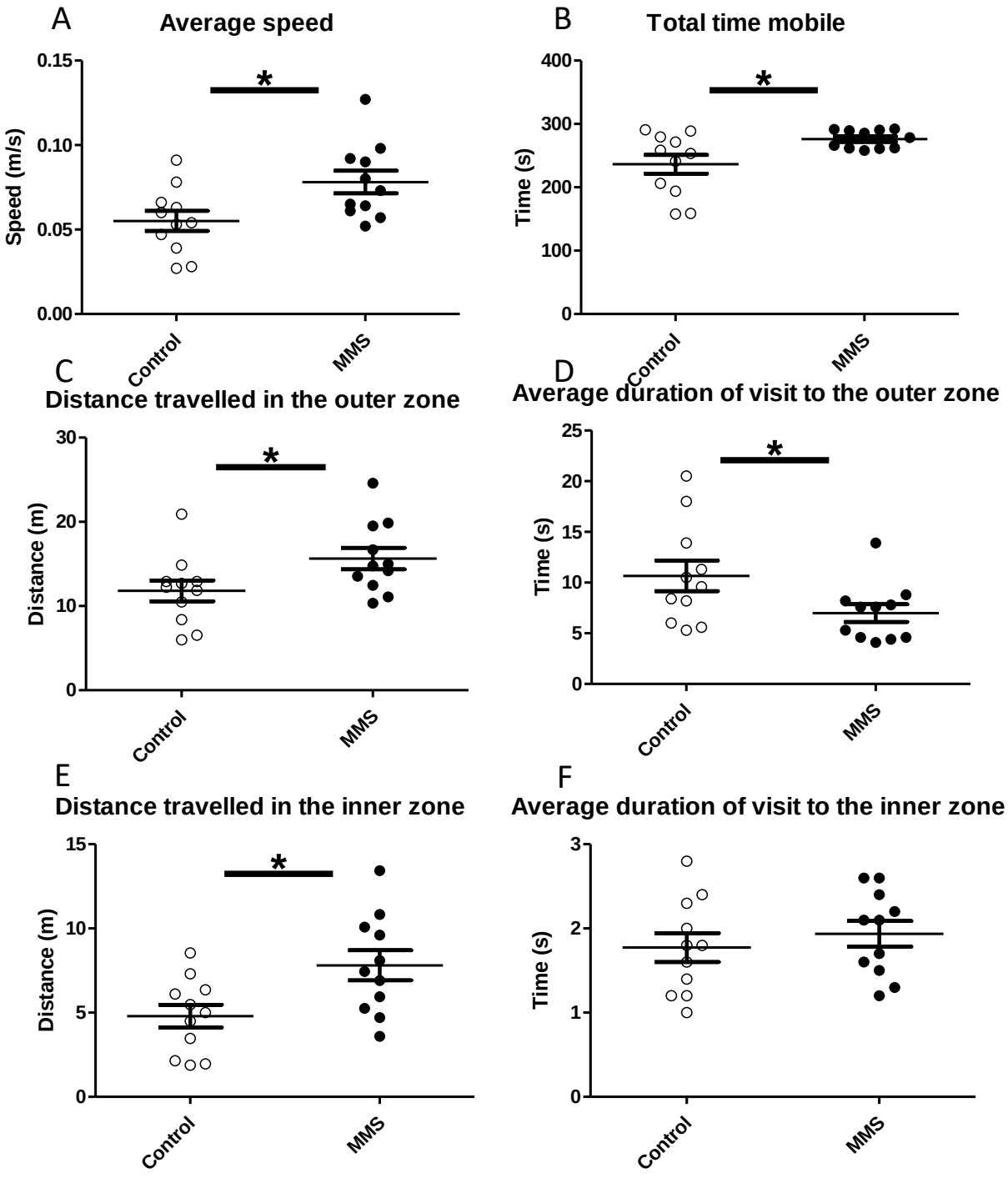

*Figure 4.17 Mice from the MMS group also moved quicker (p=0.02, df=20) and spent more time mobile (p=0.02, df=20), as seen in A and B. In the outer zone only mice from the MMS group travelled further (p=0.04) with a shorter duration of visit to this zone (p=0.048, df=20), as seen in C and D. In the inner zone only, mice from the MMS group travelled further (p=0.01, df=20) but there was no difference in the duration of visit to this zone (p=0.48, df=20), as seen in E and F. All statistical comparisons were made using independent t-tests, n=11 for both groups in all graphs. * indicates p<0.05. Error bars indicate standard error of the mean.*

On the same day as the OF, mice were tested with the tail suspension test for 360 seconds. Total immobile time was not different between control and MMS groups as seen in Figure 4.18.

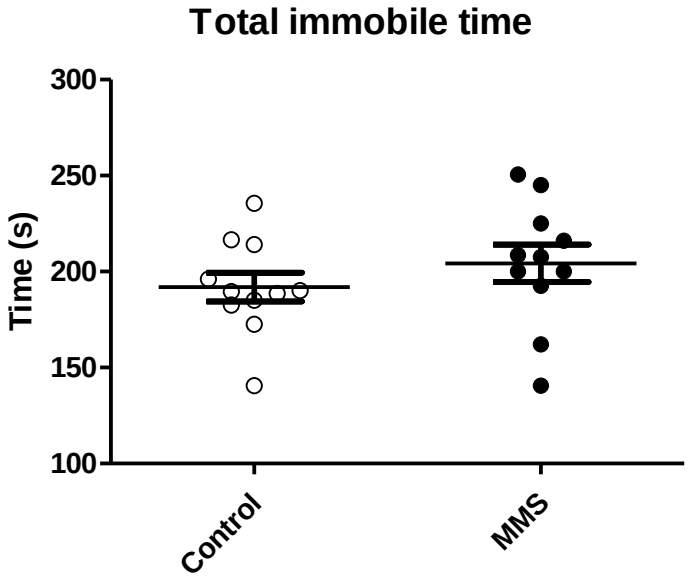

Figure 4.18 Tail suspension test was carried out following the OF. Total test time was 360 s and there was no difference between control and MMS groups (clear and black circles respectively) (p=0.32, df=20) as indicated by an independent t-test, n=11 for both groups. Error bars indicate standard error of the mean.

Considering the EPM and OF constitutes a novel stressful environment, I next investigated if the increased activity observed in those mazes was representative of habitual hyperactivity in mice following MMS. To do this I used the TSE-Systems PhenoMaster to analyse various behaviours with respect to time. In Figure 4.19A the activity of control and MMS groups over 24 hours is shown. This is quantified in B, which shows there was no difference in movement between control and MMS groups during either the light or dark phase.

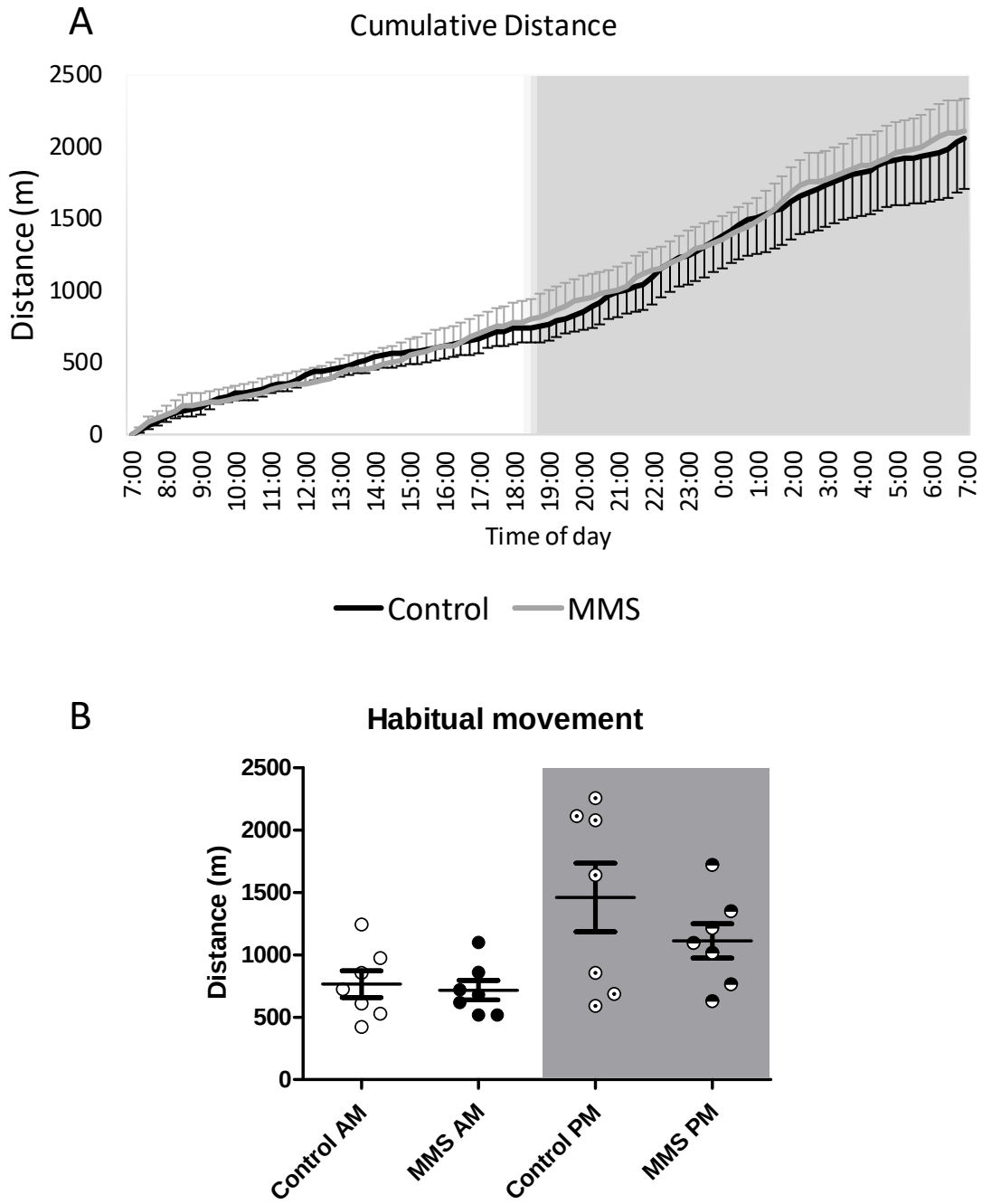

Figure 4.19 In cage behavioural monitoring using the TSE-Systems PhenoMaster was done at 4 months of age. In A the cumulative distance moved by the control (black line) and MMS (grey line) are shown with respect to time. The lighter aspect of the graph indicates when the lights were on, with the darker aspect indicating when the lights were off (n=7 for both groups). This is quantified in B, which shows no difference in movement between control and MMS animals during lights on or off (as indicated by the backgrounded shading and the nomenclature AM and PM) (p=0.36; f-statistic=1.004; df=24 for a group effect, p=0.35; f-statistic=0.348; df=24 for an interaction between group and time, and p=0.001; f-statistic=35.684; df=24 for an effect of time-significance not indicated on

graph). Statistical analysis was done using a two-way ANOVA with repeated measures. Error bars indicate standard error of the mean.

I next wanted to assess the effect of MMS on self-care behaviour following MMS. I used the PhenoMaster system to quantify grooming behaviour in control and MMS groups. As seen in Figure 4.20A and B, there were no differences in grooming behaviour in the x or y-axis over the course of 24 hours, as assessed by repetitive beam breaks in the designated plane of interest.

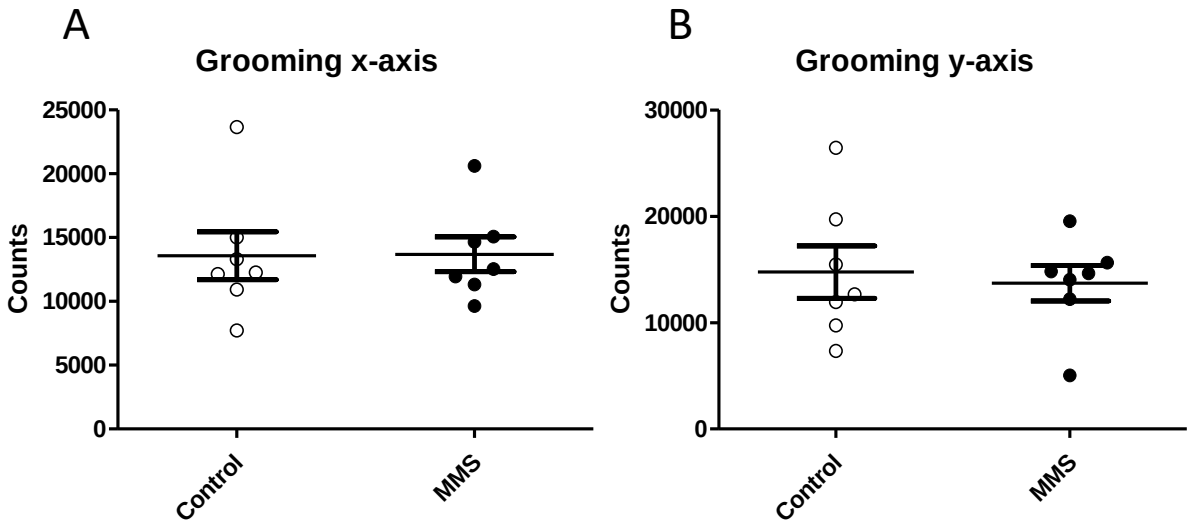

Figure 4.20 There were no differences in self-grooming behaviours of the control (clear circles) and MMS (black circles) groups along the x-axis (p=0.96, df=12) or y-axis (p=0.73, df=12) as measured by the PhenoMaster system and quantified as number of repetitive beam breaks. Independent t-tests were used for all comparison, n=7/group for both graphs. Error bars indicate standard error of the mean.

Using the PhenoMaster system I also evaluated the respiratory exchange ratio of each animal. This is a ratio of O_2 inspired and CO_2 expired, providing an approximation of fuel source used during habitual activity. This was measured every 15 minutes throughout the course of a 24 hour period. The respiratory exchange ratio for control and MMS groups can be seen in Figure 4.21, with no clear differences between groups.

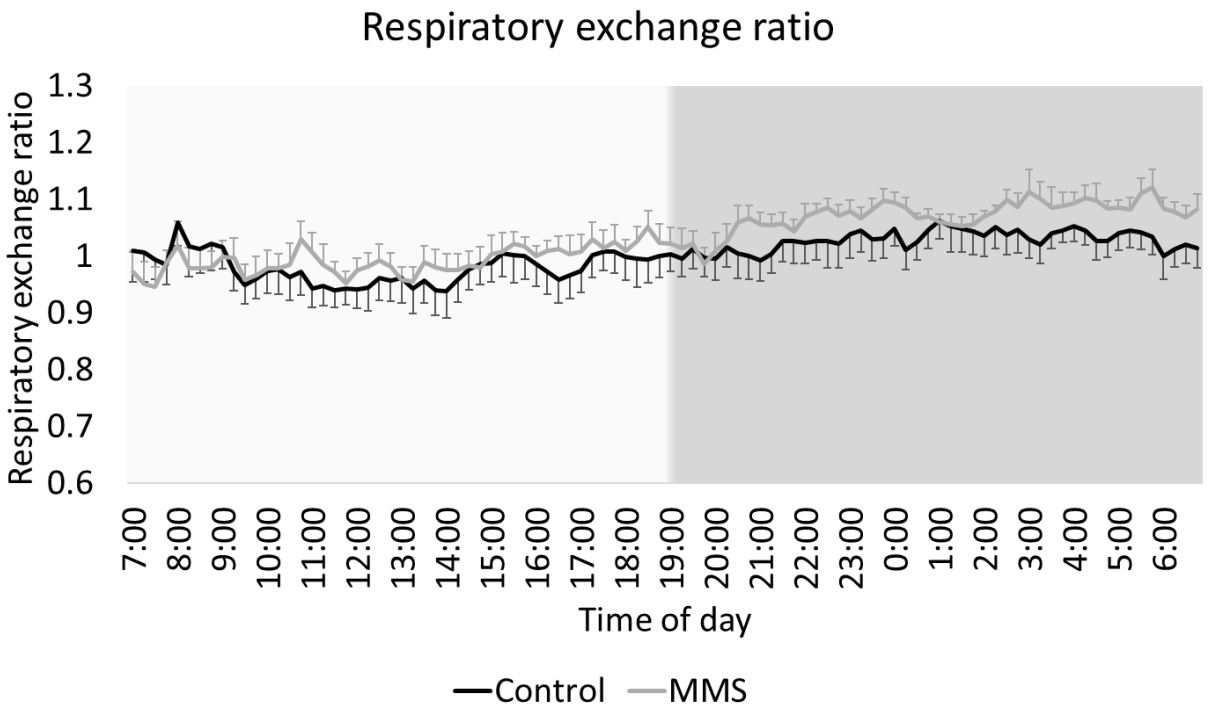

Figure 4.21 The respiratory exchange ratio was calculated using the PhenoMaster system for control (black lines) and MMS (grey lines) with respect to time of day. The light aspect of the graph indicates when the lights were on, with the dark aspect indicating when the lights were off. There was no subjective difference between groups so no further statistical analysis was performed. Error bars indicate standard error of the mean.

I also monitored cumulative food intake over the course of 24 hours using the PhenoMaster. As seen in Figure 4.22A and quantified in B, there was a trend towards a decreased food

consumption during the day and an increased food consumption at night in the MMS group but there were no statistically significant differences found.

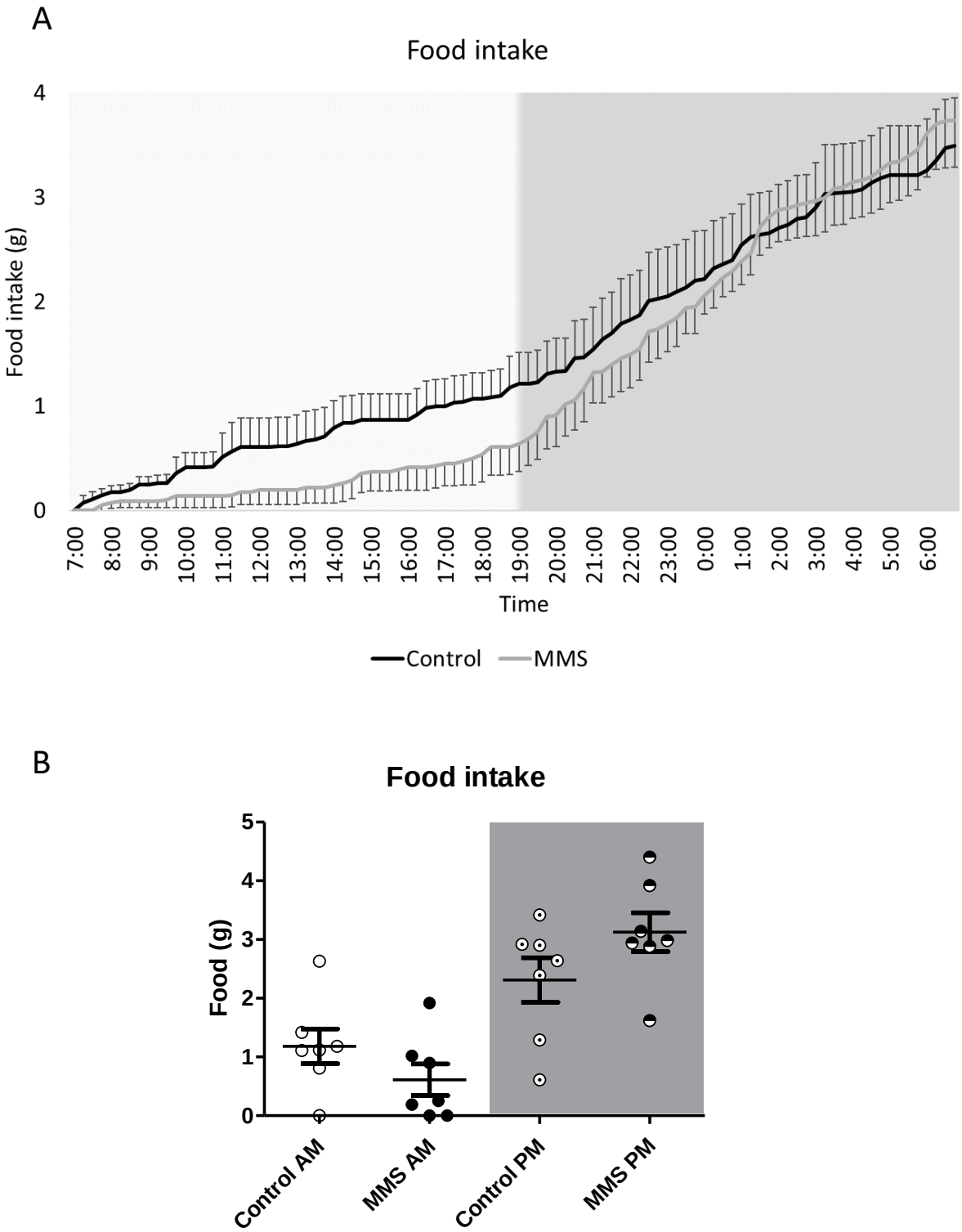

Figure 4.22 Food intake was measured over the course of 24 hours for control (black line) and MMS (grey line), as seen in A. The light aspect of the graph indicates when the lights were on with the dark aspect indicating when the lights were off. This is quantified in B, where there is an effect of time (p>0.001, f-statistic=106.558, df=24), but no effect of MMS (p=0.75, f-statistic=0.114, df=24) or an interaction between MMS and time (p=0.15, f-

statistic=2.768, df=24), as indicated by a two-way ANOVA with repeated measures, n=7 for each group. Error bars indicate standard error of the mean.

To further characterise the metabolic phenotype of these animals, their daily caloric expenditure was measured indirectly using heat given off during a 24 hour period in the closed PhenoMaster system. Daily calorie expenditure was normalised to lean mass and was not different between groups, nor was gross weight or fat mass (Figure 4.23A-D).

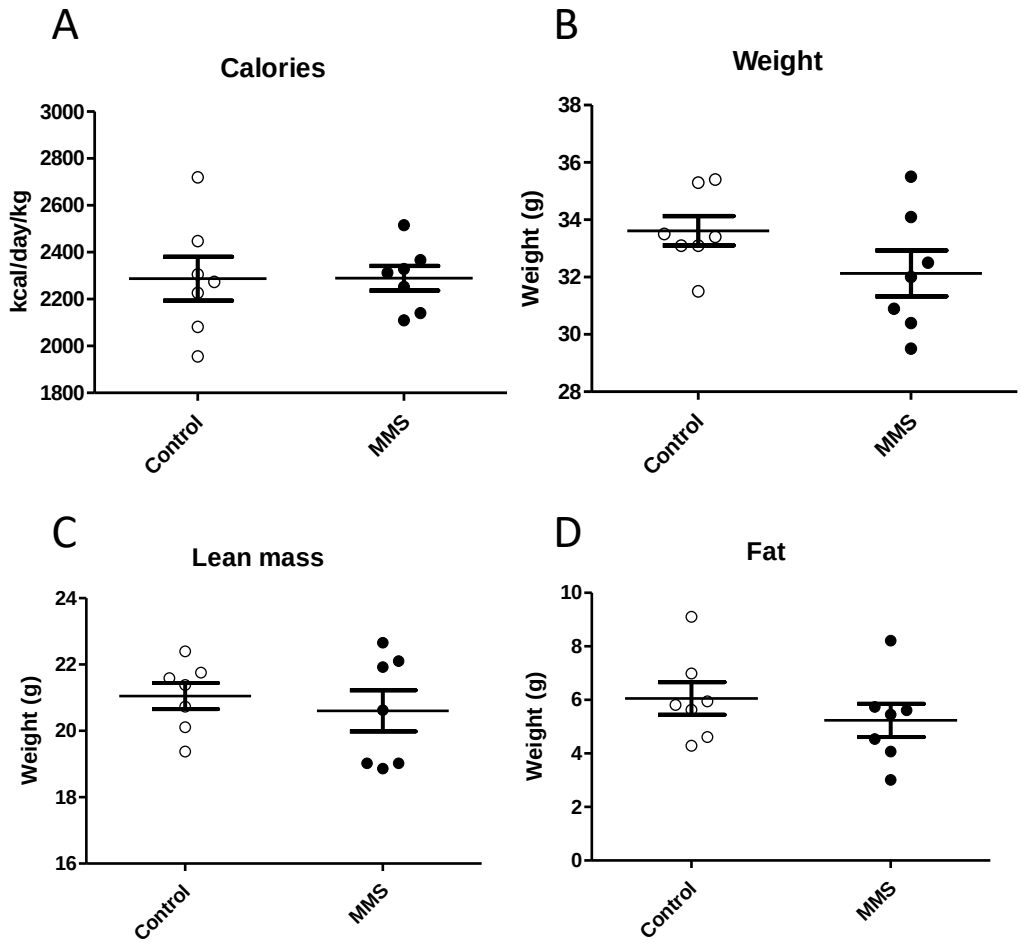

Figure 4.23 Calories spent per day/kg were quantified as heat given off in the PhenoMaster system at 4 months of age and data were normalised to lean body mass. As seen in A, there were no differences between control (clear circles) and MMS (black circles) groups (p=0.99, df=12). There were also no differences in gross weight (p=0.14, df=12), lean mass (p=0.55, df=12) or fat (p=0.36, df=12) as seen in B, C and D respectively, which were quantified using TD-NMR. All statistical comparisons were made using independent t-tests, n=7 for both groups in all graphs. Error bars indicate standard error of the mean.

I next measured plasma corticosterone at 7:00 and 19:00, timed to assess the peak and trough in circadian corticosterone secretion. As seen in Figure 4.24, there was no effect of group or an interaction between group and time but as expected there was an effect of time.

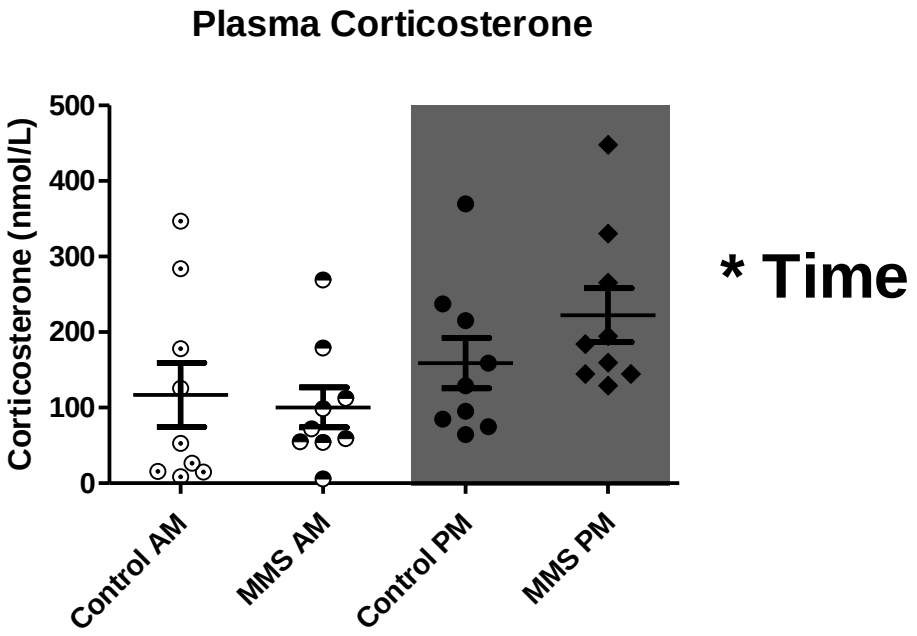

Figure 4.24 Plasma corticosterone was sampled at 7am and 7pm at 3 months of age. The 7am timepoint is indicated by the light aspect of the graph and the AM nomenclature, the 7pm timepoint is indicated by the dark aspect of the graph and the PM nomenclature. There was no difference between groups (p=0.506, f-statistic=0.453, df=32) or an interaction with time (p=0.26, f-statistic= 1.317, df=32). There was an effect of time (p=0.025, f-statistic=5.512, df=32). Statistical comparison was done using a two-way ANOVA, n=8-9 for all groups. Error bars indicate standard error of the mean.

4.5.6 The effect of MMS on candidate gene expression during adulthood

Next I assessed candidate gene expression in genes associated with stress signaling in the tissues of the HPA axis at 4 months of age using qPCR. In the hypothalamus there were no changes in the expression of the *GR*, *MR*, *Per1* or *FKBP5* as seen in Figure 4.25A. In the adrenal gland there were no alterations in the expression of *Cyp11b1*, *MC2R* or *stAr*, as seen in Figure

4.25B. In the pituitary gland there were no changes in the expression of the *GR*, *MR*, *Per1*, *FKBP5* or *POMC*, as seen in Figure 4.25C.

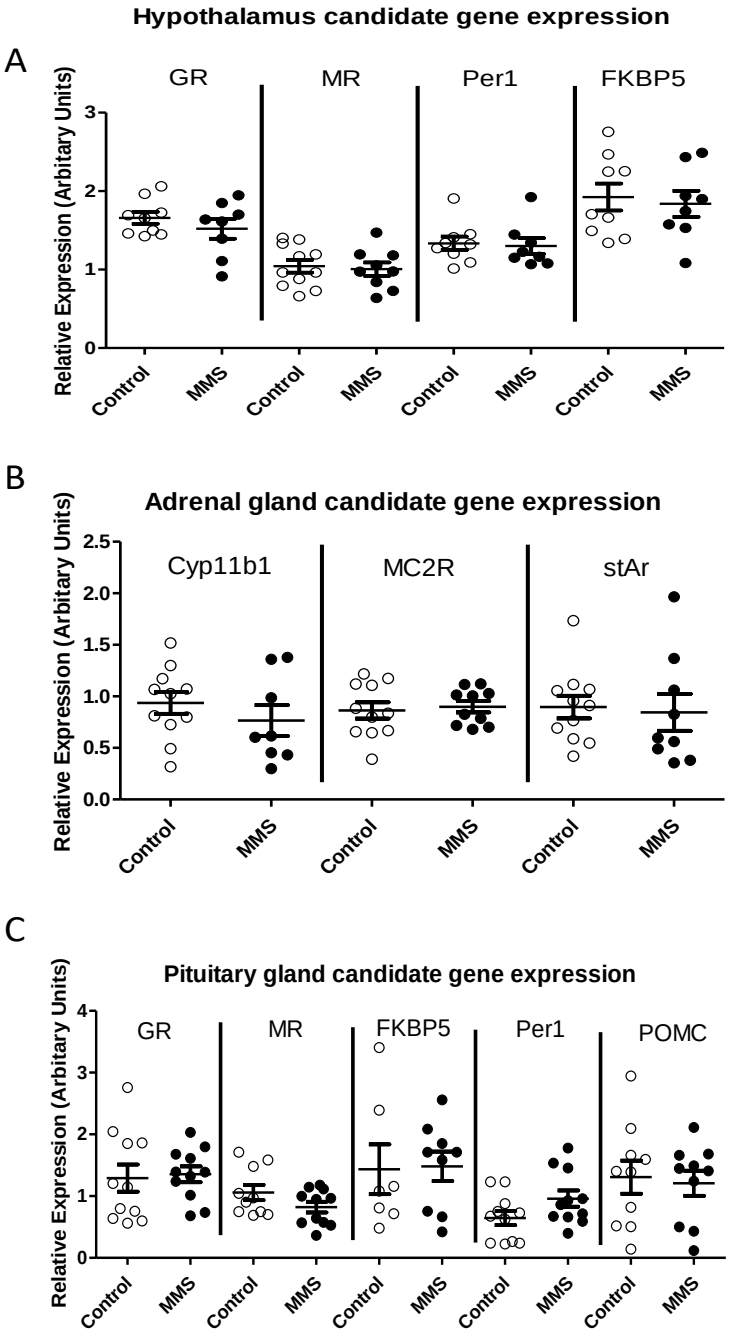

Figure 4.25 Candidate gene expression was assessed in the hypothalamus (A), adrenal gland (B) and pituitary gland (C) at 4 months of age in control (clear circles) and MMS (black filled circles) groups, and normalised to TBP. In A, there were no differences in the expression of the GR (p=0.35, df=15), MR (p=0.76, df=18), Per1 (p=0.80, df=) or FKBP5 (p=0.72, df=15) in the hypothalamus. In B, there were no differences in the expression of Cyp11b1 (p=0.35, df=17), MC2R (p=0.72, df=19) or stAr (p=0.80, df=18) in the adrenal gland. In C, there were no differences in expression of the GR (p=0.81, df=20), the MR (p=0.12, df=19), FKBP5 (p=0.92, df=14), Per1 (p=0.09, df=20) or

POMC (p=0.78, df=18) in the pituitary gland. All statistical comparisons were done using independent t-tests, n=7-11 for all tests. Error bars indicate standard error of the mean.

Considering the crucial role of the hippocampus as an input to the HPA axis, I also examined candidate gene expression changes here in control and MMS groups. As seen in Figure 4.26, there were increases in expression of the *GR*, *FKBP5* and *Per1* associated with MMS. No differences were observed for expression of the *MR* or *HSD11B1*.

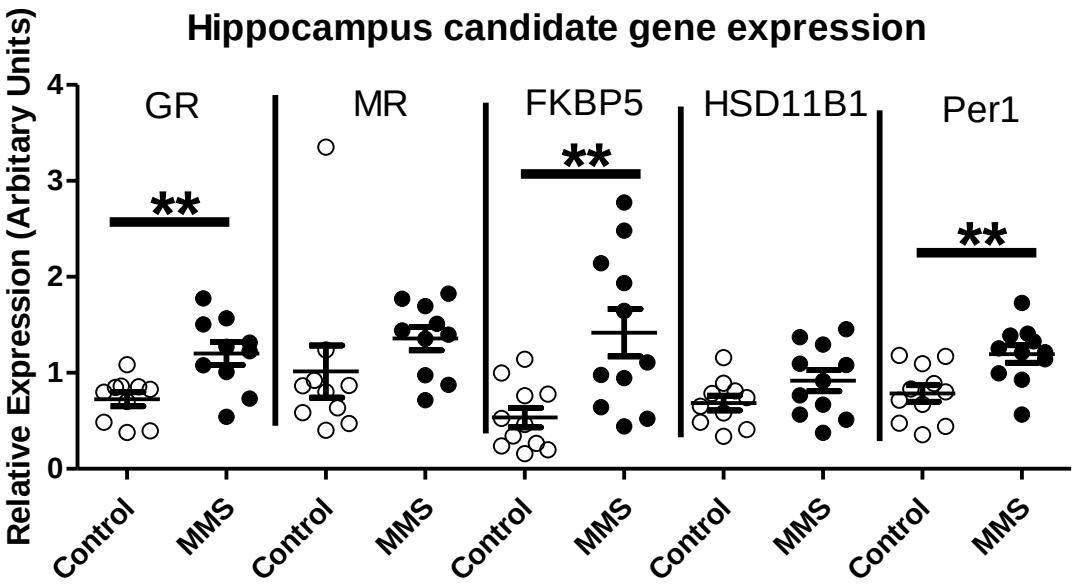

Figure 4.26 Candidate gene expression was measured in the hippocampus and normalised to TBP. There were increases in the expression of the GR (p=0.003, df=18), FKBP5 (p=0.003, df=20) and Per1 (p=0.004, df=20), but no changes in the expression of the MR (p=0.37, df=19) or HSD11b1 (p=0.08, df=20). Statistical comparisons were made using independent t-tests. Error bars indicate standard error of the mean.

4.5.7 The effect of MMS on DNA methylation at candidate loci during adulthood

I next investigated DNA methylation at candidate loci in the hypothalamus at 4 months of age at 4 loci. Two of the candidate regions chosen were those associated with the *Auts2* and *Astn2* loci which I found to be differentially methylated immediately following MMS on P6 (from the meDIP sequencing dataset). These genes also have characterised roles in the genetics of ASD [564,569]. The other 2 loci were analogous regions to those within the GR [570] and AVP [303] loci, which have previously been described in the literature to be susceptible to early life stress mediated alterations in DNA methylation. As seen in Figure 4.27 there were no changes seen across any of the loci assessed.

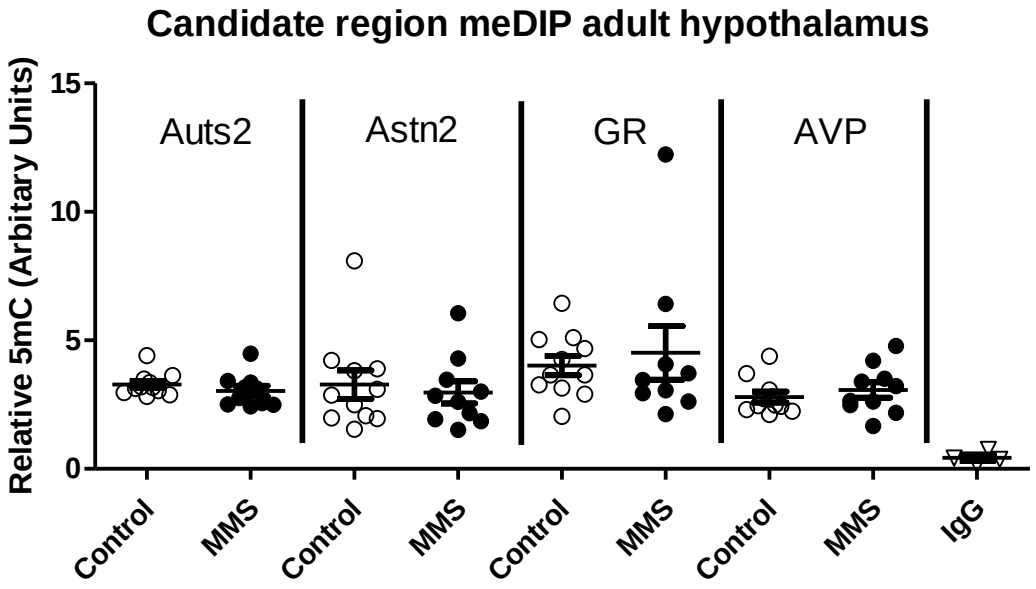

Figure 4.27 DNA methylation was assessed at candidate loci at 4 months of age in control (clear circles) and MMS (black circles) groups. Immunoprecipitated DNA was normalised to 10% input and an IgG control was included with each assay (grouped as triangles). There were no differences in DNA methylation at loci associated with Auts2 (p=0.31, df=19), Astn2 (p=0.68, df=19), GR (p=0.63, df=18) or AVP (p=0.45, df=19) genes. Statistical comparisons were made using independent t-tests, n=10-11 for all groups and comparisons. Error bars indicate standard error of the mean.

4.6 Discussion

In this chapter I have outlined a novel model of early life stress which has relevance to PTB. I have shown that:

1. MMS was not associated with differences in weight gain or blood glucose levels
2. There were no changes in Iba1+, Olig2+ or GFAP+ cellular composition in the hypothalamus following MMS
3. MMS was associated with only subtle changes in the hypothalamic transcriptome immediately following the paradigm
4. MMS was associated with widespread alterations in the DNA methylation landscape of the hypothalamus immediately following the paradigm
5. There was a stress specific hyperactivity seen in adult mice who were exposed to MMS
6. There were significant alterations in stress related gene expression in the hippocampus of adult mice exposed to MMS in the neonatal period
7. There were no effects seen in DNA methylation at candidate genes in the hypothalamus of adult animals exposed to MMS in the neonatal period

4.6.1 Corticosterone in the neonatal period

I found no difference in plasma corticosterone immediately following MMS on P6. Corticosterone is the primary hormonal mediator of stress and is therefore typically elicited by stress. However during the neonatal period in mice (P1-P12), there is a stress hyporesponsive period, which is characterised by reduced corticosterone secretion in response to various stimuli [572]. This is primarily caused by reduced adrenal activation by ACTH upon HPA stimulation [573]. I also found only subtle transcriptomic changes seen using 3' mRNA sequencing in the hypothalamus. Moreover, upon transcription factor binding enrichment analysis there was no signature of GR transcriptional targeting. However, I did see an enrichment for transcription factors associated with NFkB signalling. NFkB signalling can be stimulated during stress through canonical GR activation and the FKBP51 protein [574]. I also found a significant increase in *Per1* expression following MMS on P6. I will now discuss the possible interpretations of these results.

Per1 is highly responsive to stress signalling [448] and this could be an indication of canonical GR mediated effects, but the lack of a transcriptome wide signature (and only a minor NFkB signature which was not validated) indicates this may only be subtle with an effect size too

small to survive the statistical corrections necessary for transcriptome wide comparisons. As I found no differences in plasma corticosterone, this scenario necessitates a mechanism for local glucocorticoid activation or accumulation. However, corticosterone plasma levels were analysed using an ELISA which does not discriminate between free corticosterone and bound corticosterone. Only free corticosterone is biologically active, as such it is possible there was a shift in the ratio of bound and unbound corticosterone following MMS which was sufficient to induce *Per1* expression but insufficient to leave a strong transcriptome wide signature. There may also be an increased local conversion of dihydrocortisone into corticosterone by the enzyme HSD11b1.

An alternative possibility is the increase in *Per1* expression is not caused by glucocorticoids. *Per1* is a core regulator of circadian rhythms and its expression is controlled by other circadian regulators. Sleep deprivation is a central component of MMS and MMS was performed under excessive lighting. As described in the introduction, both light and sleep are potent regulators of the transcription-translation feedback loops which underpin circadian rhythmicity. Therefore, MMS may induce effects on *Per1* through altered circadian feedback rather than glucocorticoids. This theory is furthered by the lack of an enrichment in glucocorticoid binding motifs among genes with a logFC greater than 1.5, as well as the overall minimal transcriptional phenotype associated with MMS in the hypothalamus.

Future work could look to further investigate this in a number of ways. Firstly, MMS could be performed in *HSD11b1*$^{-/-}$ mice. As such, the local conversion of dihydrocortisone to its active form of corticosterone could not occur. Therefore, if *Per1* was still increased in expression, this mechanism could be ruled out. Secondly, mass spectrometry could be used to fully characterise the presence of glucocorticoids within the hypothalamus following MMS. Commercially available ELISAs are only validated for use on plasma, as such tissue corticosterone was not evaluated here. The local tissue level of glucocorticoids can vary independently of plasma levels [575] and therefore local accumulation should be investigated in the future. Finally, the expression of *Per1* could be measured following MMS at multiple timepoints to fully characterise the circadian oscillation of *Per1* following MMS. This would indicate whether *Per1* was transiently increased or if its circadian oscillation was affected by MMS.

4.6.2 Corticosterone at 3 months

At 3 months of age that there were no differences between control and MMS animals in baseline AM or PM plasma corticosterone levels. I also show at 4 months of age there were no differences in candidate gene expression related to stress signalling in any of the HPA axis depots. Together these data suggest MMS is not associated with alterations in baseline glucocorticoid signalling at 3-4 months of age. Previous studies using the traditional maternal separation paradigm have shown increases in baseline corticosterone at 6 weeks and 3 months but not at 1 year of age [303]. This discrepancy may be due to the different type of stress associated with MMS and other models. At 3 days, MMS also occurs for a much shorter period than other models (typically 10+ days), this increased length and developmental timing of stress may also play a role.

However, I do demonstrate stress specific hyperactivity associated with MMS. Future studies should investigate glucocorticoid signalling characteristics under stress conditions in the MMS model. Important experiments would include analysis of plasma corticosterone following stress (i.e. a 15-minute restraint stress or a social stress such as introduction of an aggressive male) and subsequent expression characteristics of stress related genes through the HPA axis and hippocampus.

4.6.3 Immunohistochemistry

As described previously, specific cell lineages are associated with distinct transcriptional and DNA methylation profiles. Therefore, changes seen using 3' mRNA sequencing or meDIP sequencing could be attributed to shifts in cellular proportions. To investigate this in a candidate approach, I used Iba1, Olig2 and GFAP to evaluate cell populations in the hypothalamus following MMS. Iba1 was used as it labels cells of the myeloid lineage and would label any infiltrating macrophages as well as resident microglia. Olig2 is a pan marker of the oligodendrocyte lineage and was chosen as a general indicator of oligodendrocyte proportions but alterations in subpopulations of oligodendrocytes cannot be ruled out. GFAP labels a subpopulation of astrocytes and was chosen as it is upregulated during astrocytosis. Even though GFAP is not a comprehensive marker of astrocytes, a previous studying using single cell sequencing in the mouse hypothalamus identified only a small number of astrocytes in the hypothalamus (~4% of all cells [576]). Although the method I used for quantification does not facilitate a direct comparison with percent of total cells, I saw sparse GFAP labelling.

4.6.4 3’ mRNA sequencing

3’ mRNA sequencing differs from traditional RNA sequencing as only the 3’ fragment is sequenced following library preparation. This allows accurate sequencing with comparable differential expression power to traditional methods but with much less depth required [534]. However, 3’ mRNA sequencing cannot measure non-coding RNA or alternative splicing in mRNA (as only a single 3’ read per transcript is obtained).

Following sequencing, Gene Ontology of genes with a logFC of greater than 1.5 showed enrichment for terms related to motile cilia. The only site which motile cilia are present in the hypothalamus is along the third ventricle, where they facilitate CSF flow. Considering these cells account for only a small proportion of total cells within the hypothalamus, enrichment of terms related to cilia movement may indicate profound alterations in their function even among the admittedly small changes seen in this dataset. CSF movement is impaired following sleep deprivation with a decrease in associated molecular clearance mechanisms, in adult animals [577]. The relevance of these mechanisms for the neonatal brain are unknown but it is likely that the clearance of molecules from CSF during sleep also plays a crucial role. These concepts will be explored in greater detail in the next chapter.

Following MMS on P6, the brains from control and MMS mice were divided along the midline. As such, an alternative possibility for enrichment of cilia related terms is asymmetric division of the hemispheres resulting in a larger ventricular surface area, and thereby more motile cilia included in one group over the other. There is no evidence of this from immunohistochemistry but considering the small number of cells lining the ventricle it is difficult to rule this possibility out.

Gene Ontology analysis also implicated increased neuronal activation within the hypothalamus. Previous work using the limited nesting material model of early life stress has described increased glutamatergic transmission in the hypothalamus [571]. Stress in adult animals also results in CRH neuronal activation which occurs independently of corticosterone, and this is an important mechanism in stress adaption [578] but this has not yet been demonstrated in neonatal animals. Glucocorticoid signalling may also act independently of its traditional cytosolic receptors to induce neuronal activation in a mechanism dependent on endocannabinoid signalling [388].

Upon transcription factor binding enrichment analysis, I saw enrichment of several transcription factors associated with NFkB signalling. NFkB signalling is classically associated with inflammation and this link will be expanded upon further in the next chapter.

4.6.5 meDIP

The first paper indicating that DNA methylation may be involved in the response to early life stress was a candidate approach by Murgatroyd *et al*, 2009 [303] which described changes in DNA methylation at the *AVP* locus at 6 weeks, 3 months and 1 year of age within the paraventricular nucleus following the traditional version of maternal separation. In contrast, I found no *AVP* associated loci to be differentially methylated at P6 or in my candidate approach at 4 months of age (see Figure 4.27). The discrepancy between these findings may be because Murgatroyd *et al,* 2009 looked only at the paraventricular nucleus where I looked at the entire hypothalamus. Of course, MMS is also a different model to traditional maternal separation and as such may have different effects.

Similar to the transcriptomic dataset, these effects may be glucocorticoid dependent or independent. Considering the dramatic nature of these changes and the only minor evidence for glucocorticoid mediated transcriptional effects, the effect on DNA methylation is more likely to be independent of glucocorticoids. Future experiments could clarify this by repeating these experiments but including a group with pharmacological inhibition of the GR, for example with the molecule RU-43044 [581].

A possible mechanism for glucocorticoid mediated effects is through FKBP51, which can modulate the activity of DNMT1 through CDK5 [366]. FKBP51 is a crucial binding partner and regulator of GR signalling. Its primary role within the cell is to bind proteins, and as such it is involved with the integration of stress signalling with several cellular pathways. Therefore, it is a primary candidate to mediate the effects of stress signalling on alternative pathways. A way to investigate the role of FKBP51 in this capacity is to immunoprecipitate FKBP51 from hypothalamic tissue following MMS, which could then be analysed with a proteomics approach to assess FKBP51 binding partners under control and MMS conditions. This is an experiment I attempted but unfortunately the poor quality of FKBP51 antibodies available made this impossible. Future work should expand on this mechanism and perhaps repeat this experiment using mice with a tagged FKBP51, which would facilitate efficient pulldown.

Alternatively, as with the transcriptomic dataset, neuronal activity is a prime candidate for glucocorticoid independent effects. Neuronal activity in the dentate gyrus of adult mice is a potent inducer of alterations in DNA methylation, with accumulation at plasticity related genes [582]. However, to my knowledge a similar mechanism has not been described in the hypothalamus or in the neonatal brain. Also in the adult hippocampus DNA methylation has been described to be crucial in synaptic function, with both DNMT1 and DNMT3a required [583]. Again I am unaware of any studies which demonstrate a similar effect in the neonatal brain or hypothalamus but Gene Ontology analysis of differentially methylated regions which were associated with protein coding regions in my dataset (see Figure 4.11), revealed strong enrichment for synapse related terms. Therefore, this is a good candidate mechanism for the effects seen here. To investigate this mechanism in the future, a comprehensive analysis of neuronal activity in the hypothalamus following MMS should be done. This analysis should include immunohistochemistry for markers of neuronal activation such as c-FOS. Areas of c-FOS accumulation should then be assessed with electrophysiological techniques *in vivo* or using acute *ex vivo* slices. Then the coupling of DNA methylation to neuronal activity could be investigated in naïve animals using optogenetic mediated stimulation of neuronal activity following by microdissection and assessment of DNA methylation. Differentially methylated regions could then be compared with those from MMS, significant overlap in differential methylation would strongly suggest neuronal activation was the mechanism responsible for changes in DNA methylation following MMS.

I saw no correlation between differentially methylated regions and gene expression. This may seem surprising, as DNA methylation is classically associated with gene expression. Indeed, the promoter regions of genes with high levels of expression are typically entirely unmethylated, and the promoter regions of genes with little or no expression are typically highly methylated [584]. In my dataset there were fewer than 20 promoter regions differentially methylated. The biological significance of changes in DNA methylation at these loci is not clear as small changes in DNA methylation, at loci with already low levels of DNA methylation may lead to a large fold change but have little or no physiological consequences. Outside of promoter regions the relationship between DNA methylation and gene expression is far less clear [584] and it is, therefore, not surprising to see that differential methylation does not associate with differential gene expression in these regions.

The physiological impact of the alterations in DNA methylation seen in this chapter are not clear. DNA methylation is highly dynamic during human brain development [110] and thereby, altered DNA methylation caused by stress may alter developmental trajectories and thereby affect long-term neurodevelopment. I demonstrate differential methylation at synapse associated genes, and this may have an important role in neuronal circuit development. An important future experiment will be to evaluate the presence of synapses both following MMS at P6 and in the adult period. This could simply be done using protein extraction and western blotting for synaptic markers such as PSD95 or vGlut. Alternatively, serial sectioning of embedded brain tissue and subsequent immunohistochemistry for pre and post synaptic markers could be done, followed by imaging and co-localisation analysis to investigate the spatial distribution of synapses following MMS, as per Zhu *et al*, 2018 [585].

4.6.6 Behaviours

4.6.6.1 EPM, OF and PhenoMaster

Here I demonstrate stress specific hyperactivity in adult male mice following MMS. Studies have previously reported hyperactivity in the EPM and OF following early life stress but to my knowledge none have also performed in cage behavioural monitoring, to demonstrate this is truly a stress specific phenotype.

The EPM and OF are often used in combination to assess anxiety in mice and the results of both tests have been shown to positively correlate in both C57BL/6JOlaHsd and BALB/c mice [539]. Previous literature describing hyperactivity in the EPM and OF have used the traditional maternal separation paradigms with at least 30 hours of total separation time. The power of MMS is underscored by similar results occurring with only 4.5 hours of total separation. A primary motivator to create MMS was the variance in behavioural outcome following traditional maternal separation. For instance, using 3 hours/day of maternal separation from P2-P14 female mice had altered behaviour in the EPM, with males being resilient [588]. Another study using the same paradigm but for 4 hours/day, saw no effect on female behaviour [589], whilst a different study showed maternal separation (6 hours/day from P15-P21) had no effect on behaviour in the EPM or OF in mice [590]. Maternal separation (6 hours/day P5-P21 or 3 hours/day P3-P14) in rats seems to more consistently show changes in the EPM and OF tests [591,592].

With respect to the limited nesting model of fragmented maternal care, studies have reported no differences in behaviour in the EPM or OF [593].

4.6.6.2 Tail suspension

Early life abuse is associated with an increased incidence of depression in adult life [594]. Therefore, I tested for depressive symptoms in adult mice exposed to MMS. The tail suspension test is a commonly used measure of depression related behaviour in mice [540]. The primary outcome is immobile time, which was not different between groups. The forced swim test (which I did not use) is another commonly used test for depressive symptoms, in which the time immobile is also the primary outcome. The forced swim and tail suspension tests do not always correlate [595], perhaps indicating that they measure distinct behaviours. Therefore, it may be useful in the future to use the forced swim test. The tail suspension test was chosen here as it provides a widely used test of depressive symptoms but is associated with less stress than the forced swim test. However, even though these are the most common preclinical tests for depressive symptoms, there are pressing questions about their relevance to human depression. To reduce a condition as heterogeneous as depression to a single metric is inherently reductionist and non-scientific, there have also been variable results using these models [596]. The ability of selective serotonin reuptake inhibitors (SSRIs) to decrease immobile time in these tests has led to a form of validity. However, these effects occur with hours/days of administration whereas anti-depressive effects of SSRIs in humans can take months to be seen [597].

Future studies should focus on aspects of depression related traits rather than single metric tests. For instance testing taste preference between water and a 1% sucrose solution has previously been used to model the reduced enjoyment of food associated with human depression [536]. Alternatively studies should analyse habitual behaviour and activity using, as done here with the PhenoMaster or variations in which novel objects can be introduced [598].

There are gender differences in depression associated with early life stress in humans and mice, with females preferentially affected [593,599]. Here, I only used male mice, which is the principal limitation of this work. A comprehensive study of MMS in female mice is needed.

4.6.6.3 Assessment of in cage behaviour

Here I assessed in cage behaviour using the TSE Systems PhenoMaster. To my knowledge this is the first study to use this or a related system to follow up the effects of a model of early life stress. This system provides a variety of data with both high temporal and spatial resolution but is associated with some caveats. As this system cannot track multiple objects independently, animals must be single housed during this experiment. This single housing

extends to 4 days before introduction to the system as the PhenoMaster uses a novel waterspout which necessitates isolated training. Mice are social animals and single housing in this manner is not recommended and constitutes a chronic stressor. Moreover, the system uses lasers to track mouse behaviour which can be interrupted by the build-up of nesting material. As such only limited nesting material can be used within the cage and there is also a completely lack of any environmental enrichment. Therefore, this entire experiment took place during 8 days of continuous chronic stress. The first 24 hours of data from the PhenoMaster were not used as the mice acclimatised to the environment, this first 24 hours could be viewed as an acute stress similar to the introduction into the EPM or OF. It is nonetheless interesting that the MMS group were not different among any of the measured variables during this period of chronic stress. Therefore, the most plausible interpretation of these behavioural results is that MMS results in acute stress specific hyperactivity.

To my knowledge there are no human studies which characterise the behavioural response to acute stress in individuals exposed to early life stress, but this may be an interesting validation of my results. It is obviously unethical to expose people to acute stress with the hypothesis they will have an exaggerated reaction, therefore a behavioural response to an acute stress which is an unavoidable part of habitual activity would be required. A study such as this would require extensive cross discipline collaboration with respect to feasibility and design.

4.6.7 Candidate gene expression changes in the hippocampus

I did not find any changes in candidate gene expression throughout the HPA axis, but I did find changes within the hippocampus. The hippocampus has a crucial role in regulating the HPA axis [287]. As such these data indicate that the stress-induced hyperactivity seen in the EPM and OF may not be due to fundamental alterations in the HPA axis, but changes in its regulation from the hippocampus. I found a signature of neuronal activation in the 3' mRNA sequencing dataset and previous work has shown DNA methylation can be altered by neuronal activity [582]. Therefore, all the effects I describe may be driven by hippocampal input into the HPA axis.

Future studies should focus on the hippocampus and fully characterise its role in MMS, in both the neonatal and adult stages. An experiment to investigate hippocampal input to the hypothalamus both immediately following MMS and in adulthood could be done by using single cell patch clamp techniques in acute brain slices, followed by reverse labelling of

neurons with biotin. The hippocampus innervates numerous nuclei within the hypothalamus which then relay information to the paraventricular nucleus so there are many possible locations and mechanisms involved. However, immunohistochemistry could then be done on biotin labelled cells to identify specific cellular subtypes and their hippocampal location.

4.6.8 Therapeutic targets

The endocannabinoid system can interact with stress through a number of mechanisms, mostly to limit the extent of stress signalling [605]. The CBR1 can control glutamate release, and *CBR1*$^{-/-}$ mice show enhanced glutamatergic signalling in the PFC following chronic stress in adult animals [606]. CBR1 agonists have anxiolytic properties in adult mice in the EPM and OF [607] but their use in the neonatal period to attenuate the effects of early life stress is unknown. Therefore, CBR1 agonists would be an interesting candidate to administer with MMS.

Previously, pharmacological inhibition of FKBP51 has been difficult due to its homology with FKBP52. However recently, specific inhibitors have been generated named SAFit1 and 2 [374]. Their use has been associated with anxiolytic effects in adult animals [375]. These would also be interesting candidates to investigate if their co-administration with MMS could abrogate the effects described here.

Increased maternal care may also be beneficial. Brief removal and handling of pups for 15 minutes is associated with an increased level of maternal grooming when the pups are returned to the cage [608]. Therefore, increased maternal contact and care may be an easier method of mitigating the effects of stress in the perinatal period.

4.7 Conclusion

The effects of stress associated with PTB on brain development are largely unknown and studying this in humans is difficult due to the confounders associated with preterm birth. This necessitates the use of animal models to understand the consequences and mechanisms involved. However, many models of early life stress fail to accurately recapitulate the stress associated with PTB. Therefore, I created a novel model of early life stress, called MMS. Using MMS, I demonstrate that DNA methylation is particularly vulnerable to alterations following early life stress and that the amount of stress needed to produce behavioural effects in later life is much less than in previously published studies.

5 The effect of LPS administration prior to MMS in the cortex and hippocampus

5.1 Introduction

In the previous results chapter, I showed an enrichment for NFkB binding motifs among differentially expressed genes in the hypothalamus immediately following MMS. NFkB signalling is classically associated with immune activation and inflammation and in this chapter, I tested the hypothesis that exposure to LPS and associated activation of NFkB signalling prior to MMS would potentiate the transcriptional response and other outcomes.

In this chapter I use a single dose of 1mg/kg LPS to model neonatal sepsis. LPS is a component of the bacterial cell wall and an agonist of the TLR4 receptor. It is commonly used to model bacterial infections and has previously been used at 1mg/kg to model sepsis [609]. In preterm infants, perinatal sepsis is associated with an adverse neurodevelopmental outcome independent of other factors [610] and in animal models it is associated with hypomyelination in the brain, altered growth, altered behaviour in adulthood and has been shown to sensitise to other early life insults [250,611,612].

LPS in animal models potentiates subsequent hypoxia/ischemia [517,613] and in human neonatal imaging studies, different patterns of brain injury are seen in term born infants with neonatal encephalopathy with or without additional exposure to chorioamnionitis [236]. LPS in animal models or inflammation in human neonates may also interact with stress to impact on the later phenotype. For instance the interaction between early life inflammation and neonatal stress may explain some of the developmental heterogeneity in individuals with schizophrenia or bipolar disorder [614]. It is also known that pregnant women with depression have increased circulating cytokine levels which correlate with the infant stress response at one year [615]. However this is a complicated relationship, and early life stress may also influence circulating cytokine levels, as has been observed in adult rhesus monkeys [616]. Early life stress and inflammation seem to be mechanistically linked, as administration of non-steroidal anti-inflammatory drugs can ameliorate hyperactivity in adult animals exposed to stress *in utero* [617]. In adult rats, evidence also suggests stress can prolong an inflammatory event [618]. However, the consequences of this for the neonatal brain are unclear.

Sleep deprivation is a central component of the MMS model, and sleep deprivation has been shown to reduce the glymphatic clearance of inflammatory molecules from the brains of adult animals [577]. Glymphatic vessels have been found in humans and resemble those in mice,

and a similar clearance process through glymphatic vessels is thought to operate in humans [619]. These processes have not been described in neonatal animals to date most likely due to the associated technical difficulties, but it is known that both CSF flow through the brain [620] and sleep [621] are of critical importance for brain development.

Individuals with ASD have an increased number of synapses [84] and individuals with schizophrenia have fewer synapses [82,96] across several brain regions when compared to typically developing individuals, and altered synaptic pruning is a potential mechanism involved. As discussed in the introduction, many immune related genes also have functions related to synaptic pruning e.g. MEGF10 [622], C4 [100] , CSMD1 [101], TGFβ [623] and CX3CR1 [624]. In this chapter I will investigate the effect of LPS and/or MMS on aspects of synaptic pruning. Much of the evidence for microglia mediated synaptic pruning comes from the mouse hippocampus [501,624,625], which is where I focus my area of investigation during this chapter.

The importance of glial cells to brain development is widely appreciated and the local redistribution or reduction/expansion of these cells can have a large effect on brain function and development [626]. As outlined previously here and in the introduction, microglia are involved in key processes such as synaptic pruning and the central inflammatory response. In post mortem tissue from individuals with ASD there are specific alterations in microglia [33]. Studies in mice indicate that individual microglia are extremely long lived [268] and therefore early life factors such as stress or inflammation may program future dysfunction in the same cell. Astrocytes are important for brain development [626] and also have a role in microglia mediated synaptic pruning [627,628]. In my first results chapter I showed that LPS exposure in primary cultured mouse OPCs resulted in a trend towards a reduced production of mature myelinating oligodendrocytes, which has also previously been described in the literature. Neonatal inflammation models produce hypomyelination [629], and WMI is a predictor of neurodevelopmental outcome [59]. In this chapter I investigate markers of microglia, astrocytes and oligodendrocytes in the hippocampus and cortex following LPS and/or MMS.

Finally, in the central dogma of molecular biology RNA is transcribed from DNA before its translation into protein. The transcriptome plays an integral role in defining cellular identity and is highly dynamic and plastic through development as well as reflecting responses to environmental perturbation. As described in the introduction, cortical dysfunction has been linked to many neurodevelopmental disorders and early life insults. In this chapter I

interrogate the cortical transcriptome in an unbiased manner using 3’ mRNA sequencing following LPS and/or MMS.

5.2 Hypothesis and aims

5.2.1 Hypotheses

Administration of LPS will potentiate the effects of subsequent MMS in the hippocampus and cortex

5.2.2 Aims

1. To assess the effect of LPS and/or MMS on weight gain
2. To investigate the expression of inflammation related genes in the brain 24 hours after LPS (which would be the onset of the MMS paradigm)
3. To examine aspects of synaptic pruning in the hippocampus following LPS and/or MMS
4. To investigate glial cell populations in the cortex following LPS and/or MMS
5. To examine the cortical transcriptome following LPS and/or MMS
6. To compare the cortical and hypothalamic transcriptomes after MMS to identify common regulators

5.3 Methods

5.3.1 Animals

C57BL/6JOLAHSD male mice were used for the following experiments. A single male was housed with 2 females under a 12-hour light/dark schedule with constant temperature and humidity. Litters were randomly reduced to 4 males on P2. On P3, these 4 males were then randomised to the following 4 groups:

1. Control group- PBS via IP injection and no MMS
2. LPS group- 1mg/kg LPS via IP injection and no MMS
3. MMS group- PBS via IP injection and MMS
4. LPS+MMS group- 1mg/kg LPS via IP injection and MMS

Pups then received subcutaneous ink injections to their footpad for identification purposes. Offspring were killed by decapitation at P6 for all experiments (except in Figure 5.2 where animals were killed at P4). See Figure 5.1 for full outline.

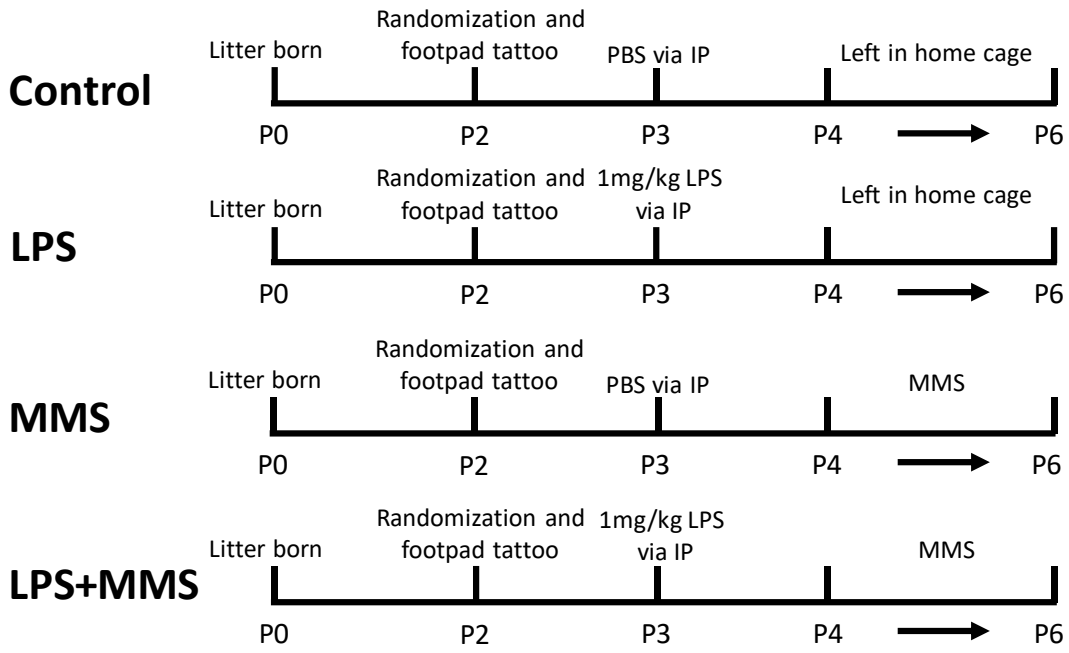

Figure 5.1 Full outline of experimental groups used in Figure 5.3-Figure 5.12

5.3.2 Gene expression response to LPS

Pups were administered either 1mg/kg of LPS or PBS on P3. After 24 hours (the time point which would be the initiation point of MMS for subsequent experiments), pups were killed and whole brain tissue removed and snap frozen on dry ice. RNA was then extracted from tissue before cDNA synthesis and qPCR analysis of candidate gene expression.

5.3.3 LPS and MMS experiments

Pups received 1mg/kg LPS or PBS on P3, 24 hours later MMS was performed and repeated on the 2 subsequent days for 1.5 hours (see Figure 5.1). All pups were weighed consecutively on each day, immediately prior to MMS. Weights were normalised to the starting weight of each pup at the time of LPS or PBS injection. At the end of the paradigm the animals were killed, and brains extracted. Brains were then halved down the midline with one half placed in 4% PFA for 24 hours before transferring to 70% ethanol and subsequent embedding in paraffin wax, from the other half the cortex and hippocampus were dissected and snap frozen on dry ice. Tissue was kept at -80° until RNA was extracted.

5.3.4 Immunohistochemistry

After embedding in wax, the fixed tissue was then cut into 6µm sections using a microtome with three consecutive sections per slide. Slides were dewaxed, then antigen retrieval was carried out before immunohistochemistry as previously outlined in the materials and methods section. Stained slides were imaged using an Axioscan slidescanner and image quantification done using Image J. Olig2+ and Iba1+ cells were manually counted and normalised to area. GFAP+ cells were analysed by percent area coverage using a universally applied threshold [496]. For each animal three consecutive brain sections were analysed which were then averaged to produce an n of 1.

5.3.5 3' mRNA sequencing

RNA was extracted from frozen tissue before determination of concentration using a Qubit Fluorometer. Library preparation was done using 500ng of RNA. Sequencing and analysis were done as described previously in the materials and methods section. Briefly, data were mapped to the mm10 genome before differential gene expression analysis using the Voom sample weights method. This method was chosen to account for variation often seen in sequencing experiments using a low n [630].

5.4 Results

5.4.1 Candidate gene expression 24 hours after 1mg/kg LPS or PBS

To ensure the dose of LPS given to pups at P3 produced an inflammatory response in the brain, 1mg/kg of LPS was given at P3 and candidate gene expression analysed in whole brain tissue 24 hours later. As seen in Figure 5.2, there was a significant upregulation of *Iba1*, *IL1α* and *TNFα* 24 hours after LPS administration compared to PBS control. This indicates that at the onset of the MMS paradigm there was a pro-inflammatory environment in the brain.

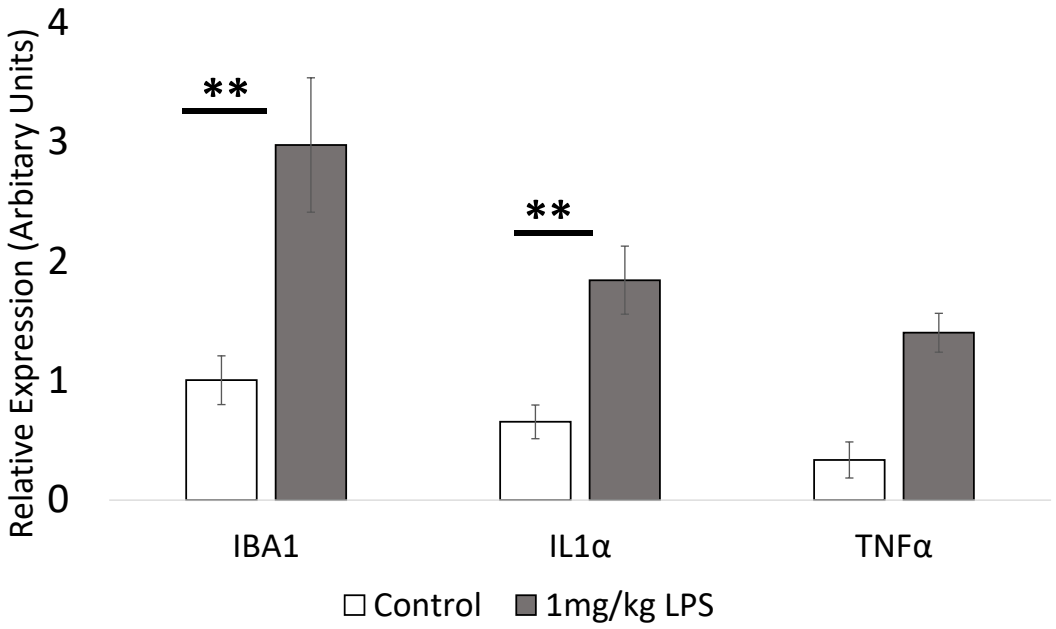

*Figure 5.2 The expression of candidate inflammatory genes was assessed 24 hours after 1mg/kg of LPS or PBS administration. An increase in Iba1 (p=0.002, df=6), IL1α (p=0.009, df=6) and TNFα (p=0.02, df=6) can be seen following LPS. Expression was normalised to TBP. Comparisons were made using independent t-tests. ** indicates p<0.01. n=4 for all groups. A p-value<0.016 was deemed to be statistically significant following Bonferroni adjustment for multiple comparisons.*

5.4.2 Growth dynamics following LPS and/or MMS

To examine alterations in growth dynamics following LPS and/or MMS, pups were weighed at the same time on consecutive days. Brain weight was also measured in a subset of animals after killing. Figure 5.3A shows the growth trajectories of pups from all 4 groups. The associated area under the curve is quantified in Figure 5.3B with a reduction in weight gain following LPS with no effect of MMS or an interaction between LPS and MMS. There were no differences in brain weight when normalised to body weight among any of the groups, as seen in Figure 5.3C.

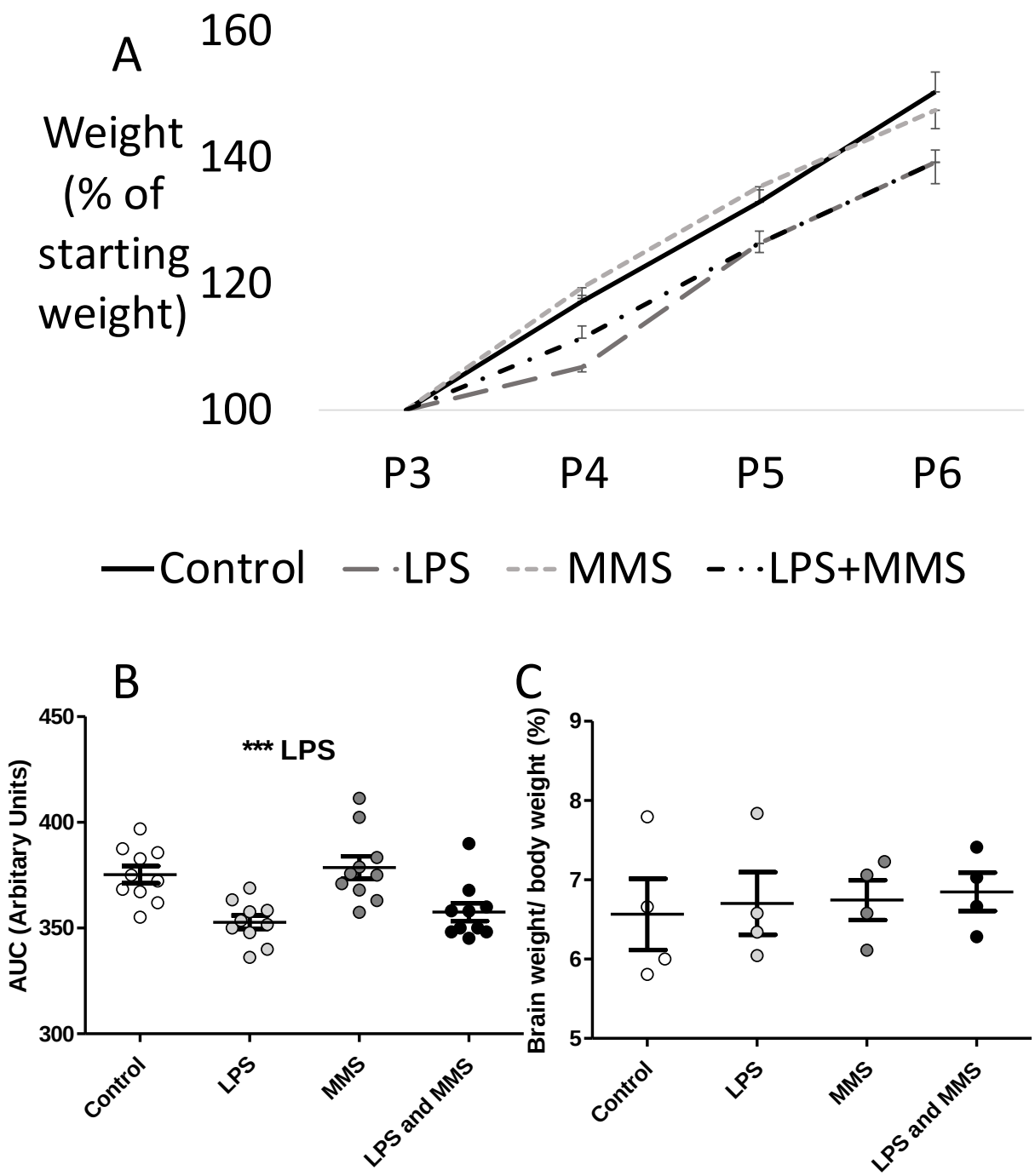

*Figure 5.3 In A), the weight gain of pups from the control (solid black line), LPS (dashed dark grey line), MMS (dashed light grey line) and LPS and MMS (dashed black line) groups can be seen as a percentage of weight on P3 (the day of injection with either 1mg/kg LPS or PBS). In B) the area under the curve of the data presented in A) shows an effect of LPS ($p<0.001$, f-statistic=26.136, df=36) with no effect of MMS ($p=0.347$, f-statistic=0.909, df=36) or interaction between LPS and MMS ($p=0.866$, f-statistic=0.029, df=36). In C) there were no main effects for LPS ($p=0.736$, f-statistic=0.119, df=12) or MMS ($p=0.646$, f-statistic=0.221, df=12), and no interaction ($p=0.963$, f-statistic=0.002, df=12) in the brain to body weight ratio. In A) and B) n=10 for all groups, and n=4 for all groups in C). All comparisons were made using a 2-way ANOVA. *** indicates $p<0.001$.*

5.4.3 Investigation of processes related to synaptic pruning in the hippocampus

Considering the important role of glia in both brain development and the response to LPS, I characterised the distribution of several markers associated with glial cells within the hippocampus immediately following the paradigm in all 4 groups (control, LPS, MMS and LPS+MMS). Representative images for all groups can be seen in Figure 5.4A-L. There was a borderline significant decrease ($p=0.05$) in GFAP (Figure 5.4M) following LPS but no effect of MMS or interaction between LPS and MMS. I found no difference in the numbers of Iba+ (Figure 5.4N) or Olig2+ (Figure 5.4O) cells in the hippocampus following LPS or MMS and there was no evidence for an interaction between LPS and MMS either.

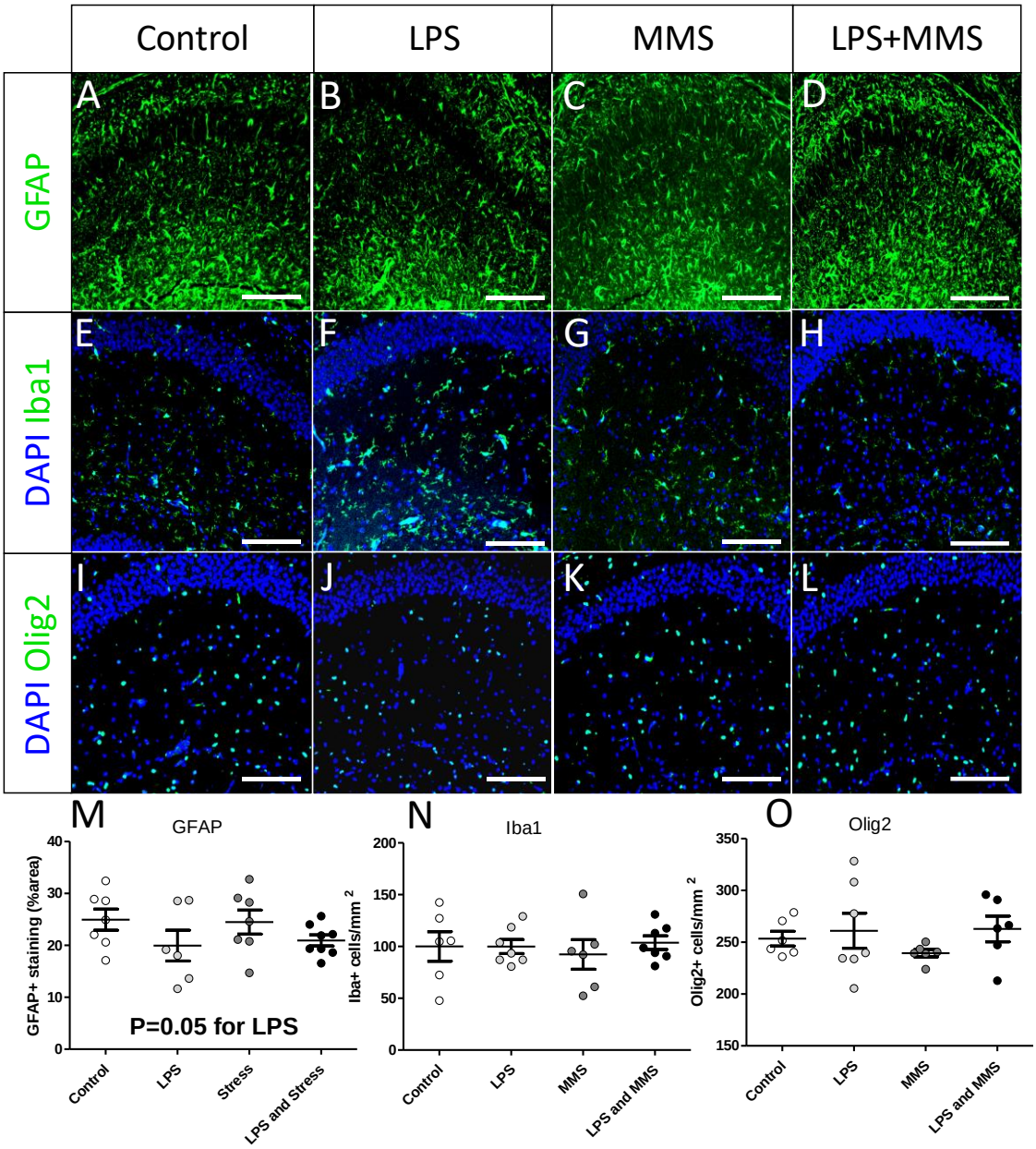

Figure 5.4 Assessment of candidate glial populations in the hippocampus in the 4 groups: control (A, E, I), LPS (B, F, J), MMS (C, G, K), LPS+MMS (D, H, L). In A-D representative images of hippocampal GFAP staining across the 4 groups are shown. This is quantified as percent area in M with a borderline effect (p=0.05, f-statistic=4.165, df=22) with no effect of MMS (p=0.901, f-statistic=0.016, df=22) or an interaction between LPS and MMS (p=0.122, f-statistic=0.73, df=22). In E-H, representative images of Iba1+ cells (green) and DAPI+ cells (blue) from all 4 groups are shown. This is quantified as Iba1+ cells/mm² in N) with no differences seen for an effect of LPS (p=0.889, f-statistic=0.02, df=22), MMS (p=0.447, f-statistic=0.598, df=22) or an interaction (p=0.772, f-statistic=0.086, df=22) between them. Similarly, in I-L representative images for Olig2+ cells (green) and DAPI+ cells (blue) are seen from all 4 groups, with this quantified in O) as Olig2+ cells/mm². No differences were seen for an effect of LPS (p=0.209, f-statistic=1.681, df=21), MMS (p=0.612, f-statistic=0.265, df=21) or an interaction (p=0.515, f-statistic=0.438,

df=21) between them. Experiment was analysed using a 2-way ANOVA, n=6-7 for all groups and comparisons. Scale bars indicate 100μm.

Several inflammatory molecules are involved in synaptic pruning within the hippocampus during development. Therefore, I examined the effect of LPS and/or MMS on the expression of these molecules in the hippocampus immediately following the paradigm, which is shown in Figure 5.5. There were no effects of either LPS or MMS and no evidence of an interaction between them for any of the genes tested (MEGF10, C4b, CSMD1, TGFβ, CX3CR1 and synapsin), as seen in Figure 5.5A-F. As such there was insufficient evidence to pursue the investigation of synaptic pruning within the hippocampus following LPS and/or MMS.

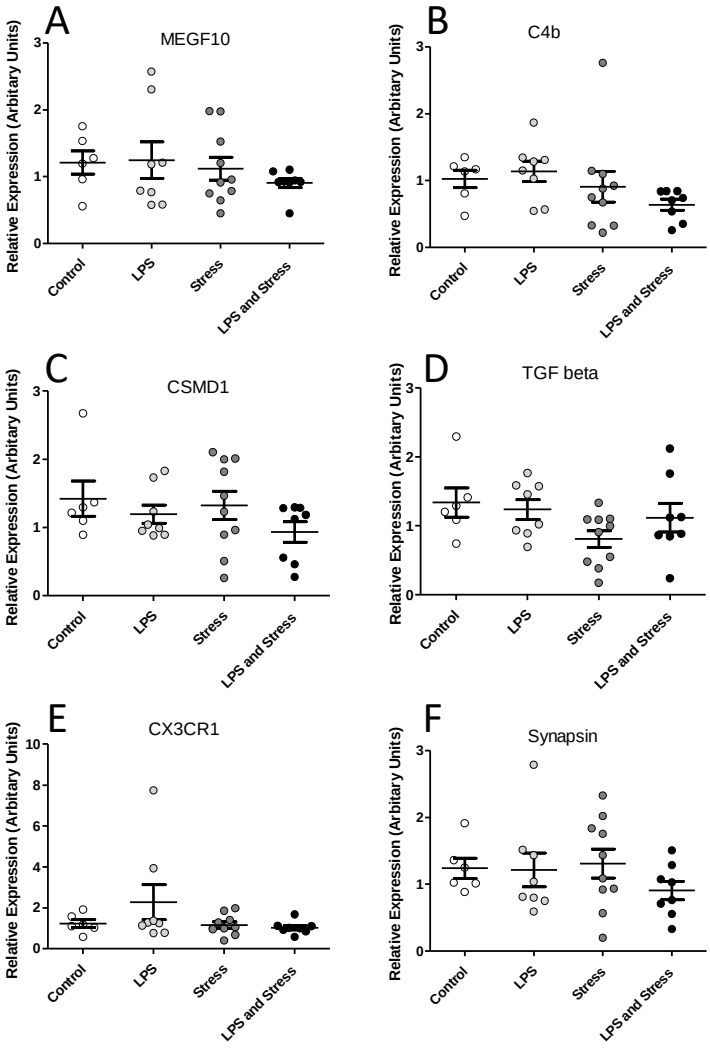

Figure 5.5 Candidate gene expression in the hippocampus following control, LPS, MMS or LPS + MMS. In A there were no differences found for an effect of MMS (p=0.267, f-statistic=1,28, df=28), LPS (p=0.65, f-statistic=0.211, df=28) or an interaction (p=0.525, f-statistic=0.414, df=28) in the expression of MEGF10. In B there were no

differences found for an effect of MMS (p=0.098, f-statistic=2.922, df=30), LPS (p=0.664, f-statistic=0.192, df=30) or an interaction (p=0.293, f-statistic=1.15, df=30) in the expression of C4b. In C there were no differences found for an effect of MMS (p=0.238, f-statistic=1.453, df=29), LPS (p=0.241, f-statistic=1.431, df=29) or an interaction (p=0.248, f-statistic=1.387, df=29) in the expression of CSMD1. In D there were no differences found for an effect of MMS (p=0.065, f-statistic=3.684, df=29), LPS (p=0.538, f-statistic=0.389, df=29) or an interaction (p=0.236, f-statistic=1.464, df=29) in the expression of TGF-beta. In E there were no differences found for an effect of MMS (p=0.567, f-statistic=0.336, df=30), LPS (p=0.317, f-statistic=1.037, df=30) or an interaction (p=0.375, f-statistic=0.814, df=30) in the expression of CX3CR1. In F there were no differences found for an effect of MMS (p=0.161, f-statistic=2.076, df=31), LPS (p=0.322, f-statistic=1.017, df=31) or an interaction (p=0.207, f-statistic=1.666, df=31) in the expression of Synapsin. Expression was normalised to TBP. Data were analysed using a 2-way ANOVA, n=6-9 in all groups shown. Error bars indicate standard error of the mean.

5.4.4 Immunohistochemistry for GFAP, Iba1 and Olig2 in the cortex

As discussed in the introduction, alterations in Iba1+, Olig2+ and GFAP+ cells in the cortex are associated with various perinatal pathologies. I profiled GFAP, Iba1 and Olig2 positive cells within the cortex immediately following the paradigm. Representative images of GFAP (A-D), Iba1 (E-H) and Olig2 (I-L) can be seen in Figure 5.6. I found no difference in GFAP percentage area (Figure 5.6M), Iba1+ cell number (Figure 5.6N) or Olig2+ cell number (Figure 5.6O) following LPS or MMS, and no evidence of interaction between LPS and MMS for any of the comparisons.

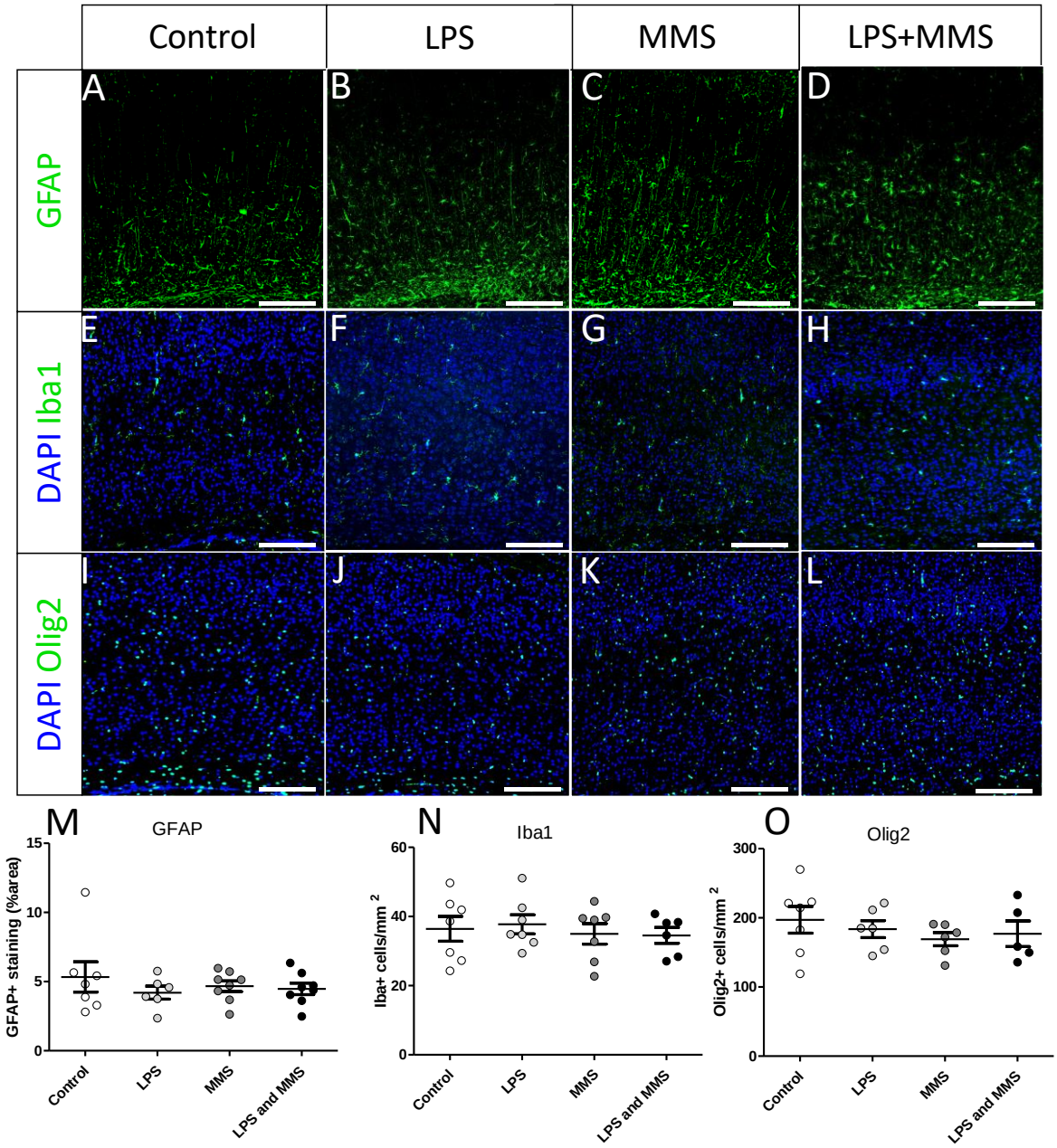

Figure 5.6 Assessment of candidate glial populations in the cortex in control (A, E, I), LPS (B, F, J), MMS (C, G, K) and LPS+MMS (D, H, L) groups. A-D show representative images of cortical GFAP staining across the 4 groups. This is quantified as percent area in M with no effect of LPS (p=0.767, f-statistic=0.09, df=22), MMS (p=0.316, f-statistic=1.048, df=22) or an interaction (p=0.476, f-statistic=0.525, df=22) between them. In E-H, representative images of Iba1+ cells (green) and DAPI+ cells (blue) from all 4 groups are shown. This is quantified as Iba1+ cells/mm^2 in N) with no difference seen for an effect of LPS (p=0.889, f-statistic=0.02, df=23), MMS (p=0.447, f-statistic=0.598, df=23) or an interaction (p=0.772, f-statistic=0.086, df=23) between them. Similarly, in I-L representative images for Olig2+ cells (green) and DAPI+ cells (blue) are seen from all 4 groups, with this quantified in O) as Olig2+ cells/mm^2. No differences were seen for an effect of LPS (p=0.857, f-statistic=0.033, df=22), MMS (p=0.286, f-statistic=1.203, df=22) or an interaction (p=0.51, f-statistic=0.451, df=22) between them. Experiments were analysed using a 2-way ANOVA, n=6-9 for all groups and comparisons. Scale bars indicate 100µm.

5.4.5 3’ mRNA sequencing

The cortical transcriptomes from the LPS, MMS and LPS+MMS groups were compared to the control group following 3’ mRNA sequencing. An n of 3 samples/ group were sequenced.

5.4.5.1 Control vs LPS

First, as seen in Figure 5.7, I compared the control and LPS groups. Following differential expression analysis 28 genes reached an FDR corrected <0.05. The volcano plot shown in Figure 5.7A shows all genes analysed for differential expression (all dots), with those with a logFC change greater than 1.5 shown in blue (downregulated) or red (upregulated). The genes failing to reach this threshold are seen in grey. In Figure 5.7B an MDS plot describes the data in 2 dimensions, which explain the vast majority of variance within the dataset. See Table 5.1 for a list of genes with an FDR<0.05 from the control vs LPS dataset along with their unadjusted p-values and LogFC.

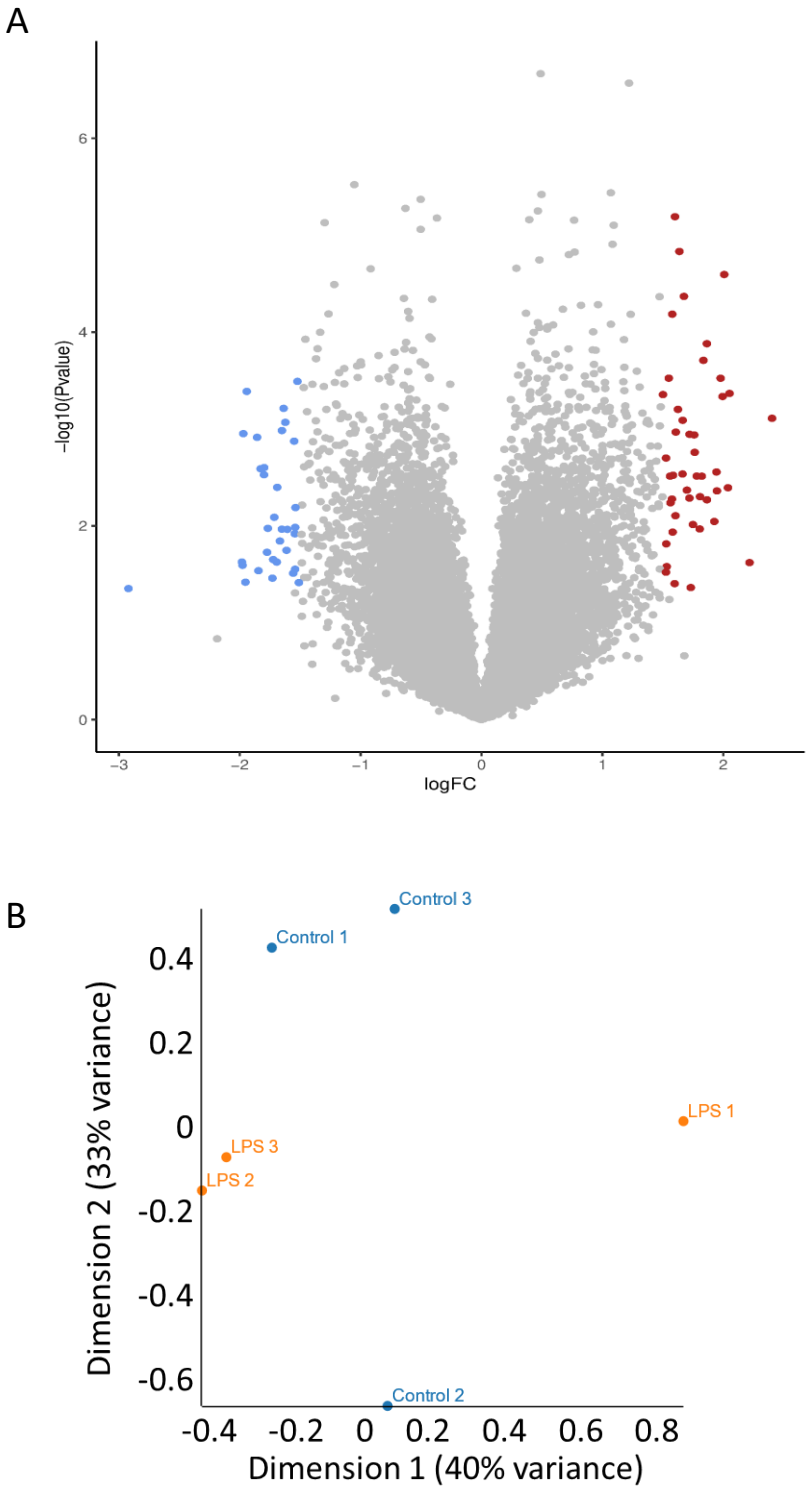

Figure 5.7 3' mRNA sequencing of cortical tissue from the control and LPS group (N=3/group) with differential gene expression analysis using VOOM with sample weights. In A) a volcano plot is shown which indicates, in blue and red, genes with a logFC of more than 1.5. In B) an MDS plot describes control (blue dots) and LPS (orange dots) group data in 2 dimensions, representing 40% and 33% of the variance within the data respectively.

Table 5.1 Genes with an FDR <0.05, listed alongside their unadjusted p-value and LogFC for the control vs LPS dataset

LPS			
Gene name	FDR	Unadjusted p-value	LogFC
RP24-468O23.2	0.006775	3.13E-07	1.214946
Col5a1	0.015074	3.93721E-06	1.071448
Gm9968	0.015074	5.89624E-06	-0.62805
Mfap5	0.015074	7.32723E-06	1.597705
RP24-323H7.4	0.015074	3.3439E-06	-1.05004
Hcn1	0.015226	8.09552E-06	-1.29473
Hgfac	0.015226	8.44339E-06	0.764093
H2-Q6	0.015606	9.20014E-06	1.093671
Gm29415	0.023281	1.45236E-05	1.083055
Cdhr3	0.026449	1.73206E-05	1.626322
H2-Oa	0.026449	1.77222E-05	0.768181
Prame	0.027063	1.87592E-05	0.718175
Hmgb1-ps6	0.030084	2.22431E-05	-0.91915
Gm10775	0.038194	3.00043E-05	1.994702
Herc6	0.04305	3.4814E-05	-1.21821

To functionally classify genes which had a logFC in expression of more than 1.5 (indicated by blue and red dots in Figure 5.7A), Gene Ontology analysis for cellular component, molecular function and biological processes were carried out, as can be seen in Figure 5.8A. To analyse over-representation of transcription factor binding sites among genes with a change in expression of more than 2-fold, a transcription factor binding enrichment analysis was carried out using the Opossum software. The results are listed in Figure 5.8B and are ranked by Z-score.

A

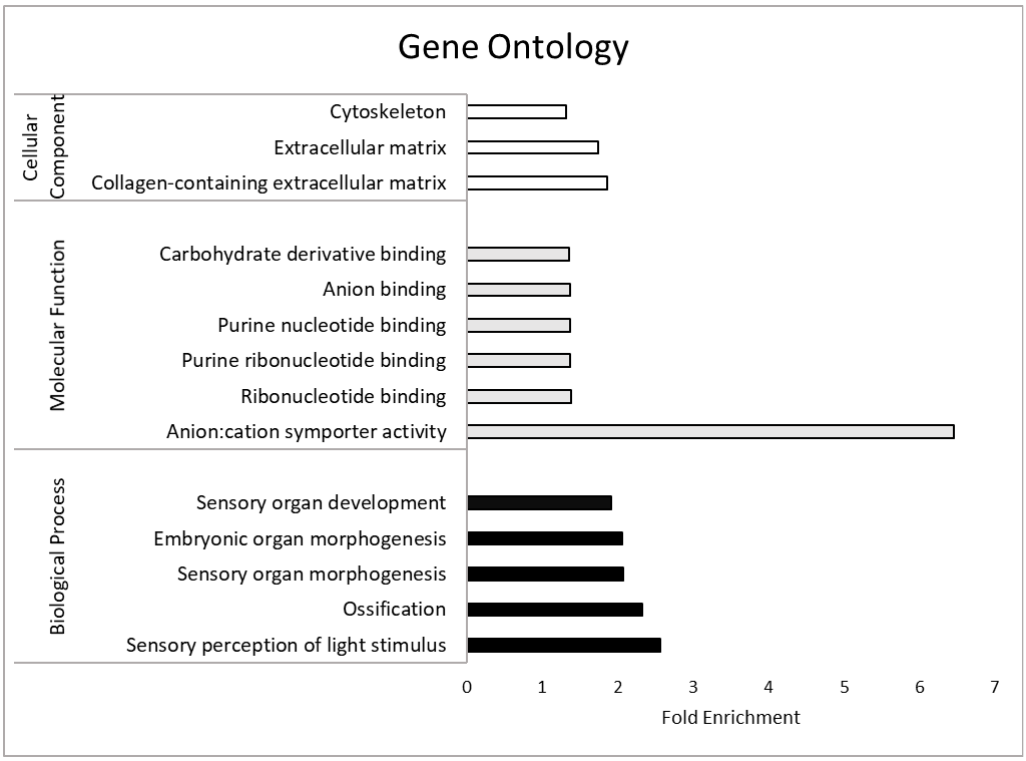

B

Rank	Transcription Factor	Family	Z-score	Fischer Score
1	MZF1_1-4	BetaBetaAlpha-zinc finger	9.598	70.306
2	IRF1	IRF	9.074	13.503
3	Hand1::Tcfe2a	Helix-Loop-Helix	8.298	35.625
4	ZNF354C	BetaBetaAlpha-zinc finger	8.013	78.334
5	SP1	BetaBetaAlpha-zinc finger	6.809	35.398
6	Zfp423	BetaBetaAlpha-zinc finger	7.627	13.548
7	Myf	Helix-Loop-Helix	7.406	21.274
8	Sox2	High Mobility Group	7.378	6.97
9	SRF	MADS	7.295	6.103
10	TAL1::TCF3	Helix-Loop-Helix	7.002	15.151

Figure 5.8 Analysis of genes with a greater than 1.5 logFC from the 3' sequencing dataset of control vs LPS. In A), Gene Ontology analysis of genes between control and LPS groups is shown for cellular component (open bars), molecular function (grey bars) and biological function (black bars). In B) a transcription factor binding enrichment analysis of genes is shown. Transcription factors are ranked by Z-score.

5.4.5.2 Control vs MMS groups

Next, I compared the control group to the MMS group as seen in Figure 5.9. Following differential expression analysis, a total 61 genes had an FDR corrected <0.05. The volcano plot shown in Figure 5.9A shows all genes analysed for differential expression (all dots), and those with a logFC of greater than 1.5 are coloured blue (downregulated) or red (upregulated) The genes failing to reach this threshold are seen in grey. In Figure 5.9B an MDS plot describes the data in 2 dimensions, which explain the vast majority of variance

within the dataset. See Table 5.2 for a list of genes with an FDR<0.05 from the control vs MMS dataset along with their unadjusted p-values and LogFC.

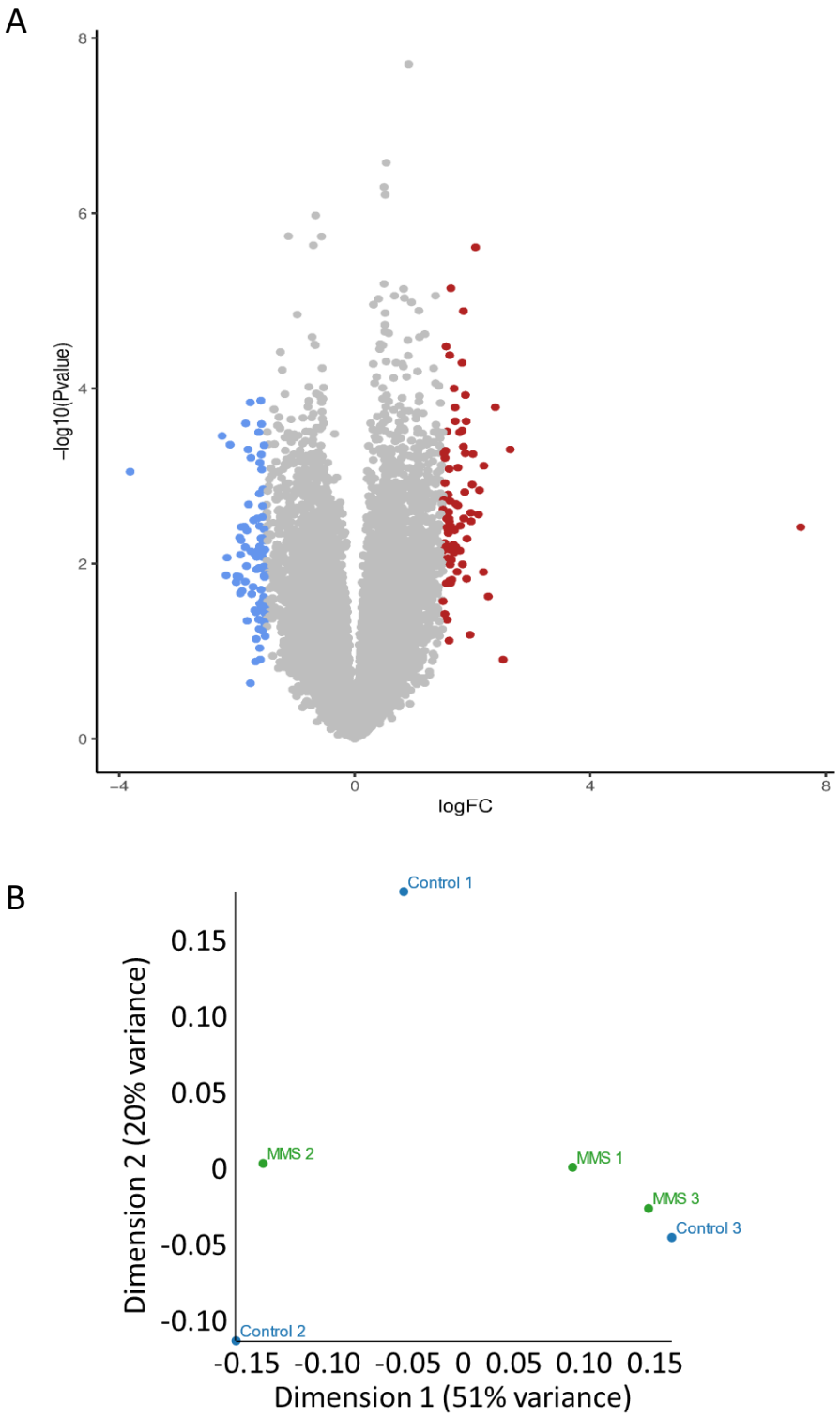

Figure 5.9 3' mRNA sequencing of cortical tissue from the control and MMS group (n=3/group) with differential gene expression analysis using VOOM with sample weights. In A) a volcano plot is shown which indicates, in blue

and red, genes with a logFC of more than 1.5. In B) an MDS plot describes control (blue dots) and MMS group (green dots) data in 2 dimensions, representing 51% and 20% of the variance within the data respectively.

Table 5.2 Genes with an FDR <0.05, listed alongside their unadjusted p-value and LogFC for the control vs MMS dataset

MMS			
Gene name	FDR	Unadjusted p-value	LogFC
Gm26884	0.001079064	2.49E-08	0.915564
Zfhx2	0.010467917	1.20933E-06	-0.66157
RP24-323H7.4	0.012627306	2.04231E-06	-1.12375
Gm9968	0.013639318	2.6013E-06	-0.70177
Sult1a1	0.013639318	2.83627E-06	2.050215
C030037D09Rik	0.026857183	9.87355E-06	1.368087
Col5a1	0.026857183	1.17498E-05	0.963867
Gm11895	0.026857183	9.17324E-06	0.824531
Gm20945	0.026857183	9.17324E-06	0.824531
Gm28979	0.026857183	1.17904E-05	0.838962
Samd11	0.026857183	7.82725E-06	1.630807
Tnfrsf18	0.026857183	1.17904E-05	0.838962
Zfp810	0.026857183	9.92458E-06	0.676586
Hmgb1-ps6	0.029911243	1.45133E-05	-0.97942
RP23-247A1.7	0.030061227	1.66698E-05	1.832265
Try5	0.030061227	1.65031E-05	1.082082
Ccdc86	0.039150045	3.25821E-05	0.898725
Erv3	0.039150045	3.32351E-05	1.093053
Gm15982	0.039150045	3.64426E-05	-0.66586
Gm6341	0.039150045	2.80825E-05	1.192692
RP23-240E15.2	0.039150045	3.64426E-05	-0.66586
Ubac2	0.039150045	2.94501E-05	-0.72013
Vax2os	0.039150045	3.57634E-05	-0.67812
Gm5117	0.039387572	4.14167E-05	1.542863
She	0.040802884	4.431E-05	-1.25531
Gm8349	0.044500303	4.97106E-05	0.908804
Rimbp3	0.044500303	5.03816E-05	1.608737
Polr2k	0.048474041	5.71205E-05	0.705397
Slco4a1	0.048930424	5.96356E-05	1.808948

To functionally classify the genes which had a logFC in expression of more than 1.5 (indicated by blue and red dots in Figure 5.9A), Gene Ontology analysis for cellular component, molecular function and biological processes were carried out, as seen in Figure 5.10A. To analyse the over representation of transcription factor binding sites among genes differentially expressed by more than 4-fold, a transcription factor binding enrichment analysis was carried out using the Opossum software. The results are listed in Figure 5.10B and show enrichment for the NFkB family of transcription factors.

A

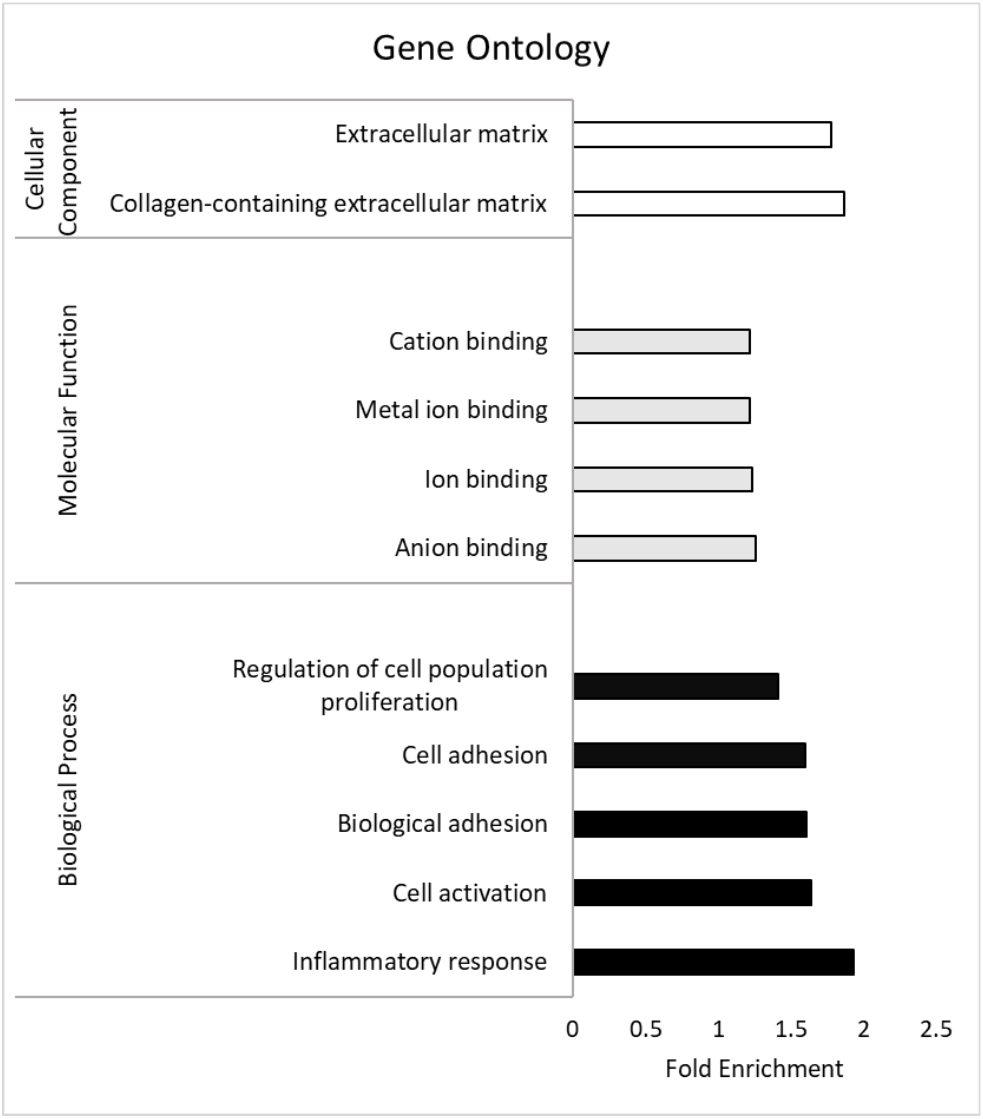

B

Rank	Transcription Factor	Family	Z-score	Fischer Score
1	EWSR1-FLI1	Ets	21.024	3.054
2	RELA	Rel	18.371	1.955
3	NFKB1	Rel	12.537	2.455
4	RXRA::VDR	Hormone-nuclear Receptor	11.291	2.183
5	NF-kappaB	Rel	9.984	1.337
6	GABPA	Ets	9.466	2.546
7	REL	Rel	8.371	0.725
8	FOXF2	Forkhead	8.061	1.319
9	Tal1::Gata1	Helix-Loop-Helix	7.463	1.413
10	SPIB	Ets	7.218	2.443

Figure 5.10 Analysis of genes with a greater than 1.5 logFC from the 3' sequencing dataset of control vs MMS. In A), Gene Ontology analysis of genes between control and MMS groups is shown for cellular component (open bars), molecular function (grey bars) and biological function (black bars). In B) transcription factor binding

enrichment analysis of genes with over a 4-fold change in expression is shown, with high representation of the NFkB family of transcription factors. Transcription factors are ranked by Z-score.

5.4.5.3 Control v LPS+MMS groups

Next, I compared the control group to the LPS+MMS group as seen in Figure 5.11. Following differential expression analysis 28 genes in total had an FDR corrected <0.05. The volcano plot shown in Figure 5.11A shows all genes analysed for differential expression (all dots), and those with a logFC of greater than 1.5 are shown in blue (downregulated) and red (upregulated). The genes failing to reach this threshold are seen in grey. In Figure 5.11B an MDS plot describes the data in 2 dimensions, which explain the vast majority of variance within the dataset. See Table 5.3 for a list of genes with an FDR<0.05 from the control vs LPS+MMS dataset along with their unadjusted p-values and LogFC.

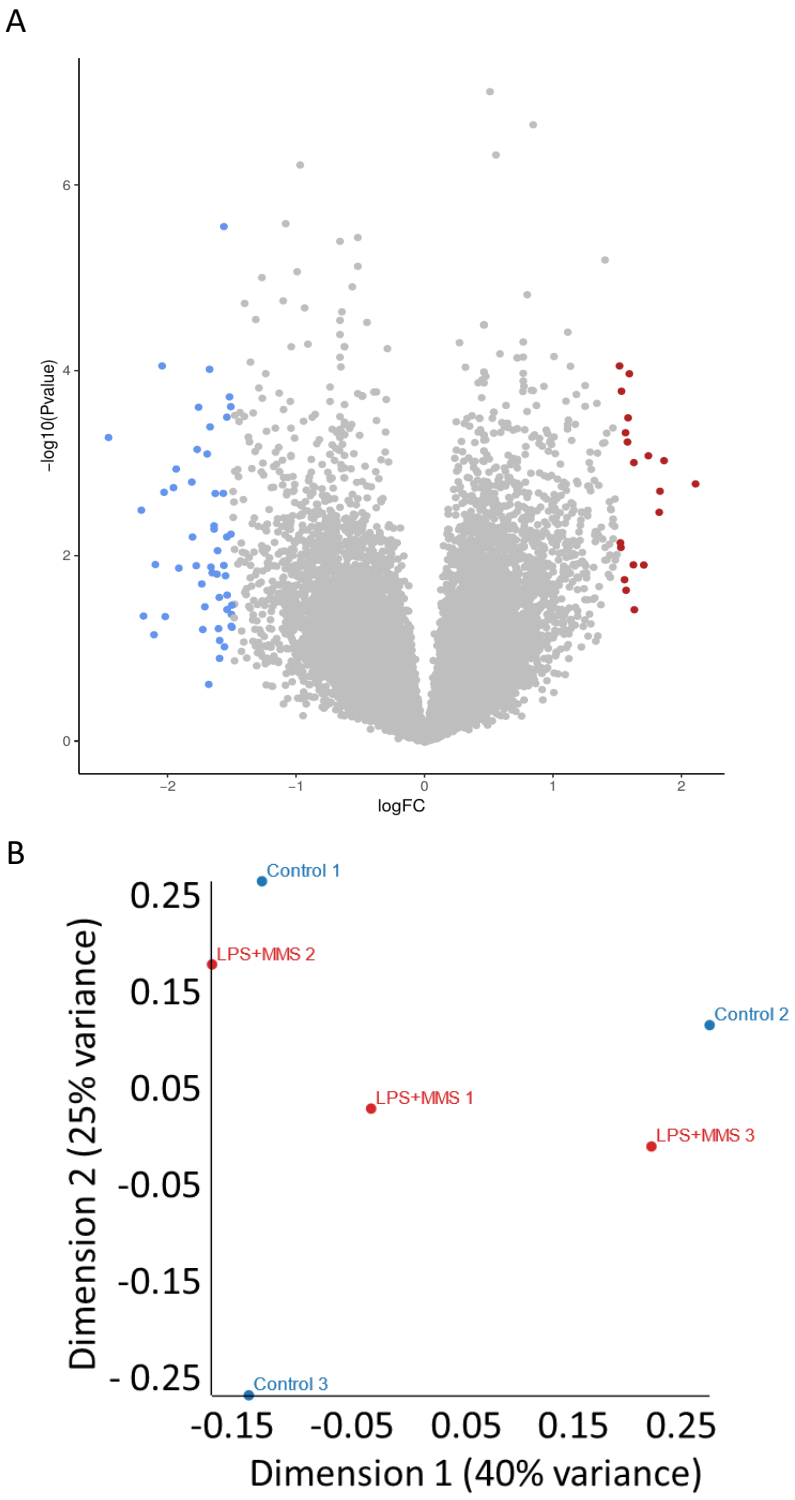

Figure 5.11 3'm RNA sequencing of cortical tissue from the control and LPS+MMS group (n=3/group) with differential gene expression analysis done using VOOM with sample weights. In A) a volcano plot is shown which indicates, in blue and red, genes with a logFC of more than 1.5. In B) an MDS plot describes the control (blue dots) and LPS + MMS (red dots) data in 2 dimensions, representing 40% and 25% of the variance within the dataset respectively.

Table 5.3 Genes with an FDR <0.05, listed alongside their unadjusted p-value and LogFC for the control vs LPS+MMS dataset

LPS+MMS			
Gene name	FDR	Unadjusted p-value	LogFC
Gm14335	0.00542	2.50E-07	0.84188
Lemd1	0.006962	6.43E-07	-0.96952
Gm4969	0.020541	2.84761E-06	-1.56267
RP24-323H7.4	0.020541	2.81017E-06	-1.08325
Gm9968	0.023502	4.34411E-06	-0.66127
Gm6341	0.03404	7.16398E-06	1.397551
Ptn	0.036553	9.29016E-06	-0.9929
Cchcr1	0.038337	1.06295E-05	-1.26753

To functionally classify the genes which had a logFC in expression of more than 1.5 (indicated by blue and red dots in Figure 5.11A), Gene Ontology analysis for cellular component, molecular function and biological processes were carried out, as seen in Figure 5.12A. To analyse the over representation of transcription factor binding sites among the genes differentially expressed by more than 2-fold, a transcription factor binding enrichment analysis was carried out using the Opossum software. The results are listed in Figure 5.12B and are not indicative of enhanced or potentiated NFkB signaling.

A

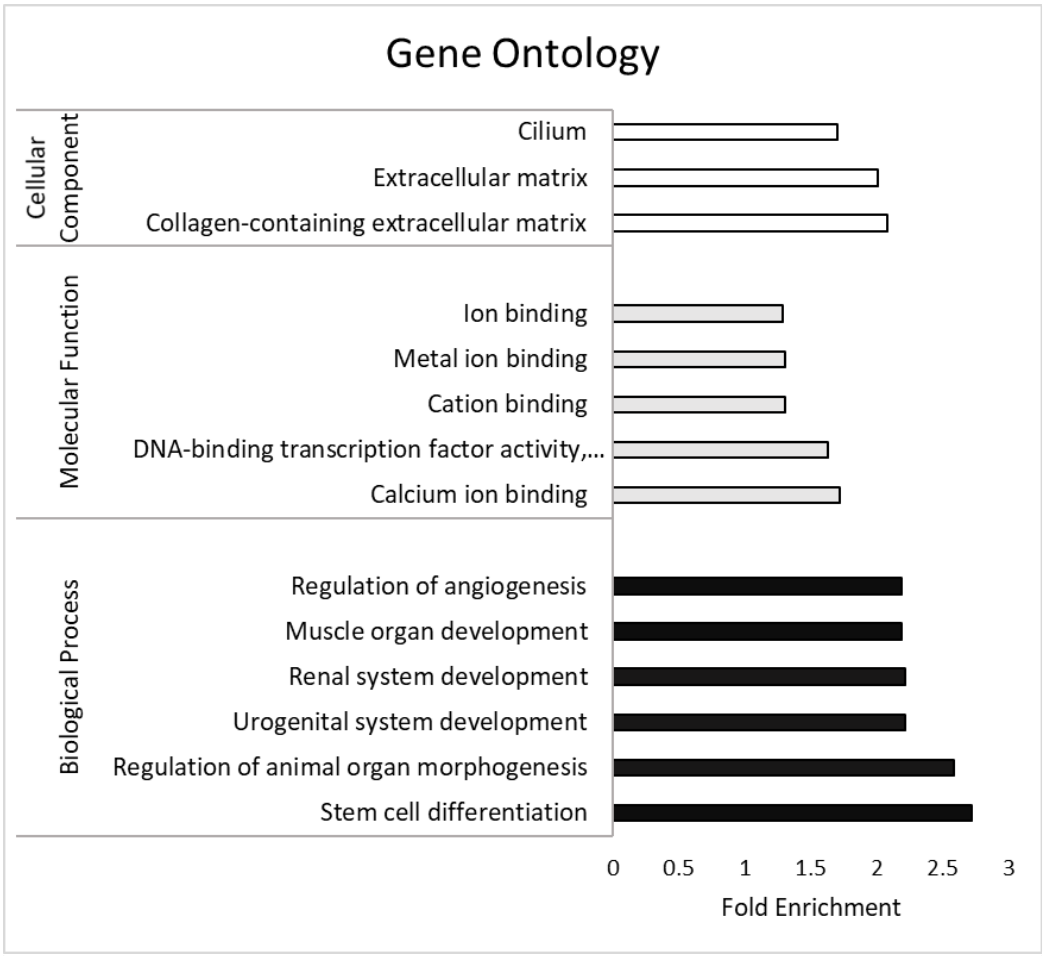

B

Rank	Transcription Factor	Family	Z-score	Fischer Score
1	Klf4	Zinc-coordinating	11.96	16.046
2	Zfp423	Zinc-coordinating	11.929	5.637
3	SP1	Zinc-coordinating	11.037	13.576
4	STAT1	Ig-fold	10.091	7.856
5	Tcfcp2l1	Other	9.193	7.274
6	MZF1_1-4	Zinc-coordinating	9.168	21.855
7	IRF2	Winged Helix-Turn-Helix	8.896	3.137
8	NFKB1	Ig-fold	7.807	5.261
9	NF-kappaB	Ig-fold	7.614	7.149
10	MIZF	Zinc-coordinating	7.26	3.348

Figure 5.12 Analysis of genes with a greater than 1.5 logFC from the 3' sequencing dataset of control vs LPS+MMS. In A), Gene Ontology analysis of genes is shown for cellular component (open bars), molecular function (grey bars) and biological function (black bars). In B) transcription factor binding enrichment analysis of genes with over a 2-fold change in expression is shown. Transcription factors are ranked by Z-score.

5.4.6 Comparison of cortical and hypothalamic transcriptome following MMS

Considering the evidence for NFkB signalling in both the hypothalamic 3' mRNA sequencing dataset presented in the previous chapter and the cortical 3' sequencing of the MMS group presented here in Figure 5.9 and Figure 5.10. I wanted to understand if similar processes were driving differential expression of genes in the cortex and hypothalamus. I therefore compared these 3' mRNA sequencing datasets.

Genes which were differentially expressed in both datasets were identified and are shown in Figure 5.13A. Six out of 17 genes (*Ccdc158*, *Sult1a1*, *Fam180a*, *8430408G22Rik*, *Fam179a* and *Ncf4*) were differentially expressed in the same direction i.e. up or down. A Gene Ontology analysis of all genes in Figure 5.13A did not identify any enriched terms, likely due to the small number of genes. Transcription factor binding enrichment analysis of these genes using Opossum, as seen in Figure 5.13B showed an over representation of NFkB motifs among all genes commonly differentially expressed between the 2 datasets.

A

Gene	Cortex	Hypothalamus
Ttr	↑	↓
Ccdc158	↓	↓
Sult1a1	↑	↑
Iyd	↓	↑
Lhx8	↓	↑
Tmem212	↑	↓
Fam180a	↑	↑
Mroh7	↑	↓
Gm14636	↓	↑
Cd14	↓	↑
8430408G22Rik	↑	↑
Gm6792	↑	↓
Gzmm	↑	↓
Fam179a	↓	↓
RP23-82P18.4	↓	↑
RP24-178N19.2	↓	↑
Ncf4	↑	↑

B

Transcription Factor	Function	Z-Score	Fisher Score
NR1H2::RXRA	Nuclear receptor	18.942	2.904
REL	Inflammatory signalling	9.941	0.641
RELA	Inflammatory signalling	9.602	0.65
NFATC2	Inflammatory signalling	6.576	3.296
NFKB1	Inflammatory signalling	5.255	1.377

Figure 5.13 Genes which were commonly differentially expressed (greater than logFC 1.5) following MMS in the cortex and hypothalamus were identified. In A) these genes are listed along with arrows indicating whether they were upregulated (grey box with white arrow) or downregulated (white box and black arrow) in the tissue specified. In B) a transcription factor binding enrichment analysis on these genes indicates an over representation of NFkB motifs associated with these genes.

5.5 Discussion

In this chapter I tested the hypothesis that the effects of MMS would be potentiated by prior exposure to LPS. I show that:

1. Pups exposed to LPS gained significantly less weight than PBS injected controls during the MMS paradigm
2. There was a significant upregulation of inflammation related gene expression in the brain 24 hours after LPS injection (i.e. onset of MMS)
3. There was no evidence from candidate gene expression or immunohistochemistry to suggest an alteration in synaptic pruning in the hippocampus following LPS and/or MMS
4. There were no changes in Iba1+, Olig2+ or GFAP+ cell composition of the cortex in any of the groups examined
5. LPS did not potentiate the effect of MMS with respect to cortical gene expression
6. There were 17 genes which were changed by more than 1.5 fold in both the hypothalamus (described in the previous chapter) and cortex, following MMS

5.5.1 LPS effects

Here I show a reduction in growth following LPS administration. Similar results have been seen in other animal models (i.e. mice [631] and rats [632]) and inflammation is also associated with poor growth in very preterm infants [633]. I did not see any differences in the brain: body weight ratio between groups (see Figure 5.3C), which implies there was no brain sparing effect as has been described for intrauterine growth restriction in humans [634] and animal models [635].

As shown in Figure 5.4 and Figure 5.6, there were no changes in Iba1+, Olig2+ or GFAP+ cells in the hippocampus or cortex respectively, there was also little change associated with LPS administration throughout these experiments. This is surprising as LPS is associated with profound effects on the brain at various concentrations (see introduction for further details). I ruled out poor quality LPS and inaccurate IP injections as the cause of this for the following reasons. Firstly, the consistent reduction in growth seen across all animals which received LPS is indicative of a physiological response and as outlined earlier in the discussion this result

agrees with both clinical and preclinical studies on inflammation. Secondly, using the same batch of LPS and injection technique, there were highly significant differences in the expression of candidate inflammatory molecules within whole brain tissue 24 hours after injection (as seen in Figure 5.2).

5.5.1.1 LPS dynamics

I administered LPS systemically through IP injection, through this route LPS is absorbed by the mesenteric blood vessels and circulated throughout the body [636]. Systemic administration of LPS in adult mice results in minimal LPS crossing the BBB. Interestingly when LPS is given repeatedly, which results in the opening of the BBB (which more accurately represents the neonatal BBB) the vast majority of LPS still does not cross the BBB [637]. This implies that LPS mediated brain inflammation results from peripheral mediators rather than central LPS mediated TLR4 activation. LPS has an extremely short half-life in adult mice (2-4 minutes) [638] and therefore the peripheral inflammatory mediators driving the central transcriptional changes at 24 hours (see Figure 5.2) may have subsided by 73.5 hours (duration of experiments described in Figure 5.3-Figure 5.12 from initial LPS administration). This may have led to a limited interaction between LPS and the MMS paradigm. This is a central limitation to these experiments, as an infant with sepsis would likely experience prolonged exposure to these inflammatory mediators. A way to overcome this in the future would be to use daily dosing of LPS alongside MMS induction.

5.5.2 Immunohistochemistry

5.5.2.1 Iba1

It was surprising to see no changes in Iba1+ cells within the LPS group but as outlined earlier this may be due to the resolution of inflammation by the time of assessment. Iba1 marks all myeloid cells and under homeostatic conditions most of these cells consist of microglia. However, perinatal insults have been associated with the infiltration of peripheral myeloid cells [641]. Saavedra *et al*, using the traditional maternal separation paradigm (3 hours/day for 2 weeks), saw a decrease in microglial density in the hippocampus. In their study mice received 1mg/kg of LPS on P14 (end of the maternal separation paradigm) which also resulted in a decreased microglial density within the hippocampus with the largest effect seen when maternal separation was combined with LPS [642]. Delpech *et al*, using the same maternal separation paradigm as Saavedra *et al* showed an increase in microglial density within the hippocampus at P14 and P28 [643]. The differences between the findings in these papers and

my own could be explained in several ways. Firstly, MMS is distinct from maternal separation and as such different effects are not surprising. Secondly, microglial assessment was done at P14 in these studies, compared to P6 in this chapter. As described in the introduction microglia assume distinct phenotypes during development, therefore at P14 microglia in the hippocampus may respond differently to stress and LPS challenge compared to at P6. Finally, LPS was given after the stress paradigm in these studies and therefore these studies model a different aspect to the interaction between early life stress and inflammation I aimed to investigate.

5.5.2.2 Olig2

As discussed in the introduction and the first results chapter, oligodendrocytes are particularly susceptible to PTB related brain injury [69] and hypomyelination has been seen in animal models of perinatal inflammation [250]. Also, in my first results chapter I showed a trend towards a reduction in mature myelinating oligodendrocytes after LPS exposure in a primary mouse OPC culture model. Stress has also been linked to oligodendrocyte alterations, a study by Teissier *et al* using 2 weeks of maternal separation for 3 hours/day showed altered myelination within the cortex [644]. I used Olig2 to label all cells of the oligodendrocyte lineage, therefore, even though I do not see alterations in Olig2 cell number, it is possible there are alterations within cellular subtypes of the lineage. For instance, a premature differentiation to mature oligodendrocytes would not necessarily reduce Olig2+ cell numbers immediately but it would reduce the number of OPCs and increase the number of mature oligodendrocytes. Future investigations using specific labels for the entire oligodendrocyte lineage would assist with understanding this further.

5.5.2.3 GFAP

Astrocytes have recently been described to be much more heterogenous than once thought, and the traditional marker GFAP is thought to label only about 5-10% of all astrocytes [645]. GFAP was used in this study as it is increased during astrogliosis, which is an important mechanistic response to inflammation [646]. As such it was not intended to be indicative of the astrocyte population at large and future work to investigate this could use the marker Sox9 to more comprehensively assess astrocyte proportions following MMS.

In adult rats exogenous administration of corticosterone results in a decrease in GFAP staining throughout the brain [647]. Maternal separation (3 hours/day for 2 weeks from P1) studies have also shown a marginal reduction in GFAP staining in the hippocampus at P14 [642].

However, in my experiments there were no differences in GFAP in the cortex or hippocampus following MMS. This discrepancy with the literature may be due to several reasons. Firstly, I assessed the presence of GFAP at P6, and the presence of GFAP is known to increase with age [648]. Secondly, as discussed in the introduction P6 is associated with a hyporesponsive period to stress in mice and as such may be associated with differential GFAP responses to stress. A marginal reduction in GFAP staining in the hippocampus following LPS in mice at P14 has previously been reported [642]. This is similar to the trend I report here, of a borderline significant decrease in GFAP following LPS. This may be an effect of LPS on astrocytes and astrogliosis which is independent of age.

It should also be noted that the areas which I quantified glial cells were not exhaustive and may not be representative of the entire cortex or hippocampus. In the future, studies such as this should strongly consider the use of single cell RNA sequencing for deep phenotyping of cellular tissue composition.

5.5.3 Investigation of synaptic pruning

Using maternal separation for 3 hours/day for 2 weeks (P1-P14), Wei *et al* show decreased synaptic protein levels and an increased number of immature dendritic spines in the hippocampus at P28 [649]. These results imply alterations in synaptic maturation or pruning following early life stress, which I provide no evidence for using the MMS model. It is possible the time point I used was too early to see functional alterations in synaptic maturation associated with MMS.

Considering I saw no difference in microglial cell number and no expression differences in candidate genes, I did not further investigate deficits in synaptic pruning. To do this would require a multi-faceted approach using high magnification confocal imaging to look at the co-localisation of synaptic proteins such as PSD95 or V-GLUT1, Iba1 (or the microglial specific marker Tmem119) and a lysosomal marker such as LAMP1. Also, the co-labelling of the pre and post-synapse with PSD95 and V-GLUT1 and the optimisation of a Matlab script to quantify their co-localisation within a certain distance to assess synapse number *in situ* as per Zhu *et al* [585]. Another option would be whole tissue protein extraction and western blotting for these markers, but this lacks spatial specificity.

5.5.4 3’ mRNA sequencing

Here as in the previous chapter, I used 3’ mRNA sequencing to interrogate the cortical transcriptome. However, to account for the smaller sample size used here (n=3/group), I used the method VOOM with sample weights to analyse differentially expressed genes. This consists of a statistical approach to minimize gene expression variation within data groups by weighting samples appropriately. Low levels of variation are of particular importance in experiments with a low n. This method of variation minimisation results in less false discoveries and higher powered experiments (as data removal isn’t necessary) when compared to traditional methods [630].

A study from Delpech *et al* using 3 hours of maternal separation/day for 2 weeks demonstrated widespread changes in the microglial transcriptome at P14 using a Nanostring immune panel. In their study, promoter analysis of differentially expressed genes indicated an enrichment in NFkB activity [643]. I see a similar transcriptional signature across multiple brain regions (the hypothalamus and cortex) and among genes which are commonly differentially expressed between these two regions following MMS. My data set and that from Delpech *et al*, differ in many ways (i.e. brain region, cellular heterogeneity, age of mice, mouse strain, stress paradigm and technique used for transcriptome analysis), this suggests that dysregulation of NFkB signaling may be a fundamental mechanism in the acute stress response in the developing brain which acts independently of brain region and cellular subtype. However, this needs to be validated further in female mice as well as other brain regions and cellular subtypes in the future as well as using other techniques such as western blotting.

Due to the unique nature of the transcriptome in specific cell subtypes, a shift in Iba1+, Olig2+ or GFAP+ cells would consequently underlie many of the changes seen in any sequencing dataset. Even though this is a far from exhaustive list of cell types within the cortex, the lack of changes seen here for these markers suggest this is not an explanation for any alterations seen in the sequencing dataset. However, with the advent and proliferation of single cell sequencing, this method should be the method of choice for the transcriptomic investigation of brain areas in the future as it can fully account for subtle changes in cellular composition.

5.5.5 Interaction between LPS and early life stress

The results in this chapter do not support my hypothesis that MMS would potentiate and prolong a prior inflammatory exposure. As outlined in the introduction to this chapter, I

hypothesised this for 2 main reasons. Firstly, in my previous results chapter I saw a strong NFkB signature among differentially expressed genes in the hypothalamus and considering the canonical role of LPS mediated TLR4 activation I reasoned this would sustain and potentiate the effect of LPS. Secondly, sleep deprivation is a central component of the MMS paradigm and sleep deprivation has been shown to decrease the clearance of inflammatory molecules from the brain and the CSF. As such I considered that the, albeit brief, sleep deprivation used here as part of the MMS paradigm would prolong the inflammatory response. My ultimate prediction therefore was that there would be more differential expression of genes related to inflammation and NFkB signalling in the LPS+MMS group. However, as shown in Figure 5.11 and Figure 5.12, there was a slight reduction in differentially expressed genes when compared to the MMS alone group with no enhancement of NFkB signalling. The reasons discussed above with respect to LPS dosing are a possible reason for this result.

5.5.6 Similar effects of MMS in the cortex and hypothalamus

In **Error! Reference source not found.**Figure 5.13 I compare the cortical and hypothalamic transcriptome following MMS. Of the genes which were commonly differentially expressed between the cortex and hypothalamus, most were not changed in the same direction. This may be due to brain region specific differences. Of the 17 genes which were commonly altered in both tissue depots, 6 were changed in the same direction. As the criteria used to identify commonly differentially expressed genes was not statistically stringent, to promote discovery, it would be incorrect to interpret the physiological relevance of these commonly dysregulated genes individually, and they are too few to undergo Gene Ontology.

Gene Ontology terms related to the cilium were enriched in both the hypothalamic and cortical MMS datasets. Considering both brain regions have a ventricular surface this could indicate altered ciliary function at the ventricular surface and perhaps altered CSF flow as a result. This would be an extremely interesting question to address in the future, but it comes with significant technical problems. CSF penetration (which relates to metabolite clearance) can be measured following fluorophore injection into the CSF via the cisterna magna and allowing the animal to recover for a period of time before perfusion and serial brain sectioning to measure penetration. However, this is extremely technically difficult in neonatal mice and to my knowledge has not been done before. Sophisticated imaging techniques such as two-photon microscopy can also be used to image CSF flow *in vivo* using

particle tracking [650]. However, to my knowledge this also has not been done in neonatal animals.

5.5.7 Conclusion

In this chapter I show LPS administration via IP injection, but not MMS, results in decreased weight gain, but this does not interact with MMS in neonatal animals. I also provide evidence to suggest an inflammatory response is present within the brain 24 hours after the administration of LPS, at the onset of MMS. I did not see any specific effects of MMS or any interaction with LPS on Iba1, Olig2 or GFAP positive cells in the hippocampus or cortex. I also did not see any effect of MMS or interaction with LPS on the expression of candidate genes which have previously been implicated in synaptic pruning. I carried out 3' mRNA sequencing and showed an enrichment of NFkB binding motifs among the differentially expressed genes in the MMS group, which is not potentiated with prior exposure to LPS. I also show this enrichment of NFkB binding motifs is present within the genes commonly differentially expressed between MMS in the cortex and hypothalamus.

6 Discussion

Mechanistic insight into the pathogenic processes associated with PTB is difficult to discern in humans. In this thesis, I have examined how insults associated with PTB can affect brain development in mice at timepoints with neurodevelopmental relevance to PTB. To do this I used several *in vitro* (organotypic forebrain slice culture and primary cell culture) and *in vivo* (MMS and LPS administration) models, as well as a variety of both candidate (e.g. qPCR, immunohistochemistry, ELISAs, etc) and unbiased (3' mRNA and meDIP sequencing) approaches. Using these methods, I investigated the role of LPS and hypoxia on various biochemical and physiological outputs, how a novel model of early life stress can affect the biochemical and physiological characteristics of the neonatal brain and behaviour in adulthood, as well as the interaction between early life inflammation and stress.

6.1 Heterogeneity of PTB related insults

PTB can be associated with, among other insults, inflammation, stress, hyperoxia/hypoxia and synthetic glucocorticoid exposure. The incidence and/or severity of these vary dramatically among preterm infants [651], making it difficult to generalise results. As such,

increasing our understanding of these factors and their interactions may be important in helping us to elucidate the mechanisms involved in PTB related brain injury.

In this thesis I investigated the ability of LPS (to model bacterial induced infection) to sensitise to subsequent hypoxia and MMS (as described in the first and third results chapters respectively). For the investigation of LPS and hypoxia, I focused on candidate gene expression and 5hmC in an organotypic forebrain slice culture model, cytokine release in primary mouse microglia culture and differentiation in primary mouse OPC culture. Previous work has convincingly shown that exposure to LPS can sensitise to the effects of subsequent hypoxia in animal models [517,652] with respect to cell death, inflammation and myelination and that inflammatory sensitisation might also occur in neonates [612]. It is therefore somewhat surprising that I saw no effect in the primary OPC and primary microglial culture models. One explanation may be that this previous work did not examine the same metrics as I did here. A major weakness of my work is that it was performed *in vitro*, and as discussed previously the oxygen saturation used in control conditions may not have be physiologically relevant despite its wide use. Future work should investigate these mechanisms in an unbiased fashion *in vivo* and use the culture systems outlined here to investigate the finer mechanisms associated with these processes or as an earlier stage screening tool for therapeutics.

I also hypothesised that LPS would sensitise mice to the subsequent effects of MMS due to the NFkB signature seen in the hypothalamic transcriptome. However, I showed that this was not the case with respect to gene expression. However, as I demonstrated, MMS is only associated with subtle gene expression changes in the first instance and as such any potentiation would likely also have a small effect size. Therefore, other methods, such as DNA methylation which are associated with many changes following MMS, could be used in future studies. I also saw no differences in Iba1, Olig2 or GFAP positive cells following LPS and MMS, but this may have been due to the limitations previously discussed. As such, these results do not preclude an interaction between LPS and MMS. Future work on this should take a more all-encompassing approach by evaluating characteristics which have larger effect sizes, such as DNA methylation, as well correlating them to behavioural outcome.

6.2 Genetics and polygenetics of neurodevelopmental disorders

Even in instances of monogenic cases of ASD which are inherited in a mendelian fashion, such as tuberous sclerosis complex (TSC), there is significant phenotypic heterogeneity. For instance, TSC is associated with abnormal DTI (diffusion tensor imaging) findings on MRI, but

no one region has been consistently identified as being affected across studies [653,654] suggesting the involvement of other genetic and/or environmental factors [655].

As discussed previously, a small proportion of neurodevelopmental disorders are caused by a single genetic alteration with a large effect size [656]. However, it is now clear that a large proportion of neurodevelopmental disorders are characterised by genetic effects with many small effect sizes [34]. Moreover, most of the heritability of ASD [657] and schizophrenia [658] is due to common genetic variation rather than specific mutations, copy number variants or other genetic events. Understanding how this normal genetic variation can lead to neurodevelopmental disorders is central to understanding their aetiology.

Normal genetic variation can also contribute to variation in DNA methylation and large scale chromatin architecture [659,660], which as discussed previously are changed in many neurodevelopmental disorders. However, the effects of other processes such as further cytosine modifications, RNA dynamics such as alternative splicing, RNA processing, methylation and degradation also need to be assessed. To characterise these features, large collaborative efforts such as the PscyhENCODE consortium are required, but it also requires a mechanistic understanding of how the environment interacts with these processes. This is only currently possible using experimental models whose biochemical and physiological processes can be more thoroughly interrogated.

In most instances the mechanisms by which genetic variation associates with atypical development are not fully understood. Previous studies have shown an enrichment for hypoxia and vascular related genes among genetic risk factors for schizophrenia [56]. Therefore, the risk carried by these alleles could potentially be mediated through perinatal exposure to hypoxia. Similarly, early life stress has been shown to interact with risk loci for schizophrenia and major depressive disorder [530]. Polygenic risk may therefore interact with various perinatal insults to affect neurodevelopmental trajectories.

Moreover ASD, schizophrenia, ADHD bi-polar and major depressive disorder share a substantial overlap in SNPs [661], and a cross disorder (ADHD, anorexia, affective disorders, ASD, bipolar disorder and schizophrenia) GWAS from the iPSYCH study showed several significant associations [662], indicating a shared genetic aetiology among neurodevelopmental disorders. Therefore, identical environmental exposures may interact with distinct polygenetic compositions to result in divergent neurodevelopmental trajectories.

Several neurodevelopmental disorders are associated with altered synaptic characteristics [663,664]. The investigation of early life events which can result in alterations involving synapse associated loci, such as my findings of DNA methylation alterations at synapse associated genes following MMS, may therefore provide mechanistic insight into this association. This may ultimately be useful for the therapeutic facilitation of optimal brain development in the neonatal period.

Even though genetics can explain an increasingly large portion of neurodevelopmental disorders, the environment undoubtably also plays a crucial role. Therefore, studies which investigate the effect of insults associated with PTB on gene expression and DNA methylation, as carried out in this thesis, can contribute to the wider integration of data from genetic/epigenetic studies in humans or animal models in an attempt to better understand human neurodevelopmental outcomes.

6.3 Assessment of models used in this thesis

6.3.1 *In vitro* models

In this thesis I use both *in vitro* and *in vivo* models to assess the impact of various insults associated with PTB on brain development. *In vitro* models included primary cell culture and forebrain organotypic slice cultures. I have previously discussed the practical limitations of these models and have recommend they be used in the future to investigate specific mechanisms which have been identified through *in vivo* experimentation. These systems are also conducive to a first line screening tool for therapeutics. For instance, the organotypic slice culture system would be a good model to investigate the efficacy of SAFit1, SAFit2 and CBR1 agonists (which I previously suggested as good candidates to target MMS related effects) in response to either Dexamethasone (to induce GR activation) or glutamate (to activate hypothalamic neurons), before larger *in vivo* studies.

Alternatively therapeutic efficacy could be evaluated in human iPSCs or organoids, however as discussed earlier these models are prohibitively expensive to scale up and are associated with large heterogeneity, but recent protocols describe more homogenous organoid generation [665].

6.3.1.1 LPS alternatives

The TLR family is the most well studied family of pathogen recognition receptors (PRR) and consists of over 13 characterised members [639], of which many are expressed in the forebrain

through development [640]. LPS specifically activates TLR4 and as such the experiments outlined here fail to account for the dynamic TLR (and wider PRR) activation associated with clinical neonatal inflammation [611].

Poly I:C is a TLR3 agonist and is commonly given to pregnant dams between E14-E18 to model viral infection during pregnancy. LPS was used here and it activates canonical NFkB signalling through the intracellular MyD88 domain of TLR4. However, TLR3 does not have an intracellular MyD88 domain, due to its cytoplasmic localisation, but can activate NFkB signalling through the TRIF pathway. As such the NFkB activation dynamics associated with TLR3 signalling are different to that of TLR4 signalling [639] and it would be interesting in the future to examine the effect of TLR3 stimulation, with Poly I:C, on NFkB signalling before and/or during MMS.

6.3.2 Stress associated with PTB in humans

The ultimate goal of this research is to identify mechanisms which can be targeted during the neonatal period to mitigate any adverse effects of stress on brain development. However, for now there are many obstacles in this path. First and foremost, to my knowledge there is no conclusive human evidence to suggest perinatal stress in preterm infants results in atypical brain development. There are a number of reasons why these are difficult experiments to carry out. Firstly, there is no logical control group for comparison. Infants which will be born at term remain *in utero* during the time which preterm infants experience stress associated with the NICU, which precludes biological sampling. A within subject study would, therefore, be needed to identify stress and associate it with neurodevelopmental outcome. This design necessitates a biomarker which is responsive to stress. Cortisol only begins circadian secretion by 2 months of age [293] but at this point it is responsive to stress [602]. However, the use of cortisol would require sampling before and after an event such to determine associated stress. Aside from the ethical and practical considerations associated with frequent blood sampling, the procedure itself would induce stress and thereby render the “before” value redundant. Salivary α-amylase has been used as a stress responsive biomarker and could be measured non-invasively, but studies suggest stress responsiveness in this enzyme only initiates at 2 months [602]. Heart rate variation is likely the best candidate as it can be measured non-invasively for long periods and is decreased with the use of kangaroo care [603]. However, this is also a measure of general health and thereby susceptible

to the other confounders associated with the use of “painful procedures” as a method to quantify stress [604].

6.3.3 Future behavioural tests

Future work should expand on these behavioural studies outlined here. As mentioned previously the EPM and the OF constitute novel stressful environments. It is important to understand if this abnormal behaviour is also relevant in novel social or intellectual environments. For instance a 3 chamber social approach assay, previously validated for abnormal sociability associated with atypical neurodevelopment by Reed *et al*, 2019 [600]. A test of learning or working memory in a stressful environment such as the Barnes maze would also be particularly insightful considering the gene expression changes I show in the hippocampus at 4 months of age (see Figure 4.26).

6.4 Epigenetics in PTB related insults

Throughout this thesis I examined the role of cytosine modifications in response to environmental perturbations. However, the importance of these changes is difficult to assess. DNA methylation is crucial to brain development; deletion of *DNMT1* results in an almost 90% loss of DNA methylation and is embryonically lethal in mice[669] and *DNMT1* is comparably important in humans [670]. DNA methylation is also crucial for key neurodevelopmental processes such as neurogenesis [671], gliogenesis [672] and myelination [673]. Considering this in combination with the energetic requirements for the generation and maintenance of differential methylation [674], it is highly likely the differential methylation seen following MMS represents an important component of the response.

A key aspect to understanding the role of DNA methylation in the pathogenesis of perinatal brain injury is to first understand the role of DNA methylation in normal brain development. In recent years, many DNA methylation maps of healthy human and mouse brain tissue, of various ages, have been generated [110,204,675,676]. These are crucial to the fundamental understanding of cytosine modifications in the brain, however, more neonatal timepoints are needed. Also, many of these maps depict only bulk tissue DNA methylation patterns and not within cell lineages. As discussed previously, the technologies for single cell epigenetic

analysis are emerging and their use will be central to our future understanding of DNA methylation in typical and atypical brain development.

Currently some therapies which target DNA methylation are used to treat some forms of cancer but these are usually associated with many off target effects and are not typically front line treatments [677]. When the importance of DNA methylation to a range of brain processes [671–673] is also considered, it is highly unlikely that DNA methylation is a clinically viable target during development. However, the inhibition of DNA methylation using 5-Azacytidine (intercalates with DNA to inhibit methylation) [678], Procainamide (DNMT1 inhibitor) [679] or 3-nitroflavones (DNMT3a inhibitor) [680] could provide valuable mechanistic insight into the role of DNA methylation following MMS. This could also be achieved through genetic means by the conditional deletion of *DNMT1* and/ or *DNMT3a* using Cre-Lox recombination in specific cell types or local deletion in the hypothalamus using the injection of viral vectors prior to MMS. These methods would allow for the non-specific modulation of DNA methylation and thereby allow for inference about the importance of DNA methylation in the behavioural effects seen following MMS.

It is unlikely that changes in DNA methylation occur in isolation, previous work has described a close relationship between DNA methylation and chromatin architecture [681] and huge efforts to map genome wide epigenetic data in cells such as ENCODE have demonstrated the co-localisation of many epigenetic marks [682,683]. Moreover, proteins such as MeCP2 can affect DNA methylation and chromatin architecture co-operatively [684,685]. Future work should focus on comprehensively assessing the effect of MMS on the wider epigenetic landscape.

6.5 Single cell level investigations

For a more comprehensive understanding of cellular proportions and cell specific transcriptomic information, single cell sequencing following MMS could be performed. This would also provide information on transcriptional alterations in specific neuronal populations, perhaps indicating particular circuits involved in MMS.

Techniques to analyse DNA methylation at the single cell level are still relatively novel. Techniques which use bisulphite conversion followed by sequencing at the single cell level have been associated with DNA degradation problems, as well as having prohibitive costs due to the depth required for accuracy. Also many non-bisulphite based methods cannot assess genome wide methylation [586].

Techniques are also emerging for the combined single cell assessment of the transcriptome, chromatin accessibility and DNA methylome in a single sample, but these techniques require the generation of a large reference data set for accurate cell lineage mapping [587]. These large datasets are not available for neonatal tissue yet but offer a promising future strategy.

6.6 Conclusions

Throughout this thesis I have examined how insults associated with PTB affect neonatal mouse brain development. Understanding how these processes are involved in atypical neurodevelopment is central to better understanding and managing neurodevelopmental disorders. The results presented here contribute to the wider body of literature concerning PTB related brain injury and may be important in understanding the aetiology of neurodevelopmental disorders.

7 References

1. Ananth, C. V & Vintzileos, A. M. Epidemiology of preterm birth and its clinical subtypes. *J. Matern. Fetal. Neonatal Med.* **19**, 773–82 (2006).

2. Blencowe, H. *et al.* Born too soon: the global epidemiology of 15 million preterm births. *Reprod. Health* **10 Suppl 1**, S2 (2013).

3. Slattery, M. M. & Morrison, J. J. Preterm delivery. *Lancet (London, England)* **360**, 1489–97 (2002).

4. Office for National Statistics. *Gestation-specific infant mortality in England and Wales*. (2012).

5. Wilson-Costello, D. *et al.* Improved Neurodevelopmental Outcomes for Extremely Low Birth Weight Infants in 2000–2002. *Pediatrics* **119**, (2007).

6. Wilson-Costello, D., Friedman, H., Minich, N., Fanaroff, A. A. & Hack, M. Improved Survival Rates With Increased Neurodevelopmental Disability for Extremely Low Birth Weight Infants in the 1990s. *Pediatrics* **115**, (2005).

7. Moore, T. *et al.* Neurological and developmental outcome in extremely preterm children born in England in 1995 and 2006: the EPICure studies. *BMJ* **345**, e7961–e7961 (2012).

8. Douglas-Escobar, M. & Weiss, M. D. Hypoxic-Ischemic Encephalopathy. *JAMA Pediatr.* **169**, 397 (2015).

9. Allen, K. A. & Brandon, D. H. Hypoxic Ischemic Encephalopathy: Pathophysiology and Experimental Treatments. *Newborn Infant Nurs. Rev.* **11**, 125–133 (2011).

10. Nelson, K. B. Causative factors in cerebral palsy. *Clin. Obstet. Gynecol.* **51**, 749–62 (2008).

11. Trønnes, H., Wilcox, A. J., Lie, R. T., Markestad, T. & Moster, D. Risk of cerebral palsy in relation to pregnancy disorders and preterm birth: a national cohort study. *Dev. Med. Child Neurol.* **56**, 779–785 (2014).

12. Kolevzon, A., Gross, R. & Reichenberg, A. Prenatal and Perinatal Risk Factors for Autism. *Arch. Pediatr. Adolesc. Med.* **161**, 326 (2007).

13. Movsas, T. Z. & Paneth, N. The Effect of Gestational Age on Symptom Severity in Children with Autism Spectrum Disorder. *J. Autism Dev. Disord.* **42**, 2431–2439 (2012).

14. Schendel, D. & Bhasin, T. K. Birth Weight and Gestational Age Characteristics of Children With Autism, Including a Comparison With Other Developmental Disabilities. *Pediatrics* **121**, 1155–1164 (2008).

15. Abel, K. M. *et al.* Birth Weight, Schizophrenia, and Adult Mental Disorder. *Arch. Gen. Psychiatry* **67**, 923 (2010).

16. Dalman, C., Allebeck, P., Cullberg, J., Grunewald, C. & Köster, M. Obstetric complications and the risk of schizophrenia: a longitudinal study of a national birth cohort. *Arch. Gen. Psychiatry* **56**, 234–40 (1999).

17. Bhutta, A. T., Cleves, M. A., Casey, P. H., Cradock, M. M. & Anand, K. J. S. Cognitive

and behavioral outcomes of school-aged children who were born preterm: a meta-analysis. *JAMA* **288**, 728–37 (2002).

18. Khalifeh, A., Quist-Nelson, J. & Berghella, V. Universal cervical length screening for preterm birth prevention in the United States (.). *J. Matern. Fetal. Neonatal Med.* 1–4 (2016) doi:10.1080/14767058.2016.1220521.

19. Sherf, Y. *et al.* Recurrence of Preterm Delivery in Women with a Family History of Preterm Delivery. *Am. J. Perinatol.* (2016) doi:10.1055/S-0036-1592131.

20. Zhang, G. *et al.* Genetic Associations with Gestational Duration and Spontaneous Preterm Birth. *N. Engl. J. Med.* **377**, 1156–1167 (2017).

21. Adhikari, K. *et al.* Does neighborhood socioeconomic status predict the risk of preterm birth? A community-based Canadian cohort study. *BMJ Open* **9**, e025341 (2019).

22. Karuppagounder, S. S. *et al.* Metabolism and epigenetics in the nervous system: Creating cellular fitness and resistance to neuronal death in neurological conditions via modulation of oxygen-, iron-, and 2-oxoglutarate-dependent dioxygenases. *Brain Res.* **1628**, 273–287 (2015).

23. Agrawal, V. & Hirsch, E. Intrauterine infection and preterm labor. *Semin. Fetal Neonatal Med.* **17**, 12–9 (2012).

24. Behrman, R. E., Butler, A. S. & Outcomes, I. of M. (US) C. on U. P. B. and A. H. Mortality and Acute Complications in Preterm Infants. (2007).

25. Baird, G. *et al.* Prevalence of disorders of the autism spectrum in a population cohort of children in South Thames: the Special Needs and Autism Project (SNAP). *Lancet* **368**, 210–215 (2006).

26. American Psychiatric Association. *Diagnostic and statistical manual of mental disorders (5th ed.). Arlington, VA: American Psychiatric Publishing.* (2013).

27. Lee, P. F., Thomas, R. E. & Lee, P. A. Approach to autism spectrum disorder: Using the new DSM-V diagnostic criteria and the CanMEDS-FM framework. *Can. Fam. Physician* **61**, 421–4 (2015).

28. Werling, D. M. & Geschwind, D. H. Sex differences in autism spectrum disorders. *Curr. Opin. Neurol.* **26**, 146–153 (2013).

29. Taylor, B., Jick, H. & Maclaughlin, D. Prevalence and incidence rates of autism in the UK: time trend from 2004-2010 in children aged 8 years. *BMJ Open* **3**, e003219 (2013).

30. Carter, M. & Scherer, S. Autism spectrum disorder in the genetics clinic: a review. *Clin. Genet.* **83**, 399–407 (2013).

31. Miles, J. H. Autism spectrum disorders—A genetics review. *Genet. Med.* **13**, 278–294 (2011).

32. Neale, B. M. *et al.* Patterns and rates of exonic de novo mutations in autism spectrum disorders. *Nature* **485**, 242–245 (2012).

33. Gandal, M. J. *et al.* Shared molecular neuropathology across major psychiatric

disorders parallels polygenic overlap. *Science (80-.).* **359**, 693–697 (2018).

34. Consortium, C.-D. G. of the P. G. *et al.* Genomic Relationships, Novel Loci, and Pleiotropic Mechanisms across Eight Psychiatric Disorders. *Cell* **179**, 1469-1482.e11 (2019).

35. Hack, M. *et al.* Behavioral outcomes of extremely low birth weight children at age 8 years. *J. Dev. Behav. Pediatr.* **30**, 122–30 (2009).

36. Samara, M., Marlow, N., Wolke, D. & EPICure Study Group. Pervasive Behavior Problems at 6 Years of Age in a Total-Population Sample of Children Born at <=25 Weeks of Gestation. *Pediatrics* **122**, 562–573 (2008).

37. Hultman, C. M., Sparén, P. & Cnattingius, S. Perinatal risk factors for infantile autism. *Epidemiology* **13**, 417–23 (2002).

38. Meldrum, S. J. *et al.* Autism spectrum disorder in children born preterm-role of exposure to perinatal inflammation. *Front. Neurosci.* **7**, 123 (2013).

39. Meyer, U., Feldon, J. & Dammam, O. Schizophrenia and Autism: Both Shared and Disorder-Specific Pathogenesis Via Perinatal Inflammation? *Pediatr. Res.* **69**, 26R-33R (2011).

40. Atladóttir, H. Ó. *et al.* Maternal Infection Requiring Hospitalization During Pregnancy and Autism Spectrum Disorders. *J. Autism Dev. Disord.* **40**, 1423–1430 (2010).

41. Brown, A. S. Epidemiologic studies of exposure to prenatal infection and risk of schizophrenia and autism. *Dev. Neurobiol.* **72**, 1272–1276 (2012).

42. Zerbo, O. *et al.* Is Maternal Influenza or Fever During Pregnancy Associated with Autism or Developmental Delays? Results from the CHARGE (CHildhood Autism Risks from Genetics and Environment) Study. *J. Autism Dev. Disord.* **43**, 25–33 (2013).

43. Zerbo, O. *et al.* Association Between Influenza Infection and Vaccination During Pregnancy and Risk of Autism Spectrum Disorder. *JAMA Pediatr.* **171**, e163609 (2017).

44. Tandon, R. Schizophrenia and Other Psychotic Disorders in Diagnostic and Statistical Manual of Mental Disorders (DSM)-5: Clinical Implications of Revisions from DSM-IV. *Indian J. Psychol. Med.* **36**, 223 (2014).

45. Messias, E. L., Chen, C.-Y. & Eaton, W. W. Epidemiology of schizophrenia: review of findings and myths. *Psychiatr. Clin. North Am.* **30**, 323–38 (2007).

46. Knud Larsen, J., Bendsen, B. B., Foldager, L. & Munk-Jørgensen, P. Prematurity and low birth weight as risk factors for the development of affective disorder, especially depression and schizophrenia: a register study. *Acta Neuropsychiatr.* **22**, 284–291 (2010).

47. Mednick, S. A., Machon, R. A., Huttunen, M. O. & Bonett, D. Adult schizophrenia following prenatal exposure to an influenza epidemic. *Arch. Gen. Psychiatry* **45**, 189–92 (1988).

48. Brown, A. S. *et al.* Prenatal Exposure to Maternal Infection and Executive Dysfunction in Adult Schizophrenia. *Am. J. Psychiatry* **166**, 683–690 (2009).

49. Buka, S. L. *et al.* Maternal Cytokine Levels during Pregnancy and Adult Psychosis. *Brain. Behav. Immun.* **15**, 411–420 (2001).

50. Brown, A. S. *et al.* Elevated maternal C-reactive protein and autism in a national birth cohort. *Mol. Psychiatry* **19**, 259–264 (2014).

51. Fatemi, S. H. *et al.* Defective corticogenesis and reduction in Reelin immunoreactivity in cortex and hippocampus of prenatally infected neonatal mice. *Mol. Psychiatry* **4**, 145–54 (1999).

52. Fatemi, S. H. *et al.* Human influenza viral infection in utero alters glial fibrillary acidic protein immunoreactivity in the developing brains of neonatal mice. *Mol. Psychiatry* **7**, 633–640 (2002).

53. Urakubo, A., Jarskog, L. F., Lieberman, J. A. & Gilmore, J. H. Prenatal exposure to maternal infection alters cytokine expression in the placenta, amniotic fluid, and fetal brain. *Schizophr. Res.* **47**, 27–36 (2001).

54. Goudriaan, A. *et al.* Specific Glial Functions Contribute to Schizophrenia Susceptibility. *Schizophr. Bull.* **40**, 925–935 (2014).

55. Zornberg, G. L., Buka, S. L. & Tsuang, M. T. Hypoxic-Ischemia-Related Fetal/Neonatal Complications and Risk of Schizophrenia and Other Nonaffective Psychoses: A 19-Year Longitudinal Study. *Am. J. Psychiatry* **157**, 196–202 (2000).

56. Schmidt-Kastner, R., van Os, J., Esquivel, G., Steinbusch, H. W. M. & Rutten, B. P. F. An environmental analysis of genes associated with schizophrenia: hypoxia and vascular factors as interacting elements in the neurodevelopmental model. *Mol. Psychiatry* **17**, 1194–1205 (2012).

57. Volpe, J. J. Dysmaturation of Premature Brain: Importance, Cellular Mechanisms, and Potential Interventions. *Pediatr. Neurol.* **95**, 42–66 (2019).

58. Back, S. A. & Miller, S. P. Brain injury in premature neonates: A primary cerebral dysmaturation disorder? *Ann. Neurol.* **75**, 469–86 (2014).

59. Martinez-Biarge, M. *et al.* Neurodevelopmental Outcomes in Preterm Infants with White Matter Injury Using a New MRI Classification. *Neonatology* **116**, 227–235 (2019).

60. Back, S. A. White matter injury in the preterm infant: pathology and mechanisms. *Acta Neuropathol.* **134**, 331–349 (2017).

61. Riddle, A. *et al.* Histopathological correlates of magnetic resonance imaging-defined chronic perinatal white matter injury. *Ann. Neurol.* **70**, 493–507 (2011).

62. Buser, J. R. *et al.* Arrested preoligodendrocyte maturation contributes to myelination failure in premature infants. *Ann. Neurol.* **71**, 93–109 (2012).

63. Gilles, F. H., Averill, D. R. & Kerr, C. S. Neonatal endotoxin encephalopathy. *Ann. Neurol.* **2**, 49–56 (1977).

64. Dambska, M., Laure-Kamionowska, M. & Schmidt-Sidor, B. Early and late neuropathological changes in perinatal white matter damage. *J. Child Neurol.* **4**, 291–8 (1989).

65. Volpe, J. J. Neurobiology of Periventricular Leukomalacia in the Premature Infant. *Pediatr. Res.* **50**, 553–562 (2001).

66. Yeargin-Allsopp, M. *et al.* Prevalence of Cerebral Palsy in 8-Year-Old Children in Three Areas of the United States in 2002: A Multisite Collaboration. *Pediatrics* **121**, (2008).

67. Graham, E. M., Ruis, K. A., Hartman, A. L., Northington, F. J. & Fox, H. E. A systematic review of the role of intrapartum hypoxia-ischemia in the causation of neonatal encephalopathy. *Am. J. Obstet. Gynecol.* **199**, 587–595 (2008).

68. Rumajogee, P., Bregman, T., Miller, S. P., Yager, J. Y. & Fehlings, M. G. Rodent Hypoxia–Ischemia Models for Cerebral Palsy Research: A Systematic Review. *Front. Neurol.* **7**, 57 (2016).

69. Back, S. A. *et al.* Late Oligodendrocyte Progenitors Coincide with the Developmental Window of Vulnerability for Human Perinatal White Matter Injury. *J. Neurosci.* **21**, (2001).

70. Boardman, J. P. *et al.* A common neonatal image phenotype predicts adverse neurodevelopmental outcome in children born preterm. *Neuroimage* **52**, 409–414 (2010).

71. Shah, D. K. *et al.* Electrographic seizures are associated with brain injury in newborns undergoing therapeutic hypothermia. *Arch. Dis. Child. - Fetal Neonatal Ed.* **99**, F219–F224 (2014).

72. Malik, S. *et al.* Neurogenesis Continues in the Third Trimester of Pregnancy and Is Suppressed by Premature Birth. *J. Neurosci.* **33**, (2013).

73. Paredes, M. F. *et al.* Extensive migration of young neurons into the infant human frontal lobe. *Science (80-.).* **354**, (2016).

74. Burmeister, M., McInnis, M. G. & Zöllner, S. Psychiatric genetics: progress amid controversy. *Nat. Rev. Genet.* **9**, 527–540 (2008).

75. Craig, F. *et al.* Overlap Between Autism Spectrum Disorders and Attention Deficit Hyperactivity Disorder: Searching for Distinctive/Common Clinical Features. *Autism Res.* **8**, 328–337 (2015).

76. Simonoff, E. *et al.* Psychiatric Disorders in Children With Autism Spectrum Disorders: Prevalence, Comorbidity, and Associated Factors in a Population-Derived Sample. *J. Am. Acad. Child Adolesc. Psychiatry* **47**, 921–929 (2008).

77. Lee, D. O. & Ousley, O. Y. Attention-Deficit Hyperactivity Disorder Symptoms in a Clinic Sample of Children and Adolescents with Pervasive Developmental Disorders. *J. Child Adolesc. Psychopharmacol.* **16**, 737–746 (2006).

78. Gottesman, I. I. & Shields, J. A polygenic theory of schizophrenia. *Proc. Natl. Acad. Sci. U. S. A.* **58**, 199–205 (1967).

79. Cross-Disorder Group of the Psychiatric Genomics Consortium, C.-D. G. of the P. G. *et al.* Genetic relationship between five psychiatric disorders estimated from genome-wide SNPs. *Nat. Genet.* **45**, 984–94 (2013).

80. Huttenlocher, P. R. Synaptic density in human frontal cortex - developmental

changes and effects of aging. *Brain Res.* **163**, 195–205 (1979).

81. Glantz, L. A. & Lewis, D. A. Decreased dendritic spine density on prefrontal cortical pyramidal neurons in schizophrenia. *Arch. Gen. Psychiatry* **57**, 65–73 (2000).

82. Selemon, L. D. & Goldman-Rakic, P. S. The reduced neuropil hypothesis: a circuit based model of schizophrenia. *Biol. Psychiatry* **45**, 17–25 (1999).

83. Tang, G. *et al.* Loss of mTOR-dependent macroautophagy causes autistic-like synaptic pruning deficits. *Neuron* **83**, 1131–43 (2014).

84. Hutsler, J. J. & Zhang, H. Increased dendritic spine densities on cortical projection neurons in autism spectrum disorders. *Brain Res.* **1309**, 83–94 (2010).

85. Weir, R. K., Bauman, M. D., Jacobs, B. & Schumann, C. M. Protracted dendritic growth in the typically developing human amygdala and increased spine density in young ASD brains. *J. Comp. Neurol.* **526**, 262–274 (2018).

86. Voineagu, I. *et al.* Transcriptomic analysis of autistic brain reveals convergent molecular pathology. *Nature* **474**, 380–384 (2011).

87. Redcay, E. & Courchesne, E. When Is the Brain Enlarged in Autism? A Meta-Analysis of All Brain Size Reports. *Biol. Psychiatry* **58**, 1–9 (2005).

88. Nardone, S. *et al.* DNA methylation analysis of the autistic brain reveals multiple dysregulated biological pathways. *Transl. Psychiatry* **4**, e433 (2014).

89. Naisbitt, S. *et al.* Shank, a novel family of postsynaptic density proteins that binds to the NMDA receptor/PSD-95/GKAP complex and cortactin. *Neuron* **23**, 569–82 (1999).

90. Monteiro, P. & Feng, G. SHANK proteins: roles at the synapse and in autism spectrum disorder. *Nat. Rev. Neurosci.* **18**, 147–157 (2017).

91. Qin, L. *et al.* Social deficits in Shank3-deficient mouse models of autism are rescued by histone deacetylase (HDAC) inhibition. *Nat. Neurosci.* 1 (2018) doi:10.1038/s41593-018-0110-8.

92. Südhof, T. C. Neuroligins and neurexins link synaptic function to cognitive disease. *Nature* **455**, 903–911 (2008).

93. Feinberg, I. Schizophrenia: caused by a fault in programmed synaptic elimination during adolescence? *J. Psychiatr. Res.* **17**, 319–34 (1982).

94. Hoffman, R. E. & Dobscha, S. K. Cortical pruning and the development of schizophrenia: a computer model. *Schizophr. Bull.* **15**, 477–90 (1989).

95. Kolomeets, N. S., Orlovskaya, D. D., Rachmanova, V. I. & Uranova, N. A. Ultrastructural alterations in hippocampal mossy fiber synapses in schizophrenia: A postmortem morphometric study. *Synapse* **57**, 47–55 (2005).

96. Matosin, N. *et al.* Molecular evidence of synaptic pathology in the CA1 region in schizophrenia. *npj Schizophr.* **2**, 16022 (2016).

97. Sellgren, C. M. *et al.* Increased synapse elimination by microglia in schizophrenia patient-derived models of synaptic pruning. *Nat. Neurosci.* 1 (2019)

doi:10.1038/s41593-018-0334-7.

98. Chen, C., Liu, H. & Hsueh, Y. TLR3 downregulates expression of schizophrenia gene *Disc1* via MYD88 to control neuronal morphology. *EMBO Rep.* **18**, 169–183 (2017).

99. Lipska, B. K. *et al.* Functional genomics in postmortem human brain: abnormalities in a DISC1 molecular pathway in schizophrenia. *Dialogues Clin. Neurosci.* **8**, 353–7 (2006).

100. Sekar, A. *et al.* Schizophrenia risk from complex variation of complement component 4. *Nature* **530**, 177–183 (2016).

101. Escudero-Esparza, A., Kalchishkova, N., Kurbasic, E., Jiang, W. G. & Blom, A. M. The novel complement inhibitor human CUB and Sushi multiple domains 1 (CSMD1) protein promotes factor I-mediated degradation of C4b and C3b and inhibits the membrane attack complex assembly. *FASEB J.* **27**, 5083–5093 (2013).

102. Donohoe, G. *et al.* Neuropsychological effects of the *CSMD1* genome-wide associated schizophrenia risk variant rs10503253. *Genes, Brain Behav.* **12**, 203–209 (2013).

103. Consortium, T. S. P. G.-W. A. S. (GWAS) *et al.* Genome-wide association study identifies five new schizophrenia loci. *Nat. Genet.* **43**, 969–976 (2011).

104. Bálint, S. *et al.* Attention deficit hyperactivity disorder (ADHD): gender- and age-related differences in neurocognition. *Psychol. Med.* **39**, 1337–1345 (2009).

105. Van Wijngaarden-Cremers, P. J. M. *et al.* Gender and Age Differences in the Core Triad of Impairments in Autism Spectrum Disorders: A Systematic Review and Meta-analysis. *J. Autism Dev. Disord.* **44**, 627–635 (2014).

106. McGrath, J., Saha, S., Chant, D. & Welham, J. Schizophrenia: A Concise Overview of Incidence, Prevalence, and Mortality. *Epidemiol. Rev.* **30**, 67–76 (2008).

107. O'Driscoll, D. N., McGovern, M., Greene, C. M. & Molloy, E. J. Gender disparities in preterm neonatal outcomes. *Acta Paediatr.* **107**, 1494–1499 (2018).

108. Hattier, M. A., Matson, J. L., Tureck, K. & Horovitz, M. The effects of gender and age on repetitive and/or restricted behaviors and interests in adults with autism spectrum disorders and intellectual disability. *Res. Dev. Disabil.* **32**, 2346–2351 (2011).

109. Kaczkurkin, A. N., Raznahan, A. & Satterthwaite, T. D. Sex differences in the developing brain: insights from multimodal neuroimaging. *Neuropsychopharmacology* **44**, 71–85 (2019).

110. Spiers, H. *et al.* Methylomic trajectories across human fetal brain development. *Genome Res.* **25**, 338–52 (2015).

111. Floris, D. L., Lai, M.-C., Nath, T., Milham, M. P. & Di Martino, A. Network-specific sex differentiation of intrinsic brain function in males with autism. *Mol. Autism* **9**, 17 (2018).

112. Schwarz, E. *et al.* Sex-specific serum biomarker patterns in adults with Asperger's syndrome. *Mol. Psychiatry* **16**, 1213–1220 (2011).

113. Baron-Cohen, S. *et al.* Foetal oestrogens and autism. *Mol. Psychiatry* 1–9 (2019) doi:10.1038/s41380-019-0454-9.

114. Goldenberg, R. L. *et al.* The Alabama Preterm Birth Study: Intrauterine infection and placental histologic findings in preterm births of males and females less than 32 weeks. *Am. J. Obstet. Gynecol.* **195**, 1533–1537 (2006).

115. Schwarz, J. M., Sholar, P. W. & Bilbo, S. D. Sex differences in microglial colonization of the developing rat brain. *J. Neurochem.* **120**, no-no (2012).

116. Brunwasser, S. M. *et al.* Sex-specific association between prenatal life stress exposure and infant pro-inflammatory cytokine levels during acute respiratory infection. *Brain. Behav. Immun.* **76**, 275–279 (2019).

117. ENGELAND, W. C., SHINSAKO, J., WINGET, C. M., VERNIKOS-DANELLIS, J. & DALLMAN, M. F. Circadian Patterns of Stress-Induced ACTH Secretion Are Modified by Corticosterone Responses. *Endocrinology* **100**, 138–147 (1977).

118. Griffin, A. C. & Whitacre, C. C. Sex and strain differences in the circadian rhythm fluctuation of endocrine and immune function in the rat: implications for rodent models of autoimmune disease. *J. Neuroimmunol.* **35**, 53–64 (1991).

119. Jezová, D., Juránková, E., Mosnárová, A., Kriska, M. & Skultétyová, I. Neuroendocrine response during stress with relation to gender differences. *Acta Neurobiol. Exp. (Wars).* **56**, 779–85 (1996).

120. Solomon, M. B. *et al.* Deletion of forebrain glucocorticoid receptors impairs neuroendocrine stress responses and induces depression-like behavior in males but not females. *Neuroscience* **203**, 135–143 (2012).

121. Workman, A. D., Charvet, C. J., Clancy, B., Darlington, R. B. & Finlay, B. L. Modeling transformations of neurodevelopmental sequences across mammalian species. *J. Neurosci.* **33**, 7368–83 (2013).

122. Rees, S. M. *et al.* Cerebellar Development In a Baboon Model of Preterm Delivery: Impact of Specific Ventilatory Regimes. *J. Neuropathol. Exp. Neurol.* **68**, 605 (2009).

123. Partridge, E. A. *et al.* An extra-uterine system to physiologically support the extreme premature lamb. *Nat. Commun.* **8**, 15112 (2017).

124. Bohlen, C. J. *et al.* Diverse Requirements for Microglial Survival, Specification, and Function Revealed by Defined-Medium Cultures. *Neuron* **94**, 759-773.e8 (2017).

125. Magalhães, D. M. *et al.* Ex vivo model of epilepsy in organotypic slices—a new tool for drug screening. *J. Neuroinflammation* **15**, 203 (2018).

126. Croft, C. L. & Noble, W. Preparation of organotypic brain slice cultures for the study of Alzheimer's disease. *F1000Research* **7**, 592 (2018).

127. Hamilton, N. B. *et al.* Endogenous GABA controls oligodendrocyte lineage cell number, myelination, and CNS internode length. *Glia* **65**, 309–321 (2017).

128. Neumann, J. T. *et al.* Increased BDNF Protein Expression after Ischemic Or PKC Epsilon Preconditioning Promotes Electrophysiologic Changes That Lead to Neuroprotection. *J. Cereb. Blood Flow Metab.* **35**, 121–130 (2015).

129. Trujillo, C. A. *et al.* Complex Oscillatory Waves Emerging from Cortical Organoids Model Early Human Brain Network Development. *Cell Stem Cell* **25**, 558-569.e7 (2019).

130. Pașca, A. M. *et al.* Human 3D cellular model of hypoxic brain injury of prematurity. *Nat. Med.* **25**, 784–791 (2019).

131. Bird, A. Perceptions of epigenetics. *Nature* **447**, 396–398 (2007).

132. Smith, Z. D. & Meissner, A. DNA methylation: roles in mammalian development. *Nat. Rev. Genet.* **14**, 204–220 (2013).

133. Robertson, K. D. DNA methylation and human disease. *Nat. Rev. Genet.* **6**, 597–610 (2005).

134. Lim, D. H. K. & Maher, E. R. DNA methylation: a form of epigenetic control of gene expression. *Obstet. Gynaecol.* **12**, 37–42 (2010).

135. Leitch, H. G. *et al.* Naive pluripotency is associated with global DNA hypomethylation. *Nat. Struct. Mol. Biol.* **20**, 311–316 (2013).

136. Habibi, E. *et al. Whole-Genome Bisulfite Sequencing of Two Distinct Interconvertible DNA Methylomes of Mouse Embryonic Stem Cells*. *Cell Stem Cell* vol. 13 (2013).

137. Theunissen, T. W. *et al.* Systematic Identification of Culture Conditions for Induction and Maintenance of Naive Human Pluripotency. *Cell Stem Cell* **15**, 471–487 (2014).

138. Chédin, F. The DNMT3 family of mammalian de novo DNA methyltransferases. *Prog. Mol. Biol. Transl. Sci.* **101**, 255–85 (2011).

139. Dhe-Paganon, S., Syeda, F. & Park, L. DNA methyl transferase 1: regulatory mechanisms and implications in health and disease. *Int. J. Biochem. Mol. Biol.* **2**, 58–66 (2011).

140. Tahiliani, M. *et al.* Conversion of 5-Methylcytosine to 5-Hydroxymethylcytosine in Mammalian DNA by MLL Partner TET1. *Science (80-.).* **324**, 930–935 (2009).

141. Gorres, K. L. & Raines, R. T. Prolyl 4-hydroxylase. *Crit. Rev. Biochem. Mol. Biol.* **45**, 106–24 (2010).

142. Aravind, L. *et al.* CHAPTER 11. The TET/JBP Family of Nucleic Acid Base-Modifying 2-Oxoglutarate and Iron-Dependent Dioxygenases. in 289–308 (2015). doi:10.1039/9781782621959-00289.

143. Shimozaki, K. Ten-Eleven Translocation 1 and 2 Confer Overlapping Transcriptional Programs for the Proliferation of Cultured Adult Neural Stem Cells. *Cell. Mol. Neurobiol.* 1–14 (2016) doi:10.1007/s10571-016-0432-6.

144. Hajkova, P. *et al.* Genome-Wide Reprogramming in the Mouse Germ Line Entails the Base Excision Repair Pathway. *Science (80-.).* **329**, (2010).

145. Gu, T.-P. *et al.* The role of Tet3 DNA dioxygenase in epigenetic reprogramming by oocytes. *Nature* **477**, 606–610 (2011).

146. Perera, A. *et al.* TET3 Is Recruited by REST for Context-Specific Hydroxymethylation and Induction of Gene Expression. *Cell Rep.* **11**, 283–294 (2015).

147. Kriaucionis, S. & Heintz, N. The nuclear DNA base 5-hydroxymethylcytosine is present in Purkinje neurons and the brain. *Science* **324**, 929–30 (2009).

148. Ito, S. *et al.* Tet proteins can convert 5-methylcytosine to 5-formylcytosine and 5-carboxylcytosine. *Science* **333**, 1300–3 (2011).

149. Hu, L. *et al.* Structural insight into substrate preference for TET-mediated oxidation. *Nature* **527**, 118–122 (2015).

150. Sang, Y., Cheng, C., Tang, X.-F., Zhang, M.-F. & Lv, X.-B. Hypermethylation of TET1 promoter is a new diagnosic marker for breast cancer metastasis. *Asian Pac. J. Cancer Prev.* **16**, 1197–200 (2015).

151. Musialik, E., Bujko, M., Wypych, A., Matysiak, M. & Siedlecki, J. A. TET2 promoter DNA methylation and expression analysis in pediatric B-cell acute lymphoblastic leukemia. *Hematol. Rep.* **6**, 5333 (2014).

152. Bahari, G., Hashemi, M., Naderi, M. & Taheri, M. TET2 Promoter DNA Methylation and Expression in Childhood Acute Lymphoblastic Leukemia. *Asian Pac. J. Cancer Prev.* **17**, 3959–62 (2016).

153. Thienpont, B. *et al.* Tumour hypoxia causes DNA hypermethylation by reducing TET activity. *Nature* **537**, 63–68 (2016).

154. Dhliwayo, N., Sarras, M. P., Luczkowski, E., Mason, S. M. & Intine, R. V. Parp Inhibition Prevents Ten-Eleven Translocase Enzyme Activation and Hyperglycemia-Induced DNA Demethylation. *Diabetes* **63**, (2014).

155. Hore, T. A. *et al.* Retinol and ascorbate drive erasure of epigenetic memory and enhance reprogramming to naïve pluripotency by complementary mechanisms. *Proc. Natl. Acad. Sci. U. S. A.* **113**, 12202–12207 (2016).

156. Jiang, H. *et al.* Immune Regulator MCPIP1 Modulates TET Expression during Early Neocortical Development. *Stem Cell Reports* **7**, 439–453 (2016).

157. Fu, X. *et al.* MicroRNA-26a targets ten eleven translocation enzymes and is regulated during pancreatic cell differentiation. *Proc. Natl. Acad. Sci.* **110**, 17892–17897 (2013).

158. Chuang, K.-H. *et al.* MicroRNA-494 is a master epigenetic regulator of multiple invasion-suppressor microRNAs by targeting ten eleven translocation 1 in invasive human hepatocellular carcinoma tumors. *Hepatology* **62**, 466–480 (2015).

159. Li, Y. *et al.* Aberrant expression of miR-153 is associated with overexpression of hypoxia-inducible factor-1α in refractory epilepsy. *Sci. Rep.* **6**, 32091 (2016).

160. Caputo, V. *et al.* Brain Derived Neurotrophic Factor (BDNF) Expression Is Regulated by MicroRNAs miR-26a and miR-26b Allele-Specific Binding. *PLoS One* **6**, e28656 (2011).

161. Bauer, C. *et al.* Phosphorylation of TET proteins is regulated via O-GlcNAcylation by the O-linked N-acetylglucosamine transferase (OGT). *J. Biol. Chem.* **290**, 4801–12 (2015).

162. Iyer, L. M., Tahiliani, M., Rao, A. & Aravind, L. Prediction of novel families of enzymes involved in oxidative and other complex modifications of bases in nucleic acids. *Cell*

Cycle **8**, 1698–1710 (2009).

163. Szulwach, K. E. *et al.* 5-hmC–mediated epigenetic dynamics during postnatal neurodevelopment and aging. *Nat. Neurosci.* **14**, 1607–1616 (2011).

164. Lister, R. *et al.* Global Epigenomic Reconfiguration During Mammalian Brain Development. *Science (80-.).* **341**, (2013).

165. Wang, T. *et al.* Genome-wide DNA hydroxymethylation changes are associated with neurodevelopmental genes in the developing human cerebellum. *Hum. Mol. Genet.* **21**, 5500–5510 (2012).

166. Jin, S.-G., Wu, X., Li, A. X. & Pfeifer, G. P. Genomic mapping of 5-hydroxymethylcytosine in the human brain. *Nucleic Acids Res.* **39**, 5015–5024 (2011).

167. Kozlenkov, A. *et al.* Substantial DNA methylation differences between two major neuronal subtypes in human brain. *Nucleic Acids Res.* **44**, 2593–2612 (2016).

168. Spruijt, C. G. *et al.* Dynamic Readers for 5-(Hydroxy)Methylcytosine and Its Oxidized Derivatives. *Cell* **152**, 1146–1159 (2013).

169. Mellén, M., Ayata, P., Dewell, S., Kriaucionis, S. & Heintz, N. MeCP2 Binds to 5hmC Enriched within Active Genes and Accessible Chromatin in the Nervous System. *Cell* **151**, 1417–1430 (2012).

170. Wang, L. *et al.* Molecular basis for 5-carboxycytosine recognition by RNA polymerase II elongation complex. *Nature* **523**, 621–625 (2015).

171. Raiber, E.-A. *et al.* 5-Formylcytosine alters the structure of the DNA double helix. *Nat. Struct. Mol. Biol.* **22**, 44–49 (2014).

172. Venkatesh, S. & Workman, J. L. Histone exchange, chromatin structure and the regulation of transcription. *Nat. Rev. Mol. Cell Biol.* **16**, 178–189 (2015).

173. Bannister, A. J. & Kouzarides, T. Regulation of chromatin by histone modifications. *Cell Res.* **21**, 381–395 (2011).

174. Berger, S. L. Histone modifications in transcriptional regulation. *Curr. Opin. Genet. Dev.* **12**, 142–8 (2002).

175. Klose, R. J., Kallin, E. M. & Zhang, Y. JmjC-domain-containing proteins and histone demethylation. *Nat. Rev. Genet.* **7**, 715–727 (2006).

176. Lyst, M. J. & Bird, A. Rett syndrome: a complex disorder with simple roots. *Nat. Rev. Genet.* **16**, 261–275 (2015).

177. Weemaes, C. M. *et al.* Heterogeneous clinical presentation in ICF syndrome: correlation with underlying gene defects. *Eur. J. Hum. Genet.* **21**, 1219–1225 (2013).

178. Lokody, I. Epigenetics: Mechanisms underlying fragile X syndrome. *Nat. Rev. Genet.* **15**, 218–218 (2014).

179. Rangasamy, S., D'Mello, S. R. & Narayanan, V. Epigenetics, autism spectrum, and neurodevelopmental disorders. *Neurotherapeutics* **10**, 742–56 (2013).

180. Cruickshank, M. N. *et al.* Analysis of epigenetic changes in survivors of preterm birth

reveals the effect of gestational age and evidence for a long term legacy. *Genome Med.* **5**, 96 (2013).

181. Schroeder, J. W. *et al.* Neonatal DNA methylation patterns associate with gestational age. *Epigenetics* **6**, 1498–504 (2011).

182. Parets, S. E. *et al.* Fetal DNA Methylation Associates with Early Spontaneous Preterm Birth and Gestational Age. *PLoS One* **8**, e67489 (2013).

183. Lee, H. *et al.* DNA methylation shows genome-wide association of *NFIX* , *RAPGEF2* and *MSRB3* with gestational age at birth. *Int. J. Epidemiol.* **41**, 188–199 (2012).

184. Sparrow, S. *et al.* Epigenomic profiling of preterm infants reveals DNA methylation differences at sites associated with neural function. *Transl. Psychiatry* **6**, e716 (2016).

185. Piyasena, C. *et al.* Dynamic Changes in DNA Methylation Occur during the First Year of Life in Preterm Infants. *Front. Endocrinol. (Lausanne).* **7**, 158 (2016).

186. Tărlungeanu, D. C. *et al.* Impaired Amino Acid Transport at the Blood Brain Barrier Is a Cause of Autism Spectrum Disorder. *Cell* **167**, 1481-1494.e18 (2016).

187. Ladd-Acosta, C. *et al.* Common DNA methylation alterations in multiple brain regions in autism. *Mol. Psychiatry* **19**, 862–871 (2014).

188. Voineagu, I. *et al.* Transcriptomic analysis of autistic brain reveals convergent molecular pathology. *Nature* **474**, 380–384 (2011).

189. Wong, C. C. Y. *et al.* Methylomic analysis of monozygotic twins discordant for autism spectrum disorder and related behavioural traits. *Mol. Psychiatry* **19**, 495–503 (2014).

190. Casey, K. F. *et al.* Birth weight discordance, DNA methylation, and cortical morphology of adolescent monozygotic twins. *Hum. Brain Mapp.* (2016) doi:10.1002/hbm.23503.

191. Sun, W. *et al.* Histone Acetylome-wide Association Study of Autism Spectrum Disorder. *Cell* **167**, 1385-1397.e11 (2016).

192. Bourgeron, T. From the genetic architecture to synaptic plasticity in autism spectrum disorder. *Nat. Rev. Neurosci.* **16**, 551–563 (2015).

193. Christensen, J. *et al.* Prenatal Valproate Exposure and Risk of Autism Spectrum Disorders and Childhood Autism. *JAMA* **309**, 1696 (2013).

194. Zheng, F. *et al.* Mutation of the CH1 Domain in the Histone Acetyltransferase CREBBP Results in Autism-Relevant Behaviors in Mice. *PLoS One* **11**, e0146366 (2016).

195. Wockner, L. F. *et al.* Genome-wide DNA methylation analysis of human brain tissue from schizophrenia patients. *Transl. Psychiatry* **4**, e339 (2014).

196. Ruzicka, W. B. *et al.* Selective epigenetic alteration of layer I GABAergic neurons isolated from prefrontal cortex of schizophrenia patients using laser-assisted microdissection. *Mol. Psychiatry* **12**, 385–397 (2007).

197. Mill, J. *et al.* Epigenomic Profiling Reveals DNA-Methylation Changes Associated with Major Psychosis. *Am. J. Hum. Genet.* **82**, 696–711 (2008).

198. Montano, C. *et al.* Association of DNA Methylation Differences With Schizophrenia in an Epigenome-Wide Association Study. *JAMA Psychiatry* **73**, 506 (2016).

199. Shi, J. *et al.* Common variants on chromosome 6p22.1 are associated with schizophrenia. *Nature* **460**, 753–7 (2009).

200. Jakovcevski, M. *et al.* Prefrontal cortical dysfunction after overexpression of histone deacetylase 1. *Biol. Psychiatry* **74**, 696–705 (2013).

201. Schroeder, F. A. *et al.* Expression of *HDAC2* but Not *HDAC1* Transcript Is Reduced in Dorsolateral Prefrontal Cortex of Patients with Schizophrenia. *ACS Chem. Neurosci.* acschemneuro.6b00372 (2016) doi:10.1021/acschemneuro.6b00372.

202. Tang, B., Dean, B. & Thomas, E. A. Disease- and age-related changes in histone acetylation at gene promoters in psychiatric disorders. *Transl. Psychiatry* **1**, e64 (2011).

203. Akbarian, S. *et al.* Chromatin Alterations Associated With Down-regulated Metabolic Gene Expression in the Prefrontal Cortex of Subjects With Schizophrenia. *Arch. Gen. Psychiatry* **62**, 829 (2005).

204. Spiers, H., Hannon, E., Schalkwyk, L. C., Bray, N. J. & Mill, J. 5-hydroxymethylcytosine is highly dynamic across human fetal brain development. *BMC Genomics* **18**, 738 (2017).

205. Reuter, S., Moser, C. & Baack, M. Respiratory distress in the newborn. *Pediatr. Rev.* **35**, 417–28; quiz 429 (2014).

206. Cooper, J. M. *et al.* Neonatal Hypoxia, Hippocampal Atrophy, and Memory Impairment: Evidence of a Causal Sequence. *Cereb. Cortex* **25**, 1469–1476 (2015).

207. Sweet, D. G. *et al.* European Consensus Guidelines on the Management of Respiratory Distress Syndrome - 2016 Update. *Neonatology* **111**, 107–125 (2017).

208. Ghafoor, T., Mahmud, S., Ali, S. & Dogar, S. A. Incidence of respiratory distress syndrome. *J. Coll. Physicians Surg. Pak.* **13**, 271–3 (2003).

209. Tin, W. & Gupta, S. Optimum oxygen therapy in preterm babies. *Arch. Dis. Child. Fetal Neonatal Ed.* **92**, F143-7 (2007).

210. Gaynor, J. W. *et al.* Neurodevelopmental Outcomes After Cardiac Surgery in Infancy. *Pediatrics* **135**, 816–825 (2015).

211. Marino, B. S. *et al.* Neurodevelopmental Outcomes in Children With Congenital Heart Disease: Evaluation and Management. *Circulation* **126**, (2012).

212. Marelli, A. J. *et al.* Lifetime Prevalence of Congenital Heart Disease in the General Population From 2000 to 2010CLINICAL PERSPECTIVE. *Circulation* **130**, (2014).

213. Morton, P. D., Ishibashi, N., Jonas, R. A. & Gallo, V. Congenital cardiac anomalies and white matter injury. *Trends Neurosci.* **38**, 353–363 (2015).

214. McQuillen, P. S. & Miller, S. P. Congenital heart disease and brain development. *Ann.*

N. Y. Acad. Sci. **1184**, 68–86 (2010).

215. Clouchoux, C. *et al.* Delayed Cortical Development in Fetuses with Complex Congenital Heart Disease. *Cereb. Cortex* **23**, 2932–2943 (2013).

216. Donofrio, M. T., duPlessis, A. J. & Limperopoulos, C. Impact of congenital heart disease on fetal brain development and injury. *Curr. Opin. Pediatr.* **23**, 502–511 (2011).

217. Escobar, J. *et al.* Prolonging in utero-like oxygenation after birth diminishes oxidative stress in the lung and brain of mice pups. *Redox Biol.* **1**, 297–303 (2013).

218. Lofaso, F. *et al.* Inhibitory effects of repeated hyperoxia on breathing in newborn mice. *Eur. Respir. J.* **29**, (2006).

219. Ritter, J. *et al.* Neonatal Hyperoxia Exposure Disrupts Axon–Oligodendrocyte Integrity in the Subcortical White Matter. *J. Neurosci.* **33**, (2013).

220. Xiao, M. *et al.* Inhibition of α-KG-dependent histone and DNA demethylases by fumarate and succinate that are accumulated in mutations of FH and SDH tumor suppressors. *Genes Dev.* **26**, 1326–38 (2012).

221. Intlekofer, A. M. *et al. Hypoxia Induces Production of L-2-Hydroxyglutarate*. *Cell Metabolism* vol. 22 (2015).

222. Chinopoulos, C. Which way does the citric acid cycle turn during hypoxia? The critical role of α-ketoglutarate dehydrogenase complex. *J. Neurosci. Res.* **91**, 1030–1043 (2013).

223. Brekke, E. *et al.* Direct measurement of backflux between oxaloacetate and fumarate following pyruvate carboxylation. *Glia* **60**, 147–158 (2012).

224. LaNoue, K., Nicklas, W. J. & Williamson, J. R. Control of citric acid cycle activity in rat heart mitochondria. *J. Biol. Chem.* **245**, 102–11 (1970).

225. Jans, A. W. & Willem, R. Metabolism of [2-13C]succinate in renal cells determined by 13C NMR. *Eur. J. Biochem.* **195**, 97–101 (1991).

226. Hoberman, H. D. & Prosky, L. Evidence of reduction of fumarate to succinate in perfused rat liver under conditions of reduced O2 tension. *Biochim. Biophys. Acta - Gen. Subj.* **148**, 392–399 (1967).

227. Folbergrova´, J., Ljunggren, B., Norberg, K. & Siesjo¨, B. K. *Influence of complete ischemia on glycolytic metabolites, citric acid cycle intermediates, and associated amino acids in the rat cerebral cortex*. *Brain Research* vol. 80 (1974).

228. Fréminet, A., Leclerc, L., Poyart, C., Huel, C. & Gentil, M. Alanine and succinate accumulation in the perfused rat heart during hypoxia. *J. Physiol. (Paris).* **76**, 113–7 (1980).

229. Sonnewald, U. *et al.* NMR spectroscopic study of cell cultures of astrocytes and neurons exposed to hypoxia: Compartmentation of astrocyte metabolism. *Neurochem. Int.* **24**, 473–483 (1994).

230. Bakken, I. J., White, L. R., Aasly, J., Unsgård, G. & Sonnewald, U. Lactate formation from [U-13C]aspartate in cultured astrocytes: compartmentation of pyruvate

metabolism. *Neurosci. Lett.* **237**, 117–120 (1997).

231. Semenza, G. L. *et al.* Structural and functional analysis of hypoxia-inducible factor 1. *Kidney Int.* **51**, 553–555 (1997).

232. Ziello, J. E., Jovin, I. S. & Huang, Y. Hypoxia-Inducible Factor (HIF)-1 regulatory pathway and its potential for therapeutic intervention in malignancy and ischemia. *Yale J. Biol. Med.* **80**, 51–60 (2007).

233. Kewley, R. J., Whitelaw, M. L. & Chapman-Smith, A. The mammalian basic helix-loop-helix/PAS family of transcriptional regulators. *Int. J. Biochem. Cell Biol.* **36**, 189–204 (2004).

234. Mariani, C. J. *et al.* TET1-mediated hydroxymethylation facilitates hypoxic gene induction in neuroblastoma. *Cell Rep.* **7**, 1343–52 (2014).

235. Hagberg, H. *et al.* The role of inflammation in perinatal brain injury. *Nat. Rev. Neurol.* **11**, 192–208 (2015).

236. Jenster, M. *et al.* Maternal or neonatal infection: association with neonatal encephalopathy outcomes. *Pediatr. Res.* **76**, 93–99 (2014).

237. Goldenberg, R. L., Culhane, J. F., Iams, J. D. & Romero, R. Epidemiology and causes of preterm birth. *Lancet* **371**, 75–84 (2008).

238. Galinsky, R., Polglase, G. R., Hooper, S. B., Black, M. J. & Moss, T. J. M. The consequences of chorioamnionitis: preterm birth and effects on development. *J. Pregnancy* **2013**, 412831 (2013).

239. Hagberg, H., Wennerholm, U.-B. & Sävman, K. Sequelae of chorioamnionitis. *Curr. Opin. Infect. Dis.* **15**, 301–6 (2002).

240. Wu, Y. W. *et al.* Chorioamnionitis and Cerebral Palsy in Term and Near-Term Infants. *JAMA* **290**, 2677 (2003).

241. Simonsen, K. A., Anderson-Berry, A. L., Delair, S. F. & Davies, H. D. Early-onset neonatal sepsis. *Clin. Microbiol. Rev.* **27**, 21–47 (2014).

242. Cortese, F. *et al.* Early and Late Infections in Newborns: Where Do We Stand? A Review. *Pediatr. Neonatol.* **57**, 265–273 (2016).

243. Stoll, B. J. *et al.* Late-onset sepsis in very low birth weight neonates: the experience of the NICHD Neonatal Research Network. *Pediatrics* **110**, 285–91 (2002).

244. Mitha, A. *et al.* Neonatal infection and 5-year neurodevelopmental outcome of very preterm infants. *Pediatrics* **132**, e372-80 (2013).

245. van der Ree, M., Tanis, J. C., Van Braeckel, K. N. J. A., Bos, A. F. & Roze, E. Functional impairments at school age of preterm born children with late-onset sepsis. *Early Hum. Dev.* **87**, 821–826 (2011).

246. Lee, I. *et al.* The impact of prenatal and neonatal infection on neurodevelopmental outcomes in very preterm infants. *J. Perinatol.* **34**, 741–7 (2014).

247. Rand, K. M., Austin, N. C., Inder, T. E., Bora, S. & Woodward, L. J. Neonatal Infection and Later Neurodevelopmental Risk in the Very Preterm Infant. *J. Pediatr.* **170**, 97–

104 (2016).

248. Kawasaki, T. & Kawai, T. Toll-like receptor signaling pathways. *Front. Immunol.* **5**, 461 (2014).

249. Kawai, T. & Akira, S. The role of pattern-recognition receptors in innate immunity: update on Toll-like receptors. *Nat. Immunol.* **11**, 373–384 (2010).

250. Favrais, G. *et al.* Systemic inflammation disrupts the developmental program of white matter. *Ann. Neurol.* **70**, 550–565 (2011).

251. Krishnan, M. L. *et al.* Integrative genomics of microglia implicates DLG4 (PSD95) in the white matter development of preterm infants. *Nat. Commun.* **8**, 428 (2017).

252. Van Steenwinckel, J. *et al.* Decreased microglial Wnt/β-catenin signalling drives microglial pro-inflammatory activation in the developing brain. *Brain* **142**, 3806–3833 (2019).

253. Stolp, H. B. *et al.* Interneuron Development Is Disrupted in Preterm Brains With Diffuse White Matter Injury: Observations in Mouse and Human. *Front. Physiol.* **10**, 955 (2019).

254. Rangon, C.-M. *et al.* Myelination induction by a histamine H3 receptor antagonist in a mouse model of preterm white matter injury. *Brain. Behav. Immun.* **74**, 265–276 (2018).

255. Christian, F. *et al.* The Regulation of NF-κB Subunits by Phosphorylation. *Cells* **5**, 12 (2016).

256. Gilmore, T. D. Introduction to NF-κB: players, pathways, perspectives. *Oncogene* **25**, 6680–6684 (2006).

257. Hoffmann, A., Natoli, G. & Ghosh, G. Transcriptional regulation via the NF-κB signaling module. *Oncogene* **25**, 6706–6716 (2006).

258. Bonello, S. *et al.* Reactive Oxygen Species Activate the HIF-1α Promoter Via a Functional NFκB Site. *Arterioscler. Thromb. Vasc. Biol.* **27**, 755–761 (2007).

259. Cummins, E. P. *et al.* Prolyl hydroxylase-1 negatively regulates I B kinase-beta, giving insight into hypoxia-induced NF B activity. *Proc. Natl. Acad. Sci.* **103**, 18154–18159 (2006).

260. Garside, H. *et al.* Glucocorticoid ligands specify different interactions with NF-kappaB by allosteric effects on the glucocorticoid receptor DNA binding domain. *J. Biol. Chem.* **279**, 50050–9 (2004).

261. Widén, C., Gustafsson, J.-A. & Wikström, A.-C. Cytosolic glucocorticoid receptor interaction with nuclear factor-kappa B proteins in rat liver cells. *Biochem. J.* **373**, 211–20 (2003).

262. Zhang, Y. *et al.* Nuclear Factor Kappa B Signaling Initiates Early Differentiation of Neural Stem Cells. *Stem Cells* **30**, 510–524 (2012).

263. Fitzpatrick, L. M. *et al.* Stem Cell Reports Article NF-kB Activity Initiates Human ESC-Derived Neural Progenitor Cell Differentiation by Inducing a Metabolic Maturation Program. *Stem Cell Reports* **10**, 1766–1781 (2018).

264. Romano, A., Freudenthal, R., Merlo, E. & Routtenberg, A. Evolutionarily-conserved role of the NF-κB transcription factor in neural plasticity and memory. *Eur. J. Neurosci.* **24**, 1507–1516 (2006).

265. Gutierrez, H., Hale, V. A., Dolcet, X. & Davies, A. NF-κB signalling regulates the growth of neural processes in the developing PNS and CNS. *Development* **132**, 1713–1726 (2005).

266. Li, J. *et al.* Nna1 Mediates Purkinje Cell Dendritic Development via Lysyl Oxidase Propeptide and NF-κB Signaling. *Neuron* **68**, 45–60 (2010).

267. Nazmi, A. *et al.* Lymphocytes Contribute to the Pathophysiology of Neonatal Brain Injury. *Front. Neurol.* **9**, 159 (2018).

268. Füger, P. *et al.* Microglia turnover with aging and in an Alzheimer's model via long-term in vivo single-cell imaging. *Nat. Neurosci.* **20**, 1371–1376 (2017).

269. Ueno, M. *et al.* Layer V cortical neurons require microglial support for survival during postnatal development. *Nat. Neurosci.* **16**, 543–551 (2013).

270. Galatro, T. F. *et al.* Transcriptomic analysis of purified human cortical microglia reveals age-associated changes. *Nat. Neurosci.* **20**, 1162–1171 (2017).

271. Wendeln, A.-C. *et al.* Innate immune memory in the brain shapes neurological disease hallmarks. *Nature* **556**, 332–338 (2018).

272. Matcovitch-Natan, O. *et al.* Microglia development follows a stepwise program to regulate brain homeostasis. *Science* **353**, aad8670 (2016).

273. Chen, X. *et al.* PSD-95 is required to sustain the molecular organization of the postsynaptic density. *J. Neurosci.* **31**, 6329–38 (2011).

274. Feyder, M. *et al.* Association of Mouse *Dlg4* (PSD-95) Gene Deletion and Human *DLG4* Gene Variation With Phenotypes Relevant to Autism Spectrum Disorders and Williams' Syndrome. *Am. J. Psychiatry* **167**, 1508–1517 (2010).

275. Hormozdiari, F., Penn, O., Borenstein, E. & Eichler, E. E. The discovery of integrated gene networks for autism and related disorders. *Genome Res.* **25**, 142–54 (2015).

276. de Bartolomeis, A., Latte, G., Tomasetti, C. & Iasevoli, F. Glutamatergic Postsynaptic Density Protein Dysfunctions in Synaptic Plasticity and Dendritic Spines Morphology: Relevance to Schizophrenia and Other Behavioral Disorders Pathophysiology, and Implications for Novel Therapeutic Approaches. *Mol. Neurobiol.* **49**, 484–511 (2014).

277. Won, S., Incontro, S., Nicoll, R. A. & Roche, K. W. PSD-95 stabilizes NMDA receptors by inducing the degradation of STEP61. *Proc. Natl. Acad. Sci. U. S. A.* **113**, E4736-44 (2016).

278. Kaindl, A. M. *et al.* Activation of microglial N-methyl-D-aspartate receptors triggers inflammation and neuronal cell death in the developing and mature brain. *Ann. Neurol.* **72**, 536–549 (2012).

279. Rabacchi, S., Bailly, Y., Delhaye-Bouchaud, N. & Mariani, J. Involvement of the N-methyl D-aspartate (NMDA) receptor in synapse elimination during cerebellar development. *Science* **256**, 1823–5 (1992).

280. Kessler, R. C. *et al.* Childhood adversities and adult psychopathology in the WHO World Mental Health Surveys. *Br. J. Psychiatry* **197**, 378–385 (2010).

281. Li, D., Liu, L. & Odouli, R. Presence of depressive symptoms during early pregnancy and the risk of preterm delivery: a prospective cohort study. *Hum. Reprod.* **24**, 146–153 (2008).

282. Wisner, K. L. *et al.* Major Depression and Antidepressant Treatment: Impact on Pregnancy and Neonatal Outcomes. *Am. J. Psychiatry* **166**, 557–566 (2009).

283. Nestler, E. J. *et al.* Neurobiology of Depression. *Neuron* **34**, 13–25 (2002).

284. Edwards, V. J., Holden, G. W., Felitti, V. J. & Anda, R. F. Relationship Between Multiple Forms of Childhood Maltreatment and Adult Mental Health in Community Respondents: Results From the Adverse Childhood Experiences Study. *Am. J. Psychiatry* **160**, 1453–1460 (2003).

285. Heim, C., Newport, D. J., Mletzko, T., Miller, A. H. & Nemeroff, C. B. The link between childhood trauma and depression: Insights from HPA axis studies in humans. *Psychoneuroendocrinology* **33**, 693–710 (2008).

286. Heim, C. *et al.* The role of early adverse experience and adulthood stress in the prediction of neuroendocrine stress reactivity in women: A multiple regression analysis. *Depress. Anxiety* **15**, 117–125 (2002).

287. Herman, J. P. *et al.* Regulation of the hypothalamic-pituitary-adrenocortical stress response. *Compr. Physiol.* **6**, 603 (2016).

288. JACOBSON, L. & SAPOLSKY, R. The Role of the Hippocampus in Feedback Regulation of the Hypothalamic-Pituitary-Adrenocortical Axis*. *Endocr. Rev.* **12**, 118–134 (1991).

289. Dunn, J. D. & Orr, S. E. Differential plasma corticosterone responses to hippocampal stimulation. *Exp. brain Res.* **54**, 1–6 (1984).

290. Diamond, D. M., Bennett, M. C., Fleshner, M. & Rose, G. M. Inverted-U relationship between the level of peripheral corticosterone and the magnitude of hippocampal primed burst potentiation. *Hippocampus* **2**, 421–430 (1992).

291. Champagne, D. L. *et al.* Maternal care and hippocampal plasticity: evidence for experience-dependent structural plasticity, altered synaptic functioning, and differential responsiveness to glucocorticoids and stress. *J. Neurosci.* **28**, 6037–45 (2008).

292. Gray, J. D., Rubin, T. G., Hunter, R. G. & McEwen, B. S. Hippocampal gene expression changes underlying stress sensitization and recovery. *Mol. Psychiatry* **19**, 1171–1178 (2014).

293. Ivars, K. *et al.* Development of salivary cortisol circadian rhythm in preterm infants. *PLoS One* **12**, e0182685 (2017).

294. Newnham, C. A., Inder, T. E. & Milgrom, J. Measuring preterm cumulative stressors within the NICU: The neonatal infant stressor scale. *Early Hum. Dev.* **85**, 549–555 (2009).

295. Smith, G. C. *et al.* Neonatal intensive care unit stress is associated with brain

development in preterm infants. *Ann. Neurol.* **70**, 541–9 (2011).

296. Ranger, M. *et al.* Neonatal Pain-Related Stress Predicts Cortical Thickness at Age 7 Years in Children Born Very Preterm. *PLoS One* **8**, e76702 (2013).

297. Brummelte, S. *et al.* Cortisol levels in former preterm children at school age are predicted by neonatal procedural pain-related stress. *Psychoneuroendocrinology* **51**, 151–163 (2015).

298. McGauran, M. *et al.* Long-term alteration of the hypothalamic-pituitary-adrenal axis in children undergoing cardiac surgery in the first 6 months of life. *Stress* **20**, 505–512 (2017).

299. Brinks, V., van der Mark, M., de Kloet, R. & Oitzl, M. Emotion and cognition in high and low stress sensitive mouse strains: a combined neuroendocrine and behavioral study in BALB/c and C57BL/6J mice. *Front. Behav. Neurosci.* **1**, 8 (2007).

300. Kember, R. L. *et al.* Maternal separation is associated with strain-specific responses to stress and epigenetic alterations to *Nr3c1* , *Avp* , and *Nr4a1* in mouse. *Brain Behav.* **2**, 455–467 (2012).

301. WALKER, C.-D., SCRIBNER, K. A., CASCIO, C. S. & DALLMAN, M. F. The Pituitary-Adrenocortical System of Neonatal Rats Is Responsive to Stress throughout Development in a Time-Dependent and Stressor-Specific Fashion*. *Endocrinology* **128**, 1385–1395 (1991).

302. Schmidt, M. V. Stress-Hyporesponsive Period. *Stress Physiol. Biochem. Pathol.* 49–56 (2019) doi:10.1016/B978-0-12-813146-6.00004-7.

303. Murgatroyd, C. *et al.* Dynamic DNA methylation programs persistent adverse effects of early-life stress. *Nat. Neurosci.* **12**, 1559–1566 (2009).

304. Yamazaki, A., Ohtsuki, Y., Yoshihara, T., Honma, S. & Honma, K. Maternal deprivation in neonatal rats of different conditions affects growth rate, circadian clock, and stress responsiveness differentially. *Physiol. Behav.* **86**, 136–144 (2005).

305. van Oers HJ, de Kloet ER & Levine. Persistent, but Paradoxical, Effects on HPA Regulation of Infants Maternally Deprived at Different Ages. *Stress* **1**, 249–262 (1997).

306. Bonapersona, V. *et al.* The behavioral phenotype of early life adversity: A 3-level meta-analysis of rodent studies. *Neurosci. Biobehav. Rev.* **102**, 299–307 (2019).

307. Murthy, S. & Gould, E. Early Life Stress in Rodents: Animal Models of Illness or Resilience? *Front. Behav. Neurosci.* **12**, 157 (2018).

308. Millstein, R. A. & Holmes, A. Effects of repeated maternal separation on anxiety- and depression-related phenotypes in different mouse strains. *Neurosci. Biobehav. Rev.* **31**, 3–17 (2007).

309. Cartier, J., Piyasena, C., Sparrow, S. A., Boardman, J. P. & Drake, A. J. Alterations in glucose concentrations affect DNA methylation at *Lrg1* in an *ex vivo* rat cortical slice model of preterm brain injury. *Eur. J. Neurosci.* **47**, 380–387 (2018).

310. Wickström, R., Skiöld, B., Petersson, G., Stephansson, O. & Altman, M. Moderate neonatal hypoglycemia and adverse neurological development at 2-6 years of age.

Eur. J. Epidemiol. **33**, 1011–1020 (2018).

311. Feng, X. *et al.* Maternal separation produces lasting changes in cortisol and behavior in rhesus monkeys. *Proc. Natl. Acad. Sci. U. S. A.* **108**, 14312–7 (2011).

312. Rawashdeh, O. & Dubocovich, M. L. Long-term effects of maternal separation on the responsiveness of the circadian system to melatonin in the diurnal nonhuman primate (Macaca mulatta). *J. Pineal Res.* **56**, 254–63 (2014).

313. Reite, M., Seiler, C., Crowley, T. J., Hydinger-Macdonald, M. & Short, R. Circadian rhythm changes following maternal separation. *Chronobiologia* **9**, 1–11.

314. Ivy, A. S., Brunson, K. L., Sandman, C. & Baram, T. Z. Dysfunctional nurturing behavior in rat dams with limited access to nesting material: A clinically relevant model for early-life stress. *Neuroscience* **154**, 1132–1142 (2008).

315. Shair, H. N., Brunelli, S. A., Masmela, J. R., Boone, E. & Hofer, M. A. Social, thermal, and temporal influences on isolation-induced and maternally potentiated ultrasonic vocalizations of rat pups. *Dev. Psychobiol.* **42**, 206–222 (2003).

316. Raineki, C., Cortes, M. R., Belnoue, L. & Sullivan, R. M. Effects of Early-Life Abuse Differ across Development: Infant Social Behavior Deficits Are Followed by Adolescent Depressive-Like Behaviors Mediated by the Amygdala. *J. Neurosci.* **32**, 7758–7765 (2012).

317. Raineki, C., Moriceau, S. & Sullivan, R. M. Developing a Neurobehavioral Animal Model of Infant Attachment to an Abusive Caregiver. *Biol. Psychiatry* **67**, 1137–1145 (2010).

318. Rice, C. J., Sandman, C. A., Lenjavi, M. R. & Baram, T. Z. A Novel Mouse Model for Acute and Long-Lasting Consequences of Early Life Stress. *Endocrinology* **149**, 4892–4900 (2008).

319. Wang, X.-D. *et al.* Early-life stress-induced anxiety-related behavior in adult mice partially requires forebrain corticotropin-releasing hormone receptor 1. *Eur. J. Neurosci.* **36**, 2360–2367 (2012).

320. Walker, C.-D. *et al.* Chronic early life stress induced by limited bedding and nesting (LBN) material in rodents: critical considerations of methodology, outcomes and translational potential. *Stress* **20**, 421–448 (2017).

321. LEVINE, S. Infantile experience and resistance to physiological stress. *Science* **126**, 405 (1957).

322. Meaney, M. J. *et al.* Cellular mechanisms underlying the development and expression of individual differences in the hypothalamic-pituitary-adrenal stress response. *J. Steroid Biochem. Mol. Biol.* **39**, 265–74 (1991).

323. PARFITT, D., WALTON, J., CORRIVEAU, E. & HELMREICH, D. Early life stress effects on adult stress-induced corticosterone secretion and anxiety-like behavior in the C57BL/6 mouse are not as robust as initially thought. *Horm. Behav.* **52**, 417–426 (2007).

324. Kiryanova, V., Smith, V. M., Dyck, R. H. & Antle, M. C. Circadian behavior of adult mice exposed to stress and fluoxetine during development. *Psychopharmacology*

(Berl). **234**, 793–804 (2017).

325. Blaze, J., Scheuing, L. & Roth, T. L. Differential methylation of genes in the medial prefrontal cortex of developing and adult rats following exposure to maltreatment or nurturing care during infancy. *Dev. Neurosci.* **35**, 306–16 (2013).

326. Blaze, J. & Roth, T. L. Caregiver maltreatment causes altered neuronal DNA methylation in female rodents. *Dev. Psychopathol.* **29**, 477–489 (2017).

327. Roth, T. L., Lubin, F. D., Funk, A. J. & Sweatt, J. D. Lasting Epigenetic Influence of Early-Life Adversity on the BDNF Gene. *Biol. Psychiatry* **65**, 760–769 (2009).

328. Naninck, E. F. G. *et al.* Chronic early life stress alters developmental and adult neurogenesis and impairs cognitive function in mice. *Hippocampus* **25**, 309–328 (2015).

329. Macrì, S. Neonatal corticosterone administration in rodents as a tool to investigate the maternal programming of emotional and immune domains. *Neurobiol. Stress* **6**, 22–30 (2017).

330. McPherson, R. J. *et al.* A New Model of Neonatal Stress Which Produces Lasting Neurobehavioral Effects in Adult Rats. *Neonatology* **92**, 33–41 (2007).

331. Girardi, C. E. N., Zanta, N. C. & Suchecki, D. Neonatal stress-induced affective changes in adolescent Wistar rats: early signs of schizophrenia-like behavior. *Front. Behav. Neurosci.* **8**, 319 (2014).

332. Weaver, I. C. G. *et al.* Epigenetic programming by maternal behavior. *Nat. Neurosci.* **7**, 847–854 (2004).

333. Kantake, M., Yoshitake, H., Ishikawa, H., Araki, Y. & Shimizu, T. Postnatal epigenetic modification of glucocorticoid receptor gene in preterm infants: a prospective cohort study. *BMJ Open* **4**, e005318 (2014).

334. Mulligan, C., D'Errico, N., Stees, J. & Hughes, D. Methylation changes at *NR3C1* in newborns associate with maternal prenatal stress exposure and newborn birth weight. *Epigenetics* **7**, 853–857 (2012).

335. McGowan, P. O. *et al.* Epigenetic regulation of the glucocorticoid receptor in human brain associates with childhood abuse. *Nat. Neurosci.* **12**, 342–348 (2009).

336. Vangeel, E. B. *et al.* Newborn genome-wide DNA methylation in association with pregnancy anxiety reveals a potential role for GABBR1. *Clin. Epigenetics* **9**, 107 (2017).

337. Papale, L. A., Seltzer, L. J., Madrid, A., Pollak, S. D. & Alisch, R. S. Differentially Methylated Genes in Saliva are linked to Childhood Stress. *Sci. Rep.* **8**, 10785 (2018).

338. Harms, M. B. *et al.* Early life stress, FK506 binding protein 5 gene (FKBP5) methylation, and inhibition-related prefrontal function: A prospective longitudinal study. *Dev. Psychopathol.* **29**, 1895–1903 (2017).

339. Klengel, T. *et al.* Allele-specific FKBP5 DNA demethylation mediates gene–childhood trauma interactions. *Nat. Neurosci.* **16**, 33–41 (2012).

340. Bockmühl, Y. *et al.* Methylation at the CpG island shore region upregulates *Nr3c1*

promoter activity after early-life stress. *Epigenetics* **10**, 247–257 (2015).

341. Murgatroyd, C. & Spengler, D. Polycomb Binding Precedes Early-Life Stress Responsive DNA Methylation at the Avp Enhancer. *PLoS One* **9**, e90277 (2014).

342. Chandramohan, Y., Droste, S. K., Arthur, J. S. C. & Reul, J. M. H. M. The forced swimming-induced behavioural immobility response involves histone H3 phospho-acetylation and c-Fos induction in dentate gyrus granule neurons via activation of the *N* -methyl-d-aspartate/extracellular signal-regulated kinase/mitogen- and stress-activated kinase signalling pathway. *Eur. J. Neurosci.* **27**, 2701–2713 (2008).

343. Suri, D. *et al.* Early Stress Evokes Age-Dependent Biphasic Changes in Hippocampal Neurogenesis, Bdnf Expression, and Cognition. *Biol. Psychiatry* **73**, 658–666 (2013).

344. Weikum, E. R., Knuesel, M. T., Ortlund, E. A. & Yamamoto, K. R. Glucocorticoid receptor control of transcription: precision and plasticity via allostery. *Nat. Rev. Mol. Cell Biol.* **18**, 159–174 (2017).

345. Picard, D. *et al.* Reduced levels of hsp90 compromise steroid receptor action in vivo. *Nature* **348**, 166–168 (1990).

346. Fries, G. R., Gassen, N. C. & Rein, T. The FKBP51 Glucocorticoid Receptor Co-Chaperone: Regulation, Function, and Implications in Health and Disease. *Int. J. Mol. Sci.* **18**, (2017).

347. Wochnik, G. M. *et al.* FK506-binding Proteins 51 and 52 Differentially Regulate Dynein Interaction and Nuclear Translocation of the Glucocorticoid Receptor in Mammalian Cells. *J. Biol. Chem.* **280**, 4609–4616 (2005).

348. E Ortí, D B Mendel, L. I. S. and A. M. Agonist-dependent phosphorylation and nuclear dephosphorylation of glucocorticoid receptors in intact cells. *J. Biol. Chem.* (1989).

349. Yongue, B. G. & Roy, E. J. Endogenous aldosterone and corticosterone in brain cell nuclei of adrenal-intact rats: regional distribution and effects of physiological variations in serum steroids. *Brain Res.* **436**, 49–61 (1987).

350. De Kloet, E. R. & Reul, J. M. H. M. Feedback action and tonic influence of corticosteroids on brain function: A concept arising from the heterogeneity of brain receptor systems. *Psychoneuroendocrinology* **12**, 83–105 (1987).

351. REUL, J. M. H. M. & KLOET, E. R. DE. Two Receptor Systems for Corticosterone in Rat Brain: Microdistribution and Differential Occupation. *Endocrinology* **117**, 2505–2511 (1985).

352. Arriza, J. L., Simerly, R. B., Swanson, L. W. & Evans, R. M. The neuronal mineralocorticoid eeceptor as a mediator of glucocorticoid response. *Neuron* **1**, 887–900 (1988).

353. de Kloet, E. R., Meijer, O. C., de Nicola, A. F., de Rijk, R. H. & Joëls, M. Importance of the brain corticosteroid receptor balance in metaplasticity, cognitive performance and neuro-inflammation. *Front. Neuroendocrinol.* **49**, 124–145 (2018).

354. Pearce, D., Náray-Fejes-Tóth, A. & Fejes-Tóth, G. Determinants of Subnuclear Organization of Mineralocorticoid Receptor Characterized through Analysis of Wild Type and Mutant Receptors. *J. Biol. Chem.* **277**, 1451–1456 (2002).

355. Galigniana, M. D., Erlejman, A. G., Monte, M., Gomez-Sanchez, C. & Piwien-Pilipuk, G. The hsp90-FKBP52 Complex Links the Mineralocorticoid Receptor to Motor Proteins and Persists Bound to the Receptor in Early Nuclear Events. *Mol. Cell. Biol.* **30**, 1285–1298 (2010).

356. Savory, J. G. A. *et al.* Glucocorticoid Receptor Homodimers and Glucocorticoid-Mineralocorticoid Receptor Heterodimers Form in the Cytoplasm through Alternative Dimerization Interfaces. *Mol. Cell. Biol.* **21**, 781–793 (2001).

357. Mifsud, K. R. & Reul, J. M. H. M. Acute stress enhances heterodimerization and binding of corticosteroid receptors at glucocorticoid target genes in the hippocampus. *Proc. Natl. Acad. Sci.* **113**, 11336–11341 (2016).

358. Muhtz, C., Zyriax, B.-C., Bondy, B., Windler, E. & Otte, C. Association of a common mineralocorticoid receptor gene polymorphism with salivary cortisol in healthy adults. *Psychoneuroendocrinology* **36**, 298–301 (2011).

359. DeRijk, R. H., de Kloet, E. R., Zitman, F. G. & van Leeuwen, N. Mineralocorticoid Receptor Gene Variants as Determinants of HPA Axis Regulation and Behavior. in *Endocrine development* vol. 20 137–148 (Karger Publishers, 2011).

360. Pirkl, F. & Buchner, J. Functional analysis of the hsp90-associated human peptidyl prolyl Cis/Trans isomerases FKBP51, FKBP52 and cyp40 1 1Edited by R. Huber. *J. Mol. Biol.* **308**, 795–806 (2001).

361. Wochnik, G. M. *et al.* FK506-binding Proteins 51 and 52 Differentially Regulate Dynein Interaction and Nuclear Translocation of the Glucocorticoid Receptor in Mammalian Cells. *J. Biol. Chem.* **280**, 4609–4616 (2005).

362. Paakinaho, V., Makkonen, H., Jääskeläinen, T. & Palvimo, J. J. Glucocorticoid Receptor Activates Poised *FKBP51* Locus through Long-Distance Interactions. *Mol. Endocrinol.* **24**, 511–525 (2010).

363. Bouwmeester, T. *et al.* A physical and functional map of the human TNF-α/NF-κB signal transduction pathway. *Nat. Cell Biol.* **6**, 97–105 (2004).

364. Yu, H.-M., Wang, Q. & Sun, W.-B. Silencing of FKBP51 alleviates the mechanical pain threshold, inhibits DRG inflammatory factors and pain mediators through the NF-kappaB signaling pathway. *Gene* **627**, 169–175 (2017).

365. Erlejman, A. G. *et al.* NF-κB transcriptional activity is modulated by FK506-binding proteins FKBP51 and FKBP52: a role for peptidyl-prolyl isomerase activity. *J. Biol. Chem.* **289**, 26263–76 (2014).

366. Gassen, N. C. *et al.* Chaperoning epigenetics: FKBP51 decreases the activity of DNMT1 and mediates epigenetic effects of the antidepressant paroxetine. *Sci. Signal.* **8**, ra119–ra119 (2015).

367. Binder, E. B. *et al.* Polymorphisms in FKBP5 are associated with increased recurrence of depressive episodes and rapid response to antidepressant treatment. *Nat. Genet.* **36**, 1319–1325 (2004).

368. Klengel, T. *et al.* Allele-specific FKBP5 DNA demethylation mediates gene–childhood trauma interactions. *Nat. Neurosci.* **16**, 33–41 (2013).

369. Patel, N., Crider, A., Pandya, C. D., Ahmed, A. O. & Pillai, A. Altered mRNA Levels of Glucocorticoid Receptor, Mineralocorticoid Receptor, and Co-Chaperones (FKBP5 and PTGES3) in the Middle Frontal Gyrus of Autism Spectrum Disorder Subjects. *Mol. Neurobiol.* **53**, 2090–2099 (2016).

370. Misiak, B. *et al.* Interactions Between Variation in Candidate Genes and Environmental Factors in the Etiology of Schizophrenia and Bipolar Disorder: a Systematic Review. *Mol. Neurobiol.* **55**, 5075–5100 (2018).

371. Isaksson, J., Allen, M., Nilsson, K. W. & Lindblad, F. Polymorphisms in the FK506 binding protein 5 gene are associated with attention deficit hyperactivity disorder and diurnal cortisol levels. *Acta Paediatr.* **104**, 910–915 (2015).

372. Minelli, A. *et al.* ROLE OF ALLELIC VARIANTS OF FK506-BINDING PROTEIN 51 (FKBP5) GENE IN THE DEVELOPMENT OF ANXIETY DISORDERS. *Depress. Anxiety* **30**, 1170–1176 (2013).

373. Lee, R. S. *et al.* Chronic Corticosterone Exposure Increases Expression and Decreases Deoxyribonucleic Acid Methylation of *Fkbp5* in Mice. *Endocrinology* **151**, 4332–4343 (2010).

374. Gaali, S. *et al.* Selective inhibitors of the FK506-binding protein 51 by induced fit. *Nat. Chem. Biol.* **11**, 33–37 (2015).

375. Hartmann, J. *et al.* Pharmacological Inhibition of the Psychiatric Risk Factor FKBP51 Has Anxiolytic Properties. *J. Neurosci.* **35**, 9007–9016 (2015).

376. Balsevich, G. *et al.* Stress-responsive FKBP51 regulates AKT2-AS160 signaling and metabolic function. *Nat. Commun.* **8**, 1725 (2017).

377. Liggins, G. C. Premature delivery of foetal lambs infused with glucocorticoids. *J. Endocrinol.* **45**, 515–23 (1969).

378. Liggins, G. C. & Howie, R. N. A controlled trial of antepartum glucocorticoid treatment for prevention of the respiratory distress syndrome in premature infants. *Pediatrics* **50**, 515–25 (1972).

379. Bennet, L., Davidson, J. O., Koome, M. & Gunn, A. J. Glucocorticoids and preterm hypoxic-ischemic brain injury: the good and the bad. *J. Pregnancy* **2012**, 751694 (2012).

380. Siebe, H. *et al.* Metabolism of dexamethasone: sites and activity in mammalian tissues. *Ren. Physiol. Biochem.* **16**, 79–88 (1993).

381. Gonzalez-Rodriguez, P. J., Xiong, F., Li, Y., Zhou, J. & Zhang, L. Fetal hypoxia increases vulnerability of hypoxic-ischemic brain injury in neonatal rats: role of glucocorticoid receptors. *Neurobiol. Dis.* **65**, 172–9 (2014).

382. Doyle, L. W. *et al.* Low-Dose Dexamethasone Facilitates Extubation Among Chronically Ventilator-Dependent Infants: A Multicenter, International, Randomized, Controlled Trial. *Pediatrics* **117**, 75–83 (2006).

383. Jefferies, A. L. Postnatal corticosteroids to treat or prevent chronic lung disease in preterm infants. *Paediatr. Child Health* **17**, 573–4 (2012).

384. Orchinik, M., Murray, T. F. & Moore, F. L. A corticosteroid receptor in neuronal

membranes. *Science* **252**, 1848–51 (1991).

385. Liu, X.-H. *et al.* Rapid Inhibition of ATP-Induced Currents by Corticosterone in Rat Dorsal Root Ganglion Neurons. *Pharmacology* **82**, 164–170 (2008).

386. Karst, H. *et al.* Mineralocorticoid receptors are indispensable for nongenomic modulation of hippocampal glutamate transmission by corticosterone. *Proc. Natl. Acad. Sci. U. S. A.* **102**, 19204–7 (2005).

387. Karst, H., Berger, S., Erdmann, G., Schütz, G. & Joëls, M. Metaplasticity of amygdalar responses to the stress hormone corticosterone. *Proc. Natl. Acad. Sci. U. S. A.* **107**, 14449–54 (2010).

388. Di, S., Malcher-Lopes, R., Halmos, K. C. & Tasker, J. G. Nongenomic glucocorticoid inhibition via endocannabinoid release in the hypothalamus: a fast feedback mechanism. *J. Neurosci.* **23**, 4850–7 (2003).

389. Di, S. *et al.* Activity-dependent release and actions of endocannabinoids in the rat hypothalamic supraoptic nucleus. *J. Physiol.* **569**, 751–760 (2005).

390. Qiu, J. *et al.* Nongenomic Mechanisms of Glucocorticoid Inhibition of Nicotine-Induced Calcium Influx in PC12 Cells: Involvement of Protein Kinase C**This work was supported by a research grant from the Natural Science Foundation of China. *Endocrinology* **139**, 5103–5108 (1998).

391. Lou, S. & Chen, Y. The Rapid Inhibitory Effect of Glucocorticoid on Cytosolic Free Ca2+Increment Induced by High Extracellular K+and Its Underlying Mechanism in PC12 Cells. *Biochem. Biophys. Res. Commun.* **244**, 403–407 (1998).

392. Danese, A., Pariante, C. M., Caspi, A., Taylor, A. & Poulton, R. Childhood maltreatment predicts adult inflammation in a life-course study. *Proc. Natl. Acad. Sci.* **104**, 1319–1324 (2007).

393. Takizawa, R., Danese, A., Maughan, B. & Arseneault, L. Bullying victimization in childhood predicts inflammation and obesity at mid-life: a five-decade birth cohort study. *Psychol. Med.* **45**, 2705–2715 (2015).

394. Redlich, R. *et al.* Evidence of an IFN-γ by early life stress interaction in the regulation of amygdala reactivity to emotional stimuli. *Psychoneuroendocrinology* **62**, 166–173 (2015).

395. Wolf, J. M., Rohleder, N., Bierhaus, A., Nawroth, P. P. & Kirschbaum, C. Determinants of the NF-κB response to acute psychosocial stress in humans. *Brain. Behav. Immun.* **23**, 742–749 (2009).

396. Ross, K. M., Cole, S. W., Carroll, J. E. & Dunkel Schetter, C. Elevated pro-inflammatory gene expression in the third trimester of pregnancy in mothers who experienced stressful life events. *Brain. Behav. Immun.* **76**, 97–103 (2019).

397. Doenni, V. M., Song, C. M., Hill, M. N. & Pittman, Q. J. Early-life inflammation with LPS delays fear extinction in adult rodents. *Brain. Behav. Immun.* **63**, 176–185 (2017).

398. Ben-Yehuda, H. *et al.* Maternal Type-I interferon signaling adversely affects the microglia and the behavior of the offspring accompanied by increased sensitivity to

stress. *Mol. Psychiatry* 1–18 (2019) doi:10.1038/s41380-019-0604-0.

399. Bekhbat, M. *et al.* Chronic adolescent stress sex-specifically alters central and peripheral neuro-immune reactivity in rats. *Brain. Behav. Immun.* **76**, 248–257 (2019).

400. Doucas, V. *et al.* Cytoplasmic catalytic subunit of protein kinase A mediates cross-repression by NF-kappa B and the glucocorticoid receptor. *Proc. Natl. Acad. Sci.* **97**, 11893–11898 (2000).

401. Bhadra, U., Thakkar, N., Das, P. & Pal Bhadra, M. Evolution of circadian rhythms: from bacteria to human. *Sleep Med.* **35**, 49–61 (2017).

402. Takahashi, J. S. Transcriptional architecture of the mammalian circadian clock. *Nat. Rev. Genet.* **18**, 164–179 (2017).

403. Yoo, S.-H. *et al.* PERIOD2::LUCIFERASE real-time reporting of circadian dynamics reveals persistent circadian oscillations in mouse peripheral tissues. *Proc. Natl. Acad. Sci. U. S. A.* **101**, 5339–46 (2004).

404. Zhang, R., Lahens, N. F., Ballance, H. I., Hughes, M. E. & Hogenesch, J. B. A circadian gene expression atlas in mammals: implications for biology and medicine. *Proc. Natl. Acad. Sci. U. S. A.* **111**, 16219–24 (2014).

405. Hastings, M. H., Maywood, E. S. & Brancaccio, M. Generation of circadian rhythms in the suprachiasmatic nucleus. *Nat. Rev. Neurosci.* **19**, 453–469 (2018).

406. Colwell, C. S. Linking neural activity and molecular oscillations in the SCN. *Nat. Rev. Neurosci.* **12**, 553–569 (2011).

407. Leak, R. K. & Moore, R. Y. Topographic organization of suprachiasmatic nucleus projection neurons. *J. Comp. Neurol.* **433**, 312–334 (2001).

408. Jones, J. R., Tackenberg, M. C. & McMahon, D. G. Manipulating circadian clock neuron firing rate resets molecular circadian rhythms and behavior. *Nat. Neurosci.* **18**, 373–375 (2015).

409. Silver, R., LeSauter, J., Tresco, P. A. & Lehman, M. N. A diffusible coupling signal from the transplanted suprachiasmatic nucleus controlling circadian locomotor rhythms. *Nature* **382**, 810–813 (1996).

410. Maywood, E. S., Chesham, J. E., O'Brien, J. A. & Hastings, M. H. A diversity of paracrine signals sustains molecular circadian cycling in suprachiasmatic nucleus circuits. *Proc. Natl. Acad. Sci. U. S. A.* **108**, 14306–11 (2011).

411. Lee, I. T. *et al.* Neuromedin S-Producing Neurons Act as Essential Pacemakers in the Suprachiasmatic Nucleus to Couple Clock Neurons and Dictate Circadian Rhythms. *Neuron* **85**, 1086–1102 (2015).

412. Bailey, M. & Silver, R. Sex differences in circadian timing systems: Implications for disease. *Front. Neuroendocrinol.* **35**, 111–139 (2014).

413. Fernandez-Guasti, A., Kruijver, F. P. M., Fodor, M. & Swaab, D. F. Sex differences in the distribution of androgen receptors in the human hypothalamus. *J. Comp. Neurol.* **425**, 422–435 (2000).

414. Iwahana, E., Karatsoreos, I., Shibata, S. & Silver, R. Gonadectomy reveals sex differences in circadian rhythms and suprachiasmatic nucleus androgen receptors in mice. *Horm. Behav.* **53**, 422–430 (2008).

415. Kruijver, F. P. M. & Swaab, D. F. Sex hormone receptors are present in the human suprachiasmatic nucleus. *Neuroendocrinology* **75**, 296–305 (2002).

416. Provencio, I. *et al.* A novel human opsin in the inner retina. *J. Neurosci.* **20**, 600–5 (2000).

417. Coomans, C. P. *et al.* The suprachiasmatic nucleus controls circadian energy metabolism and hepatic insulin sensitivity. *Diabetes* **62**, 1102–8 (2013).

418. Prendergast, B. J. *et al.* Impaired leukocyte trafficking and skin inflammatory responses in hamsters lacking a functional circadian system. *Brain. Behav. Immun.* **32**, 94–104 (2013).

419. Easton, A., Meerlo, P., Bergmann, B. & Turek, F. W. The suprachiasmatic nucleus regulates sleep timing and amount in mice. *Sleep* **27**, 1307–18 (2004).

420. Santhi, N. *et al.* Sex differences in the circadian regulation of sleep and waking cognition in humans. *Proc. Natl. Acad. Sci.* **113**, E2730–E2739 (2016).

421. Videnovic, A., Lazar, A. S., Barker, R. A. & Overeem, S. 'The clocks that time us'—circadian rhythms in neurodegenerative disorders. *Nat. Rev. Neurol.* **10**, 683–693 (2014).

422. Ripperger, J. A. & Schibler, U. Rhythmic CLOCK-BMAL1 binding to multiple E-box motifs drives circadian Dbp transcription and chromatin transitions. *Nat. Genet.* **38**, 369–374 (2006).

423. Gekakis, N. *et al.* Role of the CLOCK protein in the mammalian circadian mechanism. *Science* **280**, 1564–9 (1998).

424. Sato, T. K. *et al.* A Functional Genomics Strategy Reveals Rora as a Component of the Mammalian Circadian Clock. *Neuron* **43**, 527–537 (2004).

425. Preitner, N. *et al.* The orphan nuclear receptor REV-ERBalpha controls circadian transcription within the positive limb of the mammalian circadian oscillator. *Cell* **110**, 251–60 (2002).

426. Stratmann, M., Suter, D. M., Molina, N., Naef, F. & Schibler, U. Circadian Dbp Transcription Relies on Highly Dynamic BMAL1-CLOCK Interaction with E Boxes and Requires the Proteasome. *Mol. Cell* **48**, 277–287 (2012).

427. Lipton, J. O. *et al.* The Circadian Protein BMAL1 Regulates Translation in Response to S6K1-Mediated Phosphorylation. *Cell* **161**, 1138–1151 (2015).

428. DeBruyne, J. P. *et al.* A Clock Shock: Mouse CLOCK Is Not Required for Circadian Oscillator Function. *Neuron* **50**, 465–477 (2006).

429. Tamiya, H., Ogawa, S., Ouchi, Y. & Akishita, M. Rigid Cooperation of Per1 and Per2 proteins. *Sci. Rep.* **6**, 32769 (2016).

430. Husse, J., Hintze, S. C., Eichele, G., Lehnert, H. & Oster, H. Circadian Clock Genes Per1 and Per2 Regulate the Response of Metabolism-Associated Transcripts to Sleep

Disruption. *PLoS One* **7**, e52983 (2012).

431. Horst, G. T. J. van der *et al.* Mammalian Cry1 and Cry2 are essential for maintenance of circadian rhythms. *Nature* **398**, 627–630 (1999).

432. Cho, H. *et al.* Regulation of circadian behaviour and metabolism by REV-ERB-α and REV-ERB-β. *Nature* **485**, 123–127 (2012).

433. Takeda, Y., Jothi, R., Birault, V. & Jetten, A. M. RORγ directly regulates the circadian expression of clock genes and downstream targets in vivo. *Nucleic Acids Res.* **40**, 8519–35 (2012).

434. Masana, M. I., Sumaya, I. C., Becker-Andre, M. & Dubocovich, M. L. Behavioral characterization and modulation of circadian rhythms by light and melatonin in C3H/HeN mice homozygous for the RORβ knockout. *Am. J. Physiol. Integr. Comp. Physiol.* **292**, R2357–R2367 (2007).

435. Lopez-Molina, L., Conquet, F., Dubois-Dauphin, M. & Schibler, U. The DBP gene is expressed according to a circadian rhythm in the suprachiasmatic nucleus and influences circadian behavior. *EMBO J.* **16**, 6762–6771 (1997).

436. Tso, C. F. *et al.* Astrocytes Regulate Daily Rhythms in the Suprachiasmatic Nucleus and Behavior. *Curr. Biol.* **27**, 1055–1061 (2017).

437. Brancaccio, M., Patton, A. P., Chesham, J. E., Maywood, E. S. & Hastings, M. H. Astrocytes Control Circadian Timekeeping in the Suprachiasmatic Nucleus via Glutamatergic Signaling. *Neuron* **93**, 1420-1435.e5 (2017).

438. Barca-Mayo, O. *et al.* Astrocyte deletion of Bmal1 alters daily locomotor activity and cognitive functions via GABA signalling. *Nat. Commun.* **8**, 14336 (2017).

439. Girotti, M., Weinberg, M. S. & Spencer, R. L. Diurnal expression of functional and clock-related genes throughout the rat HPA axis: system-wide shifts in response to a restricted feeding schedule. *Am. J. Physiol. Metab.* **296**, E888–E897 (2009).

440. Dickmeis, T. Glucocorticoids and the circadian clock. *J. Endocrinol.* **200**, 3–22 (2009).

441. Moore, R. Y. & Eichler, V. B. Loss of a circadian adrenal corticosterone rhythm following suprachiasmatic lesions in the rat. *Brain Res.* **42**, 201–6 (1972).

442. Son, G. H. *et al.* Adrenal peripheral clock controls the autonomous circadian rhythm of glucocorticoid by causing rhythmic steroid production. *Proc. Natl. Acad. Sci. U. S. A.* **105**, 20970–5 (2008).

443. Balsalobre, A. *et al.* Resetting of circadian time in peripheral tissues by glucocorticoid signaling. *Science* **289**, 2344–7 (2000).

444. Koch, C. E., Leinweber, B., Drengberg, B. C., Blaum, C. & Oster, H. Interaction between circadian rhythms and stress. *Neurobiol. Stress* **6**, 57–67 (2017).

445. Ikeda, Y., Kumagai, H., Skach, A., Sato, M. & Yanagisawa, M. Modulation of circadian glucocorticoid oscillation via adrenal opioid-CXCR7 signaling alters emotional behavior. *Cell* **155**, 1323–36 (2013).

446. Tahara, Y. *et al.* Entrainment of the mouse circadian clock by sub-acute physical and psychological stress. *Sci. Rep.* **5**, 11417 (2015).

447. Lamia, K. A. *et al.* Cryptochromes mediate rhythmic repression of the glucocorticoid receptor. *Nature* **480**, 552–556 (2011).

448. Al-Safadi, S., Branchaud, M., Rutherford, S. & Amir, S. Glucocorticoids and Stress-Induced Changes in the Expression of PERIOD1 in the Rat Forebrain. *PLoS One* **10**, e0130085 (2015).

449. Takahashi, S. *et al.* Physical and Inflammatory Stressors Elevate Circadian Clock Gene *mPer1* mRNA Levels in the Paraventricular Nucleus of the Mouse. *Endocrinology* **142**, 4910–4917 (2001).

450. Schwichtenberg, A. J., Christ, S., Abel, E. & Poehlmann-Tynan, J. A. Circadian Sleep Patterns in Toddlers Born Preterm. *J. Dev. Behav. Pediatr.* **37**, 358–369 (2016).

451. Sun, W. *et al.* Association of Sleep and Circadian Activity Rhythm with Emotional Face Processing among 12-month-old Infants. *Sci. Rep.* **8**, 3200 (2018).

452. Tordjman, S. *et al.* Altered circadian patterns of salivary cortisol in low-functioning children and adolescents with autism. *Psychoneuroendocrinology* **50**, 227–245 (2014).

453. Kotagal, S. & Broomall, E. Sleep in Children With Autism Spectrum Disorder. *Pediatr. Neurol.* **47**, 242–251 (2012).

454. Limoges, É., Mottron, L., Bolduc, C., Berthiaume, C. & Godbout, R. Atypical sleep architecture and the autism phenotype. *Brain* **128**, 1049–1061 (2005).

455. Baker, E. K., Richdale, A. L. & Hazi, A. Employment status is related to sleep problems in adults with autism spectrum disorder and no comorbid intellectual impairment. *Autism* 136236131774585 (2018) doi:10.1177/1362361317745857.

456. Nir, I. *et al.* Brief report: circadian melatonin, thyroid-stimulating hormone, prolactin, and cortisol levels in serum of young adults with autism. *J. Autism Dev. Disord.* **25**, 641–54 (1995).

457. Tordjman, S., Anderson, G. M., Pichard, N., Charbuy, H. & Touitou, Y. Nocturnal excretion of 6-sulphatoxymelatonin in children and adolescents with autistic disorder. *Biol. Psychiatry* **57**, 134–138 (2005).

458. Olde Loohuis, N. F. M. *et al.* Altered expression of circadian rhythm and extracellular matrix genes in the medial prefrontal cortex of a valproic acid rat model of autism. *Prog. Neuro-Psychopharmacology Biol. Psychiatry* **77**, 128–132 (2017).

459. Cusmano, D. M. & Mong, J. A. In Utero Exposure to Valproic Acid Changes Sleep in Juvenile Rats: A Model for Sleep Disturbances in Autism. *Sleep* **37**, 1489–1499 (2014).

460. Fountain, M. D., Tao, H., Chen, C.-A., Yin, J. & Schaaf, C. P. *Magel2* knockout mice manifest altered social phenotypes and a deficit in preference for social novelty. *Genes, Brain Behav.* **16**, 592–600 (2017).

461. Angelakos, C. C. *et al.* Hyperactivity and male-specific sleep deficits in the 16p11.2 deletion mouse model of autism. *Autism Res.* **10**, 572–584 (2017).

462. Sare, R. M., Levine, M. & Smith, C. B. Behavioral Phenotype of Fmr1 Knock-Out Mice during Active Phase in an Altered Light/Dark Cycle. *eNeuro* **3**, (2016).

463. Tsuchiya, Y. *et al.* Disruption of MeCP2 attenuates circadian rhythm in CRISPR/Cas9-based Rett syndrome model mouse. *Genes to Cells* **20**, 992–1005 (2015).

464. Lyall, L. M. *et al.* Association of disrupted circadian rhythmicity with mood disorders, subjective wellbeing, and cognitive function: a cross-sectional study of 91 105 participants from the UK Biobank. *The lancet. Psychiatry* **5**, 507–514 (2018).

465. Wulff, K., Dijk, D.-J., Middleton, B., Foster, R. G. & Joyce, E. M. Sleep and circadian rhythm disruption in schizophrenia. *Br. J. Psychiatry* **200**, 308–316 (2012).

466. Oliver, P. L. *et al.* Disrupted circadian rhythms in a mouse model of schizophrenia. *Curr. Biol.* **22**, 314–9 (2012).

467. Takaesu, Y. Circadian rhythm in bipolar disorder: A review of the literature. *Psychiatry Clin. Neurosci.* **72**, 673–682 (2018).

468. McCarthy, M. J. *et al.* Chronotype and cellular circadian rhythms predict the clinical response to lithium maintenance treatment in patients with bipolar disorder. *Neuropsychopharmacology* **44**, 620–628 (2019).

469. Li, J. Z. *et al.* Circadian patterns of gene expression in the human brain and disruption in major depressive disorder. *Proc. Natl. Acad. Sci. U. S. A.* **110**, 9950–5 (2013).

470. Giannakoulopoulos, X., Sepulveda, W., Kourtis, P., Glover, V. & Fisk, N. M. Fetal plasma cortisol and beta-endorphin response to intrauterine needling. *Lancet (London, England)* **344**, 77–81 (1994).

471. Swaab, D. F., Hofman, M. A. & Honnebier, M. B. Development of vasopressin neurons in the human suprachiasmatic nucleus in relation to birth. *Brain Res. Dev. Brain Res.* **52**, 289–93 (1990).

472. Bolt, R. J. *et al.* Maturity of the Adrenal Cortex in Very Preterm Infants Is Related to Gestational Age. *Pediatr. Res.* **52**, 405–410 (2002).

473. Ivars, K. *et al.* Development of Salivary Cortisol Circadian Rhythm and Reference Intervals in Full-Term Infants. *PLoS One* **10**, e0129502 (2015).

474. Bauer, J. *et al.* Circadian variation on oxygen consumption in preterm infants. *J. Perinat. Med.* **37**, 413–7 (2009).

475. Mirmiran, M. *et al.* Circadian rhythms in preterm infants: a preliminary study. *Early Hum. Dev.* **23**, 139–146 (1990).

476. Rivkees, S. A., Mayes, L., Jacobs, H. & Gross, I. Rest-activity patterns of premature infants are regulated by cycled lighting. *Pediatrics* **113**, 833–9 (2004).

477. Vásquez-Ruiz, S. *et al.* A light/dark cycle in the NICU accelerates body weight gain and shortens time to discharge in preterm infants. *Early Hum. Dev.* **90**, 535–540 (2014).

478. Mirmiran, M., Baldwin, R. B. & Ariagno, R. L. Circadian and Sleep Development in Preterm Infants Occurs Independently From the Influences of Environmental Lighting. *Pediatr. Res.* **53**, 933–938 (2003).

479. Saxena, M. T. *et al.* Bioluminescence Imaging of *Period1* Gene Expression in Utero.

Mol. Imaging **6**, 7290.2007.00003 (2007).

480. Altman, J. & Bayer, S. A. Development of the diencephalon in the rat. II. Correlation of the embryonic development of the hypothalamus with the time of origin of its neurons. *J. Comp. Neurol.* **182**, 973–93 (1978).

481. Sládek, M. *et al.* Insight into molecular core clock mechanism of embryonic and early postnatal rat suprachiasmatic nucleus. *Proc. Natl. Acad. Sci. U. S. A.* **101**, 6231–6 (2004).

482. Oh, G. *et al.* Cytosine modifications exhibit circadian oscillations that are involved in epigenetic diversity and aging. *Nat. Commun.* **9**, 644 (2018).

483. Lim, A. S. P. *et al.* 24-Hour Rhythms of DNA Methylation and Their Relation with Rhythms of RNA Expression in the Human Dorsolateral Prefrontal Cortex. *PLoS Genet.* **10**, e1004792 (2014).

484. Azzi, A. *et al.* Circadian behavior is light-reprogrammed by plastic DNA methylation. *Nat. Neurosci.* **17**, 377–382 (2014).

485. Martínez de Paz, A. *et al.* Circadian Cycle-Dependent MeCP2 and Brain Chromatin Changes. *PLoS One* **10**, e0123693 (2015).

486. Young, D. *et al.* Sleep problems in Rett syndrome. *Brain Dev.* **29**, 609–16 (2007).

487. Mullegama, S. V *et al.* MBD5 haploinsufficiency is associated with sleep disturbance and disrupts circadian pathways common to Smith–Magenis and fragile X syndromes. *Eur. J. Hum. Genet.* **23**, 781–789 (2015).

488. Etchegaray, J.-P., Lee, C., Wade, P. A. & Reppert, S. M. Rhythmic histone acetylation underlies transcription in the mammalian circadian clock. *Nature* **421**, 177–182 (2003).

489. Hosoda, H. *et al.* CBP/p300 is a cell type-specific modulator of CLOCK/BMAL1-mediated transcription. *Mol. Brain* **2**, 34 (2009).

490. Doi, M., Hirayama, J. & Sassone-Corsi, P. Circadian Regulator CLOCK Is a Histone Acetyltransferase. *Cell* **125**, 497–508 (2006).

491. Asher, G. *et al.* SIRT1 Regulates Circadian Clock Gene Expression through PER2 Deacetylation. *Cell* **134**, 317–328 (2008).

492. Katada, S. & Sassone-Corsi, P. The histone methyltransferase MLL1 permits the oscillation of circadian gene expression. *Nat. Struct. Mol. Biol.* **17**, 1414–1421 (2010).

493. Valekunja, U. K. *et al.* Histone methyltransferase MLL3 contributes to genome-scale circadian transcription. *Proc. Natl. Acad. Sci. U. S. A.* **110**, 1554–9 (2013).

494. DiTacchio, L. *et al.* Histone Lysine Demethylase JARID1a Activates CLOCK-BMAL1 and Influences the Circadian Clock. *Science (80-.).* **333**, 1881–1885 (2011).

495. Schneider, J. E., Wysocki, C. J., Nyby, J. & Whitney, G. Determining the sex of neonatal mice (Mus musculus). *Behav. Res. Methods Instrum.* **10**, 105–105 (1978).

496. Jui-Cheng Yen, Fu-Juay Chang & Shyang Chang. A new criterion for automatic multilevel thresholding. *IEEE Trans. Image Process.* **4**, 370–378 (1995).

497. Thomson, J. P. *et al.* DNA immunoprecipitation semiconductor sequencing (DIP-SC-seq) as a rapid method to generate genome wide epigenetic signatures. *Sci. Rep.* **5**, 9778 (2015).

498. Boardman, J. P. *et al.* Common genetic variants and risk of brain injury after preterm birth. *Pediatrics* **133**, e1655-63 (2014).

499. Wang, T. *et al.* Genome-wide DNA hydroxymethylation changes are associated with neurodevelopmental genes in the developing human cerebellum. *Hum. Mol. Genet.* **21**, 5500–5510 (2012).

500. Wlodarczyk, A. *et al.* A novel microglial subset plays a key role in myelinogenesis in developing brain. *EMBO J.* **36**, 3292–3308 (2017).

501. Weinhard, L. *et al.* Microglia remodel synapses by presynaptic trogocytosis and spine head filopodia induction. *Nat. Commun.* **9**, 1228 (2018).

502. Ellison, V. J. *et al.* The Relationship of CSF and Plasma Cytokine Levels to Cerebral White Matter Injury in the Premature Newborn. *Pediatr. Res.* **57**, 282–286 (2005).

503. Narang, V. S. *et al.* Dexamethasone increases expression and activity of multidrug resistance transporters at the rat blood-brain barrier. *Am. J. Physiol. Cell Physiol.* **295**, C440-50 (2008).

504. Förster, C., Kahles, T., Kietz, S. & Drenckhahn, D. Dexamethasone induces the expression of metalloproteinase inhibitor TIMP-1 in the murine cerebral vascular endothelial cell line cEND. *J. Physiol.* **580**, 937–949 (2007).

505. Sidibeh, C. O. *et al.* FKBP5 expression in human adipose tissue: potential role in glucose and lipid metabolism, adipogenesis and type 2 diabetes. *Endocrine* **62**, 116–128 (2018).

506. Cronin, J. *et al.* Single dose oral dexamethasone versus multi-dose prednisolone in the treatment of acute exacerbations of asthma in children who attend the emergency department: study protocol for a randomized controlled trial. *Trials* **13**, 141 (2012).

507. Lyons, D. G., Parpaleix, A., Roche, M. & Charpak, S. Mapping oxygen concentration in the awake mouse brain. *Elife* **5**, (2016).

508. Tomita, S. *et al.* Defective Brain Development in Mice Lacking the Hif-1 Gene in Neural Cells. *Mol. Cell. Biol.* **23**, 6739–6749 (2003).

509. Terraneo, L., Virgili, E., Caretti, A., Bianciardi, P. & Samaja, M. In vivo hyperoxia induces hypoxia-inducible factor-1α overexpression in LNCaP tumors without affecting the tumor growth rate. *Int. J. Biochem. Cell Biol.* **51**, 65–74 (2014).

510. Laukka, T. *et al.* Fumarate and Succinate Regulate Expression of Hypoxia-inducible Genes via TET Enzymes. *J. Biol. Chem.* **291**, 4256–65 (2016).

511. Wang, J. *et al.* Tet1 facilitates hypoxia tolerance by stabilizing the HIF-α proteins independent of its methylcytosine dioxygenase activity. *Nucleic Acids Res.* (2017) doi:10.1093/nar/gkx869.

512. Xu, X. *et al.* High-fidelity CRISPR/Cas9- based gene-specific hydroxymethylation rescues gene expression and attenuates renal fibrosis. *Nat. Commun.* **9**, 3509 (2018).

513. Morotti, M. *et al.* Hypoxia-induced switch in SNAT2/SLC38A2 regulation generates endocrine resistance in breast cancer. *Proc. Natl. Acad. Sci. U. S. A.* **116**, 12452–12461 (2019).

514. Elorza, A. *et al.* HIF2α Acts as an mTORC1 Activator through the Amino Acid Carrier SLC7A5. *Mol. Cell* **48**, 681–691 (2012).

515. Kaira, K. *et al.* LAT1 expression is closely associated with hypoxic markers and mTOR in resected non-small cell lung cancer. *Am. J. Transl. Res.* **3**, 468–78 (2011).

516. Onishi, Y. *et al.* Hypoxia affects Slc7a5 expression through HIF-2α in differentiated neuronal cells. *FEBS Open Bio* **9**, 241–247 (2019).

517. van Tilborg, E. *et al.* Combined fetal inflammation and postnatal hypoxia causes myelin deficits and autism-like behavior in a rat model of diffuse white matter injury. *Glia* **66**, 78–93 (2018).

518. Lu, Y.-C., Yeh, W.-C. & Ohashi, P. S. LPS/TLR4 signal transduction pathway. *Cytokine* **42**, 145–151 (2008).

519. Michiels, C. *et al.* HIF-1 and AP-1 Cooperate to Increase Gene Expression in Hypoxia: Role of MAP Kinases. *IUBMB Life (International Union Biochem. Mol. Biol. Life)* **52**, 49–53 (2001).

520. Nestor, C. E. *et al.* Rapid reprogramming of epigenetic and transcriptional profiles in mammalian culture systems. *Genome Biol.* **16**, 11 (2015).

521. Voss, T. C. & Hager, G. L. Dynamic regulation of transcriptional states by chromatin and transcription factors. *Nat. Rev. Genet.* **15**, 69–81 (2014).

522. Yang, L., Chen, M., Zhang, J., Ren, D. & Hu, B. Hypoxia Delays Oligodendrocyte Progenitor Cell Migration and Myelin Formation by Suppressing Bmp2b Signaling in Larval Zebrafish. *Front. Cell. Neurosci.* **12**, 348 (2018).

523. Jablonska, B. *et al.* Oligodendrocyte regeneration after neonatal hypoxia requires FoxO1-mediated p27Kip1 expression. *J. Neurosci.* **32**, 14775–93 (2012).

524. Hopkins, S. J. & Rothwell, N. J. Cytokines and the nervous system. I: Expression and recognition. *Trends Neurosci.* **18**, 83–8 (1995).

525. Scheibel, M. *et al.* IκBβ is an essential co-activator for LPS-induced IL-1β transcription in vivo. *J. Exp. Med.* **207**, 2621–2630 (2010).

526. Folco, E. J., Sukhova, G. K., Quillard, T. & Libby, P. Moderate Hypoxia Potentiates Interleukin-1β Production in Activated Human Macrophages. *Circ. Res.* **115**, 875 (2014).

527. Zhang, W. *et al.* Evidence that hypoxia-inducible factor-1 (HIF-1) mediates transcriptional activation of interleukin-1β (IL-1β) in astrocyte cultures. *J. Neuroimmunol.* **174**, 63–73 (2006).

528. Twilhaar, E. S. *et al.* Cognitive Outcomes of Children Born Extremely or Very Preterm Since the 1990s and Associated Risk Factors. *JAMA Pediatr.* **172**, 361 (2018).

529. Fitzgerald, E., Boardman, J. P. & Drake, A. J. Preterm Birth and the Risk of Neurodevelopmental Disorders - Is There a Role for Epigenetic Dysregulation? *Curr.*

Genomics **19**, 507–521 (2018).

530. Zimmermann, C. A. *et al.* Stress dynamically regulates co-expression networks of glucocorticoid receptor-dependent MDD and SCZ risk genes. *Transl. Psychiatry* **9**, 41 (2019).

531. Mackes, N. K. *et al.* Early childhood deprivation is associated with alterations in adult brain structure despite subsequent environmental enrichment. *Proc. Natl. Acad. Sci. U. S. A.* **117**, 641–649 (2020).

532. Brummelte, S. *et al.* Procedural pain and brain development in premature newborns. *Ann. Neurol.* **71**, 385–96 (2012).

533. Al-Safadi, S. *et al.* Stress-induced changes in the expression of the clock protein PERIOD1 in the rat limbic forebrain and hypothalamus: role of stress type, time of day, and predictability. *PLoS One* **9**, e111166 (2014).

534. Ma, F. *et al.* A comparison between whole transcript and 3' RNA sequencing methods using Kapa and Lexogen library preparation methods. *BMC Genomics* **20**, 9 (2019).

535. Peña, C. J. *et al.* Early life stress alters transcriptomic patterning across reward circuitry in male and female mice. *Nat. Commun.* **10**, 5098 (2019).

536. Peña, C. J. *et al.* Early life stress confers lifelong stress susceptibility in mice via ventral tegmental area OTX2. *Science* **356**, 1185–1188 (2017).

537. Mehta, D. *et al.* Childhood maltreatment is associated with distinct genomic and epigenetic profiles in posttraumatic stress disorder. *Proc. Natl. Acad. Sci. U. S. A.* **110**, 8302–7 (2013).

538. Maniam, J., Antoniadis, C. & Morris, M. J. Early-Life Stress, HPA Axis Adaptation, and Mechanisms Contributing to Later Health Outcomes. *Front. Endocrinol. (Lausanne).* **5**, 73 (2014).

539. Carola, V., D'Olimpio, F., Brunamonti, E., Mangia, F. & Renzi, P. Evaluation of the elevated plus-maze and open-field tests for the assessment of anxiety-related behaviour in inbred mice. *Behav. Brain Res.* **134**, 49–57 (2002).

540. Can, A. *et al.* The tail suspension test. *J. Vis. Exp.* e3769 (2012) doi:10.3791/3769.

541. Lin, L. *et al.* Early-life stress leads to impaired spatial learning and memory in middle-aged ApoE4-TR mice. *Mol. Neurodegener.* **11**, 51 (2016).

542. Barone, I., Hawks-Mayer, H. & Lipton, J. O. Mechanisms of sleep and circadian ontogeny through the lens of neurodevelopmental disorders. *Neurobiol. Learn. Mem.* **160**, 160–172 (2019).

543. Reite, M., Seiler, C., Crowley, T. J., Hydinger-Macdonald, M. & Short, R. Circadian rhythm changes following maternal separation. *Chronobiologia* **9**, 1–11 (1982).

544. Lewin, M. *et al.* Early Life Trauma Has Lifelong Consequences for Sleep And Behavior. *Sci. Rep.* **9**, 16701 (2019).

545. Keunen, K., van Elburg, R. M., van Bel, F. & Benders, M. J. N. L. Impact of nutrition on brain development and its neuroprotective implications following preterm birth.

Pediatr. Res. **77**, 148–155 (2015).

546. Powell, D. R. *et al.* Cdon promotes neural crest migration by regulating N-cadherin localization. *Dev. Biol.* **407**, 289–99 (2015).

547. Qin, S. *et al.* An association study of the N-methyl-D-aspartate receptor NR1 subunit gene (GRIN1) and NR2B subunit gene (GRIN2B) in schizophrenia with universal DNA microarray. *Eur. J. Hum. Genet.* **13**, 807–814 (2005).

548. Arion, D., Unger, T., Lewis, D. A., Levitt, P. & Mirnics, K. Molecular evidence for increased expression of genes related to immune and chaperone function in the prefrontal cortex in schizophrenia. *Biol. Psychiatry* **62**, 711 (2007).

549. Varela-Nallar, L., Grabowski, C. P., Alfaro, I. E., Alvarez, A. R. & Inestrosa, N. C. Role of the Wnt receptor Frizzled-1 in presynaptic differentiation and function. *Neural Dev.* **4**, 41 (2009).

550. Tripathy, R. *et al.* Mutations in MAST1 Cause Mega-Corpus-Callosum Syndrome with Cerebellar Hypoplasia and Cortical Malformations. *Neuron* **100**, 1354-1368.e5 (2018).

551. Fahnenstich, J. *et al.* Promyelocytic leukaemia zinc finger protein (PLZF) is a glucocorticoid- and progesterone-induced transcription factor in human endometrial stromal cells and myometrial smooth muscle cells. *Mol. Hum. Reprod.* **9**, 611–623 (2003).

552. Kubota-Sakashita, M., Iwamoto, K., Bundo, M. & Kato, T. A role of ADAR2 and RNA editing of glutamate receptors in mood disorders and schizophrenia. *Mol. Brain* **7**, 5 (2014).

553. Zhang, J. *et al.* S phase-dependent interaction with DNMT1 dictates the role of UHRF1 but not UHRF2 in DNA methylation maintenance. *Cell Res.* **21**, 1723–1739 (2011).

554. Zhou, T. *et al.* Structural Basis for Hydroxymethylcytosine Recognition by the SRA Domain of UHRF2. *Mol. Cell* **54**, 879–886 (2014).

555. Wang, K. *et al.* Common genetic variants on 5p14.1 associate with autism spectrum disorders. *Nature* **459**, 528–533 (2009).

556. Smith, K. R. *et al.* Cadherin-10 Maintains Excitatory/Inhibitory Ratio through Interactions with Synaptic Proteins. *J. Neurosci.* **37**, 11127–11139 (2017).

557. Lazarides, C. *et al.* Maternal pro-inflammatory state during pregnancy and newborn leukocyte telomere length: A prospective investigation. *Brain. Behav. Immun.* **80**, 419–426 (2019).

558. Connolly, S., Anney, R., Gallagher, L. & Heron, E. A. A genome-wide investigation into parent-of-origin effects in autism spectrum disorder identifies previously associated genes including SHANK3. *Eur. J. Hum. Genet.* **25**, 234–239 (2017).

559. Fricke, C. *et al.* astray, a zebrafish roundabout homolog required for retinal axon guidance. *Science* **292**, 507–10 (2001).

560. Harripaul, R. *et al.* Mapping autosomal recessive intellectual disability: combined microarray and exome sequencing identifies 26 novel candidate genes in 192

consanguineous families. *Mol. Psychiatry* **23**, 973–984 (2018).

561. Cairo, S., Merla, G., Urbinati, F., Ballabio, A. & Reymond, A. WBSCR14, a gene mapping to the Williams--Beuren syndrome deleted region, is a new member of the Mlx transcription factor network. *Hum. Mol. Genet.* **10**, 617–27 (2001).

562. Vorstman, J. A. S. *et al.* A double hit implicates DIAPH3 as an autism risk gene. *Mol. Psychiatry* **16**, 442–451 (2011).

563. Alonso-Gonzalez, A., Calaza, M., Rodriguez-Fontenla, C. & Carracedo, A. Novel Gene-Based Analysis of ASD GWAS: Insight Into the Biological Role of Associated Genes. *Front. Genet.* **10**, 733 (2019).

564. Lionel, A. C. *et al.* Disruption of the ASTN2/TRIM32 locus at 9q33.1 is a risk factor in males for autism spectrum disorders, ADHD and other neurodevelopmental phenotypes. *Hum. Mol. Genet.* **23**, 2752–2768 (2014).

565. Lorgen-Ritchie, M. *et al.* Imprinting methylation in SNRPN and MEST1 in adult blood predicts cognitive ability. *PLoS One* **14**, e0211799 (2019).

566. Tekinay, A. B. *et al.* A role for LYNX2 in anxiety-related behavior. *Proc. Natl. Acad. Sci.* **106**, 4477–4482 (2009).

567. Peet, M. *et al.* Association of the Ban I dimorphic site at the human cytosolic phospholipase A2 gene with schizophrenia. *Psychiatr. Genet.* **8**, 191–2 (1998).

568. Hashimoto, R. *et al.* Genome-wide association study of cognitive decline in schizophrenia. *Am. J. Psychiatry* **170**, 683–4 (2013).

569. Beunders, G. *et al.* Two male adults with pathogenic AUTS2 variants, including a two-base pair deletion, further delineate the AUTS2 syndrome. *Eur. J. Hum. Genet.* **23**, 803–807 (2015).

570. Perroud, N. *et al.* Increased methylation of glucocorticoid receptor gene (NR3C1) in adults with a history of childhood maltreatment: a link with the severity and type of trauma. *Transl. Psychiatry* **1**, e59 (2011).

571. Gunn, B. G. *et al.* Dysfunctional astrocytic and synaptic regulation of hypothalamic glutamatergic transmission in a mouse model of early-life adversity: relevance to neurosteroids and programming of the stress response. *J. Neurosci.* **33**, 19534–54 (2013).

572. Schmidt, M. V. Stress-Hyporesponsive Period. *Stress Physiol. Biochem. Pathol.* 49–56 (2019) doi:10.1016/B978-0-12-813146-6.00004-7.

573. Rosenfeld, P., Suchecki, D. & Levine, S. Multifactorial regulation of the hypothalamic-pituitary-adrenal axis during development. *Neurosci. Biobehav. Rev.* **16**, 553–568 (1992).

574. Zannas, A. S. *et al.* Epigenetic upregulation of FKBP5 by aging and stress contributes to NF-κB-driven inflammation and cardiovascular risk. *Proc. Natl. Acad. Sci. U. S. A.* **116**, 11370–11379 (2019).

575. Taves, M. D., Ma, C., Heimovics, S. A., Saldanha, C. J. & Soma, K. K. Measurement of Steroid Concentrations in Brain Tissue: Methodological Considerations. *Front. Endocrinol. (Lausanne).* **2**, 39 (2011).

576. Chen, R., Wu, X., Jiang, L. & Zhang, Y. Single-Cell RNA-Seq Reveals Hypothalamic Cell Diversity. *Cell Rep.* **18**, 3227–3241 (2017).

577. Xie, L. *et al.* Sleep drives metabolite clearance from the adult brain. *Science* **342**, 373–7 (2013).

578. Kim, J. S., Han, S. Y. & Iremonger, K. J. Stress experience and hormone feedback tune distinct components of hypothalamic CRH neuron activity. *Nat. Commun.* **10**, 5696 (2019).

579. Thomson, J. P. *et al.* Comparative analysis of affinity-based 5-hydroxymethylation enrichment techniques. *Nucleic Acids Res.* **41**, e206–e206 (2013).

580. Lentini, A. *et al.* A reassessment of DNA-immunoprecipitation-based genomic profiling. *Nat. Methods* **15**, 499–504 (2018).

581. Ago, Y. *et al.* Antidepressant-like effects of the glucocorticoid receptor antagonist RU-43044 are associated with changes in prefrontal dopamine in mouse models of depression. *Neuropharmacology* **55**, 1355–63 (2008).

582. Guo, J. U. *et al.* Neuronal activity modifies the DNA methylation landscape in the adult brain. *Nat. Neurosci.* **14**, 1345–51 (2011).

583. Feng, J. *et al.* Dnmt1 and Dnmt3a maintain DNA methylation and regulate synaptic function in adult forebrain neurons. *Nat. Neurosci.* **13**, 423–430 (2010).

584. Jones, P. A. Functions of DNA methylation: islands, start sites, gene bodies and beyond. *Nat. Rev. Genet.* **13**, 484–492 (2012).

585. Zhu, F. *et al.* Architecture of the Mouse Brain Synaptome. *Neuron* **99**, 781-799.e10 (2018).

586. Karemaker, I. D. & Vermeulen, M. Single-Cell DNA Methylation Profiling: Technologies and Biological Applications. *Trends Biotechnol.* **36**, 952–965 (2018).

587. Clark, S. J. *et al.* scNMT-seq enables joint profiling of chromatin accessibility DNA methylation and transcription in single cells. *Nat. Commun.* **9**, 781 (2018).

588. Bondar, N. P., Lepeshko, A. A. & Reshetnikov, V. V. Effects of Early-Life Stress on Social and Anxiety-Like Behaviors in Adult Mice: Sex-Specific Effects. *Behav. Neurol.* **2018**, 1–13 (2018).

589. He, T., Guo, C., Wang, C., Hu, C. & Chen, H. Effect of early life stress on anxiety and depressive behaviors in adolescent mice. *Brain Behav.* e01526 (2020) doi:10.1002/brb3.1526.

590. Bahari-Javan, S. *et al.* HDAC1 links early life stress to schizophrenia-like phenotypes. *Proc. Natl. Acad. Sci. U. S. A.* **114**, E4686–E4694 (2017).

591. Daniels, W. M. U., Pietersen, C. Y., Carstens, M. E. & Stein, D. J. Maternal separation in rats leads to anxiety-like behavior and a blunted ACTH response and altered neurotransmitter levels in response to a subsequent stressor. *Metab. Brain Dis.* **19**, 3–14 (2004).

592. Troakes, C. & Ingram, C. D. Anxiety behaviour of the male rat on the elevated plus maze: associated regional increase in c-fos mRNA expression and modulation by

early maternal separation. *Stress* **12**, 362–9 (2009).

593. Goodwill, H. L. *et al.* Early life stress leads to sex differences in development of depressive-like outcomes in a mouse model. *Neuropsychopharmacology* **44**, 711–720 (2019).

594. Wise, L. A., Zierler, S., Krieger, N. & Harlow, B. L. Adult onset of major depressive disorder in relation to early life violent victimisation: a case-control study. *Lancet* **358**, 881–887 (2001).

595. Chatterjee, M., Jaiswal, M. & Palit, G. Comparative evaluation of forced swim test and tail suspension test as models of negative symptom of schizophrenia in rodents. *ISRN Psychiatry* **2012**, 595141 (2012).

596. Castagné, V., Moser, P., Roux, S. & Porsolt, R. D. Rodent models of depression: forced swim and tail suspension behavioral despair tests in rats and mice. *Curr. Protoc. Neurosci.* **Chapter 8**, Unit 8.10A (2011).

597. Mitchell, N. C., Gould, G. G., Smolik, C. M., Koek, W. & Daws, L. C. Antidepressant-like drug effects in juvenile and adolescent mice in the tail suspension test: Relationship with hippocampal serotonin and norepinephrine transporter expression and function. *Front. Pharmacol.* **4**, 131 (2013).

598. Jhuang, H. *et al.* Automated home-cage behavioural phenotyping of mice. *Nat. Commun.* **1**, 68 (2010).

599. Becker, J. B. *et al.* Stress and disease: is being female a predisposing factor? *J. Neurosci.* **27**, 11851–5 (2007).

600. Reed, M. D. *et al.* IL-17a promotes sociability in mouse models of neurodevelopmental disorders. *Nature* **577**, 249–253 (2019).

601. Kataoka, N., Shima, Y., Nakajima, K. & Nakamura, K. A central master driver of psychosocial stress responses in the rat. *Science* **367**, 1105–1112 (2020).

602. Davis, E. P. & Granger, D. A. Developmental differences in infant salivary alpha-amylase and cortisol responses to stress. *Psychoneuroendocrinology* **34**, 795–804 (2009).

603. McCain, G. C., Ludington-Hoe, S. M., Swinth, J. Y. & Hadeed, A. J. Heart rate variability responses of a preterm infant to kangaroo care. *J. Obstet. Gynecol. neonatal Nurs. JOGNN* **34**, 689–94 (2005).

604. Jost, K., Datta, A. N., Frey, U., Suki, B. & Schulzke, S. M. Heart rate variability predicts duration of respiratory support in preterm infants. in *European Respiratory Journal* vol. 48 PA1291 (European Respiratory Society, 2016).

605. McEwen, B. S. *et al.* Mechanisms of stress in the brain. *Nat. Neurosci.* **18**, 1353–1363 (2015).

606. Zoppi, S. *et al.* Regulatory Role of Cannabinoid Receptor 1 in Stress-Induced Excitotoxicity and Neuroinflammation. *Neuropsychopharmacology* **36**, 805–818 (2011).

607. Haller, J., Varga, B., Ledent, C. & Freund, T. F. CB1 cannabinoid receptors mediate anxiolytic effects: convergent genetic and pharmacological evidence with CB1-

specific agents. *Behav. Pharmacol.* **15**, 299–304 (2004).

608. Liu, D. *et al.* Maternal Care, Hippocampal Glucocorticoid Receptors, and Hypothalamic-Pituitary-Adrenal Responses to Stress. *Science (80-.).* **277**, 1659–1662 (1997).

609. Nautiyal, K. M., McKellar, H., Silverman, A.-J. & Silver, R. Mast cells are necessary for the hypothermic response to LPS-induced sepsis. *Am. J. Physiol. Integr. Comp. Physiol.* **296**, R595–R602 (2009).

610. Schlapbach, L. J. *et al.* Impact of sepsis on neurodevelopmental outcome in a Swiss National Cohort of extremely premature infants. *Pediatrics* **128**, e348-57 (2011).

611. Hagberg, H. *et al.* The role of inflammation in perinatal brain injury. *Nat. Rev. Neurol.* **11**, 192–208 (2015).

612. Fleiss, B. *et al.* Inflammation-induced sensitization of the brain in term infants. *Dev. Med. Child Neurol.* **57**, 17–28 (2015).

613. Eklind, S. *et al.* Bacterial endotoxin sensitizes the immature brain to hypoxic--ischaemic injury. *Eur. J. Neurosci.* **13**, 1101–6 (2001).

614. Fillman, S. G., Sinclair, D., Fung, S. J., Webster, M. J. & Shannon Weickert, C. Markers of inflammation and stress distinguish subsets of individuals with schizophrenia and bipolar disorder. *Transl. Psychiatry* **4**, e365–e365 (2014).

615. Osborne, S. *et al.* Antenatal depression programs cortisol stress reactivity in offspring through increased maternal inflammation and cortisol in pregnancy: The Psychiatry Research and Motherhood – Depression (PRAM-D) Study. *Psychoneuroendocrinology* **98**, 211–221 (2018).

616. Kinnally, E. L., Martinez, S. J., Chun, K., Capitanio, J. P. & Ceniceros, L. C. Early Social Stress Promotes Inflammation and Disease Risk in Rhesus Monkeys. *Sci. Rep.* **9**, 7609 (2019).

617. Bronson, S. L. & Bale, T. L. Prenatal Stress-Induced Increases in Placental Inflammation and Offspring Hyperactivity Are Male-Specific and Ameliorated by Maternal Antiinflammatory Treatment. *Endocrinology* **155**, 2635–2646 (2014).

618. Espinosa-Oliva, A. M. *et al.* Stress is critical for LPS-induced activation of microglia and damage in the rat hippocampus. *Neurobiol. Aging* **32**, 85–102 (2011).

619. Louveau, A. *et al.* Structural and functional features of central nervous system lymphatic vessels. *Nature* **523**, 337–341 (2015).

620. Lehtinen, M. K. & Walsh, C. A. Neurogenesis at the Brain–Cerebrospinal Fluid Interface. *Annu. Rev. Cell Dev. Biol.* **27**, 653–679 (2011).

621. Dahl, R. E. Sleep and the developing brain. *Sleep* **30**, 1079–80 (2007).

622. Chung, W.-S. *et al.* Astrocytes mediate synapse elimination through MEGF10 and MERTK pathways. *Nature* **504**, 394–400 (2013).

623. Bialas, A. R. & Stevens, B. TGF-β signaling regulates neuronal C1q expression and developmental synaptic refinement. *Nat. Neurosci.* **16**, 1773–1782 (2013).

624. Paolicelli, R. C. *et al.* Synaptic pruning by microglia is necessary for normal brain development. *Science* **333**, 1456–8 (2011).

625. Zhan, Y. *et al.* Deficient neuron-microglia signaling results in impaired functional brain connectivity and social behavior. *Nat. Neurosci.* **17**, 400–406 (2014).

626. Reemst, K., Noctor, S. C., Lucassen, P. J. & Hol, E. M. The Indispensable Roles of Microglia and Astrocytes during Brain Development. *Front. Hum. Neurosci.* **10**, 566 (2016).

627. Sokolowski, J. D., Chabanon-Hicks, C. N., Han, C. Z., Heffron, D. S. & Mandell, J. W. Fractalkine is a "find-me" signal released by neurons undergoing ethanol-induced apoptosis. *Front. Cell. Neurosci.* **8**, 360 (2014).

628. Vainchtein, I. D. *et al.* Astrocyte-derived interleukin-33 promotes microglial synapse engulfment and neural circuit development. *Science* **359**, 1269–1273 (2018).

629. Krishnan, M. L. *et al.* Integrative genomics study of microglial transcriptome reveals effect of DLG4 (PSD95) on white matter in preterm infants. doi:10.1101/105288.

630. Liu, R. *et al.* Why weight? Modelling sample and observational level variability improves power in RNA-seq analyses. *Nucleic Acids Res.* **43**, e97 (2015).

631. Lew, W. Y. W. *et al.* Recurrent exposure to subclinical lipopolysaccharide increases mortality and induces cardiac fibrosis in mice. *PLoS One* **8**, e61057 (2013).

632. Silva, C. S. da *et al.* LPS-Induced Systemic Neonatal Inflammation: Blockage of P2X7R by BBG Decreases Mortality on Rat Pups and Oxidative Stress in Hippocampus of Adult Rats. *Front. Behav. Neurosci.* **13**, 240 (2019).

633. Cuestas, E., Aguilera, B., Cerutti, M. & Rizzotti, A. Sustained Neonatal Inflammation Is Associated with Poor Growth in Infants Born Very Preterm during the First Year of Life. *J. Pediatr.* **205**, 91–97 (2019).

634. Cohen, E., Baerts, W. & van Bel, F. Brain-Sparing in Intrauterine Growth Restriction: Considerations for the Neonatologist. *Neonatology* **108**, 269–276 (2015).

635. Cahill, L. S. *et al.* Fetal brain sparing in a mouse model of chronic maternal hypoxia. *J. Cereb. Blood Flow Metab.* **39**, 1172–1184 (2019).

636. Lukas, G., Brindle, S. D. & Greengard, P. The route of absorption of intraperitoneally administered compounds. *J. Pharmacol. Exp. Ther.* **178**, 562–4 (1971).

637. Banks, W. A. & Robinson, S. M. Minimal penetration of lipopolysaccharide across the murine blood-brain barrier. *Brain. Behav. Immun.* **24**, 102–9 (2010).

638. Yao, Z. *et al.* Blood-Borne Lipopolysaccharide Is Rapidly Eliminated by Liver Sinusoidal Endothelial Cells via High-Density Lipoprotein. *J. Immunol.* **197**, 2390–2399 (2016).

639. Kawai, T. & Akira, S. Signaling to NF-κB by Toll-like receptors. *Trends Mol. Med.* **13**, 460–469 (2007).

640. Stridh, L., Smith, P. L., Naylor, A. S., Wang, X. & Mallard, C. Regulation of Toll-like receptor 1 and -2 in neonatal mice brains after hypoxia-ischemia. *J. Neuroinflammation* **8**, 45 (2011).

641. Smith, P. L. P. *et al.* Peripheral myeloid cells contribute to brain injury in male neonatal mice. *J. Neuroinflammation* **15**, 301 (2018).

642. Saavedra, L. M., Fenton Navarro, B. & Torner, L. Early Life Stress Activates Glial Cells in the Hippocampus but Attenuates Cytokine Secretion in Response to an Immune Challenge in Rat Pups. *Neuroimmunomodulation* **24**, 242–255 (2017).

643. Delpech, J.-C. *et al.* Early life stress perturbs the maturation of microglia in the developing hippocampus. *Brain. Behav. Immun.* **57**, 79–93 (2016).

644. Teissier, A. *et al.* Early-life stress impairs postnatal oligodendrogenesis and adult emotional behaviour through activity-dependent mechanisms. *Mol. Psychiatry* 1–16 (2019) doi:10.1038/s41380-019-0493-2.

645. Cahoy, J. D. *et al.* A transcriptome database for astrocytes, neurons, and oligodendrocytes: a new resource for understanding brain development and function. *J. Neurosci.* **28**, 264–78 (2008).

646. Sofroniew, M. V. & Vinters, H. V. Astrocytes: biology and pathology. *Acta Neuropathol.* **119**, 7–35 (2010).

647. O'Callaghan, J. P., Brinton, R. E. & McEwen, B. S. Glucocorticoids regulate the concentration of glial fibrillary acidic protein throughout the brain. *Brain Res.* **494**, 159–161 (1989).

648. Roessmann, U. & Gambetti, P. Astrocytes in the developing human brain. An immunohistochemical study. *Acta Neuropathol.* **70**, 308–13 (1986).

649. Wei, L. *et al.* Early-Life Stress Perturbs Key Cellular Programs in the Developing Mouse Hippocampus. *Dev. Neurosci.* **37**, 476–488 (2015).

650. Mestre, H. *et al.* Flow of cerebrospinal fluid is driven by arterial pulsations and is reduced in hypertension. *Nat. Commun.* **9**, 4878 (2018).

651. Galinsky, R. *et al.* Complex interactions between hypoxia-ischemia and inflammation in preterm brain injury. *Dev. Med. Child Neurol.* **60**, 126–133 (2018).

652. Martinello, K. A. *et al.* Acute LPS sensitization and continuous infusion exacerbates hypoxic brain injury in a piglet model of neonatal encephalopathy. *Sci. Rep.* **9**, 10184 (2019).

653. Garaci, F. G. *et al.* Increased Brain Apparent Diffusion Coefficient in Tuberous Sclerosis. *Radiology* **232**, 461–465 (2004).

654. Krishnan, M. L. *et al.* Diffusion Features of White Matter in Tuberous Sclerosis With Tractography. *Pediatr. Neurol.* **42**, 101–106 (2010).

655. Jeste, S. S. & Geschwind, D. H. Disentangling the heterogeneity of autism spectrum disorder through genetic findings. *Nat. Rev. Neurol.* **10**, 74–81 (2014).

656. de la Torre-Ubieta, L., Won, H., Stein, J. L. & Geschwind, D. H. Advancing the understanding of autism disease mechanisms through genetics. *Nat. Med.* **22**, 345–61 (2016).

657. Gaugler, T. *et al.* Most genetic risk for autism resides with common variation. *Nat. Genet.* **46**, 881–885 (2014).

658. Purcell, S. M. *et al.* A polygenic burden of rare disruptive mutations in schizophrenia. *Nature* **506**, 185–190 (2014).

659. Husquin, L. T. *et al.* Exploring the genetic basis of human population differences in DNA methylation and their causal impact on immune gene regulation. *Genome Biol.* **19**, 222 (2018).

660. Sadowski, M. *et al.* Spatial chromatin architecture alteration by structural variations in human genomes at the population scale. *Genome Biol.* **20**, 148 (2019).

661. Cross-Disorder Group of the Psychiatric Genomics Consortium. Identification of risk loci with shared effects on five major psychiatric disorders: a genome-wide analysis. *Lancet* **381**, 1371–1379 (2013).

662. Schork, A. J. *et al.* A genome-wide association study of shared risk across psychiatric disorders implicates gene regulation during fetal neurodevelopment. *Nat. Neurosci.* **22**, 353–361 (2019).

663. Zoghbi, H. Y. & Bear, M. F. Synaptic dysfunction in neurodevelopmental disorders associated with autism and intellectual disabilities. *Cold Spring Harb. Perspect. Biol.* **4**, (2012).

664. Forsyth, J. K. *et al.* Synaptic and Gene Regulatory Mechanisms in Schizophrenia, Autism, and 22q11.2 Copy Number Variant–Mediated Risk for Neuropsychiatric Disorders. *Biol. Psychiatry* **87**, 150–163 (2020).

665. Yoon, S.-J. *et al.* Reliability of human cortical organoid generation. *Nat. Methods* **16**, 75–78 (2019).

666. Ellenbroek, B. & Youn, J. Rodent models in neuroscience research: is it a rat race? *Dis. Model. Mech.* **9**, 1079–1087 (2016).

667. Kumar, S. & Hedges, S. B. A molecular timescale for vertebrate evolution. *Nature* **392**, 917–920 (1998).

668. Francis, C. *et al.* Divergence of RNA localization between rat and mouse neurons reveals the potential for rapid brain evolution. *BMC Genomics* **15**, 883 (2014).

669. Li, E., Bestor, T. H. & Jaenisch, R. Targeted mutation of the DNA methyltransferase gene results in embryonic lethality. *Cell* **69**, 915–26 (1992).

670. Chen, T. *et al.* Complete inactivation of DNMT1 leads to mitotic catastrophe in human cancer cells. *Nat. Genet.* **39**, 391–396 (2007).

671. Wu, H. *et al.* Dnmt3a-dependent nonpromoter DNA methylation facilitates transcription of neurogenic genes. *Science* **329**, 444–8 (2010).

672. Takizawa, T. *et al.* DNA Methylation Is a Critical Cell-Intrinsic Determinant of Astrocyte Differentiation in the Fetal Brain. *Dev. Cell* **1**, 749–758 (2001).

673. Moyon, S. *et al.* Functional Characterization of DNA Methylation in the Oligodendrocyte Lineage. *Cell Rep.* **15**, 748–760 (2016).

674. Donohoe, D. R. & Bultman, S. J. Metaboloepigenetics: interrelationships between energy metabolism and epigenetic control of gene expression. *J. Cell. Physiol.* **227**, 3169–77 (2012).

675. Meissner, A. *et al.* Genome-scale DNA methylation maps of pluripotent and differentiated cells. *Nature* **454**, 766–770 (2008).

676. Sanchez-Mut, J. V *et al.* DNA methylation map of mouse and human brain identifies target genes in Alzheimer's disease. *Brain* **136**, 3018–27 (2013).

677. Agrawal, K., Das, V., Vyas, P. & Hajdúch, M. Nucleosidic DNA demethylating epigenetic drugs – A comprehensive review from discovery to clinic. *Pharmacol. Ther.* **188**, 45–79 (2018).

678. Christman, J. K. 5-Azacytidine and 5-aza-2'-deoxycytidine as inhibitors of DNA methylation: mechanistic studies and their implications for cancer therapy. *Oncogene* **21**, 5483–5495 (2002).

679. Lee, B. H., Yegnasubramanian, S., Lin, X. & Nelson, W. G. Procainamide is a specific inhibitor of DNA methyltransferase 1. *J. Biol. Chem.* **280**, 40749–56 (2005).

680. Ceccaldi, A. *et al.* C5-DNA Methyltransferase Inhibitors: From Screening to Effects on Zebrafish Embryo Development. *ChemBioChem* **12**, 1337–1345 (2011).

681. Bartke, T. *et al.* Nucleosome-Interacting Proteins Regulated by DNA and Histone Methylation. *Cell* **143**, 470–484 (2010).

682. Natarajan, A., Yardimci, G. G., Sheffield, N. C., Crawford, G. E. & Ohler, U. Predicting cell-type-specific gene expression from regions of open chromatin. *Genome Res.* **22**, 1711–22 (2012).

683. Wang, J. *et al.* Sequence features and chromatin structure around the genomic regions bound by 119 human transcription factors. *Genome Res.* **22**, 1798–812 (2012).

684. Fuks, F. *et al.* The methyl-CpG-binding protein MeCP2 links DNA methylation to histone methylation. *J. Biol. Chem.* **278**, 4035–40 (2003).

685. Georgel, P. T. *et al.* Chromatin compaction by human MeCP2. Assembly of novel secondary chromatin structures in the absence of DNA methylation. *J. Biol. Chem.* **278**, 32181–8 (2003).